Magnetic Memory of Rocks: the Kazakhstan Orocline and Climatic Record of the Indian Monsoon

by

Alexandra Abrajevitch

A dissertation submitted in partial fulfillment
of the requirements for the degree of
Doctor of Philosophy
(Geology)
in The University of Michigan
2008

Doctoral committee:

Professor Rob Van der Voo, Chair
Professor Charles R. Cowley
Professor Ben A. van der Pluijm
Adjunct Associate Professor Josep M. Pares

2008

Acknowledgements

It is a pleasure to acknowledge the invaluable help of many people, without whom this thesis would not have been possible. I would like to express my gratitude to my advisor Rob Van der Voo for many helpful discussions and constant encouragement he provided during my study. His patience as well as his kindness in curing the injures I had inflicted on the English language are sincerely appreciated.

I would like to thank my dissertation committee members Josep Maria Pares, Ben van der Pluijm and Charles Cowley for managing to read the whole thesis so thoroughly. Kirill Degtyarev, Mikhail Bazhenov, Natalia Levashova and Phil McCausland are acknowledged for their constructive discussions on the geology of Kazakhstan, assistance in field research and for many memories, some of which still bring a smile to my face. I am also grateful to David Rea for his encouragement and assistance in the Bengal Fan study. Jim Hnat is gratefully acknowledged for his help in editing the final draft of the dissertation.

This study was supported by the U.S. National Science Foundation, grant EAR 0335882, by a Schlanger Ocean Drilling Fellowship and by an Institute of Rock Magnetism Visiting Fellowship.

It is impossible to name all the people who have contributed to the dissertation in some way; my sincere gratitude goes to all of them:

thank you all!

Table of Contents

Acknowledgements ii

List of Figures vii

List of Tables xi

List of Appendices xii

Chapter

1. Introduction 1

Kazakhstan orocline and amalgamation of Eurasia 2

Rock magnetic study of the Bengal Fan sediments 7

References 8

2. Paleomagnetic constraints on the paleogeography and oroclinal bending of the Devonian volcanic arc in Kazakhstan 12

Abstract 12

Introduction 14

Geological setting 16

Field and laboratory methods 19

Results 20

The a- and b- components 21

The c-component 23

Anomalous directions of magnetization 29

Discussion 31

Results summary and ages of magnetization 31

General pre-amble to an analysis of rotations in the Devonian volcanic arc 34

Previously published Silurian and Devonian paleomagnetic data and their corrected pre-Late Permian declinations 35

Unbending the orocline 41

Conclusions 43
Acknowledgements 44
References 44
3. Paleomagnetism of mid-Paleozoic subduction-related volcanics from the Chingiz Range in NE Kazakhstan: The evolving paleogeography of the amalgamating Eurasian composite continent 48
Abstract 48
Introduction 50
Geological Setting and Sampling 55
Locality AY (=Ayaguz; 48.0°N, 80.7°E) 57
Localities KN & DG (Kaynar-Dogolan; 49.5°N, 77.0°E) 57
Locality KU (Kurbakanas; 48.3°N, 78.3°E) 57
Methods 58
Results 59
Mid-Silurian volcanics (locality AY) 59
Lower to lower-Middle Devonian rocks of KN&DG locality 60
Givetian basalts (locality KU) 69
Discussion 70
Overview of results from the Chingiz area deemed of primary origin 70
Overprint data 77
Polarity choice 78
Declinations and rotations 81
Paleolatitudes 83
Comparison with published paleogeographic models 89
Conclusions 92
Acknowledgements 92
References 93
4. The role of the Kazakhstan orocline in the late Paleozoic amalgamation of Eurasia 99
Abstract 99
Introduction 101

The tectonics of Kazakhstan and adjacent areas 103
Sampling and laboratory methods 105
Results 107
Tokrau-A 107
Tokrau-B 111
Ayaguz-A 116
Ayaguz-B 120
Ages of magnetization 120
Tokrau 124
Ayaguz 128
Discussion 131
Rotations 131
Geodynamic implications 133
Conclusions 139
Acknowledgements 140
References 140
5. Variations in relative abundances of goethite and hematite in the Bengal Fan sediments: climatic vs. diagenetic signal 146
Introduction 146
Geological background 149
Climate change in the region 149
Himalayan foreland basin 151
The Bengal Fan 152
Sampling 153
Methods for identification of magnetic minerals in samples 154
Results 160
Identity of the components 160
Reliability of the IRM acquisition analysis in quantifying goethite and hematite 171
Results summary 171
Discussion 175
Climatic signal vs. diagenetic changes 175
Stability of the iron (oxyhydr)oxides in marine environments 178

Environmental significance of biogenic magnetite 180
Evidence for reductive dissolution 182
Summary and Conclusions 185
Acknowlegements 186
References 187
6. Conclusions 195
Kazakhstan orocline 195
Rock magnetic study of the Bengal Fan sediments 198
References 200
Appendices 202

List of Figures

Figure

1-1. Location areas of two paleomagnetic studies described in this thesis..... 4

2-1. Schematic map of central Asia, showing the location of the East Kazakhstan study area, wedged in between the Tarim, Baltica and Siberia cratons.. 15

2-2. Paleozoic subduction-related complexes showing strongly curved Devonian and late Paleozoic volcanic belts. 17

2-3. The sampled sections of the middle member of the Kurgasholak Formation at N 44 07'10", E74 47'30".. 18

2-4. Orthogonal demagnetization diagrams (Zijderveld, 1967) in geographic coordinates..... 22

2-5. Conglomerate test.. 24

2-6. Examples of great-circles used in constraining the c-component directions..... 28

2-7. Equal-angle stereoplots of the various component site-means isolated in the Kurgasholak Formation (as also listed in Table 2-1).. 30

2-8. Stereoplots showing the tilt-corrected primary site-mean directions of magnetization obtained from the Late Devonian Aral Formation (Levashova et al., 2007) and the Middle Devonian results of this study, with the third plot showing the difference in tilt-correction effects..... 32

2-9. Equal-angle stereoplot of the reference and the c-component directions..... 33

2-10. Cartoon illustrating the relationship between the structural trends and the declinations of the primary Silurian and Devonian magnetizations for the time prior to Permo-Triassic small-block rotations (A) and for the inferred Devonian (B) configuration of the belt.. 42

3-1. Location of study area. 52

3-2. Schematic map of major rock complexes in Kazakhstan..... 53

3-3. Representative thermal demagnetization plots of Silurian rocks from locality AY, in stratigraphic coordinates.. 61

3-4. Stereoplots of site-mean directions of the high-temperature components (HTC) with associated confidence circles (thin lines) of Silurian volcanic rocks from locality AY, (a) in situ (IS) and (b) after tilt correction (TC).. 62

3-5. Thermal demagnetization diagrams from the Lower-Middle Devonian volcanics from locality KN&DG in geographic coordinates. 65

3-6. Stereoplots showing site-mean directions of the A and B components isolated from Lower to lower-Middle Devonian rocks at locality KN&DG.. 66

3-7. Representative thermal demagnetization plots and stereonets of vector end-points and isolated components in Givetian volcanics from locality KU in stratigraphic coordinates (a-d).. 71

3-8. Site-mean directions of locality KU magnetizations. 72

3-9. Stereonet of locality-mean overprint directions with confidence circles (thin lines): squares, locality-means in situ; oblique cross, the result for locality KN&DG after 35% unfolding.. 79

3-10. Schematic outline of the Devonian volcanic belt (gray; simplified from Figure 3-2) with Silurian and Devonian paleomagnetic declinations (arrows).. 84

3-11. Plots of paleolatitude versus age for reference and observed data.. 88

3-12. Reconstruction of the Ural-Mongol belt and the major cratons of Baltica and Siberia (cross-hatched) for mid-Silurian time..... 91

4-1. Location of the study area.. 102

4-2. (a) Geologic sketch of the Tokrau-A sampling locality. (b-j) orthogonal demagnetization diagrams (Zijderveld, 1967) in tilt-corrected coordinates for representative samples of the Tokrau-A collection.. 109

4-3. (a) Geologic sketch of the Tokrau-B sampling locality. (b-i) orthogonal demagnetization diagrams in tilt-corrected coordinates for representative samples of the Tokrau-B collection. Conventions as in Figure 4-2. (j) examples of angular separation between site-mean magnetizations defined by “hematite” (labeled HTC) and “magnetite” (ITC) unblocking temperature ranges.. 112

4-4. Equal-area stereoplots of site-mean magnetization directions of the Tokrau locality.. 115

4-5. (a) Geologic sketch of the Ayaguz-A sampling locality. (b-e) orthogonal demagnetization diagrams in tilt-corrected coordinates for representative samples of the Ayaguz-A collection. (f-i) Examples of demagnetization diagrams (in situ) of conglomerate clasts.. 118

4-6. (a) Geologic sketch of the Ayaguz-B sampling locality, (b-g) orthogonal demagnetization diagrams (Zijderveld, 1967) in in situ coordinates for representative samples of the Ayaguz-B collection.. 121

4-7. Equal-area stereoplots of site-means magnetization directions of the Ayaguz locality.. 123

4-8. Age-correlation diagram for the Tokrau magnetizations.. 127

4-9. Baltica reference directions (black squares, plotted in 10 m.y. intervals, confidence limits are omitted for clarity) and directions of magnetization of the studied rocks.. 129

4-10. Tectonic scenario for the bending of the Kazakhstan orocline.. 136

5-1. Location map of Himalayan foreland and Bengal Fan showing ODP leg 116 drill sites..... 148

5-2. Summary of sites 717,718,719 (leg 116), showing lithostratigraphic units and correlations. 155

5-3. Basic principles of the IRM acquisition curves analysis, from Kruiver et al. (2001)..... 158

5-4. Low-temperature behavior of pedogenic iron oxides.. 159

5-5. Examples of IRM acquisition plotted as GAP (gradient acquisition plot) and SAP (standardized acquisition plot).. 162

5-6. Thermomagnetic runs for representative samples.. 163

5-7. The stepwise thermomagnetic runs on the sample 7-54-7-0.. 165

5-8. TEM micrographs of small grains from magnetic extract of sample 7-68-2-88, which shows a prominent “biogenic magnetite” peak.. 168

5-9. Low temperature cycling runs (Carter-Stiglitz et al., 2006) for representative samples.. 170

5-10. The difference in definition of the “high coercivity fraction” employed in the IRM analysis and in the low temperature cycling. 172

5-11. Values of the goethite to hematite ratio identified by two methods based on different physical principles.. 173

5-12. The variation in relative abundance of goethite vs. hematite and presence of the biogenic component in the studied sections of Holes 717 and 718. 177

5-13. Variations in biogenic and detrital magnetite, hematite and goethite components obtained in present study as well as the total organic carbon (TOC) and documented presence of pyrite (purple stars) in the sediments of the studied interval of Hole 717 (Shipboard scientific party, 1989. ODP Leg 116 initial report).…..... 184

A1. Examples of Ar release spectra and element ratios for several samples from the paleomagnetic site A493..…..... 212

A2. Micrographs of plagioclase grains..…..... 213

List of Tables

Table

2-1. Site-mean and formation-mean directions of the components isolated from the Kurgasholak Formation. 26

2-2. Summary of published Siluro-Devonian paleomagnetic data from the Devonian volcanic belt of the Kazakhstan orocline. 38

2-3. Analysis of reliability criteria for the results of Grishin et al. (1997) 39

3-1. Site-mean paleomagnetic directions for the Silurian rocks from locality AY 63

3-2. Component A data from Lower-Middle Devonian rocks from localities KN and DG 68

3-3. Component B data from Lower-Middle Devonian rocks from localities KN and DG 73

3-4. Paleomagnetic data from Givetian (Middle Devonian) volcanics (locality KU) 74

3-5. Summary of primary paleomagnetic results from northeastern Kazakhstan 76

3-6. Summary of overprint directions from northeastern Kazakhstan 80

3-7. Paleozoic paleomagnetic poles of Siberia 87

4-1. High temperature component, Tokrau-A 110

4-2. Intermediate temperature component, Tokrau 113

4-3. High temperature, Tokrau-B 114

4-4. High temperature component, Ayaguz-A 119

4-5. High temperature component, Ayaguz-B 122

4-6. Summary of paleomagnetic results 130

4-7. Rotation angles deduced for the Devonian results from the three limbs of the Kazakhstan Orocline 134

A1. $^{40}Ar/^{39}Ar$ analytical data 206

List of Appendices

Appendix

A. Ar-Ar dating of the Tokrau-A rocks 203

Ar-Ar analytical method 203

Results of Ar-Ar dating 204

References 214

B. Overview of previous studies on stability of iron (oxyhydr)oxides towards reductive dissolution 215

References 216

Chapter 1

Introduction

Natural magnetic minerals, iron (oxyhydr)oxides and iron sulfides, can provide a wealth of information on the formation, subsequent deformation and alteration of a rock. Although all minerals exhibit some form of magnetic behavior, the magnetic properties of rocks are mostly defined by their ferromagnetic content; the general term ferromagnetism, as used here, includes antiferromagnetism and ferrimagnetism, following Batler (1993). When a rock forms, the magnetic moments of ferromagnetic grains align themselves with the ambient magnetic field, thus recording the intensity and orientation of the Earth's magnetic field. Information on the past configuration of the field can be quantified as paleo–location of the rock unit, as well as any post-formational rotation or tilting. This ability to quantify displacements has made paleomagnetism, the study of remanent magnetization in ancient rocks, an important tool in tectonic studies. Since the mid-1950's, paleomagnetism has been used to identify the paleogeographic positions of major continental and oceanic lithospheric plates, to document motion histories of displaced terranes and to trace rotation and tilting of individual thrust-sheets in orogenic belts. These studies continue to provide insights into the processes by which continents grow and break-up, mountain belts form and change their shapes, etc.

During the past twenty years, a different approach has emerged concerning the interpretation of the magnetic record preserved in rocks. The various fractions of ferromagnetic grains that contribute to the total magnetization of a sedimentary rock may have different histories. The grains that were formed elsewhere were then eroded, transported by wind or water and then deposited in a new setting. In this new environment, the initial detrital assemblage can be modified by post-depositional processes, such as reductive dissolution of primary magnetic minerals and authigenic precipitation of new ferromagnetic phases. Both processes, dissolution and precipitation,

can be either abiotic or biologically controlled. Erosion, transport, deposition and diagenetic modification of the ferromagnetic grains are influenced by a complex interplay of atmospheric, hydrologic and lithoslogic factors. The climatic/physical conditions prevailing during the formation of a sedimentary rock can be deduced from the resulting ferromagnetic assemblage of the rock. The detailed information on mineralogy and grain-size distribution of a ferromagnetic fraction of sedimentary rocks has been used in environmental magnetism studies to deduce provenance of the sediments, mode of transport (aeolian, fluvial, or glaciogenic), climatic conditions in weathering environments, among others.

These two applications of paleomagnetism (tectonic and environmental) are used in the studies that constitute this thesis. Chapters 2, 3 and 4 of the thesis describe a tectonic study of Kazakhstan. The main objective of the study was to resolve the sequence of deformation that resulted in the creation of a strongly curved structure (Fig.1-1a). The second part of the thesis, Chapter 5, discusses the use of a rock magnetic parameter (the ratio of two magnetic minerals, goethite and hematite) in the sediments of the Bengal Fan to detect the changes in precipitation associated with the postulated change in the Indian monsoon system at ~ 7-8 Ma.

Kazakhstan orocline and amalgamation of Eurasia

Oroclines, or map-view bends of the tectonic elements, are common features of continental crust (Van der Voo, 2004). Curvature of initially straighter linear elements can develop in response to a variety of boundary conditions, ranging from local variations in configuration of the colliding terranes to regional changes in the stress-field (Weil and Sussman 2004). A particular mechanism, and accordingly, the boundary conditions responsible for the bending can be deduced from the kinematics of the curvature formation.

The Kazakhstan orocline - a pair of concentric horseshoe-shaped volcanic belts in Central Kazakhstan (Fig.1-1a), formed during the amalgamation of Eurasia. The ultimate cause of bending is thought to be the convergence of the large cratonic blocks of Baltica,

Figure 1-1. Location areas of two paleomagnetic studies described in this thesis.
a) Central Kazakhstan. A couple of subduction-related volcanic belts in Central Kazakhstan has an unusual, i.e. strongly curved, shape. A paleomagnetic study described in Chapters 2, 3 and 4 of this thesis was focused on understanding processes that led to the formation of the curvature.
b) The Bengal Fan. Sediments of the Bengal Fan contain iron-bearing minerals that formed in weathering environments of the Himalayan Foreland Basin. As processes of chemical weathering are climate-dependent, the resulting assemblage of iron-bearing minerals in sedimentary rocks is often interpreted as reflecting climatic conditions prevailing during the formation of the sediments. When the mineral grains are transported from terrestrial into marine conditions, an initial assemblage of the grains might be modified by diagenetic dissolution and neo-mineralization. A rock magnetic study of a sedimentary sequence recovered by the ODP Leg 116 at the distal part of the Bengal Fan (described in Chapter 5 of this thesis) investigated the applicability of a terrestrial climatic proxy (i.e., relative abundances of goethite and hematite) to studies of marine sediments.

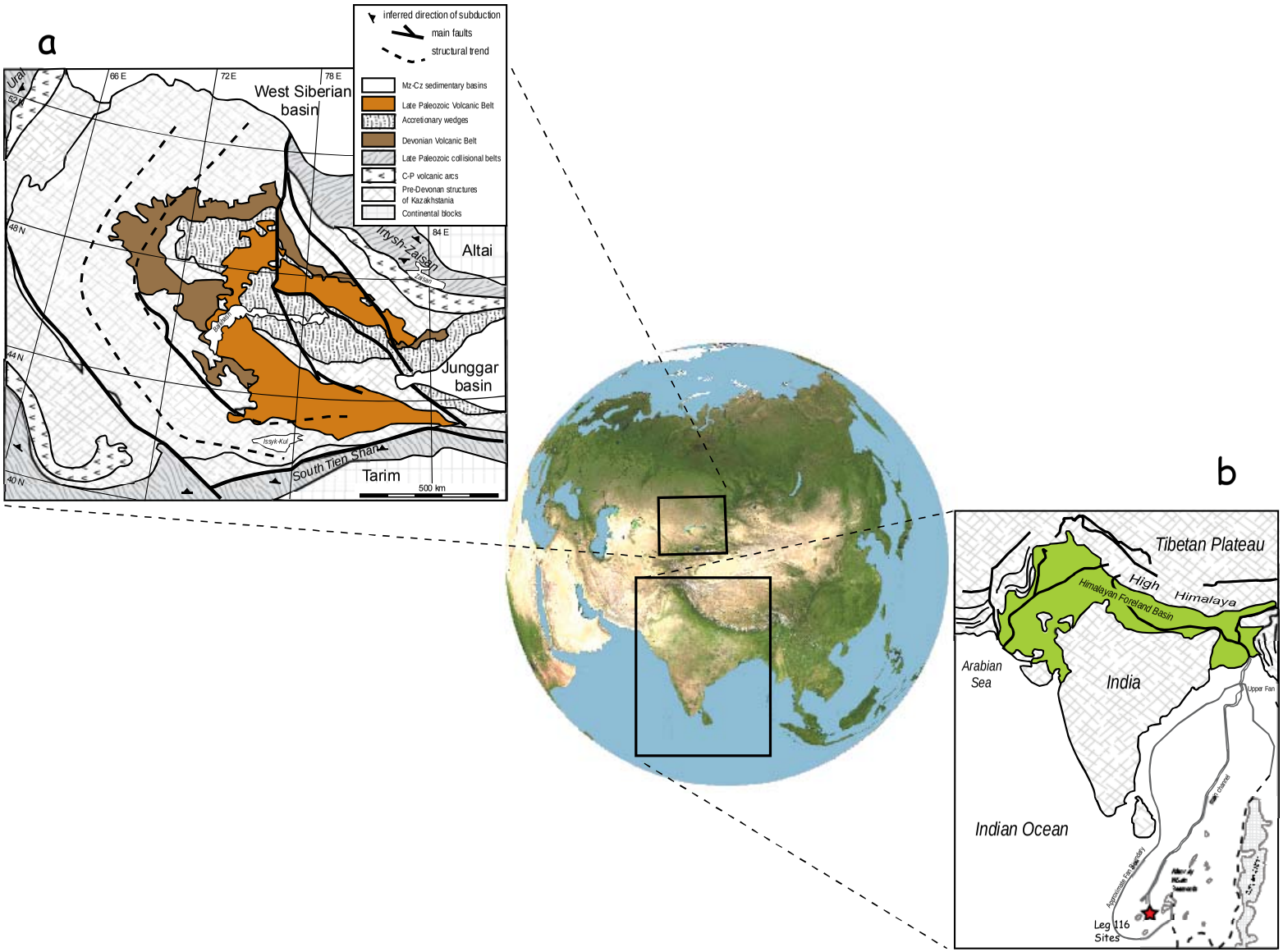
a
inferred direction of subduction
main faults
structural trend
Mz-Cz sedimentary basins
Late Paleozoic Volcanic Belt
Accretionary wedges
Devonian Volcanic Belt
Late Paleozoic collisional belts
C-P volcanic arcs
Pre-Devonan structures of Kazakhstania
Continental blocks
Ural
66 E
72 E
78 E
84 E
60 N
48 N
44 N
40 N
West Siberian basin
Irysh-Zaisan
Altai
Junggar basin
Tarim
South Tien Shan
Issyk-Kul
500 km
b
Tibetan Plateau
High
Himalaya
Himalayan Foreland Basin
Arabian Sea
India
Upper Fan
Indian Ocean
Leg 116 Sites

Siberia and Tarim (e.g. Zonenshain et al., 1990; Şengör et al., 1993; Van der Voo, 2004). Hence, both the pattern and timing of oroclinal rotations in Kazakhstan contain clues toward understanding the relative movements of these cratons prior to their final amalgamation.

The volcanic belts of the Kazakhstan orocline represent the remains of a subduction-related, Andean-type volcanic arc (Zonenshain et al., 1990; Bakhtiev, 1987, Kurchavov, 1994; Skrinnik and Horst, 1995). The area internal to the volcanic structures is dominated by rocks indicative of deeper marine environments, whereas the regions surrounding it were either non-depositional highlands or epicontinental shallow marine and non-marine basins (Zonenshain et al., 1990). Taken at face value, such a distribution implies that subduction was directed outwards from the inner part of the curved structure. In plate tectonic terms, this configuration of a plate boundary is considered unstable. The alternative explanation for the curved shape of the volcanic belts, that is of the oroclinal bending of an originally straighter arc, has been suggested by several authors (e.g., Zonenshain et al., 1990; Sengor and Natal'in, 1996; Grishin et al., 1997; Levashova et al., 2003; Van der Voo, 2004). Yet, while united in the recognition of the oroclinal nature of the curvature, the models cited above differ significantly in their estimates for the timing of the orogeny, the initial configuration of the arc and the magnitude of the relative rotation between the arms of the curved structure.

The discrepancies between the proposed oroclinal scenarios have two main reasons; a dearth of data and a multiphase deformational history of the area. Primary paleomagnetic results of suitable age (which can provide a quantitative measure of the oroclinal rotations) remain sparse in the geographical area of interest. Even when some results are available, their unambiguous interpretation is hampered by the multiple episodes of rotations. The repeated episodes of strike strip motions along the abundant east-west and northwest-southeast fault systems are well documented in the region (Allen et al., 2001; Natal'in and Şengör, 2005; Van der Voo et al., 2006). Such strike-slip faulting is frequently associated with vertical-axis rotations which cause a deviation in paleomagnetic declinations. A complex pattern of both counterclockwise and clockwise rotations (associated with sinistral east-west strike-slip faults, and dextral northwest-

southeast strike-slip faults, respectively) occurred in the region during the latest Paleozoic, after the main phase of oroclinal bending (Van der Voo et al., 2006). In making tectonic reconstructions for earlier times, a correction must be made for these late orogenic rotations.

Chapter 2 of this thesis presents new results of a paleomagnetic study of the middle Devonian formation from the southern arm of the orocline and describes the use of a Late Permian overprint to correct the primary mid-Devonian declination for the late-orogenic rotations. Declinations from other published Silurian and Devonian paleomagnetic results in the subduction-related Devonian volcanic arc of Kazakhstan have been similarly corrected for such rotations wherever the overprint directions are reasonably well documented. Using the corrected declinations as passive markers has allowed us to restore the trend of the volcanic belt to its Devonian configuration. Our analysis indicates that in the middle Devonian, the volcanic arc was nearly straight and northwest-southeast trending. This chapter has been published (as Abrajevitch et al., 2007).

Chapter 3 of this thesis presents new paleomagnetic results from three volcanic formations of mid-Silurian, Lower-to- Middle Devonian and Middle Devonian age from the Chingiz Range (the NE arm of the orocline). These new results improve the data-coverage in this part of the structure and allow us to substantiate the paleogeographic reconstructions proposed in the previous chapter. Our results also demonstrated the similarities between the northward motion of the Chingiz unit and that of Siberia, suggesting that these tectonic units were in close proximity to each other. This study has been submitted and is now in revision after review (as Levashova et al., 2008).

Chapter 4 describes a paleomagnetic study of Late Carboniferous to Late Permian subduction-related volcanics from the middle (NW) and north-eastern (NE) limbs of the orocline. Results of this study indicate that the rotation of the middle arm of the orocline was essentially complete by the earliest Permian, while the NE arm probably was still ~ 30º short of its final orientation with respect to Baltica. The rotation of, or rotation within, the NE arm was completed by the Late Permian. This study has been accepted for publication (as Abrajevitch et al., 2008).

These new constraints on the timing and amount of rotations combined with the data on the Middle Devonian configuration of the belt presented in the previous chapters have allowed us to reconstruct the main pattern of bending in the Kazakhstan orocline. We estimated that during oroclinal development, the SW arm of the curved structure underwent minimum relative displacement (~25^{o} ccw rotation), while the NE arm endured the largest amount (~ 120^{o} cw) of rotation. This pattern of rotations suggests that a dextral shear stress and drag was applied to the northern end of the structure, while its southern end was pinned down by a back-stop. Effectively, the bending of the Kazakhstan orocline can be explained as a result of relative convergence between Siberia (drag) and Tarim (backstop).

Rock magnetic study of the Bengal Fan sediments

Climate change is one of the greatest challenges facing modern society. According to the International Panel on Climate Change, some of the most profound and direct impacts of climate change over the next few decades will be felt in precipitation pattern and intensity. At present, atmospheric precipitation is the vital source of moisture used for agriculture and basic human necessities for the vast majority of the world's population. Forecasting the timing and magnitude of the regional responses of rainfall to ongoing global warming, an essential part of any long-term development plans, requires understanding of how the natural world has operated in the past. Detailed records of local and regional climatic changes can be found in sedimentary rocks, a natural archive containing a wealth of environmental information. This information, however, is often difficult to decipher. Formation of sedimentary rocks is controlled by the intricate interplay of climatic and tectonic factors, such as uplift or erosion of mountain ranges, temperature and precipitation of the weathering environment and diagenetic alteration during and after the deposition. So, it is desirable to find a generally applicable parameter that uniquely characterizes only one of these several factors, i.e., a parameter that responds to precipitation only.

In terrestrial sediments and soils of tropical and subtropical regions, a ratio of two pedogenic iron oxides, goethite and hematite was found to be a good proxy for precipitation (Cornell and Schwertmann, 2003). Detailed studies of soil sequences

showed that this ratio is very sensitive to moisture availability (e.g., Curi and Franzmeier, 1984; da Motta and Kampf, 1992) and does not depend on the parental rock composition (Kampf and Schwertmann, 1984). A relative abundance of goethite (high G/(G+H)) can be used as an indicator of higher precipitation, whereas low values imply dryer/warmer conditions. Similar climatic interpretation of the relative abundances of goethite and hematite has been increasingly applied to marine sediments (e.g. Harris and Mix, 1999; 2002; Clift, 2006; Zhang at al., 2007), i.e., the variations in the G/(G+H) parameter are thought to reflect the precipitation regime in the source area of the sediments. The validity of this approach, however, is contingent on the assumption, yet to be confirmed, that post-depositional diagenetic changes in marine environment do not modify the initial detrital ratio of these minerals.

Marine sediments of the Bengal Fan (Fig. 1-1b) provide an opportunity to test the utility of the G/(G+H) ratio in climatic studies. Various geological proxies indicate that a significant climatic change occurred in the source area of the fan (the Himalayan foreland) at ~ 7-8 Ma, yet the nature and cause of this change remain unclear. The proposed scenarios range from increased aridity (Gupta et al., 2004; Stern et al. 1997; Derry and France-Lanord, 1996) to intensification of the monsoon (e.g., Prell et al., 1992; Quade et al., 1989; Ding et al., 2001). Both options imply a significant change, albeit of opposite sense, in the average amount of precipitation in the Himalayan foreland. Consequently, the relative abundances of goethite and hematite in sediments derived from the foreland are expected to show a systematic change; the G/(G+H) parameter should increase with the intensification of the monsoon and decrease with aridification.

In an attempt to identify the nature of the climatic change in the Himalayan region and to better understand the applicability of the G/(G+H) parameter as a precipitation proxy to the studies of marine sediments, we have conducted a rock-magnetic study of Bengal Fan sediments. Results of the study are presented in Chapter 5 of this thesis.

References

Abrajevitch, A.V., Van der Voo, R., Levashova, N.M., Bazhenov, M.L. 2007. Paleomagnetism of the mid-Devonian Kurgasholak Formation, Southern

Kazakhstan: Constraints on the Devonian paleogeography and oroclinal bending of the Kazakhstan volcanic arc. *Tectonophysics*, v. 441, 67–84.

Abrajevitch, A., Van der Voo, R., Bazhenov, M. L., Levashova, N. M., McCausland, P. J. A. 2008. The role of the Kazakhstan orocline in the late Paleozoic amalgamation of Eurasia, *Tectonophysics*, in review.

Allen, M.B., Alsop, G.I., Zhemchuzhnikov, V.G. 2001. Dome and basin refolding and transpressive inversion along the Karatau fault system, southern Kazakhstan. *Journal of Geological Society of London*, 158, 83-95.

Bakhtiev, M.K. 1987. Paleozoic orogenic magmatic belts. Nauka, Moscow 168 p. (In Russian)

Clift, P.D. 2006. Controls on the erosion of Cenozoic Asia and the flux of clastic sediment to the ocean. *Earth and Planetary Science Letters*, 241, 571-580.

Cornell, R. M., Schwertmann, U. 2003. The iron oxides: structure, properties, reactions, occurrences, and uses. Weinheim Wiley-VCH, 664 pp.

Curi, N., Franzmeier, D.P. 1984. Toposequence of Oxisols from the Central Plateau of Brazil, *Soil Scientists Society America Journal,* 48(2), 341–346.

da Motta, P.E.F., Kampf, N. 1992. Iron oxide properties as support to soil morphological features for prediction of moisture regimes in oxisols of central Brazil. *Pflanzenernahrung und Bodenkunde* 155, 385-90.

Derry, L.A., France-Lanord, C. 1996. Neogene Himalayan weathering history and river (super 87) Sr/ (super 86) Sr; impact on the marine Sr record. *Earth and Planetary Science Letters*, 142(1-2), 59-74.

Ding, Z.L., Yang, S.L., Sun, J.M., Liu, T.S. 2001. Iron geochemistry of loess and red clay deposits in the Chinese Loess Plateau and implications for long-term Asian monsoon evolution in the last 7.0 Ma. *Earth and Planetary Science Letters*, 185(1-2), 99-109.

Grishin, D.V., Pechersky, D.M., Degtyarev, K.E. 1997. Paleomagnetism and reconstruction of Middle Paleozoic structure of Central Kazakhstan. *Geotectonics*, 1, 71– 81.

Gupta, A.K., Singh, R.K., Joseph, S., Thomas, E. 2004. Indian Ocean high-productivity event (10-8 Ma); linked to global cooling or to the initiation of the Indian monsoons? *Geology*, 32(9), 753-756.

Harris, S.E., Mix, A.C. 1999. Pleistocene precipitation balance in the Amazon Basin recorded in deep sea sediments. *Quaternary Research*, 51, 14-26.

Harris, S.E., Mix, A.C. 2002. Climate and tectonic influences on continental erosion of tropical South America, 0-13 Ma. *Geology*, 30(5), 447-450.

Kampf, N., Schwertmann, U. 1984. Goethite and hematite in a climosequence in southern Brazil and their application in classification of kaolinitic soils. *Geoderma*, 29, 27-39.

Kurchavov, A.M. 1994. The lateral variability and evolution of orogenic volcanism in the fold belts. *Geotectonics*, 28, 3-18.

Levashova, N.M., Degtyarev, K.E., M.L. Bazhenov, M.L., Collins, A.Q., Van der Voo, R. 2003. Permian Paleomagnetism of East Kazakhstan and the Amalgamation of Eurasia: *Geophysical Journal International*, v. 152, p. 677-687.

Levashova, N.M., Van der Voo, R., Abrajevitch, A.V., and Bazhenov, M.L. 2008. Paleomagnetism of mid-Paleozoic subduction-related volcanics from the Chingiz Range in NE Kazakhstan: The evolving paleogeography of an amalgamating Eurasian continent. *Geological Society of America Bulletin*, in revision.

Natal'in, B. A., Şengör, A. M. C. 2005. Late Palaeozoic to Triassic evolution of the Turan and Scythian platforms: the pre-history of the palaeo-Tethyan closure, Tectonophysics, 404, 175-202.

Prell, W.L., Murray, D.W., Clemens, S.C., Anderson, D.M. 1992. Evolution and variability of the Indian Ocean summer monsoon: Evidence from the western Arabian Sea drilling program, In Duncan, R.A., Rea, D.K., Kidd, R.B., von Rad, U., and Weissel, J.K. (eds.), Synthesis of Results from Scientific Drilling in the Indian Ocean, American Geophysical Union Geophysical Monograph 70, Washington, D.C., 447-469.

Quade, J., Cerling, T.E., Bowman, J.R. 1989. Development of Asian monsoon revealed by marked ecological shift during the latest Miocene in northern Pakistan. *Nature*, 342(6246), 163-166.

Şengör, A M C; Natal'in, B. A., Burtman, V. S. 1993. Evolution of the Altaid tectonic collage and Palaeozoic crustal growth in Eurasia. *Nature* (London), vol.364, pp.299-307.

Şengör, A.M.C., Natal'in, B.A. 1996. Paleotectonics of Asia: fragments of a synthesis. In: Yin, A., Harrison, M. (Eds.), The Tectonic Evolution of Asia. Cambridge Univ. Press, Cambridge, pp. 486– 640.

Skrinnik, L.I., Horst, V.E. 1995. Devonian island arc volcanic complexes in the Junggar Alatau. *Geology and exploration of Kazakhstan*, 4, 6-10.

Stern, L.A., Chamberlain, C.P., Reynolds, R.C., Johnson, G.D. 1997. Oxygen isotope evidence of climate change from pedogenic clay minerals in the Himalayan molasse. *Geochimica et Cosmochimica Acta*, 61(4), 731-744.

Van der Voo, R. 2004. Paleomagnetism, oroclines and the growth of the continental crust. *GSA Today,* 14 (12), 4-9.

Van der Voo, R., Levashova, N. M., Skrinnik, L. I., Kara, T. V., Bazhenov, M. L. 2006. Late orogenic, large-scale rotations in the Tien Shan and adjacent mobile belts in Kyrgyzstan and Kazakhstan, *Tectonophysics*, 426, 335-360.

Weil, A.B., Sussman, A.J. (eds.) 2004. Orogenic curvature: Integrating paleomagnetic and structural analyses. *Geological Society of America Special Paper*, 383, p. 271.

Zhang., Y.G., Ji, J., Balsam, W., Liu, L., Chen, J. 2007. High resolution hematite and goethite records from ODP 1143, South China Sea: Co-evolution of monsoonal

precipitation and El-Nino over the past 600,000 years. *Earth and Planetary Science Letters*, 264, 136-150.

Zonenshain, L.P., Kuzmin, M.I., Natapov, L.M. 1990. Geology of the USSR: a plate tectonic synthesis. Ed. Page, B.M. AGU, Geodynamic series, volume 21. Washington, D.C., 250p.

Chapter 2

Paleomagnetic constraints on the paleogeography and oroclinal bending of the Devonian volcanic arc in Kazakhstan

Abstract

A prominent feature of the central part of the Ural-Mongol orogenic belt is a series of concentric horse-shoe shaped volcanic arcs, with the youngest arc on the inside. This structure was long-suspected to be an orocline, but unequivocal evidence for this was lacking, mainly because paleomagnetic results of suitable age from this area remained sparse, but also because their interpretation was not straightforward due to a long history of deformations associated with the protracted late Paleozoic assembly of Asia.

Our paleomagnetic study of Middle Devonian basaltic and andesitic flows in southeastern Kazakhstan revealed two main components of magnetization. The primary nature of a high temperature magnetization (tilt corrected Dec=286.5, Inc=46.4, α_{95}=7.8, k=29.2, N=13 sites) is supported by the presence of antipodal directions and a baked-contact test. We also isolated a post-folding overprint with an *in situ* mean direction Dec=134.9, Inc=-43.0 (α_{95}=4.9, k=71.6, N=13 sites). The age of this overprint can be estimated as Early Permian with a high degree of confidence. The declination of the overprint is seen to be deflected counter-clockwise by 100±6^{o} relative to the 290-Ma reference direction, indicating that the studied locality, similar to many other localities in the region, was affected by late-orogenic rotations. We use the overprint's deflection to correct the declination of the primary Devonian magnetization for these late-orogenic block-rotations.

Declinations from other Silurian and Devonian paleomagnetic results in the subduction-related Devonian volcanic arc of Kazakhstan have been corrected for such

rotations wherever the latter are reasonably well documented. Using corrected declinations as passive markers we restored the trend of the volcanic belt to its Devonian configuration. Our analysis indicates that the presently curved belt was nearly straight and NW-SE trending. This ~1500 km long volcanic belt characterized the northeastern margin of a landmass in today's central Kazakhstan where subduction occurred towards the southwest. Oroclinal bending of this arc took place in the interval between the Middle Devonian and the Late Permian.

Introduction

It is now widely recognized that Central Asia is a composite realm assembled during the Phanerozoic by accretion of various continental blocks, island arc fragments, and accretionary complexes (Fig. 2-1). The assembly mechanism is still disputed for the early Paleozoic, however. Regardless whether authors favored collision of microcontinents that were originally separated by oceanic basins and multiple island arcs (Mossakovsky, et al., 1993; Didenko et al., 1994; Dobretsov et al., 1995; Filippova et al., 2001; Windley et al., 2007), or forearc accretion and oroclinal bending of a single, long-lived subduction system (Şengör and Natal'in, 1996), most scientists agree that by the middle Paleozoic several relatively small terranes had amalgamated into a single tectonic unit (often referred to as "Kazakhstania", but the definition of this concept may differ from author to author). Possibly from Early Silurian onwards (Degtyarev and Ryazantsev, 1993) and certainly from Late Silurian to Early Permian time, volcanic arc structures marked one of the margins of the amalgamated block (Zonenshain et al., 1990; Bakhtiev, 1987, Kurchavov, 1994; Skrinnik and Horst, 1995). In their present-day configuration, the Devonian and late Paleozoic volcanic belts are horse-shoe shaped (Fig. 2-2). The area internal to the strongly curved volcanic structures is dominated by rocks indicative of deeper marine environments, whereas the regions surrounding it were either non-depositional highlands or epicontinental shallow marine and non-marine basins (Zonenshain et al., 1990). Taken at face value, such a distribution implies that subduction was directed outwards from the inner part of the curved structure. This scenario, however, is difficult to reconcile with plate tectonic theory; oroclinal bending of an originally straighter arc was therefore suggested as a possible explanation for the shape of the volcanic belts (Zonenshain et al., 1990; Şengör and Natal'in, 1996; Grishin et al., 1997; Levashova et al., 2003; Van der Voo, 2004).

Currently several paleomagnetic efforts are underway to improve our understanding of the tectonic history of Central Asia, and especially that of the "Kazakhstan orocline" (e.g., Bazhenov et al., 2003; Collins et al., 2003; Levashova et al., 2003; Alexyutin et al., 2005; Van der Voo et al., 2006; Levashova et al., 2007). The

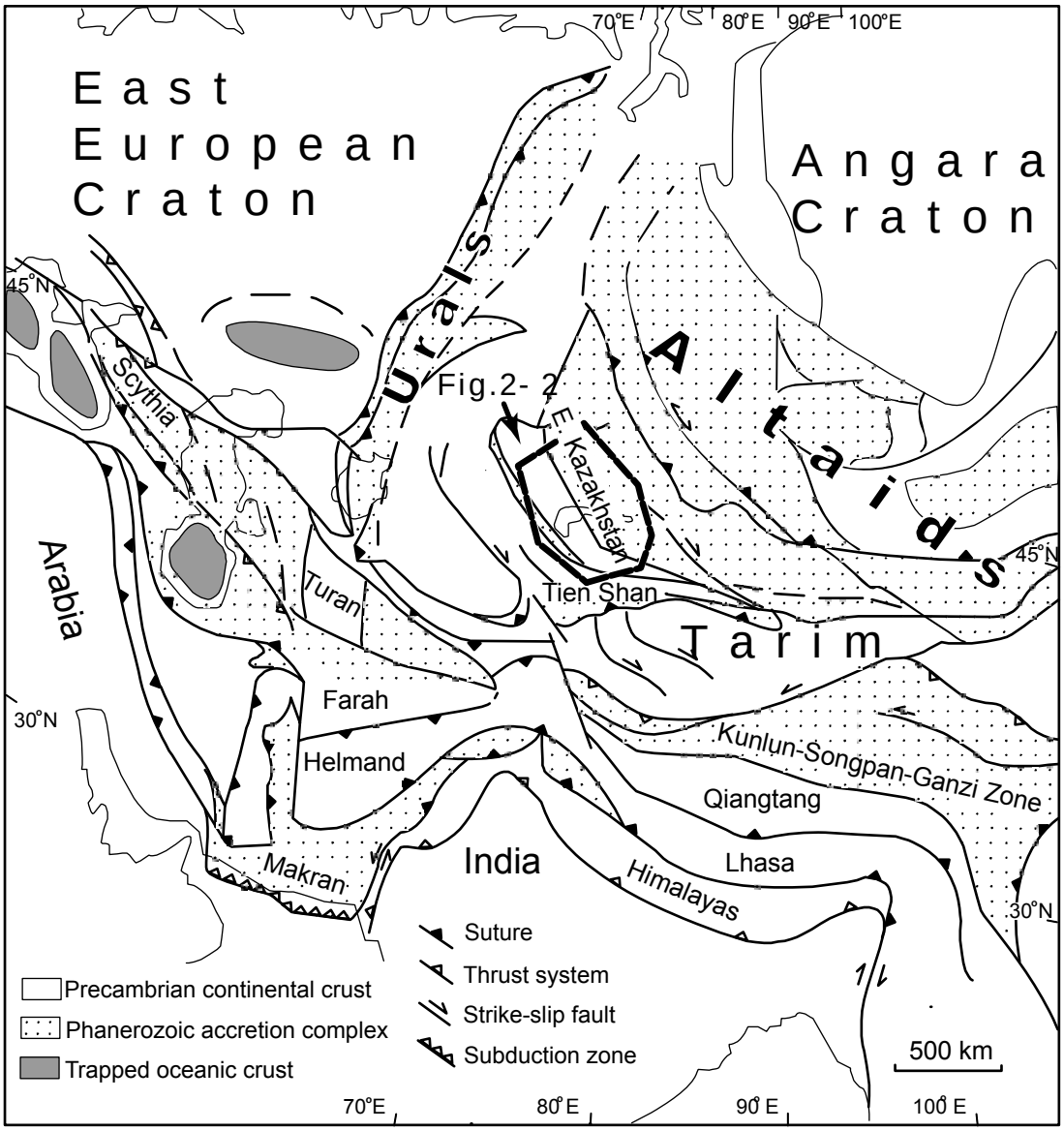

Figure 2-1. Schematic map of central Asia, showing the location of the East Kazakhstan study area, wedged in between the Tarim, Baltica and Siberia cratons. Modified after Allen et al., 2001.

declinations of primary magnetization in Ordovician rocks from the Chingiz Range (the northeastern limb of the orocline) and the North Tien Shan (south- to southwestern limb) were found to differ by about 180˚, which was interpreted by Levashova et al. (2003) as evidence for oroclinal bending. The Permian results from the same two areas (Van der Voo et al., 2006) show declination differences on the order of 90˚. The post-Permian rotations, on the other hand, were attributed to small-scale block rotations within a larger-scale sinistral wrenching zone of deformations in and around the North Tien Shan area. Thus, only about 50% of the total post-Ordovician rotation was attributed to the putative oroclinal bending that presumably happened some time between Ordovican and Late Permian.

To further constrain the timing and mode of the oroclinal bending, we studied Middle Devonian volcanics from the southwestern limb of the Kazakhstan orocline. The declination obtained in the present study will be compared with those for rocks of similar age as well as with the declination pattern of Silurian results from the entire curved volcanic arc structure (Grishin et al., 1997; Levashova et al., 2003; Alexyutin et al., 2005). Declination deviations will be taken as an indication of relative rotations of the limbs.

Geological setting

The stratotype section of the Kurgasholak Formation is located in the southeast of the Chu-Ili region (Fig.2-3; GPS location N 44^{o} 07'10", E74^{o}47'30"). This locality is the only known outcrop of the Middle Devonian volcanics in the region (Abdullin et al., 1980); basaltic extrusive volcanism here occurred along the south-west boundary of the outcrops of Precambrian metamorphic rocks (Abdullin et al., 1980).

The Kurgasholak Formation unconformably overlies the Lower to Middle Devonian Degrez Formation and in turn is unconformably overlain by the Upper Devonian (Famennian) Zhingeldy Formation (Tokmacheva et al., 1974; Senkevich, 1991). The Kurgasholak formation is subdivided into three members. The lower member (~600 m thick) comprises basal pebbly conglomerate, medium– to fine grained sandstones, rare tuffaceous sandstones, two rhyolite flows and occasional beds of

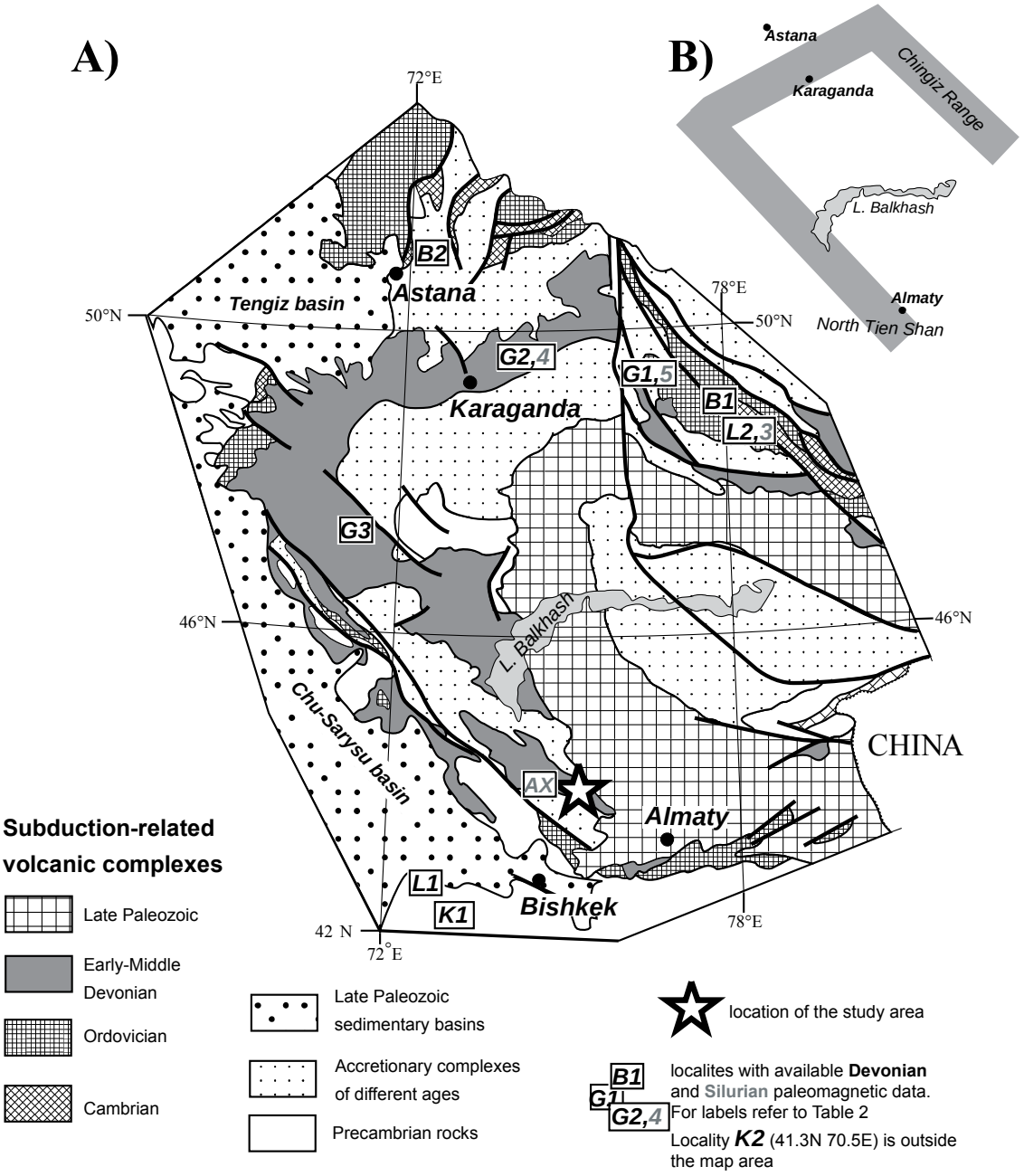

Figure 2-2. Paleozoic subduction-related complexes showing strongly curved Devonian and late Paleozoic volcanic belts. (A; modified after Degtyarev, 2003), the North Tien Shan and Chingiz Range at either end, as labeled in (B). The sampling localities of previously published Silurian and Devonian paleomagnetic results (G1 – 5, L1 – 3, B1 – 2, AX) and of this study (star) are indicated.

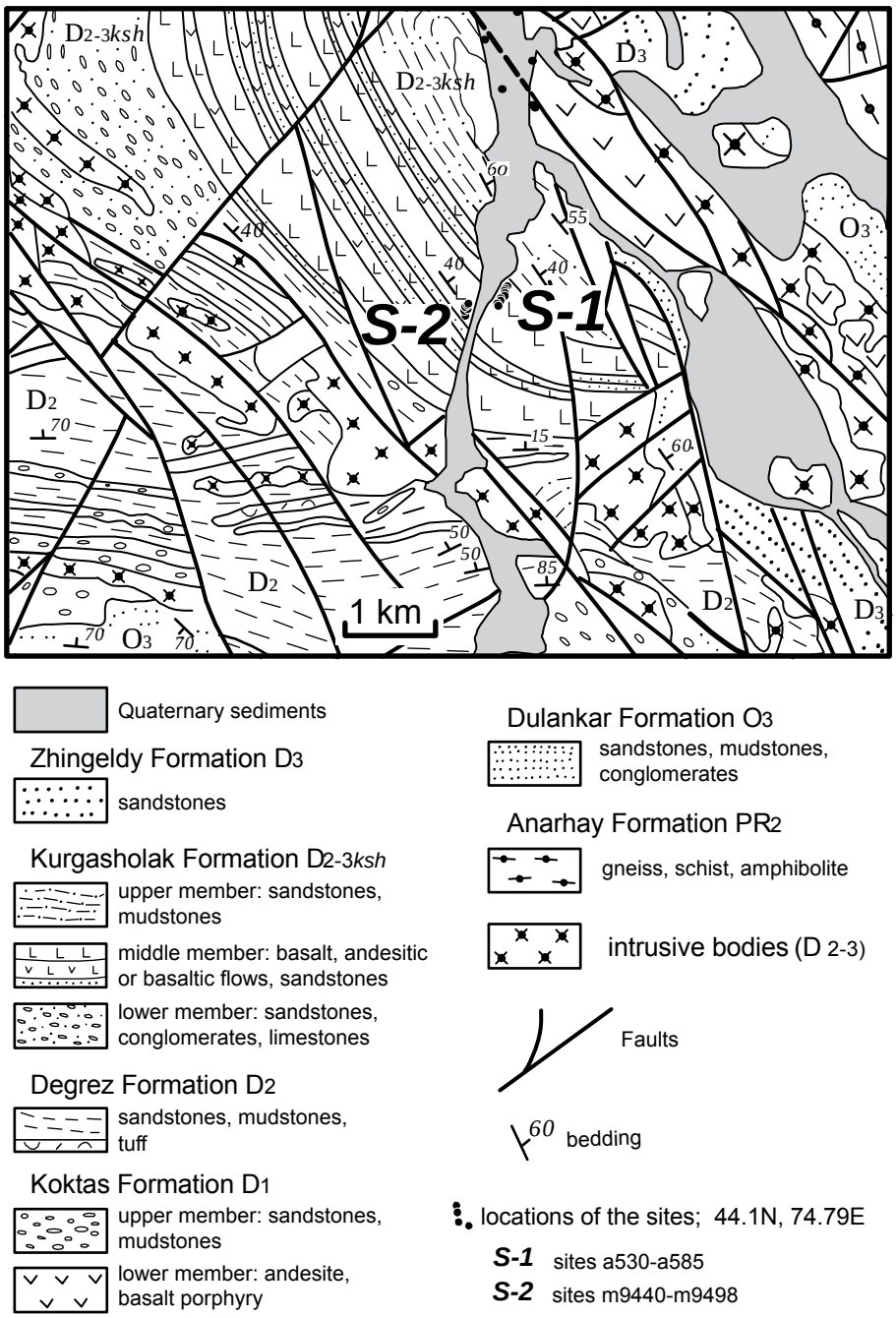

Figure 2-3. The sampled sections of the middle member of the Kurgasholak Formation at N 44 07'10", E74 47'30". Geological map from Abdullin et al. (1980).

limestone. The middle member (~1100 m thick) consists mostly of massive flows of purplish-grey, dark green and brown porphyritic basalt and andesitic basalt with rare feeder-dikes. No occurrence of tuff is known in the sequence. In the majority of the flows the upper oxidized surface is preserved, suggesting short-lived but nearly continuous volcanic activity. The flows are inter-bedded with occasional layers of sandstone and pebbly conglomerates, which contain products of erosion and re-deposition of the contemporary volcanics. The upper member of the formation (~560 m thick) comprises poorly exposed fine- to coarse-grained, cross-bedded, red sandstones and mudstones.

The age assignment of Middle Devonian for the Kurgasholak Formation is based on stratigraphic position as well as on fossil plants collected from sandstones of the lower member: *Cooksonia (?) degrezensis* Senk., *Taeniocrada* cf. *langi* Stockm., T. cf. *dubia* Kr. et W., *Lidasimophyton akkermensis* Senk., *Protolepidodendron schrianum* Kr., *Protopteridium* cf. *hostimense* Kr. The plant assemblage does not allow for a more precise age estimate within the Middle Devonian (Tokmacheva et al., 1974).

The sampling area is located in a zone (called Stepnyak-North Tien Shan) that by Devonian time was incorporated into the Kokchetav – North Tien Shan Domain (KNTD) according to Windley et al. (2007, fig. 6). This domain is approximately the same as the "Kazakhstan-Kyrghyz" block of Filippova et al. (2001). These scientists argued that this block was probably not rigid, but that it did act as a coherent paleogeographic unit in post-Ordovician times, and that an Early Devonian arc system developed on its eastern side, as illustrated in Figure 2-2, accommodating west- or southwest-dipping subduction (in present-day coordinates).

Field and laboratory methods

For this study, we collected volcanics of the middle member of the Kurgasholak Formation at the type locality for this formation (see Fig. 2-3). In total, we sampled 18 volcanic sites, each representing a cooling unit, and one layer of an intra-formational conglomerate (16 clasts, site m9476 in Table 2-1). Sample labels start with a capital letter

(A, or M), followed by sample number, whereas sites are marked with a lower-case letter and the number of the first sample collected.

Paleo-horizontal of the volcanic flows in the sampled sections and the younging direction of the section were determined from oxidized flow-tops and the intra-formational conglomerate bed. Bedding attitudes show some variation from bottom to top of the sampled section; see Table 2-1, which contains the strikes and dips of the sites, listed in stratigraphic order. Samples were collected as oriented blocks; a magnetic compass with inclinometer was used for the orientation of the samples. A lack of deflection of the magnetic compass needle by the basalts demonstrated that magnetic intensities did not significantly affect orientation readings.

In the laboratory, cubic specimens with ~20 mm side dimensions were cut from the block samples, yielding, on average, 2 specimens per sample. Measurements of natural remanent magnetization (NRM) were performed in the University of Michigan paleomagnetic laboratory. The remanent intensities and directions were measured with a three-axis 2G superconducting magnetometer. Alternating field demagnetization of a few pilot specimens failed to isolate components of magnetization successfully. The bulk of the specimens were therefore thermally demagnetized in an ASC TD-48 demagnetizer. Both demagnetization and measurement were done in a magnetically shielded room with a rest field < 200 nT. Results of the demagnetization treatments have been plotted in orthogonal vector endpoint diagrams (Zijderveld, 1967) and in stereonets. For calculation of the magnetization directions, principal component analysis (PCA, Kirschvink, 1980) was used on linear segments of the Zijderveld plots; in cases where stable endpoints were not obtained, so that successive endpoints were seen moving as trends along great circle paths, a combined analysis of remagnetization circles and direct observations (McFadden & McElhinny, 1988) was used.

Results

NRM intensities of the studied samples range from 0.2 to 11 A/m. Demagnetization diagrams (Fig. 2-4) show a wide range of behavior. Apart from a low-temperature overprint generally removed at ~ 200^{o}C, specimens revealed a number of

discrete directions that have been divided into *a*-, *b*-, and *c*-components. The site-mean directions of the intermediate- and high-temperature components and their associated statistical parameters are listed in Table 1 together with the formation mean directions.

The first-removed low-temperature components are tightly clustered (with a mean of dec/inc = 6.4º/62.7º, k = 42, α_{95} = 5.4º, N = 18 site means) around the present-day geomagnetic field direction, which is dec/inc = 5.4º/63.8º in 2005. These components are readily interpreted as of recent and most likely viscous origin and have no significance for the tectonics of the area. Even so, the good clustering of these directions testifies to the accuracy and coherency of the field-orientations of our samples.

The a- and b- components

The high temperature *a*-component, easterly and shallow up in geographic coordinates, was isolated in 10 out of 18 sampling sites. This component was usually removed between 500 and 580^{o}C, although in samples collected from the upper oxidized part of the flows, the magnetization could persist up to 675^{o}C with no significant change in direction from 350 to 470 ^{o}C to >650^{o}C (Fig.2-4a-d), suggesting that magnetite and hematite contribute similarly to the higher-temperature remanence (*a*-) directions. In some samples, the *a*-component was readily identified even though it appeared to co-exist with a lower-temperature component (which we will call *c*), as can be seen for instance in Figure 2-4c. In yet other samples, *a* and *c* appear to co-exist, but an insufficient number of steps is available to determine the *a*-component by PCA (e.g., Fig. 2-4f). In several demagnetization experiments the trajectory of the data-points did not reach a stable direction, indicating overlapping temperature spectra of two or more components. In these cases, the McFadden & McElhinny (1988) great-circle technique was used to estimate the directions of the various components.

A high-temperature *b*-component, westerly and shallow down in geographic coordinates (Fig. 2-4h, 2-4h), was found in three sites and its remanence unblocks in the same range as the *a*-component in the other sites, i.e., between 250 – 475˚C and ~600˚C.

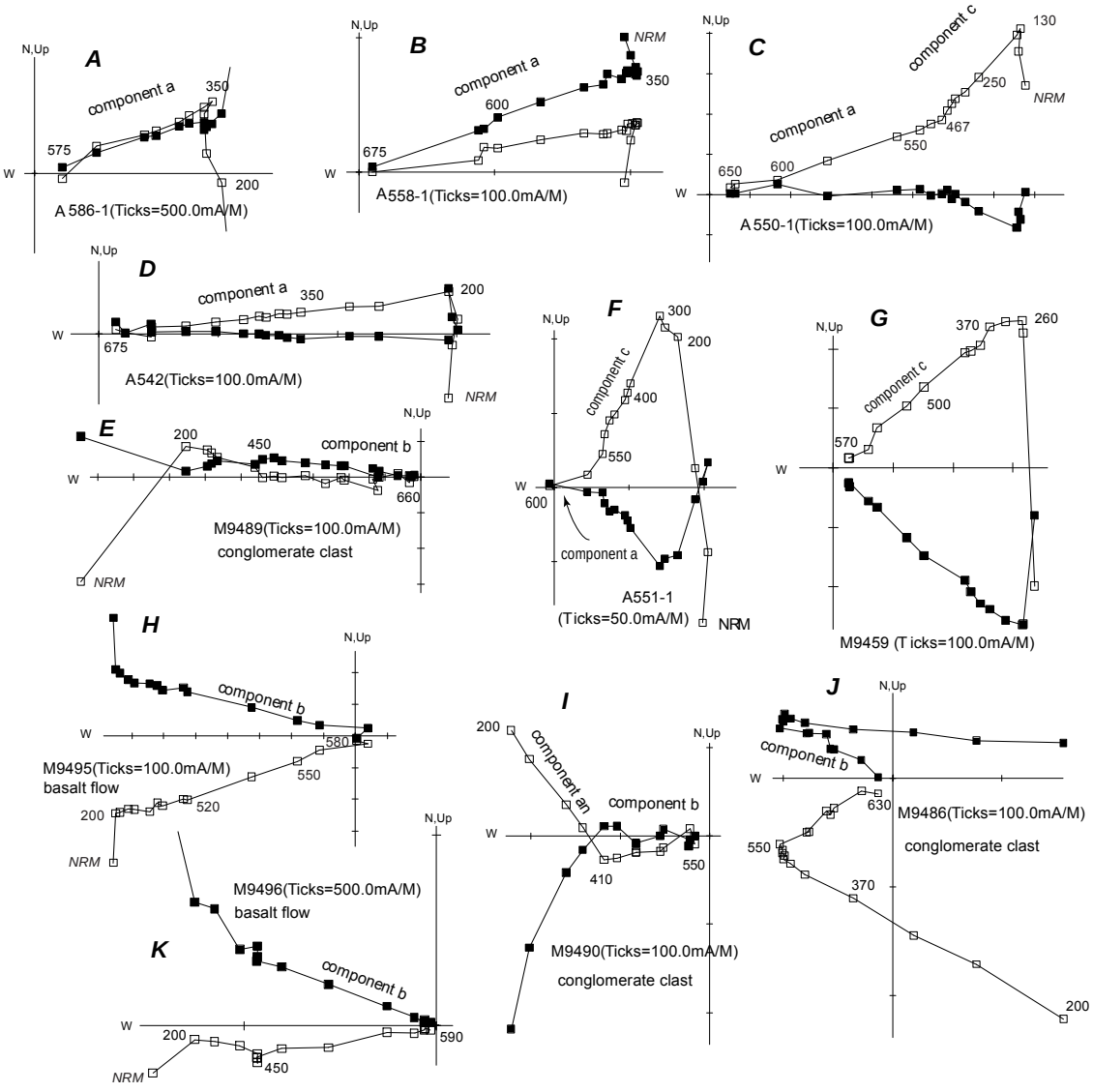

Figure 2-4. Orthogonal demagnetization diagrams (Zijderveld, 1967) in geographic coordinates. Sample numbers correspond to similarly numbered sites (see Table 2-1). Components, as labeled (a, b, c or an), are discussed in the text. Open (closed) symbols correspond to magnetization end-points projected onto the east-west vertical (horizontal) plane. Tickmarks denote intensities as labeled in mA/m.

Two of these sites are successive volcanic flows (sites m9492 and m9498; Table 2-1); the third one is a conglomerate bed just below these flows (Figs. 2-4eE, 2-4i-jJ, 5). The mean magnetization direction of the overlying flow (star in Fig. 2-5) agrees well with the characteristic directions of the conglomeratic clasts, suggesting that in all likelihood the magnetization of each individual clast represents more or less the same spot reading of the geomagnetic field. Thus, it appears that the characteristic magnetization of the conglomerate clasts is a thermoremanent magnetization (TRM) acquired during the emplacement of, and heating by, the overlying flow.

The *a*- and *b*- directions are approximately antipodal; with a deviation γ=18.9˚, it could be argued that they pass the McFadden and McElhinny (1990) reversal test, but not much significance can be given to this because of the limited number of site-means with a westerly/shallow downward *b*-direction, which, moreover, probably represents only a spot reading of the geomagnetic field. However, the very presence of a dual-polarity remanence (*a*- and *b*- components) as well as evidence for the baking of the conglomerate during the emplacement of the overlying flow suggest that the high temperature (*a* + *b*) magnetization is of primary nature. The tilt corrected mean direction of the combined *a* + *b* site-mean components is D=106.5˚; I= -46.4˚ (α_{95}=7.8˚; k= 29.2 for N=13 site-means out of 19 sites collected). Because during Devonian time, the North Tien Shan and adjacent Kazakhstan were clearly situated in the northern hemisphere (e.g. Bazhenov et al., 2003, Levashova et al., 2007), the normal-polarity direction in the study area should be pointing downward. The upward pointing direction, therefore, corresponds to that of a reversed-polarity field; the normal polarity direction of the primary magnetization of the Kurgasholak Formation is D=286.5˚; I=+46.4˚.

The c-component

The *c*-component is south-easterly and intermediate-up in geographic coordinates; it was isolated in 13 sites out of the total of 19 sites. The 6 other sites often revealed the possible presence of a c-component, but its direction could not be determined with any accuracy. The c-component generally unblocks between ~250 and 580˚C and is usually revealed as an intermediate-temperature component co-existing with the *a*-component (Fig. 2-4c, f). In five sites (a568, a573, m9470, m9464, m9458) it was found as the only

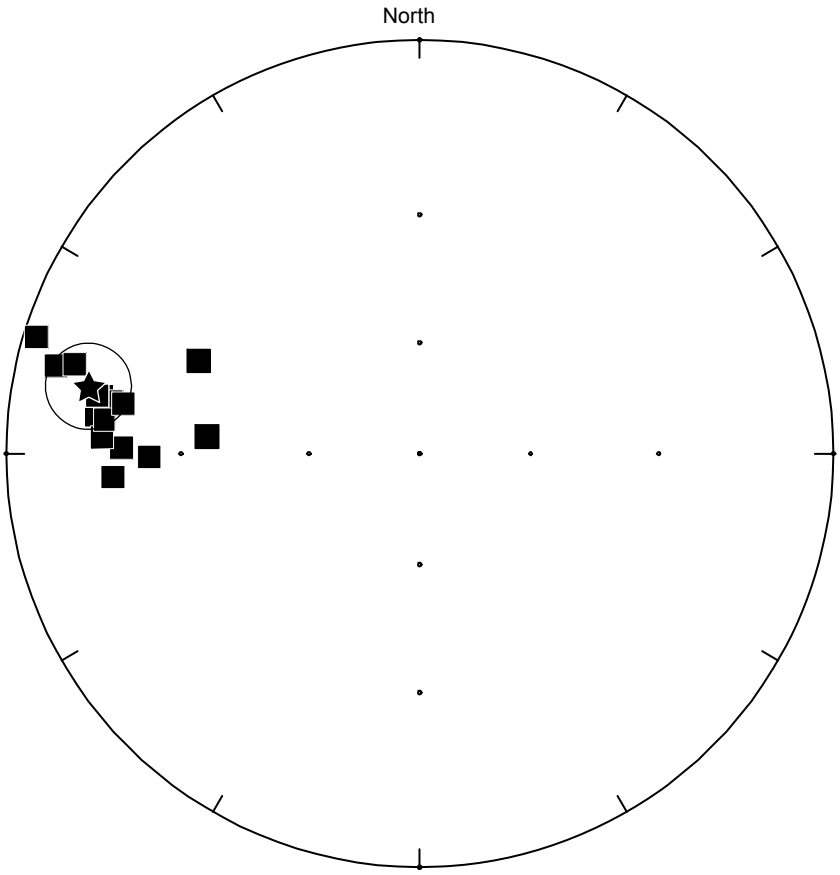

Figure 2-5. Conglomerate test. The site-mean b-direction of a basalt flow (site m9492; star) and b-component directions (filled squares), which have been obtained from clasts in the underlying, baked conglomerate of site m9476, and which have been interpreted as a thermo-remanent magnetization. Lower-hemisphere equal-angle projection.

Legend and explanation for Table 2-1: Bedding measurements are given as the strike and dip angle (down dip to the right (clockwise) of strike). Components (cmp) labeled as in the text. m indicates number of samples used in the statistical analysis: g-great circle, s-stable endpoint, hd-intersection point of two great circles (Hoffman and Day, 1978); n - number of samples demagnetized; N = number of sites. *indicates sites that showed only trends that did not reach a stable endpoint. In such cases, a site-mean direction of the nearest site with a stable endpoint estimate for the particular component was used as an anchor in the great circle analysis. TC = tectonic correction. Dec and Inc are the declination and inclination of the site-mean direction (in ˚); α95 is the radius of the 95% confidence cone about the mean direction in ˚; k is the Fisher (1953) concentration parameter. Directions (Dec/Inc values) in italics are not used in the interpretation of the results

Table 2-1. Site-mean and formation-mean directions of the components isolated from the Kurgasholak Formation.

site	bedding	cmp	m/n	Geographic				Stratigraphic	
				Dec	Inc	α_{95}	k	Dec	Inc
a530	343/30	a	(1g2s)/7	86.5	-17.4	12.0	80.5	91.8	-46.3
		c	(6g1s)/7	126.2	-48.5	12.7	47.8	166.3	-57.9
a537	343/30	a	(2g4s)/6	86.6	-15.6	7.0	100.0	91.5	-44.5
		c	(2g1s)/6	119.7	-38.0	12.2	282.5	147.4	-53.5
a543	340/35	a	(1g4s)/6	81.5	-13.2	8.2	72.5	86.6	-47.2
		c	1s/6	139.2	-49.9			182.7	-49.3
a549	338/37	a	(3g2s)/6	89.4	-21.2	9.5	100.8	103.6	-54.2
		c	(2g4s)/6	127.0	-50.7	6.8	107.4	178.7	-54.5
a555	335/40	a	4s/5	78.2	-13.2	8.4	119.4	86.0	-51.6
a561	332/45	a	1s/6	89.1	-18.4			111.1	-55.1
		c	(4g2s)/6	127.3	-38.6	11.4	43.8	168.5	-42.2
a568	332/45	c	2hd/5	143.3	-43.4	15.3	270.0	181.6	-34.3
a573	332/45	c	3g*/6	127.9	-51.9	6.8	676.8	185.9	-47.3
a579	328/45	a	(5g1s)/6	75.8	-15.2	21.7	16.8	90.4	-56.6
a585	328/45	a	(2g4s)/6	80.4	-18.0	8.0	76.4	99.9	-57.2
		c	1hd/6	133.6	-45.7			177.5	-39.0
m9498	320/40	b	5g*/6	284.9	5.5	10.3	72.9	295.2	26.2
m9492	320/40	b	5s/6	286.3	11.8	6.9	122.6	300.7	30.4
m9476 cgl.	320/40	b	(2g13s)/16	285.5	18.9	6.4	37.0	305.5	36.3
m9470	320/40	c	(4g1s)/6	133.0	-41.8	19.7	24.0	165.9	-34.7
m9464	320/40	c	5s/6	138.5	-37.4	13.9	31.2	165.2	-28.6
m9458	320/40	c	6s/6	134.8	-34.6	5.2	166.0	160.6	-28.9
m9452	320/40	a	(1g3s)/5	95.4	-12.9	10.3	64.4	111.2	-37.7
		c	(4g1s)/5	153.8	-31.2	10.3	86.0	170.5	-15.4
m9446	320/40	a	5g*/6	103.6	-31.5	18.6	22.6	135.7	-46.5
		c	(4g2s)/6	145.4	-42.2	15.7	38.0	173.3	-28.0
Mean a+b	In situ		N=13	*90.9*	*-16.6*	6.3	44.5		
	After TC		N=13			7.8	29.2	106.5	-46.4
Mean c	In situ		N=13	134.9	-43.0	4.9	71.6		
	After TC		N=13			7.6	30.4	*171.1*	*-39.9*
anomalous (an) directions (not used)									
a568	332/45	an	(3g2s)/5	*218.1*	*17.2*	14.0	46.9	*198.5*	*55.8*
a573	332/45	an	(1g5s)/6	*174.9*	*-52.3*	9.0	61.0	*204.3*	*-23.0*
a579	328/45	an	(4g2s)/6	*55.7*	*-3.4*	12.1	33.9	*54.5*	*-48.4*
m9440	290/40	an	4s/6	*346.7*	*58.5*	17.6	28.2	*2.0*	*21.9*
m9476 cgl.	320/40	an	(8g3s)/16	*218.4*	*-40.2*	13.2	13.9	*221.2*	*-0.8*

characteristic direction (e.g. Fig. 2-4g), but in two of these sites it co-existed with anomalous lower-temperature (*an*) components that have no coherence and no statistical significance (see Table 2-1).

Very often the *c*-component directions can be seen to contribute to a great-circle ("mixing") trend in the stereonet or in curved trajectories of the demagnetization diagrams, and it seems clear in many cases that overlap with *a*-components can be held responsible. In these cases, as mentioned, we used the McFadden & McElhinny (1988) technique to estimate the directions of the components. But this raises the critical question whether the mean inclination and declination of the intermediate-temperature *c*-component are accurately determined, given that many of the great circles run more or less parallel between the more easterly *a*-component and the southeasterly *c*-component. To document that the c-directions are indeed well constrained, we next examine Figure 2-6.

In the common occurrence that the *a*- and *c*-components are being removed simultaneously (Fig. 2-6a, example of site a537), the great-circles run more or less parallel to each other roughly along lines of equal inclination in the south- to southeastern part of the stereonet. This means that for this site, the inclination is reasonably well defined, but the declination is not well constrained. In contrast, the samples shown in Figure 2-6c do not appear to contain the *a*-component, but instead show great-circles that connect low-temperature, viscous (present-day) magnetization directions with the southeasterly and upward *c*-directions. In these cases the great-circles define the declination reasonably well, but the inclination less so. In Figure 2-6b, the sample illustrates the co-existence and overlapping unblocking temperatures, first of the present-day field (PDF) and c component, and subsequently of the *a* and the *c*-component; however, the unblocking temperature spectra of the PDF and *a* components do not appear to overlap. Thus, the directions define two great circles and the well-constrained intersection of these two (gray star in upper hemisphere) corresponds to the (*c*-) component in common to both.

Combining the effects of the great-circles shown in Figure 2-6a – c, one can see that their intersections, the stable endpoints of a few samples (stars in Fig. 2-6a), and the

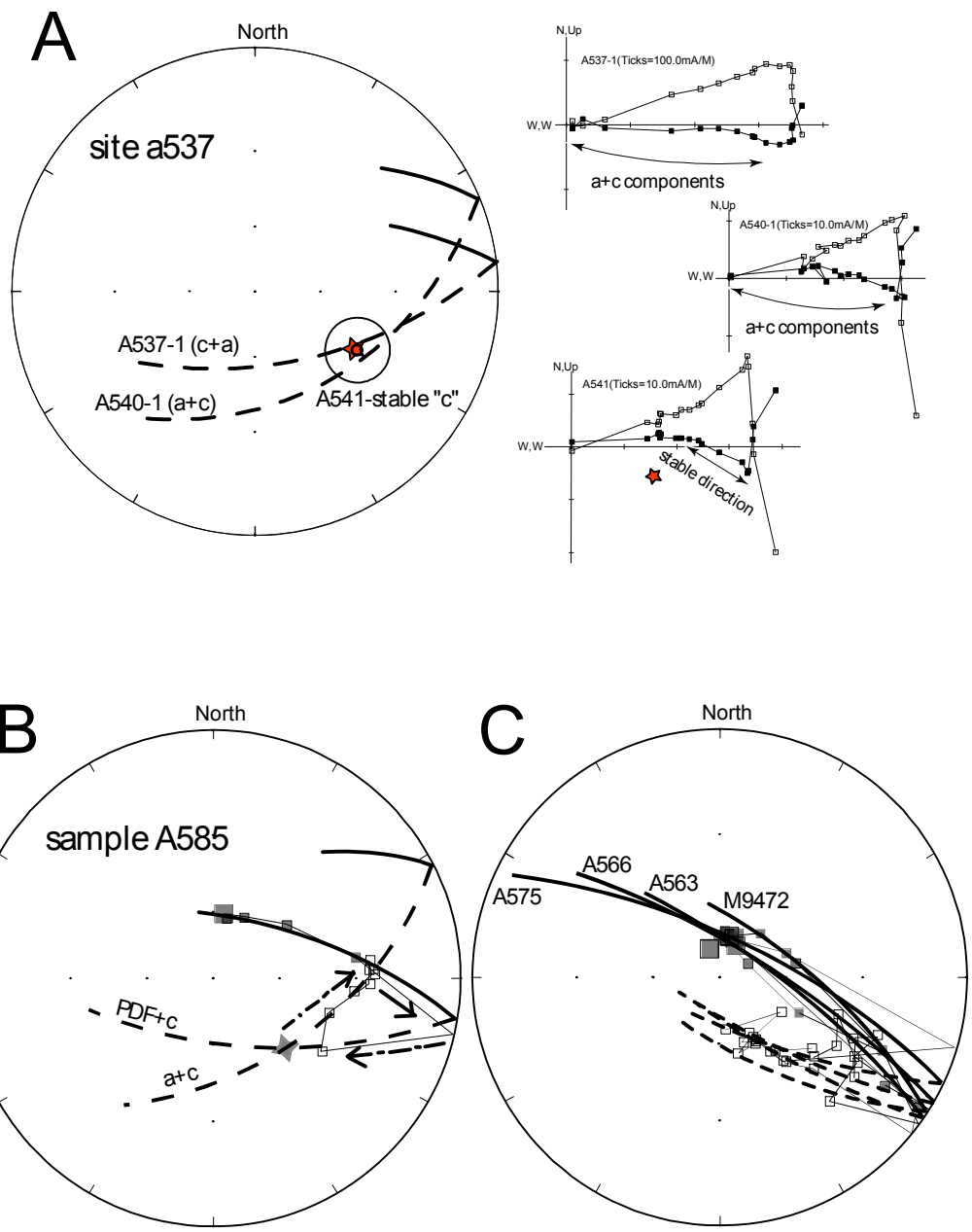

Figure 2-6. Examples of great-circles used in constraining the c-component directions. Lower-hemisphere projections are represented by solid lines and filled symbols, upper hemisphere results are shown as dashed lines and open symbols. The stars in (A) represent what we believe to be a fairly accurate isolation of the c-component without contamination by the higher-temperature a-component. In (B), the three arrows indicate the trends in the progressive locations of the magnetization end-points during thermal demagnetization, which illustrate, first, simultaneous removal of the present-day field (PDF) and c-component and then, the simultaneous removal of the c-component and the a-component. The intersection in (B) is therefore the direction of c (gray star, upper hemisphere).

clear vectorial separation of the trends in Figure 2-6b, allow us to state with confidence that the mean in-situ *c*-direction with dec/inc = 135º/-43º is well constrained.

Although the small range of variation in the bedding attitudes at our sampling locality does not allow for a statistically significant fold test for the *a* + *b* components, site-mean directions of the *c*-component group much better in geographic coordinates with the concentration parameter k decreasing from 71.6 to 30.4 upon unfolding (Table 2-1, Fig. 2-7b). The k-ratio of 2.36 (N=13) is statistically significant at the 95% confidence level, indicating a post-folding origin of this magnetization.

Anomalous directions of magnetization

Here we discuss briefly the five site-means that have been labeled anomalous in Table 2-1 and which are shown in Figure 2-7c. These site-means are listed because they correspond to magnetizations that unblocked at intermediate-to-high temperatures. One site-mean (m9440) clearly corresponds to the direction of the present-day field (PDF); it is not anomalous in that sense, but is different from all other sites in that this PDF-component persists up to higher temperatures. The shallow northeasterly direction of site a579 can readily be explained as due to simultaneous removal of PDF and an a-component, whereas the southwesterly and up intermediate-temperature directions of the conglomerate site (m9476) fall between those of the b- and the c-components. We note, however, that great-circle trends are lacking to document the suspicions that these directions are due to simultaneous removal of two directions.

The anomalous components of sites a568 and a573 are removed at intermediate-temperatures. Although these directions co-exist with c-components (see Table 2-1), they do not seem to correspond to any mixing trends. We can only speculate as to what imparted these magnetizations; perhaps these directions reflect transient geomagnetic fields during excursions.

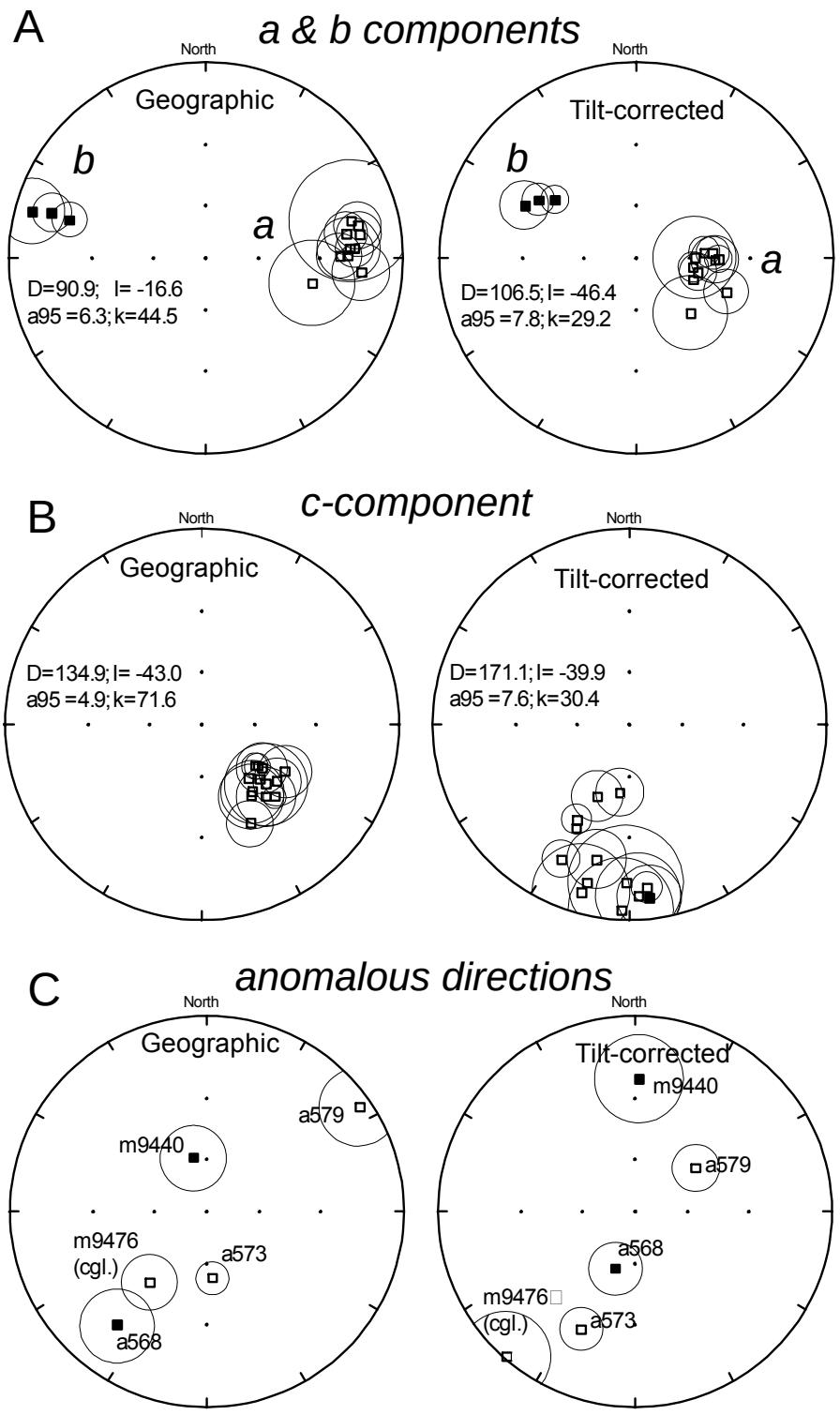

Figure 2-7. Equal-angle stereoplots of the various component site-means isolated in the Kurgasholak Formation (as also listed in Table 2-1). Open (closed) symbols represent upper (lower) hemisphere projections.

Discussion

Results summary and ages of magnetization

We conclude that the high-temperature, dual-polarity remanence (*a*- and *b*-components) with the tilt-corrected mean direction dec/inc = 286.5 º/+46.4º, represents a valuable characteristic magnetization direction for the Kurgasholak formation. The primary (Middle Devonian) age of this remanence is indicated by the normal polarity interval found in-between reversed flow sequences below and above the conglomerate and by the evidence for the baking of this conglomerate by the overlying volcanic flow (the baked contact test).

The *in-situ* inclination of the *a*-component is significantly lower than those from rocks of Devonian or any younger age in the area (Lyons et al., 2002; Bazhenov et al., 2003; Van der Voo et al., 2006), suggesting that the tilt correction is needed in order for the result to reflect the ancient magnetic field. This, in turn, implies that the magnetization is older than the folding and also, therefore, older than the post-folding *c*-component, which makes sense given the relative unblocking temperatures.

We also derive support for our arguments that the *a* + *b* remanence is of Middle Devonian age from a comparison with Late Devonian paleomagnetic directions from the Aral Formation (Levashova et al., 2007) some 250 km to the SW of our locality (Fig. 2-8). Tilts of the Aral and Kurgasholak are very different, suggesting that the remanences are both pre-folding and of approximately the same, presumably primary, age.

The *c*-component has a statistically significant negative fold-test, yielding better grouping in geographic coordinates with a southeasterly, intermediate-upward in situ mean direction (dec/inc = 134.9º/-43.0º). Eastern Kazakhstan rocks have often revealed similar overprint components, sometimes pre-folding, sometimes post-folding, depending on the age of deformation. These overprints seem to be associated with the "Pan-Asian thermal event" (Coleman, 1989) – widespread and pervasive intrusions of A-type (anorogenic) granites of late Paleozoic age that affected almost all the area of Kazakhstan

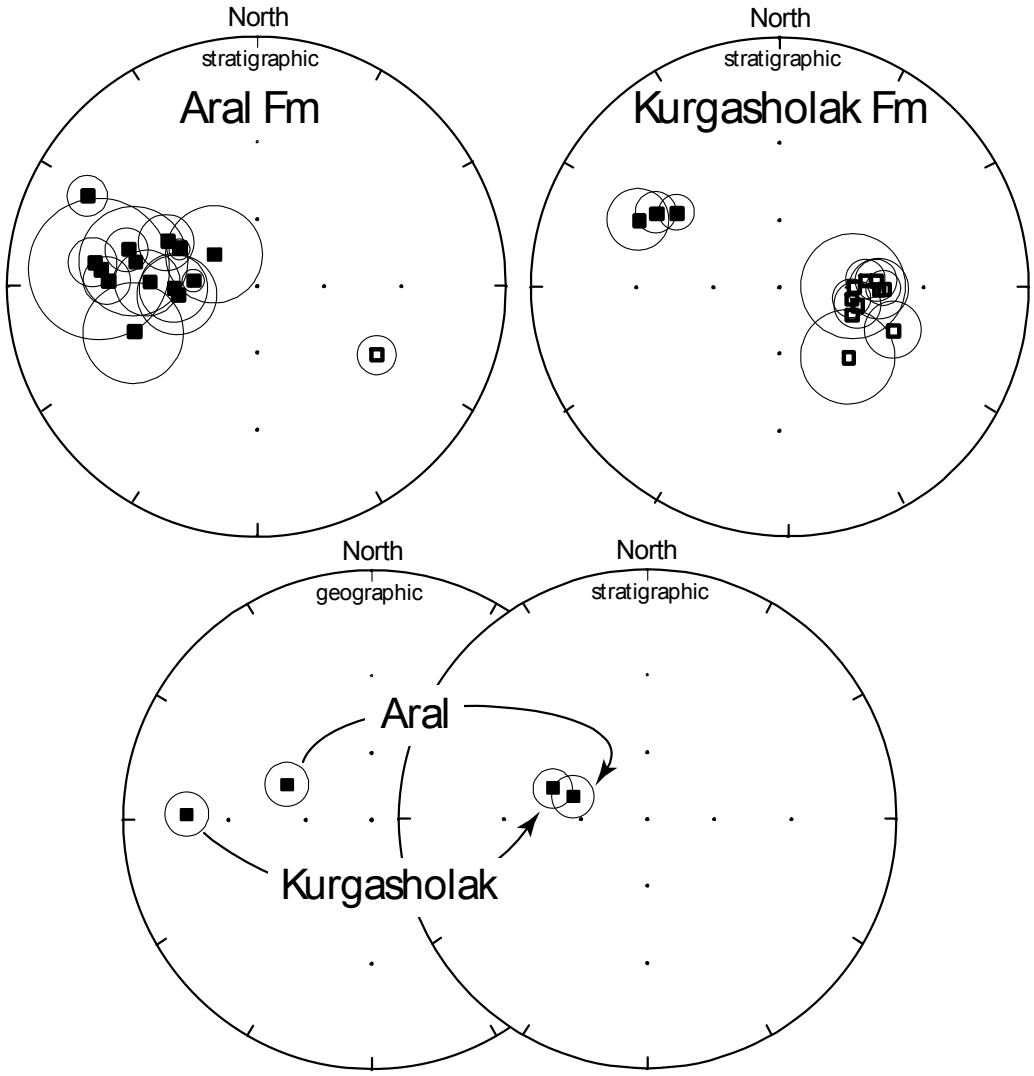

Figure 2-8. Stereoplots showing the tilt-corrected primary site-mean directions of magnetization obtained from the Late Devonian Aral Formation (Levashova et al., 2007) and the Middle Devonian results of this study, with the third plot showing the difference in tilt-correction effects.

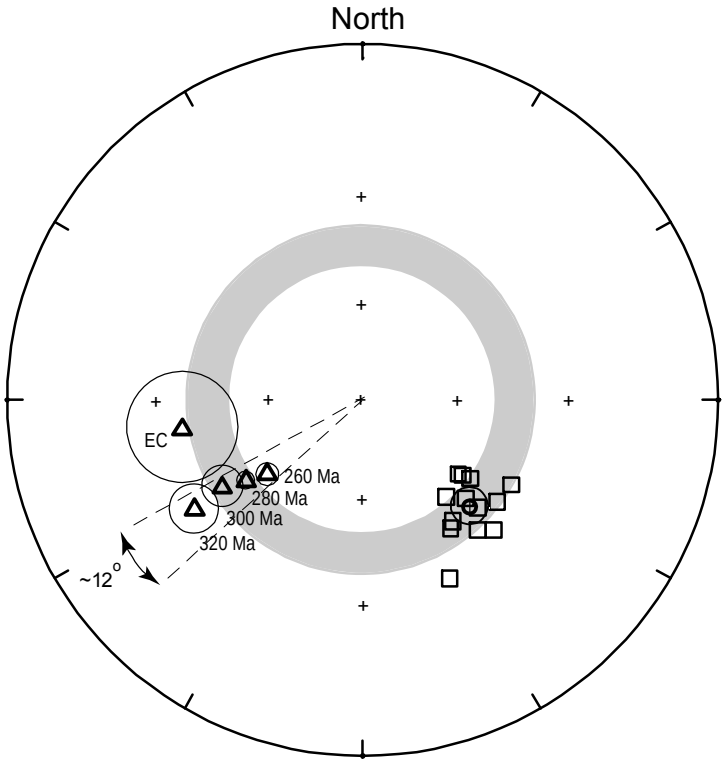

Figure 2-9. Equal-angle stereoplot of the reference and the c-component directions. Reference directions are the triangles with associated 95% confidence circles and age in Ma (EC is the early Carboniferous direction (360-320 Ma)). They are calculated by extrapolation from the APWP of Baltica (Torsvik et al., 2001; Van der Voo, 1993). Open squares represent site means of the c-component directions, with the full dot (upper hemisphere projection) showing their mean (Table 2-1). The concentric circle around this mean represents its 95% confidence limit. The shaded band marks the range of the c-component inclinations for comparison with the reference directions and their ages.

(Yakubchuk, (1997). In almost all cases, the magnetizations are of reversed polarity and usually show upward inclinations of 40 – 60º. Figure 2-9 illustrates that these inclinations are characteristic of the late Paleozoic reference directions. In Figure 2-9 these directions are calculated for the area by extrapolation from Baltica, but it must be noted that using Siberian or Tarim's late Paleozoic poles as reference poles yields very similar inclination predictions. It must also be noted that the paleolatitudes of Kazakhstan are, without exception, higher than 40ºN for the entire Mesozoic and Cenozoic, as can be seen by examining Scotese's (2000) paleogeographic maps; this indicates that the observed paleolatitude of 25±5ºN from the *c*-component implies a pre-Mesozoic age of the magnetization. All-in-all, this leads us to argue for a Permian age for the c-component.

General pre-amble to an analysis of rotations in the Devonian volcanic arc

Despite some recent accomplishments, primary paleomagnetic results from Kazakhstan and Kyrgyzstan remain sparse and frequently defy a unique interpretation. While the inclination data provide consistent paleolatitude estimates for the area of interest to this study, such as the Chingiz Range and North Tien Shan limbs of the curved Devonian orocline illustrated in Figure 2-2b (Bazhenov et al., 2003; Alexyutin et al., 2005; Collins et al., 2003; Levashova et al., 2007), an unambiguous interpretation of declination data from this region is hampered by the multiple episodes of wrench faulting and transpressional deformation during the protracted late Paleozoic assembly of this part of Asia. The repeated episodes of strike slip motions along the abundant east-west and northwest-southeast fault systems in the region are well documented (Allen et al., 2001; Natal'in and Şengör, 2005; Van der Voo et al., 2006). Such strike-slip faulting is frequently associated with vertical-axis rotations which cause a deviation in paleomagnetic declinations. Bazhenov et al. (1993) and Van der Voo et al. (2006) discussed the complex patterns of late-orogenic, Late Permian – Early Triassic rotations in Kyrgyzstan and eastern Kazakhstan. In the Chingiz Range (the northeastern limb of the orocline) the rotations are generally clock-wise and small, whereas in the North Tien Shan and adjacent areas the rotations are usually large, on the order of 90˚, and predominantly counter-clockwise. But importantly, exceptions to the latter pattern do

occur in some restricted localities of the North Tien Shan and vicinity where rotations are minor (Alexyutin et al., 2005, McCausland et al., 2005). Late orogenic rotations of larger magnitude, obviously, must be considered in making tectonic reconstructions for earlier times. In the next section we will briefly discuss the paleomagnetic data available for Silurian and Devonian volcanic rocks in the oroclinal belt of Kazakhstan, and we will also describe estimates for the declination corrections that may restore rock units to their pre-Late Permian orientation.

Previously published Silurian and Devonian paleomagnetic data and their corrected pre-Late Permian declinations

Available paleomagnetic results from rocks of Silurian and Devonian age from localities in or close to the Devonian volcanic belt are listed in Table 2-2. Primary magnetizations of Devonian age have been obtained by us from the Aral and Kurgasholak formations, with westerly and intermediate downward dual-polarity magnetizations in both formations (dec = 280 - 287º); the localities of these two formations are shown as L2 and a star in Figure 2-2. Klishevich and Khramov (1993) presented Devonian results from two localities (K1 and K2) in the North Tien Shan. Their results passed fold and reversals tests and are considered reliable. Only one other Devonian and one Silurian result have been derived from this southwestern limb of the putative orocline: G3 (Grishin et al., 1997) and AX (Alexyutin et al., 2005). The latter is of Silurian to Early Devonian age and the magnetization is demonstrably pre-Middle Devonian owing to a positive fold test; this result is clearly reliable. In contrast, the G3 result cannot be qualified as reliable; moreover, the information available in the publication is not always complete. We have analyzed the three relevant Devonian paleomagnetic results from the Grishin et al. (1997) study and in Table 2-3 we list the seven reliability criteria of Van der Voo (1993) and enumerate how well the G1 – G3 results meet these criteria. The G3 result meets only one or two of the seven criteria, and consequently cannot be considered as reliable. A negative conglomerate test and an inconclusive foldtest also argue strongly against the use of this result. Thus, we did not include G3 in our analysis.

The NE limb has yielded five results, two of which (L3, G5) are of Silurian age. The Devonian L2 result published by some of us in 2003 (Levashova et al., 2003) is in

need of substantiation as we have maintained from the beginning, but the formation seems to have some promise; work in progress has given us some confidence that the result will eventually meet minimum reliability (i.e., Q > 3). The Silurian G5 result meets minimum reliability criteria (Q = 3 or perhaps 4), and L3 is of good quality as well. Both have therefore been included in the analysis, and so has the more marginal (Q > 3?) Devonian result (G1) from Grishin et al. (1997).

The two results published by Burtman et al. (1998), on the other hand, have not been included in our analysis. These authors reported a dual polarity, pre-folding remanence from two Middle Devonian localities (B1, B2, Table 2-2). The directions of the magnetization, however, match closely the expected Late Paleozoic overprint direction in both declination and inclination. Thus, we think it likely that these rocks were remagnetized prior to the Middle Carboniferous to Early Permian folding episode that affected the sampled localities.

The third (NW) limb of the orocline connects the SW and NE limbs in the pattern shown in Figure 2-2b. It has yielded two useable results (G2, G4), one each of Devonian and of Silurian age. These results meet minimum reliability criteria (Q > 3 in both cases), and have been included in the analysis. The reliability of G4, in particular, is attested to by a positive fold-test on a syn-sedimentary slump structure.

In summary, Table 2-2 provides us with eleven declinations distributed over all three limbs of the orocline that can be analyzed for rotations. The Silurian and Devonian data sets are of mixed quality, but as we will see, the results of the two groups do not contradict each other. Our next step is to use our knowledge of the sense and magnitude of Late Permian – Early Triassic rotations to restore the declinations to their pre-Late Permian orientations.

The deflection of the "*c*-component" of this study (that we consider to be an overprint of Permian age) relative to the reference direction indicates that the sampling locality underwent a counter-clockwise rotation of about 100˚, similar sense rotations are common in the region (e.g. Van der Voo et al., 2006). The much less plausible choice of the alternative option, a rotation of 260^{o} clockwise, will, of course, result in the same corrected value of the Devonian declination. The uncertainties of this and other rotations

have been calculated by the method of Debiche and Watson (1995) and are included in Table 2-2 (labeled ΔR). As a reference direction for the calculation of rotations in the study area we chose the 290 Ma pole. It should be noted that while the reference inclinations for the study area steadily increase with younging age during the Late Paleozoic, the declinations show relatively minor changes (Fig. 2-9). Thus, somewhat imprecise dating of the *c*-component will not significantly affect the reference declination and, consequently, the estimate of the rotations.

Rotating the primary Devonian direction clockwise by 100° (or counter-clockwise by 260°), we restore the declination of the primary *a* + *b* component to its pre-Late Permian bearing of 27±13º.

For the Aral result no estimate of any late Paleozoic rotation is available from the rocks themselves, but considering that their locality is within the same shear-zone as our study area (Van der Voo et al., 2006), it is reasonable to expect that the Aral-Formation sampling area was also affected by a counterclockwise (ccw) rotation of considerable magnitude. If this rotation was of the order of 90° ccw (Van der Voo et al., 2006), then the corrected Devonian declination turns into a northerly direction, not unlike that of the corrected declination from this study. Even if the rotation was only some 60° ccw, the restored declination of 340° is northerly.

Klishevich and Khramov (1993) reported the presence of secondary overprints in some of their samples in addition to the primary Devonian K1 and K2 magnetizations. The directions of these secondary components are described as being "similar to that of the primary magnetization of the Permian rocks in the sampling regions". However, no explicit information about the direction of this component was provided in the publication. Thus, we used an average of several published Late Permian results to correct the declinations for late Paleozoic rotations (Van der Voo et al., 2006). These results come from localities closest to the K1 and K2 sampling sites. Restored to their pre-Late Permian bearings, the Devonian declinations of both sites are ~ 20 NE.

Table 2-2. Summary of published Siluro-Devonian paleomagnetic data from the Devonian volcanic belt of the Kazakhstan orocline.

Label-limb	Reference	Estim. Paleolat. ±Δλ	Dec ±ΔD	Correction Value R±ΔR	Corrected mid-Paleozoic Declination
Devonian results					
A-SW	This study	+28±10	287±11	100±6 cw	27±13
L1-SW	Levashova et al. (2007)	+36±13	286±15	~90 cw	~ 16
L2-NE	Levashova et al. (2003)	+30±17	172±19	~0	~172±19
K1-SW	Klishevich & Khramov (1993)	+21±8	334±9	~49±18	~23±20
K2-SW	Klishevich & Khramov (1993)	+19±5	309±6	~73±37	~22±37
G1-NE	Grishin et al. (1997)	+29±12	168±14	13±31 cw	181±34
G2-NW	Grishin et al. (1997)	+23±11	111±13	~0	~111±13
G3-SW	Grishin et al. (1997)	*+33±17*	*139±20*	*28±20 cw*	Not used
B1-NE	Burtman et al. (1998)	*+24±7*	*52±8*	Not avail.	Not used
B2-NW	Burtman et al. (1998)	*+17±8*	*50±10*	Not avail.	Not used
Silurian results					
AX-SW	Alexyutin et al. (2005)	+12±9	347±14	~0	~347±14
L3-NE	Levashova et al. (2003)	-1±7	217±13	~0	~217±13
G4-NW	Grishin et al. (1997)	+13±7	124±10	~0	~124±10
G5-NE	Grishin et al. (1997)	+6±7	144±13	14±3cw	158±13

Legend and explanation for Table 2-2.
Labels are the same as those described in the text and used in Figures 2-2 and 2-10; limb (NE, NW or SW) denotes one of the three branches of the strongly curved Devonian volcanic belt and its putative oroclinal model. Estimated paleolatitude is given as + (-) for northern (southern) hemisphere, respectively, together with its 95% uncertainty (±Δλ)*. Declination uncertainties are labeled ±ΔD*. The Correction Value (R, see text for further description) restores a locality's orientation to its pre-Permian value, by correcting for rotations that occurred during the Permian and Early Triassic (Van der Voo et al., 2006). The Correction Value (R) has uncertainties ±ΔR*. "Not used" (with declinations in italics) indicates that the data were of insufficient quality to be used in reconstructions (see Appendix 1).
*: Δλ is calculated from dp, the meridional semi-axis of the oval of 95% confidence around the paleopole; $\Delta D = \alpha_{95}/\cos I$. Rotations: R is the difference in the declinations of the observed and reference directions, with uncertainties ΔR calculated according to the technique of Debiche and Watson (1995). The confidence level for the corrected mid-Paleozoic declinations is calculated as $(\Delta D^2 + \Delta R^2)^{1/2}$. Correction values for G1 and G3 are taken directly from the paper, whereas that for G5 was calculated by us.

Table 2-3. Analysis of reliability criteria for the results of Grishin et al. (1997)

Devonian results

Criterion	**G1 (NE limb)**		**G2 (NW limb)**		**G3 (SW limb)**	
1. Well-determined rock age	+	Same for all	+	Same for all	+	Same for all
2. Minimum N of samples, statistical significance	–	Based on 9 samples only	+		–	An unclear or inconsistent listing of directions was used to calculate the mean. Table 2 with locality-means indicates that the G3 result is based on 27 samples from 3 objects. Table 1 with object-mean directions lists the number of samples used in statistical analysis as 7 at BA, 13 at BA+BB, and 14 at BA+BD, giving a total of 20 samples for all three objects.
3. Adequate demagnetization that demonstrably includes vector subtraction	+		+		–	No demagn. diagrams are presented in the paper. Its figure 4 with a caption indicating that the results shown are from the SW-limb (G3 locality) in fact represents examples from the objects OM and OZh. These objects, according to the description in the main text, belong to the NW-limb (G2)
4. Field tests that constrain the age of magnetization	–	No fold tests available, monocline sections	?	Ambiguous cgl. test; + test on a slump fold, but on rocks of a different (Sil.) age	–	**negative conglomerate test**; directions isolated from the clasts show a streaking distribution form SW up to NW up. (NW up direction is interpreted as primary Devonian direction in volcanics of the object BA of locality G3). The **fold test** is **inconclusive** (best grouping at 80% unfolding) and **statistically insignificant**
5. Structural control	?	Both terrestrial volcanics and marine sedimentary rocks were sampled to control for the possible primary tilt in the terrestrial volcanics	?	Both volcanics and marine sedimentary rocks were sampled to control for the possible primary tilt in terrestrial volcanics	–	In the BA locality (where the main "primary Devonian results" come from) the rocks are described as being "cut by large intrusive bodies of Late Devonian and late Paleozoic age. This fact complicates the interpretation of the paleomagnetic data". In the BB locality (another one with presumably a Devonian result), it was said "in the lower part of the section, magnetization direction depends on the bedding attitude, suggesting some tectonic re-working". It is unclear what exactly this means, but this result does not appear to have adequate structural control
6. Presence of reversals	+		+	In several sections	–	
7. No resemblance to paleopoles of younger age	?	Inc is same as Permian, Dec may be rotated	?	Dec may be rotated	?	Inc is same as Permian, Dec may be rotated
Final score	**≥3**		**≥4**		**2?**	

Table 2-3. (continued) Analysis of reliability criteria for the results of Grishin et al. (1997).

Silurian results

Criterion	G4 (NW limb)		G5 (NE limb)	
1. Well-determined rock age	+	Same for all	+	Same for all
2. Minimum N of samples, statistical significance	–	Result is based on 13 samples	–	Result is based on 12 samples
3. Adequate demagnetization that demonstrably includes vector subtraction	–	Examples for the object OM (their fig 4b) demonstrate only the late PZ direction. No examples of the component that was interpret as primary	+	Examples of the characteristic components for the object are shown in their fig 2b
4. Field tests that constrain the age of magnetization	+	+ test on a slump fold	?	Ambiguous fold test on directions defined by great-circle intersections
5. Structural control	?	Overturned section	?	2 sections with different bedding attitudes
6. Presence of reversals	–		–	
7. No resemblance to paleopoles of younger age	+	In-situ (IS) declination differs significantly from the late Paleozoic direction isolated in other localities in the immediate vicinity. Tilt-corrected (TC) dec and inc are different from younger reference directions	+	Both IS and TC directions of the characteristic component are significantly different from the expected late Paleozoic or younger directions.
Final score	**≥3**		**≥3**	

In the NE and NW limbs of the orocline, the later rotations are generally negligibly small, which is concluded from overprints of late Paleozoic age that agree well with the coeval reference declination. The Devonian declinations in the Chingiz Range (NE limb) thus remain southerly (172 and 181^{o}), whereas the Devonian declination in the NW limb is of the order of 110^{o}.

The Silurian results show the same pattern as the Devonian (Table 2-2) with a northerly (347^{o}) declination in the Kendyktas block, where no appreciable late Paleozoic rotation is observed (Alexyutin et al., 2005; McCausland et al., 2005; Van der Voo, 2006), whereas the declinations are roughly southerly (144^{o} and 217^{o}) in the Chingiz Range and east-southeasterly (about 124^{o}) in the third (NW) limb.

Unbending the orocline

The corrected declinations of the Devonian and Silurian magnetizations are plotted in Figure 2-10a within the structural trends of the strongly curved Devonian volcanic belt. In general, there is a good correlation between the change in the structural trend and the change in declination. This correlation suggests that the present-day curvature of the belt is, indeed, the result of oroclinal bending of an originally much straighter belt. One can test, to first approximation, whether the initial Devonian configuration of the belt was linear, by using the declinations as passive markers and aligning them all roughly parallel (Fig. 2-10b).

We realize, of course, that Fig. 2-10 reduces an exceedingly complex geological situation to three straight bands and a set of seemingly precise directions (arrows). Nevertheless, recognizing that the figure is a simplification, it usefully illustrates that a ~1500 km-long active volcanic arc trended approximately northwest-southeast in Devonian times. The subduction responsible for the volcanism was towards the southwest. The consistent inclination data from all segments indicate that the arc, which delineated the northeastern margin of the KNTD ("Kazakhstania") landmass, was situated at a ~ 30˚ northerly paleolatitude (see also Levashova et al., 2007). We note that the results of Klishevich and Khramov (1993) have shallower inclinations than all the

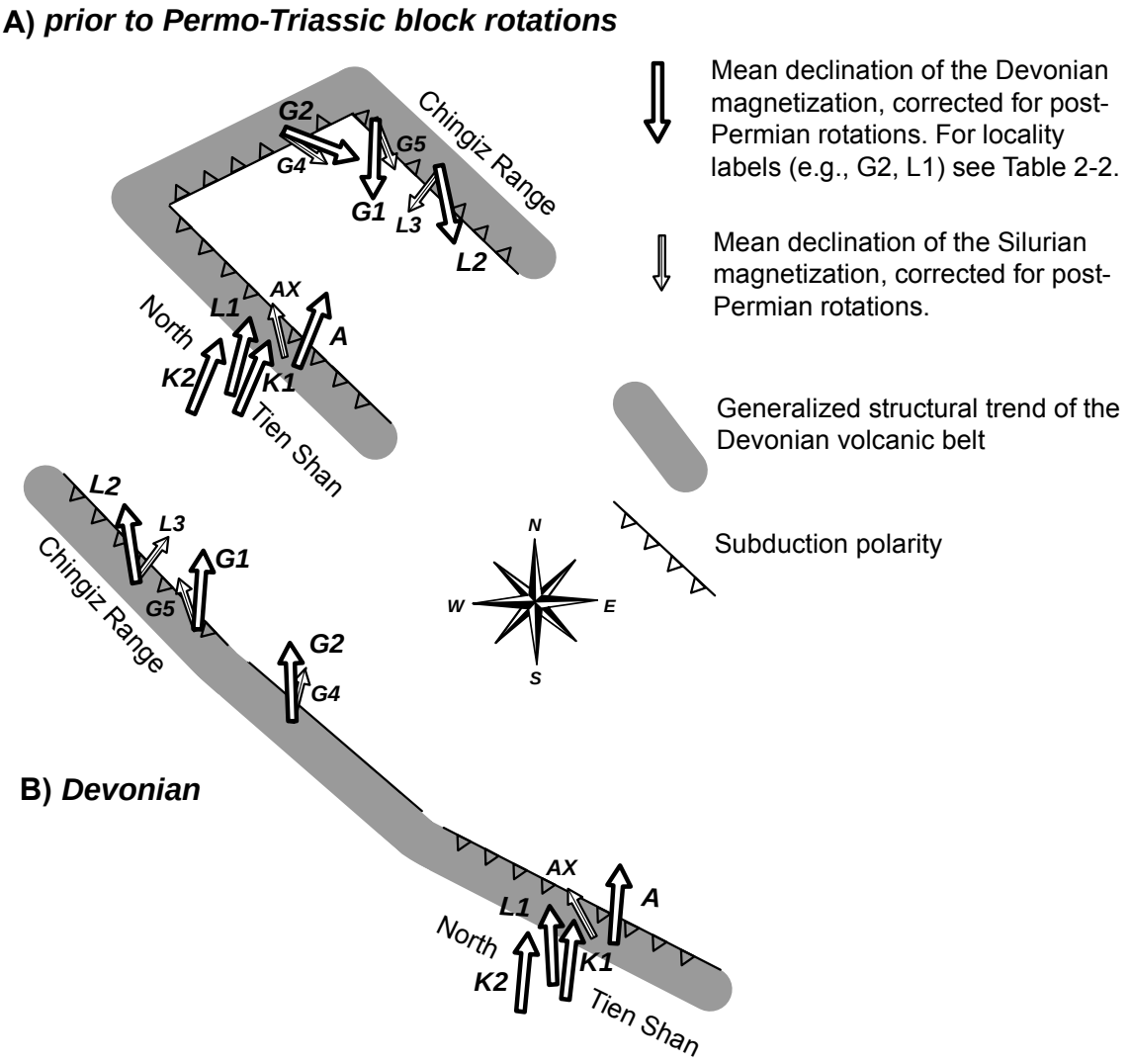

Figure 2-10. Cartoon illustrating the relationship between the structural trends and the declinations of the primary Silurian and Devonian magnetizations for the time prior to Permo-Triassic small-block rotations (A) and for the inferred Devonian (B) configuration of the belt. For locations of the schematically represented limbs of the orocline and the sampling localities of the different studies, see Figure 2-2 and Table 2-2.

other (volcanic) Devonian results, possibly due to inclination shallowing in the K1-K2 sedimentary formations.

Conclusions

Our paleomagnetic study of the Middle Devonian rocks (Kurgasholak Fm) from the southern limb of a long curved belt of the Devonian volcanics in Kazakhstan revealed two meaningful components of magnetization:

1) a high-temperature, dual-polarity remanence (*a*- and *b*- components) with a mean direction dec/inc =286.5º/+46.4 º and pole position 30.3ºN, 355.4ºE. We interpret this remanence as a primary Middle Devonian magnetization based on reversals and a baked contact test.

2) a secondary magnetization (*c*-component) with an *in situ* mean dec/inc = 134.9º/-43.0º and pole position 48.9ºN, 332.2ºE. This post-folding component is younger than the *a* + *b* remanence and likely represents a Permian (~290 Ma) overprint, as evidenced by a good agreement of the *c*-component inclination with the reference inclination for this age and as consistent with observations of similar overprints in other formations in this area of Kazakhstan. The declination of the *c*-component, however, is deflected counter-clockwise by about 100˚ relative to the reference direction. This deflection indicates that the studied locality was affected by late-orogenic small-block rotations within a shear-zone of deformations, as suggested by Van der Voo et al. (2006). Using the sense and magnitude of this deflection, we corrected for these late-orogenic rotations, and thereby restored the declination of the primary Devonian magnetization to a north-northeasterly pre-Late Permian value.

Our corrected declination combined with several other published paleomagnetic directions of Devonian and Silurian age shows a good correlation with the structural trends of the curved Devonian volcanic belt, suggesting that the curvature is, indeed, a result of oroclinal bending.

Using corrected declinations as passive markers, we restored the belt to its Devonian configuration. Our reconstruction suggests that in the Devonian the "Kazakhstania" (Kokchetav-North Tien Shan (KNTD)) landmass was situated at about

30˚N paleolatitude. The eastern margin of the landmass was delineated by a nearly straight, northwest-southeast trending, ~1500 km long volcanic arc. The subduction responsible for the volcanism was towards the southwest. The bending of this volcanic arc into its present horse-shoe shape took place sometime between Middle Devonian and the Late Permian. This ~ 180^{o} post-Devonian bending of Kazakhstania provides additional geometrical constraints on the changing positions of Baltica, Siberia and Tarim during final stages of their convergence, which should be taken into consideration by tectonic models dealing with the amalgamation of Eurasia.

Acknowledgements

This study was supported by the Division of Earth Sciences and the Office of International Science and Engineering's Eastern and Central Europe Program of the U.S. National Science Foundation, grant EAR 0335882. Support was also derived from the Russian Foundation of Basic Research, grants 04-05-64050 and 05-05-65105. Critical reviews by anonymous and B. Natal'in are gratefully acknowledged.

References

Abdullin, A.A., Volkov, V.M., Scherba, G.N. 1980. (eds.) Chu-Ili ore belt. Nauka, Almaata, 503 p. (in Russian).

Alexyutin, M.V., Bachtadse, V., Alexeiev, D.V., Nikitina, O.I. 2005. Palaeomagnetism of Ordovician and Silurian rocks from the Chu-Yili and Kendyktas Mountains, South Kazakhstan . *Geophysical Journal International*, 162, 321-331.

Allen, M.B., Alsop, G.I., Zhemchuzhnikov, V.G. 2001. Dome and basin refolding and transpressive inversion along the Karatau fault system, southern Kazakstan. *Journal of the Geological Society of London*, 158, 83-95.

Bakhtiev, M.K. 1987. Paleozoic orogenic magmatic belts. Nauka, Moscow 168 p. (In Russian).

Bazhenov, M. L., Chauvin, A., Audibert, M., Levashova, N. M. 1993. Permian and Triassic paleomagnetism of the south-west Tien Shan: the timing and mode of tectonic rotations, *Earth and Planetary Science Letters*, 118, 195-212.

Bazhenov, M.L., Collins, A.Q., Degtyarev, K.E., Levashova, N.M., Mikolaichuk, A.V., Pavlov, V.E., Van der Voo, R. 2003. Paleozoic northward drift of the North Tien Shan (Central Asia) as revealed by Ordovician and Carboniferous paleomagnetism. *Tectonophysics*, 366, 113–141.

Burtman, V.S., Gurary, G.Z., Belenky, A.V., Kudasheva, I.A. 1998. Kazakhstan and the Altai in the Devonian: paleomagnetic evidence. *Geotectonics*, 6, 63–71.

Coleman, R.G. 1989. Continental growth of Northwest China. *Tectonics*, 8, 621-635.

Collins, A.Q., Degtyarev, K.E., Levashova, N.M., Bazhenov, M.L., Van der Voo, R. 2003. Early Paleozoic paleomagnetism of East Kazakhstan: implications for paleolatitudinal drift of tectonic elements within the Ural–Mongol belt. *Tectonophysics*, 377, 229– 247.

Debiche, M. G., Watson, G. S. 1995. Confidence limits and bias correction for estimating angles between directions with applications to paleomagnetism. *Journal of Geophysical Research*, 100, 24,405 – 24,429.

Degtyarev, K. E. 2003. The position of the Aktau-Junggar microcontinent in the Paleozoides of Central Kazakhstan. *Geotectonics*, 37 (4), 14-34.

Degtyarev, K. E., Ryazantsev, A. V. 1993. Geology of the orogenic Silurian and the structures with continuous sections in the Caledonides of Kazakhstan, in: E. E. Milanovsky (ed.) Geology and metallogeny of central Kazakhstan, Moscow, Nauka, 64-82 (in Russian).

Didenko, A.L., Mossakovsky, A.A., Pechersky, D.M., Ruzhentsev, S.V., Samygin, S.G., Kheraskova, T.N. 1994. Geodynamics of Paleozoic oceans of Central Asia. *Geology and Geophysics*, 35, 118– 145 (in Russian).

Dobretsov N. L., Berzin N. A., Buslov M. M. 1995. Opening and tectonic evolution of the Paleo-Asian ocean. *International Geology Review*, 37, 335-360.

Filippova, I.B., Bush, V.A., Didenko, A.N. 2001. Middle Paleozoic subduction belts: The leading factor in the formation of the Central Asian fold-and-thrust belt. *Russian Journal of Earth Sciences*, 3 (6) 405–426.

Fisher, R.A., 1953. Dispersion on a sphere. *Proceedings of the Royal Society of London*, A 217, 295– 305.

Grishin, D.V., Pechersky, D.M., and Degtyarev, K.E. 1997. Paleomagnetism and reconstruction of Middle Paleozoic structure of Central Kazakhstan. *Geotectonics*, 1, 71– 81.

Hoffman, K.A., and Day, R. 1978. Separation of multicomponent NRM: A general method. *Earth and Planetary Science Letters*, 40, 433-438.

Kirschvink, J.L. 1980. The least-square line and plane and the analysis of palaeomagnetic data. *Geophysical Journal of the Royal Astronomical Society*, 62, 699– 718.

Kurchavov, A.M. 1994. The lateral variability and evolution of orogenic volcanism in the fold belts. *Geotectonics*, 28, 3-18.

Levashova, N.M., Degtyarev, K.E., Bazhenov, M.L., Collins, A.Q., Van der Voo, R. 2003. Middle Paleozoic paleomagnetism of east Kazakhstan: post-Middle Devonian rotations in a large-scale orocline in the central Ural–Mongol belt. *Tectonophysics*, 377, 249–268.

Levashova, N.M., Mikolaichuk, A.V., McCausland, P.J.A, Bazhenov, M.L., Van der Voo, R. 2007. Devonian paleomagnetism of the North Tien Shan: Implications for the middle-late Paleozoic paleogeography of Eurasia, *Earth and Planetary Science Letters*, 257(1-2), 104-120..

Lyons, J.J., Coe, R.S., Zhao, X.-X., Renne, P.R., Kazansky, A.Y., Izokh, A.E., Kungurtsev, L.V., and Mitrokhin, D.V. 2002. Paleomagnetism of the Early Triassic Semeitau igneous series, E. Kazakhstan, *Journal of Geophysical Research*, 107 (B7), doi: 10.1029/2001JB000521.

McCausland, P.J.A., Bazhenov, M.L., Van der Voo, R., Degtyarev, K. E., and Levashova, N. M. 2005. Carboniferous paleomagnetic study of Zhemanty, Kendyktas block, Kazakhstan (Abstract), *EOS – Transactions AGU*, GP11A-0002.

McFadden, P.L., McElhinny, M.W. 1988. The combined analysis of remagnetization circles and direct observations in paleomagnetism. *Earth and Planetary Science Letters*, 87, 161– 172.

McFadden, P.L., McElhinny, M.W. 1990. Classification of the reversal test in paleomagnetism. *Geophysical Journal International*, 103, 725– 729.

Mossakovsky, A.A., Ruzhentsev, S.V., Samygin, S.G., Kheraskova, T.N. 1993. Central Asian fold belt: geodynamic evolution and formation. *Geotectonics*, 27 (6), 3– 32.

Natal'in, B.A., Şengör, A.M.C. 2005. Late Palaeozoic to Triassic evolution of the Turan and Scythian platforms: the pre-history of the palaeo-Tethyan closure, *Tectonophysics*, 404, 175-202.

Scotese, C.R. 2000. Atlas of Earth history, Paleomap Progress Report 90-0497, University of Texas at Arlington, 45 pp.

Şengör, A.M.C., Natal'in, B.A. 1996. Paleotectonics of Asia: fragments of a synthesis. In: Yin, A., Harrison, M. (Eds.), The Tectonic Evolution of Asia. Cambridge Univ. Press, Cambridge, pp. 486– 640.

Senkevich, M.A. 1991. In: Stratigraphic glossary of the USSR. New Paleozoic stratigraphic subdivisions of the USSR. Nedra, Leningrad. (In Russian).

Skrinnik, L.I., Horst, V.E. 1995. Devonian island arc volcanic complexes in the Junggar Alatau. *Geology and exploration of Kazakhstan*, 4, 6-10.

Tokmacheva, S.G., Paretsky, I.I., Palets, L.M. 1974. Upper Silurian and Devonian of western and southwestern Balkhash area and of south-east Betpak-Dala. In: Stratigraphy of Devonian, Carboniferous and Permian in Kazakhstan. Nauka, Almaty (In Russian).

Torsvik, T.H., Van der Voo, R., Meert, J.G., Mosar, J., Walderhaug, H.J. 2001. Reconstructions of the continents around the North Atlantic at about the 60th parallel. *Earth and Planetary Science Letters*, 187, 55-69.

Van der Voo, R. 1993. Paleomagnetism of the Atlantic, Tethys and Iapetus Oceans Cambridge Univ. Press, Cambridge. 411 pp.

Van der Voo, R. 2004. Paleomagnetism, oroclines and the growth of the continental crust, *GSA Today*, 14 (12), 4-9.

Van der Voo, R., Levashova, N.M., Skrinnik, L.I., Kara, T.V., Bazhenov, M.L. 2006. Late orogenic, large-scale rotations in the Tien Shan and adjacent mobile belts in Kyrgyzstan and Kazakhstan, *Tectonophysics*, 426, 335-360.

Windley, B.F., Alexeiev, D., Xiao, W.J., Kröner, A., and Badarch, G. 2007. Tectonic models for accretion of the Central Asian Orogenic Belt, *Journal of the Geological Society of London*, 164, 31-47.

Yakubchuk, A. 1997. Kazakhstan. In: Moores and Fairbridge (Eds), Encyclopedia of European and Asian regional geology. Chapman and Hall, London, pp. 450-465.

Zijderveld, J.D.A. 1967. AC demagnetization of rocks: analysis of results. In: Collinson, D.W., Creer, K.M. (Eds.), Methods in Paleomagnetism. Elsevier, Amsterdam, pp. 254– 286.

Zonenshain, L.P., Kuzmin, M.I., Natapov, L.M. 1990. Geology of the USSR: a plate tectonic synthesis. Ed. Page, B.M. AGU, Geodynamic series, volume 21. Washington, D.C., 250p.

Chapter 3

Paleomagnetism of mid-Paleozoic subduction-related volcanics from the Chingiz Range in NE Kazakhstan: The evolving paleogeography of the amalgamating Eurasian composite continent

Abstract

The tectonic and paleogeographic evolution of the Ural-Mongol belt between the cratons of Baltica, Siberia, and Tarim is key to the formation of the Eurasian composite continent during Paleozoic time, but the views on this complicated process remain very disparate and sometimes controversial. A study of three volcanic formations of mid-Silurian, Lower-to- Middle Devonian and Middle Devonian age from the southwestern boundary of the Chingiz Range (NE Kazakhstan) yields what are interpreted as primary paleomagnetic directions that help clarify the evolution of the belt. A single-polarity characteristic component in mid-Silurian andesites yields a positive intraformational conglomerate test, whereas dual-polarity prefolding components are isolated from the two Devonian collections. Post-folding reversed-polarity overprint directions have also been isolated, and are likely of Permo-Triassic age. These new data can be evaluated together with previously published paleomagnetic results from Paleozoic rocks in the Chingiz Range, and allow us to establish with confidence the polarity of each result, and hence to determine the hemisphere in which the area was located at a given time. We conclude that NE Kazakhstan was steadily moving northward, albeit with variable velocity, crossing the equator in Silurian time. These new paleomagnetic data from the Chingiz range also agree with and reinforce the hypothesis that the strongly curved volcanic belts of Kazakhstan underwent oroclinal bending between Middle Devonian and

Middle Permian time. A comparison of the Chingiz paleolatitudes with those of Siberia shows, insofar as the sparse data allow, similarities between the northward motion of the Chingiz unit and that of Siberia, which imposes important constraints on the evolving paleogeography of the Ural-Mongol belt.

Introduction

Palinspastic reconstructions at various scales are a concise way to illustrate the paleogeographic and tectonic evolution of an area, and a certain degree of consistency between reconstructions proposed by different researchers can be expected, provided that the extent of our knowledge is adequate. Unfortunately, this is not the situation for the Ural-Mongol mobile belt (UMB) in Eurasia (Fig. 3-1). If one examines the different published reconstructions of the UMB components, it would be difficult indeed (i.e., without carefully studying the figure captions), to understand that it is the same area that is being illustrated. Names and component descriptions of the belt change from one publication to the other, whereas the spatial relationships between mobile zones and older Precambrian cratons range in distance over an order of magnitude or more, and may reveal relative orientations varying by more than a hundred degrees. Thus, one can find a slowly evolving flotilla of small fragments (Mossakovsky et al., 1993; Didenko et al., 1994; Filippova et al., 2001), or a gradually coiling serpentine island arc (Şengör and Natal'in, 1996; Yakubchuk et al., 2001; 2002), or an array of larger blocks that consume surrounding oceans according to rules that change from author to author (Stampfli and Borel, 2002; Puchkov, 1997; 2000). The co-existence of so many dissimilar models strongly indicates that we lack even first-order knowledge about the paleogeography and kinematics of the UMB constituents. Major cratons like Baltica, Siberia, and Tarim are often the only recognizable features in these reconstructions, and even their positions may be quite dissimilar – see the discussion in Cocks and Torsvik (2007) about the Siberian late Paleozoic paleopoles.

Palinspastic reconstructions at various scales are a concise way to illustrate the paleogeographic and tectonic evolution of an area, and a certain degree of consistency between reconstructions proposed by different researchers can be expected. Unfortunately, the different published reconstructions of the Ural-Mongol mobile belt (UMB) in Eurasia (Fig. 3-1) are highly controvercial and even mutually exclusive (see, for example Mossakovsky et al., 1993; Didenko et al., 1994; Filippova et al., 2001; Şengör and Natal'in, 1996; Yakubchuk et al., 2001; 2002; Stampfli and Borel, 2002; Puchkov, 1997; 2000).

It seems to us that this lack of consensus, which contrasts markedly with the much less varying syntheses of Alpine or circum-Iapetus belts, can be attributed to two main reasons. One is that the Paleozoic motions of Siberia, Tarim, Amuria (= Mongolia, south of the Mongol-Okhotsk suture; e.g., Kravchinsky et al., 2002a), and the China blocks are very incompletely known. The other is that the numbers as well as the quality of the available paleomagnetic data have been grossly inadequate.

The Ural-Mongol mobile belt stretches for nearly 10,000 km from the Arctic Ocean along the Ural Mountains between Europe and Asia and then onward through Central Asia almost to the Pacific (Fig. 3-1a). Its western part, the Urals (Fig. 3-1b), displays long narrow sets of folded and imbricated thrusts (Puchkov, 1997; 2000) and is generally akin to other orogenic belts resulting from continent-continent collisions, such as the Caledonides and Appalachians. In contrast, the central parts of the UMB, including Kazakhstan, the Altai, and northwestern Mongolia, have a mosaic structure with no prevailing structural trend (Fig. 3-1b).

In Kazakhstan the UMB reaches its maximum width and is likely to be at its most complex. The early Paleozoic structure comprises tectonically juxtaposed microcontinents with Precambrian basement, early Paleozoic subduction-related volcanic complexes, and accretionary wedges or flysch sequences. In contrast, the Middle to Late Paleozoic geology is dominated by a pair of strongly curved volcanic belts (Fig. 3-2), which are unconformably superposed on older structures. The outer belt comprises volcano-sedimentary Upper Silurian rocks and thick sequences of Lower-to-Middle Devonian subduction-related extrusives. In the Frasnian, volcanic activity shifted to a more interior belt, about 150 km to the south, and continued there in the Famennian-Tournaisian. Further inward displacement of volcanic activity occurred in the Early Carboniferous and lasted until the Middle Permian. The composition of the volcanic series strongly varies within each belt but generally progresses from basalt to andesite and/or dacite and then to rhyolite (Tectonics of Kazakhstan, 1982). After the Late Silurian, and up to the Early Permian, the volcanics are of calc-alkaline affinity and are

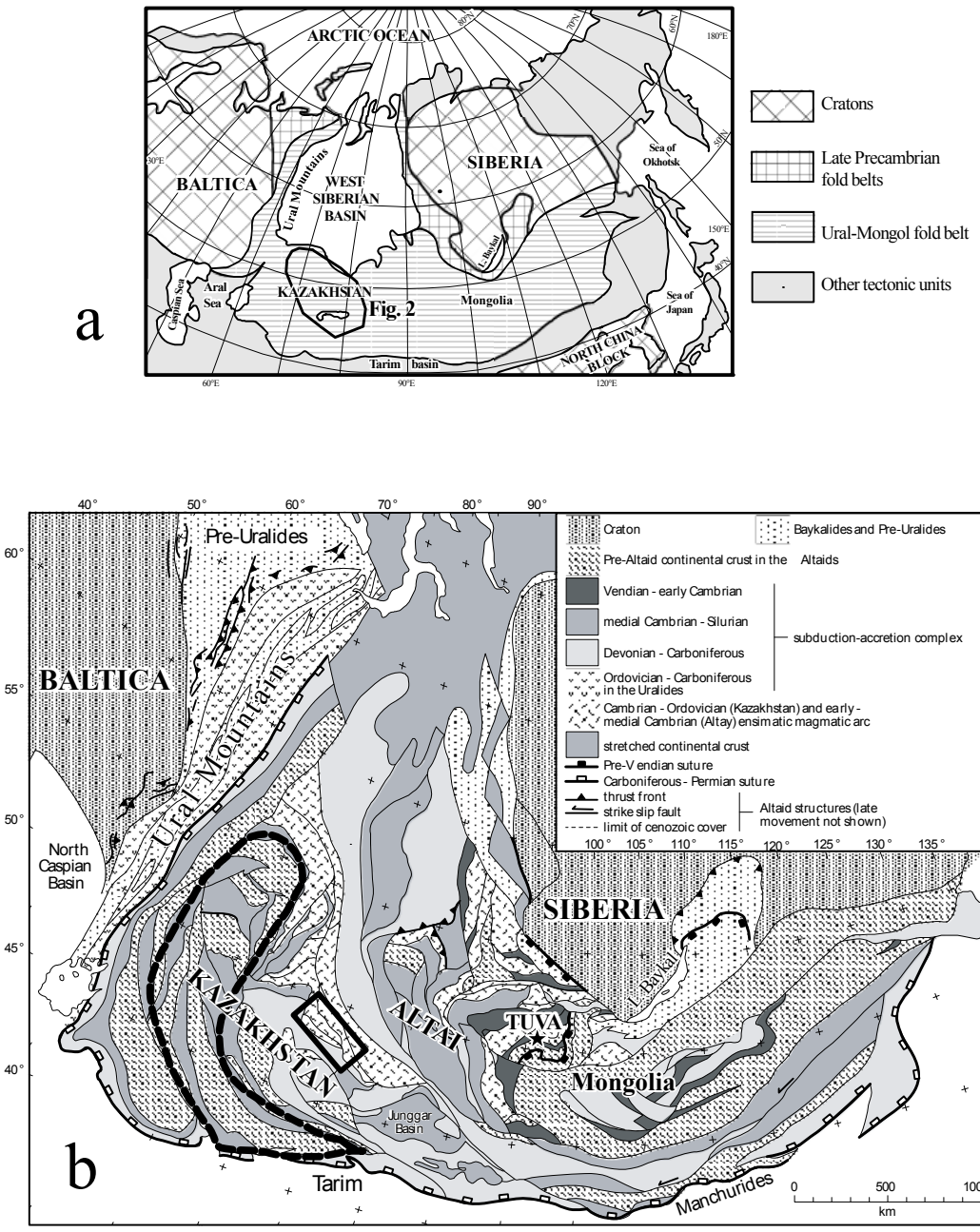

Figure 3-1. Location of study area. (a) Location of the Ural-Mongol fold belt within Eurasia. (b) Generalized tectonic map of the Ural-Mongol belts (the Altaids) and major surrounding units (modified from figure 21.18 of Şengör and Natal'in (1996). The rectangle outlines the Chingiz block. Thick dashed line denotes the boundaries of the Kokchetav-North Tien Shan domain (KNTD) as defined by Levashova et al. (2007). The star denotes the location of the field area (Tuva) of Bachtadse et al. (2000), where Upper Silurian-Lower Devonian rocks were sampled**.**

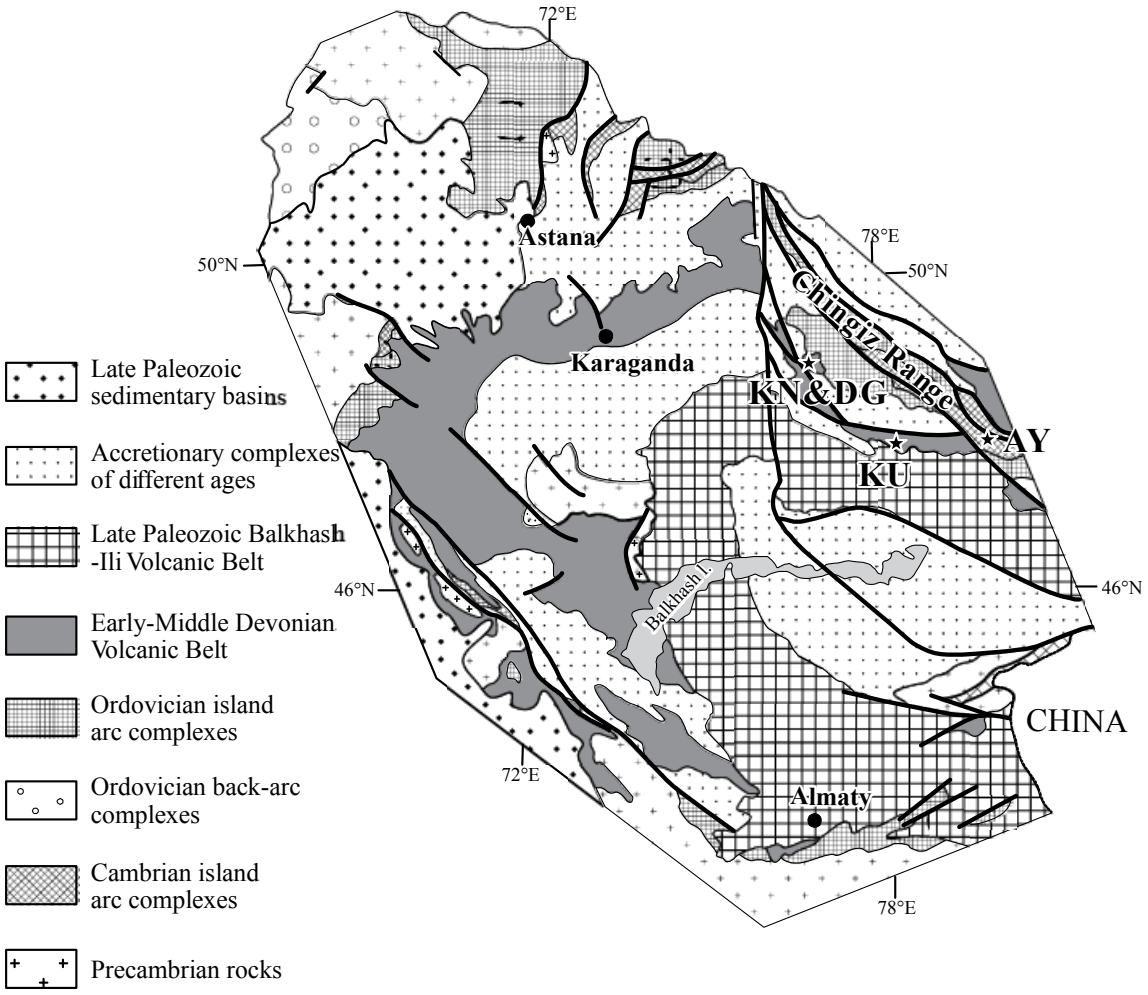

Figure 3-2. Schematic map of major rock complexes in Kazakhstan. Simplified after Degtyarev (2003). Main faults shown as thick solid lines. Stars are the study areas labeled as described in the text.

considered to be of subduction-related origin (Kurchavov, 1994; Tevelev, 2001). Volcanic activity lasted for about 150 Ma, while terrigenous sedimentation continued more and more to the interior side of the loop-like belts. As a result, Late Devonian to late Paleozoic volcanics overlie Silurian and Early Devonian flysch series and accretionary wedges.

To remedy the scarcity of paleomagnetic data, we have initiated a program in the last seven years to obtain temporal sequences of paleomagnetic results for a significant time interval for key tectonic units of Kazakhstan's UMB. This program is not yet completed, except for one major tectonic unit, which is the Kokchetav-North Tien Shan domain (KNTD; Levashova et al., 2007). The KNTD stretches from north Tarim to almost the West Siberian Basin and is outlined by a thick dashed contour in Figure 3-1b. It comprises several Precambrian microcontinents and numerous remnants of early Paleozoic island arcs, marginal basins and accretionary wedges. It is thought that in the Late Ordovician these units had amalgamated into a contiguous domain (Levashova et al., 2007). Nine paleomagnetic results from the KNTD have been combined to show its latitudinal motion from the Late Ordovician until the Late Permian; the data support the concept of a more or less coherent motion of the KNTD and Baltica (Levashova et al., 2007), and imply that Baltica and the KNTD were never very far apart after the Silurian.

A similar program (Collins et al., 2003; Levashova et al., 2003a, b) was started in the Chingiz Range, which stretches for more than 600 km in northeast Kazakhstan (Fig. 3-2). These reports noted acceptable, albeit temporally incomplete, agreement of the observed paleolatitudes with the Siberian reference values for the early Paleozoic, followed by a disparity in the middle Paleozoic. Although the possibility of coherent motion of the Chingiz arc and the Siberian craton was discussed in these papers (Collins et al., 2003; Levashova et al., 2003a), a conclusion remained rather elusive due to large time gaps between the results, poor quality of the Devonian data (Levashova et al., 2003a), and the lack of reliable middle and late Paleozoic poles for the Siberian plate, except for the about 360 Ma old pole of Kravchinsky et al. (2002b). To fill the gap in temporal coverage in NE Kazakhstan, we present here three new paleomagnetic results from Middle Silurian and Lower to Middle Devonian rocks of the Chingiz area and

compare these with the available data from SW Kazakhstan, Kyrgyzstan, Siberia, and Baltica. This will allow us to determine the paleolatitudinal movements of the tectonic units in this area and to place constraints on the tectonic evolution of the UMB.

Geological Setting and Sampling

The Chingiz Range sensu stricto is a tectonic unit that extends for about 600 km in a NW-SE direction in northeastern Kazakhstan (Fig. 3-2). It contains Cambrian to Early Silurian volcanic series of island-arc affinity (Degtyarev, 1999), some of which were studied by us earlier (Collins et al., 2003; Levashova et al., 2003a). No accretionary complexes of Cambrian or Tremadocian age are known in this area. In contrast, Arenigian to Late Ordovician accretionary complexes and Middle Ordovician to Early Silurian flysch sequences are widespread and become progressively younger from the northeast to the southwest. After the Middle Ordovician, the ages of volcanic series also show a younging trend from NE towards the SW.

The lower Paleozoic rocks of the Chingiz unit do not contain continent-derived sediments, so that it is regarded as an intra-oceanic arc (Degtyarev, 1999). Most authors agree that subduction under the Chingiz island arc was from the southwest to the northeast (in present-day coordinates) since the Middle Ordovician. Recently, detailed mapping coupled with new age determinations and restoration of displacements along the abundant strike-slip faults provided evidence that the polarity of the arc has remained the same since the Cambrian (Degtyarev and Tolmacheva, 2005), although other authors earlier hypothesized a reversal of subduction in the Early Ordovician (Samygin, 1974; Zonenshain et al., 1990). By the end of Early Silurian time, volcanism diminished in the Chingiz Range; the overlying Upper Silurian redbeds only locally and rarely contain lava flows or tuffaceous members. In a few places, these redbeds reside on older rocks with a pronounced angular unconformity, although elsewhere this unconformity is absent (Degtyarev and Ryazantsev, 1993). These authors also note that the pattern of younger Devonian volcanism generally follows the spatial distribution of the Upper Silurian sediments.

In Early Devonian time, a renewed outburst of volcanism took place in many areas of Kazakhstan. The most active volcanism is confined to a relatively narrow horseshoe-shaped band (the Early-Middle Devonian volcanic belt in Fig. 3-2), which was recognized several decades ago (Bogdanov, 1965). Generally, this belt follows the boundary between the older ("Caledonian") structures outside of the horseshoe and the younger ("Variscan") fold belt inside it. In the Chingiz area *sensu lato*, this volcanism is of mid-Lochkovian age (Schegoleva et al., 1993) and is located generally to the SW of the early Paleozoic and Silurian island-arc complexes (Fig. 3-2). These Devonian volcanics of the northeastern arm of the belt partly overlap, and generally parallel the older Chingiz structures. Volcanic activity in this belt lasted until the Givetian, whereas Late Devonian and Tournaisian volcanics are scarce or absent altogether in this Range.

In the Visean, volcanism resumed and lasted until the Late Permian (Sal'menova and Koshkin, 1990); the resulting late Paleozoic volcanic belt (see Fig. 3-2) is called the Balkhash-Ili belt. Both the Devonian and the Balkhash-Ili belts are usually considered as Andean-type active margins with subduction under them directed away from the horseshoe interior; however, the views on the evolution of these belts, their strongly curved outlines in particular, are controversial (Kurchavov, 2001; Tevelev, 2001). Judging by numerous angular unconformities in the Chingiz island-arc sequence and adjacent parts of the volcanic belts, multiple late Paleozoic deformation events affected the area. For our purposes, we need to mention the post-Early Silurian, post-Givetian, Visean and Late Permian events. As noted above, however, the magnitude of each deformation varies laterally, and the deformation pattern is not uniform (Degtyarev and Ryazantsev, 1993).

On the whole, the Chingiz island arc of intra-oceanic setting was active for more than 100 million years (Degtyarev, 1999). The clear reduction in the volcanism during the later Silurian may indicate either greatly diminished subduction, or a major reorganization of the plate boundary system. Regardless, subduction-related volcanism resumed at the Andean-type active margin in Early Devonian time and lasted well into the Permian (Tevelev, 2001, and references therein).

Our study concentrated on mid-Silurian volcanic rocks of the Chingiz island arc and Devonian rocks of the Devonian volcanic belt from the southwestern part of the Chingiz area. Brief descriptions follow, using the two-letter abbreviations that we use to identify the sampling areas (see labels in Fig. 3-2).

Locality AY (=Ayaguz; 48.0°N, 80.7°E)

Marine sediments are covered by andesite flows at this section. The youngest fossiliferous sediments, of late Wenlockian- early Ludlovian age, occur below the base of the volcanic pile, so we can consider the volcanic rocks as of Ludlovian age. We sampled 12 lava flows with clear flow contacts in a SE-dipping monocline; the total true thickness studied is more than 200 meters. Bedding attitudes were measured on several sedimentary layers intercalated with the volcanics. Also sampled were 20 lava cobbles from two conglomerate members between lava flows. We should add that, except for one strongly weathered flow, we studied all cooling units at this section, and no other Silurian volcanics are present within a reasonable distance from it.

Localities KN & DG (Kaynar-Dogolan; 49.5°N, 77.0°E)

Lower to lower-Middle Devonian volcanics and tuffs of basaltic to rhyolitic composition were sampled from a bowl-like syncline and from three adjacent but separate monoclines with different attitudes up to 15 km apart. Lava flows and tuffs were sampled at 44 sites. Bedding attitudes could usually be measured on stratified tuffs and sediments, although occasionally bedding had to be obtained from flow contacts.

Locality KU (Kurbakanas; 48.3°N, 78.3°E)

Givetian basalts with sparse interbeds of sediments occupy a large area but, due to low relief, are rather poorly exposed. Earlier, Levashova et al. (2003a) studied five flow units (sites) from a section distributed about a single sedimentary layer. We re-visited this area and sampled 13 more sites from basaltic flows with varying attitudes. All sampled sites are within twenty meters from sedimentary layers.

Methods

Generally, a set of samples collected from a separate cooling unit was called a site, wherever practical in terms of numbers and spatial distribution. Paleomagnetic samples were collected either as fist-sized blocks oriented with a magnetic compass, or were drilled with a portable drill and oriented with a magnetic or sun compass. Our convention is to label a site using the letters/numbers of its first sample but with a capital letter at the beginning; for instance, site N3814 contains samples n3814 through n3819, followed by site N3820, and so forth.

Cubic specimens of 8 cm^3 volume were sawed from hand blocks; cores were sliced into 22 mm long cylinders. The collection was studied in the paleomagnetic laboratories of the Geological Institute of the Russian Academy of Sciences in Moscow and of the University of Michigan in Ann Arbor. In Moscow, specimens were heated in a homemade oven with internal residual fields of approximately 10 nT and measured with a JR-4 spinner magnetometer with a noise level of 0.05 mA/m. In Ann Arbor, specimens were stepwise demagnetized utilizing an Analytical Services TD-48 thermal demagnetizer with internal residual fields of < 10 nT; magnetizations were measured with a 2G Enterprises cryogenic magnetometer in a magnetically shielded room. In both laboratories, the specimens were stepwise demagnetized in 15-20 increments up to 680°C. No systematic difference was found between the samples that were treated in Moscow or Ann Arbor, and the data have been pooled.

Demagnetization results were plotted in orthogonal vector diagrams (Zijderveld, 1967). Visually identified linear trajectories were used to determine directions of magnetic components by Principal Component Analysis (PCA), employing a least-squares fit comprising three or more demagnetization steps (Kirschvink, 1980), anchoring the fitting lines to the origin where appropriate.

If complete component separation is not achieved during demagnetization, the common practice is to combine the PCA-calculated sample directions (Kirschvink, 1980) and remagnetization circles employing the technique of McFadden and McElhinny (1988). When this was the case, remagnetization circles were combined with direct observations for computing site-means of both lower- and higher-temperature

components. This approach, however, is not omnipotent. For instance, if only remagnetization circles are available at a given site and, as is often the case, these circles converge at acute angles, their intersection gives a biased estimate of the least-dispersed component (Schmidt, 1985). In other sites where one can determine only component directions that form a strongly elongate distribution, a calculation of a mean direction is undesirable. In such cases, one can calculate the site-mean great circle in the first site, and the best-fitting plane in the second. For calculation of the overall mean for a formation, such great circles can be combined with "standard" site-mean directions (McFadden and McElhinny, 1988). All statistics below are calculated for 95% confidence level. Paleomagnetic software written by Jean-Pascal Cogné (2003), Randy Enkin (http://gsc.nrcan.gc.ca/dir/index_e.php?id=12377), and Stanislav V. Shipunov was used in the analysis.

Results

Mid-Silurian volcanics (locality AY)

In the dark-colored volcanics, a weak unstable component is completely removed by 350° - 400°C, and a well-defined characteristic component (ChRM) that shows rectilinear decay to the origin can be isolated (Fig. 3-3a, c). In contrast, the natural remanent magnetization (NRM) of brick-red varieties is strongly dominated by an overprint; nevertheless, a ChRM could reliably be isolated from most of these samples as well (Fig. 3-3b). All in all, every one of the 12 sites and all but 6 of the 83 samples gave useful results. ChRM site-mean directions are rather well clustered, as can be evaluated from the statistical parameters in Table 3-1, and the overall mean direction is well defined (Table 3-1). Judging by unblocking temperatures, this remanence resides in both magnetite and hematite in varying proportion, both "magnetite" and "hematite" components being directionally identical (Fig. 3-3a, c). Bedding attitudes at this section show minor variation, and, although maximum grouping occurs at 100% unfolding, the fold test is inconclusive (Table 3-1; Fig. 3-4a, b).

Thirteen cobbles out of twenty that were sampled from two beds of intraformational conglomerate show demagnetization patterns that are very similar to

those in the host rocks (Fig. 3d). In six samples, however, the "magnetite" component clearly misses the origin, whereas the "hematite" ChRM decays to it (Fig. 3e). For all ChRM's from 19 cobbles, the normalized vector-resultant of 0.165 is much less than the critical value of 0.367 (Mardia, 1972); hence the conglomerate test is positive (Fig. 3-4c), and the ChRM in Silurian volcanics can be deemed primary. The "magnetite" intermediate component in the six samples is very scattered also.

In most cases, ChRM site-mean directions from adjacent sites are statistically different. This means that no serial correlation of site-mean directions is present in this data set, and each site-mean can be regarded as an independent spot-reading of the field. The distribution of site-mean virtual geomagnetic poles has a standard angular deviation (S) of 12.3º, which agrees well with the value of about 12.5º for the geomagnetic field near the equator during the last 5 Ma (Merrill et al., 1996). This finding as well as the presence of sedimentary members among the volcanics, indicates that accumulation of the volcanic pile lasted long enough to average secular variation adequately. Hence we conclude that the ChRM in the studied section is likely to be primary, and that its mean direction originally did correspond to that of the ancient field.

Lower to lower-Middle Devonian rocks of KN&DG locality

A low-temperature component, which clusters around the present-day field before tilt correction, is usually removed below 200°-250°. Only at one site (P254) did a similar remanence persist over the entire heating range (not shown), suggesting that this is a chemical remanence due to recent weathering.

After removal of the low-temperature remanence, many sites had stable components, but not all. A few sites yielded what only can be called anomalous mean directions and eight gave very scattered and inconsistent results. In total, we had to reject 10 sites. In 28 of the remaining 34 sites, an upward-pointing component A was often isolated (Fig. 3-5a, c-e). This intermediate-temperature component may decay to the origin (Fig. 3-5a) or can miss it (Fig. 3-5c-f); even in the former case, however, vector end-points often shift along a great circle path at intermediate and high temperatures (Fig. 3-5b). This component is

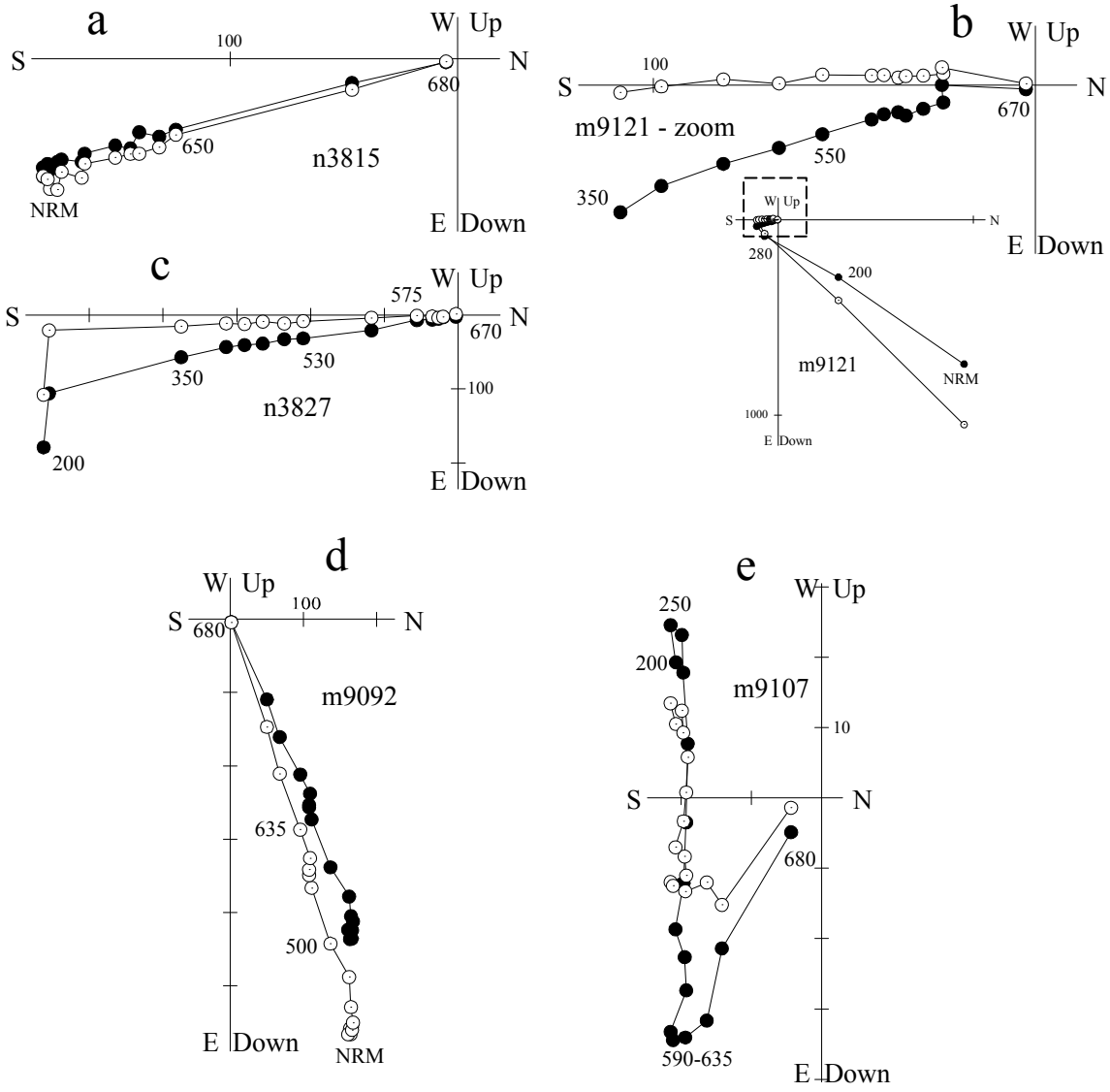

Figure 3-3. Representative thermal demagnetization plots of Silurian rocks from locality AY, in stratigraphic coordinates: a-c, andesite flows; d-e, cobbles from an intraformational conglomerate. Full (open) circles represent vector endpoints projected onto the horizontal (vertical) plane. Temperature steps are in degrees Celsius. Magnetization intensities are in mA/m. For clarity, NRM points are omitted from some plots.

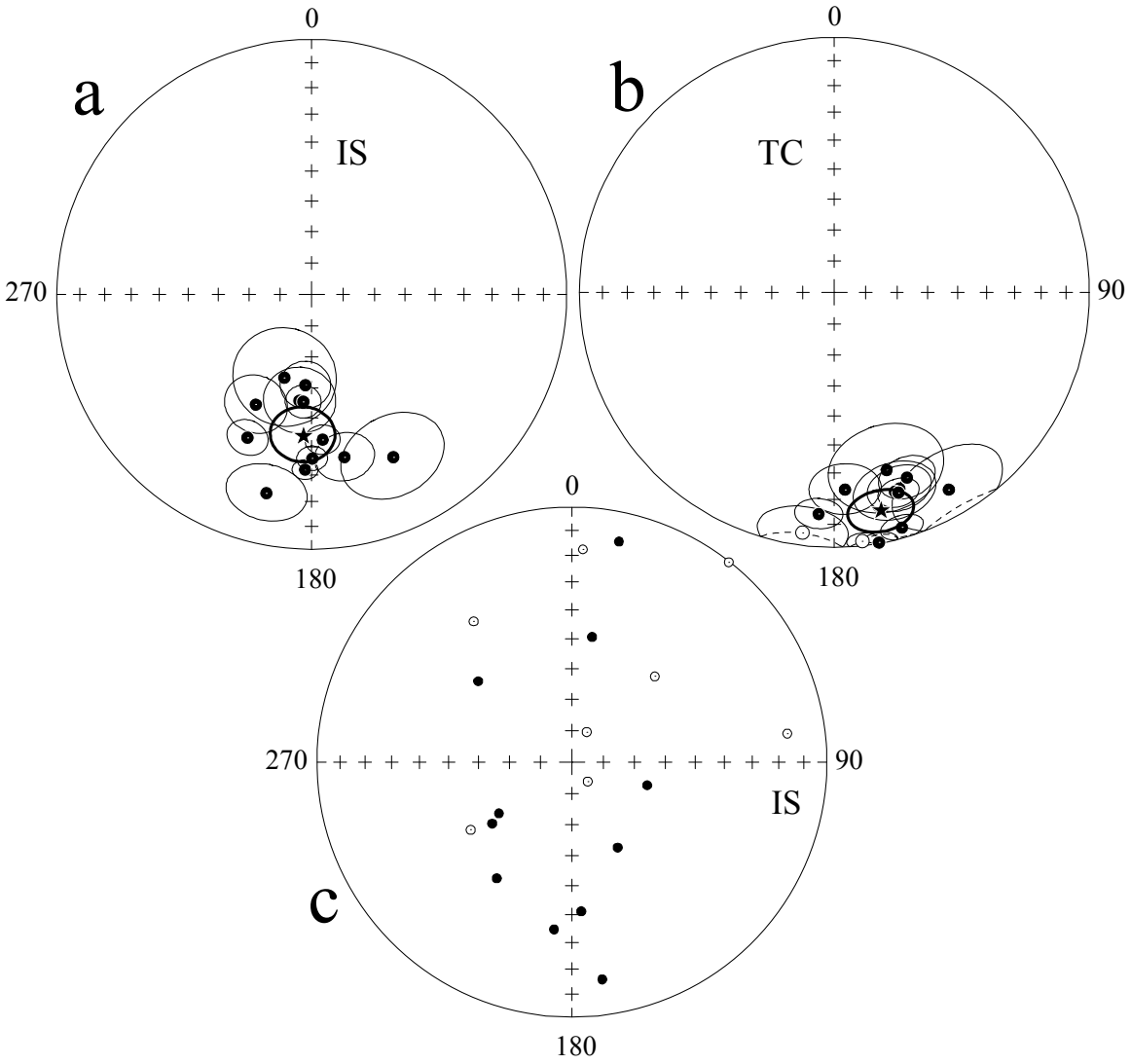

Figure 3-4. Stereoplots of site-mean directions of the high-temperature components (HTC) with associated confidence circles (thin lines) of Silurian volcanic rocks from locality AY, (a) in situ (IS) and (b) after tilt correction (TC). Star with associated confidence circle (thick line) is the overall mean directions of the characteristic remanence. (c) HTC directions from cobbles from an intraformational conglomerate. Filled (open) symbols and solid (dashed) lines are projected onto the lower (upper) hemisphere.

Table 3-1. Site-mean paleomagnetic directions for the Silurian rocks from locality AY

		In Situ					Tilt corrected			
Site	N	A	D°	I°	k	α_{95}°	D°	I°	k	α_{95}°
M9066	7/7	124/20	153.4	29.3			149.9	11.5	18	14.9
N3801	7/7	124/20	168.6	35.2			161.7	20.0	50	8.6
M9073	6/5	135/45	198.2	61.8			163.6	28.2	25	16.1
M9079	12/7	135/45	206.9	49.9			176.9	23.6	41	9.6
M9111	6/6	135/45	192.8	21.1			187.5	-5.6	40	10.8
M9117	7/7	135/45	182.1	31.8			173.6	-2.1	285	3.6
N3808	6/6	134/39	184.0	60.8			158.6	23.0	75	7.8
N3814	6/6	134/39	184.5	55.2			162.2	18.6	151	5.5
N3820	6/6	135/45	186.5	55.5			163.1	19.4	38	11.0
N3826	7/7	135/45	179.8	35.9			169.8	0.5	194	4.3
N3833	6/6	135/45	204.2	38.4			184.0	14.0	123	6.1
N3839	7/7	135/45	175.7	42.3			163.9	4.6	139	5.1
MEAN	(12/12)		183.7	44.1	22	9.5	168.0	13.2	28	8.4

Legend and explanation for Table 3-1.
N is the ratio of the number of samples (sites) studied/accepted; A is the site's azimuth of dip/dip angle; D, declination; I, inclination; k, concentration parameter; α95, radius of 95% confidence circle (Fisher, 1953). The results are presented in stratigraphic order from top to bottom.

typically isolated below 570°C suggesting magnetite as the main carrier but the corresponding linear segments on orthogonal plots sometimes extend into the hematite range (Fig. 3-5c).

The exclusively reversed-polarity component A is moderately to well grouped at most sites (Table 3-2). Its site-mean directions show a rather diffuse distribution with similar dispersions in situ and after tilt correction (Table 3-2; Fig. 3-6a, b), but a distinct maximum at 35 percent is observed during stepwise untilting (Fig. 3-6c). The maximum concentration parameter, k, of 16 differs significantly from the tilt-corrected value (8) but not from the in situ value. The latter difference only becomes significant at levels lower than 90%. Judging by demagnetization characteristics and the result of the fold test, this reversed A-component is an overprint that was acquired during deformation. Geological data, however, clearly indicate that Lower-lower Middle Devonian volcanics were deformed in the Givetian but were also affected by folding in the late Paleozoic. So it is more accurate to state that component A was acquired not during a single folding event but at the final stages of deformation in this area.

The presence of another component (labeled B) is clearly indicated in many samples, and this B component is always characterized by the highest unblocking temperatures for a given sample and by a rather different direction from that of the A-component. However, proper isolation of the B-component was prevented in several samples by the acquisition of spurious remanence at high temperatures (Fig. 3-5c). Component B has negative inclinations at six sites (Fig. 3-5f; Fig. 3-6d, e) and is of opposite polarity at 12 others (Fig. 3-5d, e; Fig. 3-6d, e). Component B site-means are rather scattered but they clearly form two nearly antipodal clusters, in particular after tilt correction (Fig. 3-6d-e). The two polarity-means differ by 175.2º (4.8º) ± 18.1, rendering the reversal test positive (Table 3-3). This remanence shows a two-fold increase in grouping upon tilt correction (Table 3-3), which is statistically significant, and renders the fold test (McElhinny, 1964) positive as well.

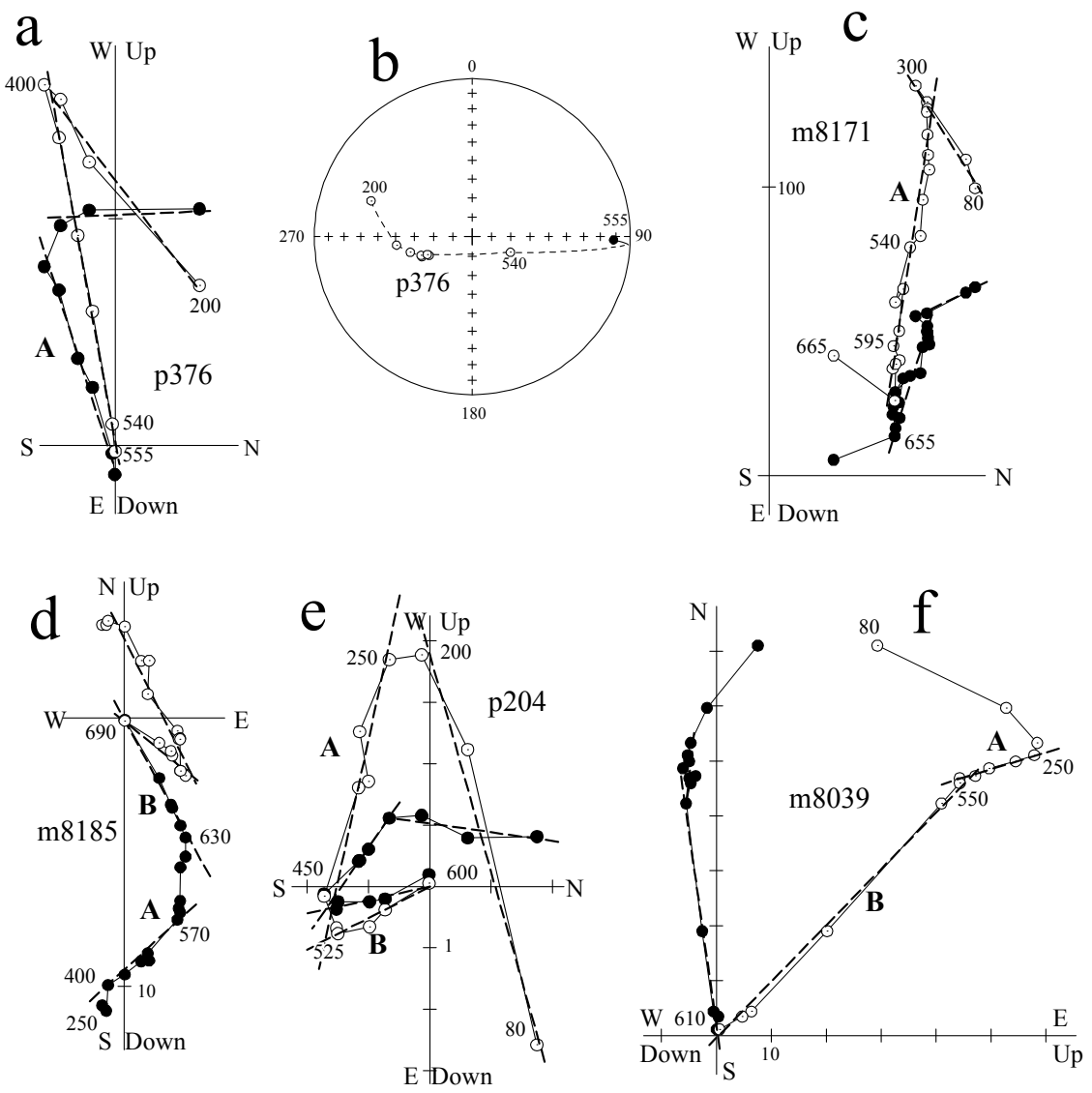

Figure 3-5. Thermal demagnetization diagrams from the Lower-Middle Devonian volcanics from locality KN&DG in geographic coordinates. For clarity, NRM points are omitted from the plots. Thick dashed lines denote identified and labeled (A, B) components (see Tables 3-2 and 3-3). Other notation for demagnetization plots and stereonet as in Figures 3-3 and 3-4.

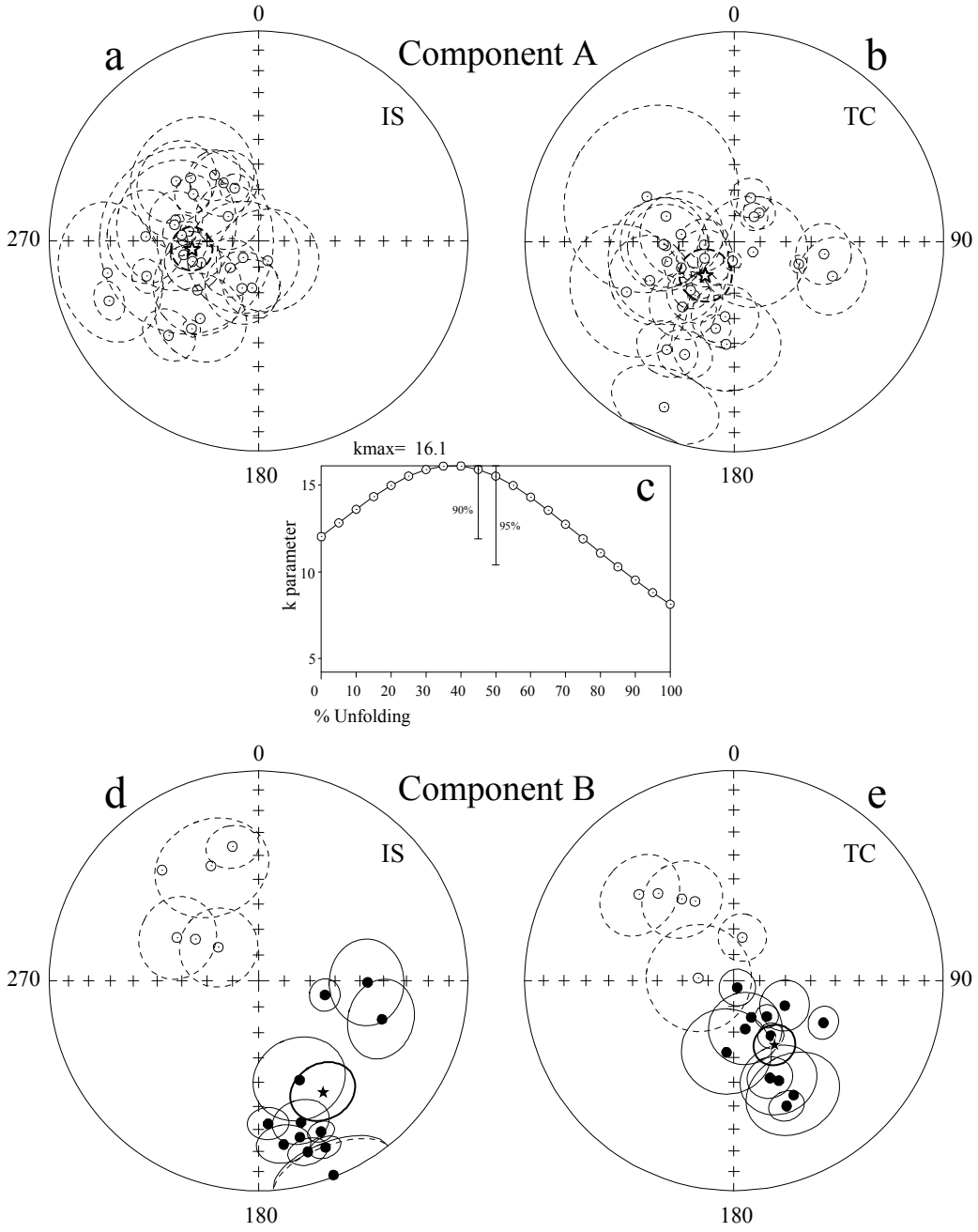

Figure 3-6. Stereoplots showing site-mean directions of the A and B components isolated from Lower to lower-Middle Devonian rocks at locality KN&DG, (a, d) in situ and (b, e) after tilt correction and (c) a plot of concentration parameter versus percent unfolding for component A data. Stars are the overall mean directions of the corresponding components with associated confidence circles (thick lines). Mean directions without confidence circles are shown when two samples are used at a site. Other notation as in Figure 3-4.

Legend and explanation for Table 3-2.
[#] – this anomalous site is excluded from computation of the overall mean.
Mean1 (Mean2) is the overall mean direction of all sites (sites with more than two samples and $\alpha_{95} < 20°$). 35% unfold is the mean direction at 35% incremental unfolding. Other notation is as in Table 3-1.

Table 3-2. Component A data from Lower-Middle Devonian rocks from localities KN and DG

			In Situ				Tilt corrected			
Site	N	A	D°	I°	k	α_{95}°	D°	I°	k	α_{95}°
A44	5/4	8/50	328.9	-63.6	52	12.9	218.6	-57.3	52	12.9
A61	7/0	328/25	No stable remanence above 250°							
A68	6/3	330/24	272.3	-45.2	55	16.7	245.3	-53.4	55	16.7
A75	6/0	fold	scattered							
A81	6/5	297/24	223.7	-37.8	63	10.0	203.8	-40.9	63	10.0
A87	4/0	313/21	No stable remanence above 250°							
A93#	6/3	216/26	224.3	-2.2	62	15.7	225.4	-27.8	62	15.7
M8019	7/4	350/28	326.3	-59.0	86	9.9	263.7	-78.2	86	9.9
M8026	9/6	350/28	305.8	-49.7	19	15.6	266.5	-63.2	19	15.6
M8044	6/4	143/15	188.2	-71.6	79	11.0	240.7	-76.9	79	11.0
M8050	5/3	168/20	231.4	-59.3	50	17.6	267.8	-62.3	50	17.6
M8056	5/2	168/20	249.2	-66.1	-	-	290.3	-61.5	-	-
M8062	5/3	168/20	270.2	-60.4	13	35.4	297.2	-51.2	13	35.4
P200	5/5	358/55	335.7	-67.5	185	5.6	192.1	-55.2	185	5.6
P218	6/4	260/14	223.2	-81.2	19	21.8	119.3	-81.8	19	21.5
P248	6/0	8/37	scattered							
P254	6/0	348/34	Main component is close to the present-day field							
P260	6/4	331/36	284.2	-56.3	74	10.8	216.5	-63.9	74	10.8
P266	6/6	294/29	278.0	-62.5	358	3.5	185.4	-82.5	358	3.5
A99	4/4	246/44	258.1	-27.1	22	23.5	277.7	-69.0	43	16.4
A112	4/0	263/44	scattered							
A190	7/4	12/34	155.2	-81.6	25	20.0	184.6	-49.4	25	20.0
A300	5/5	12/32	280.9	-56.4	11	24.3	242.6	-44.6	11	24.3
M8161	3/0	356/46	scattered							
M8167	3/0	356/46	scattered							
M8174	3/3	1/35	312.7	-53.6	37	24.1	253.5	-62.6	37	24.1
M8180	6/6	358/38	252.9	-63.0	36	11.3	212.1	-39.1	36	11.3
M8187	5/3	1/41	217.1	-51.8	51	17.4	203.0	-15.5	51	17.4
P306	6/5	252/43	248.2	-24.1	132	6.7	243.7	-66.9	132	6.7
P312	6/6	245/60	252.6	-43.3	116	6.3	41.1	-75.2	116	6.3
P317	6/6	245/60	217.5	-46.4	403	3.3	109.2	-63.4	403	3.3
P357	5/5	263/47	199.3	-70.6	30	14.2	109.4	-48.8	30	14.2
P362	9/5	263/47	226.6	-74.9	47	11.3	97.9	-54.4	47	11.3
P371	6/6	248/40	259.6	-60.2	158	5.4	38.6	-77.7	158	5.4
P377	5/5	248/40	274.4	-59.8	100	7.7	20.6	-71.9	100	7.7
P383	6/5	348/40	308.8	-74.8	38	12.7	187.1	-60.5	38	12.7
P389	6/6	348/40	305.6	-58.5	90	7.2	222.0	-64.5	90	7.2
T50	5/0	17/32	scattered							
Mean1	(44/27)		261.4	-63.2	12	8.3	220.3	-73.5	8	10.1
Mean2	(44/22)		261.4	-61.6	11	9.7	209.1	-73.4	8	11.6
35% unfold	(44/27)		251.2	-68.2	16	7.2				

The mean B-component direction ends up with acceptable statistical parameters and is confirmed by positive fold and reversal tests (Table 3-3, Fig. 3-6d, e), despite some anomalous and inconsistently scattered sites. Also heartening is the gross similarity of this result with the KU one (discussed next) .

Givetian basalts (locality KU)

Low-temperature component directions cluster around the present-day field before tilt correction, and were usually removed below 200°-250°C. At higher temperatures, two components (A and B) were isolated from most samples.

Component A persists from about 250°C until above 500° and is sometimes the only component present in a sample (Fig. 3-7a). In other samples, this remanence does not decay to the origin and is succeeded by another component (B). This can be seen as sequential rectilinear segments on orthogonal plots (Fig. 3-7b-d) or in remagnetization circles in stereonets when the decay of an A component produces a curved trajectory in the orthogonal demagnetization diagrams. Proper component separation may not always be reached in such a case, even if two apparently rectilinear segments seem evident. For instance, component B is unlikely to be fully and reliably isolated in sample n3863 (Fig. 3-7c). It can also happen that the intermediate-temperature (A) component is contaminated, as suggested by the diagram of sample m9202 (Fig. 3-7d). In this sample, overlapping of unblocking spectra of components A and B seems responsible. For several sites, remagnetization circles (Fig. 3-7e) had to be used, and for some six other sites we could not determine any well-clustered mean A-, B- or anomalous direction with any confidence. These sites are, of course, not included in Table 3-4.

Despite this occasional problematic aspect of the determination of A or B component directions, we feel confident that the site-mean directions and remagnetization circles of Table 3-4 are well enough determined. We have combined our data with the previous results from five sites of the same formation at this locality (Levashova et al., 2003a). In this combined set, twelve site-mean directions of the A-component form a tight cluster in situ (Table 3-4; Fig. 3-8a), excluding two anomalous outliers (not shown). A three-fold increase in dispersion upon tilt correction (Table 3-4; Fig. 3-8b) indicates that the A-component is postfolding.

The combined component B site-mean directions and remagnetization circle intersections form two groups on the stereonet (Fig. 3-8c, d): one with four site-means with north and up directions and another comprising four remagnetization circles and two site-means; the latter group defines a south and down cluster of directions. The corresponding polarity-means differ by 168.3° (11.7°) ± 13.8°, rendering the reversal test positive (Table 3-4; Fig. 3-8c, d). For the ten sites with B-directions, tilt-corrected data show a better grouping than in-situ directions, but this is not statistically significant; also insignificant is a slight improvement in data grouping at 80% unfolding. With some reservation, we conclude that the dual-polarity B-component is primary and of Middle Devonian age. This view is further supported by general agreement between the Early-early Middle Devonian KN&DG result and late Middle Devonian KU data (Table 3-5).

Discussion

Overview of results from the Chingiz area deemed of primary origin

Several studies reported Paleozoic paleomagnetic results from the Chingiz island arc and adjacent units and the nearby and younger complexes of the Devonian and late Paleozoic volcanic belts (Table 3-5).

Collins et al. (2003) reported paleomagnetic data from Upper Cambrian andesites and Lower Ordovician (Arenigian) redbeds from the central part of the Chingiz Range (results labeled CL and OE, respectively, in Table 3-5). The ancient nature of both magnetizations is confirmed by positive fold tests. There is a large scatter of Arenigian site-mean declinations, however, presumably because of local vertical-axis rotations. The statistical limits on the Early Ordovician mean inclination are therefore much tighter than those for the mean declination.

Lower Silurian volcanics (SI) were studied 30-40 km to the southwest from localities OE and CL. The primary origin of he dual- polarity magnetization in these

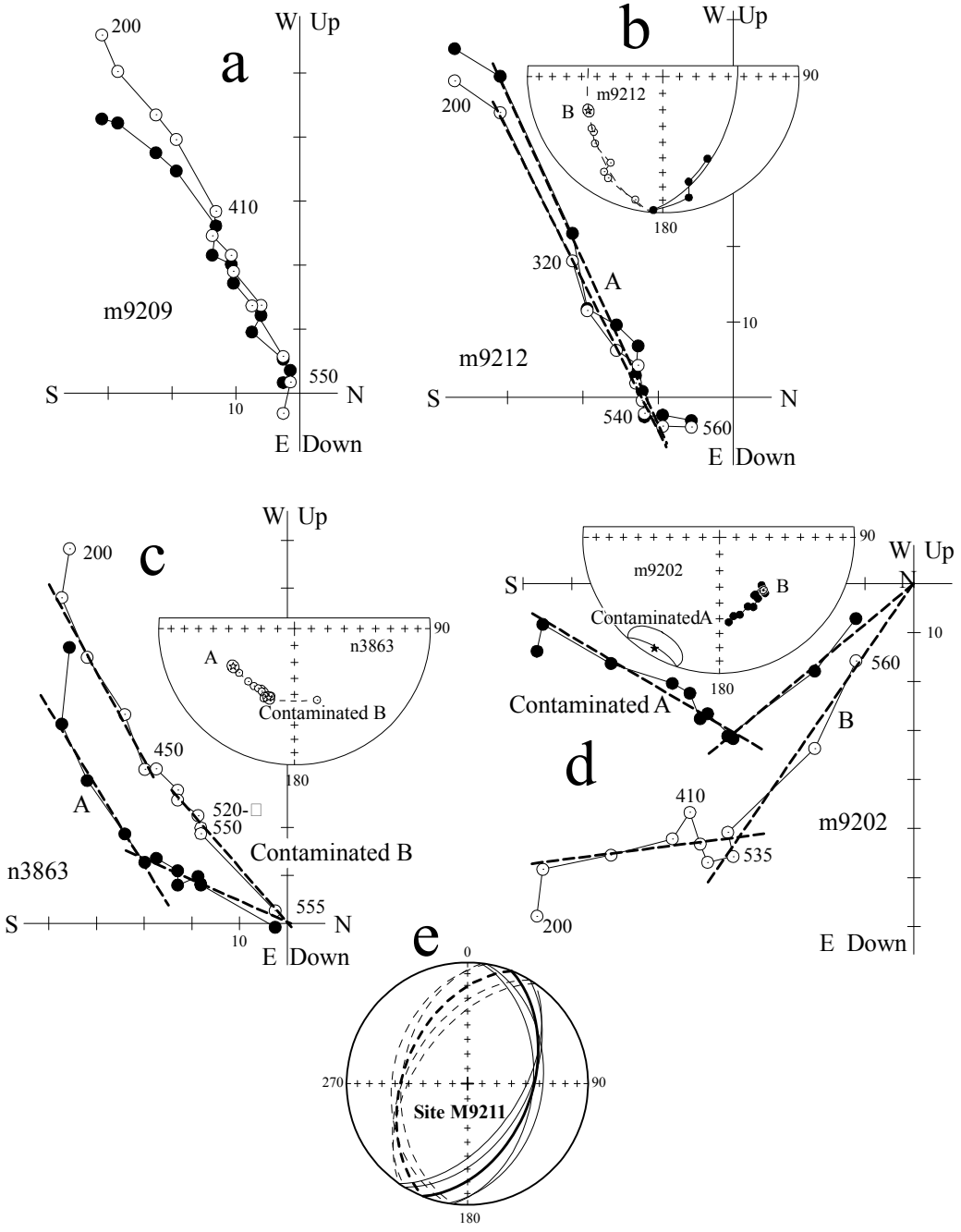

Figure 3-7. Representative thermal demagnetization plots and stereonets of vector end-points and isolated components in Givetian volcanics from locality KU in stratigraphic coordinates (a-d). Thick dashed lines denote isolated and labeled (A, B) components. Stars in stereonets are best estimates of the (A or B) component directions. (e) An example of the computation of the mean remagnetization circle (thick line) from several near-parallel sample remagnetization trajectories (thin lines) (see text for detail). Other notation for the orthogonal plots and stereonets in Figures 3-3 and 3-4.

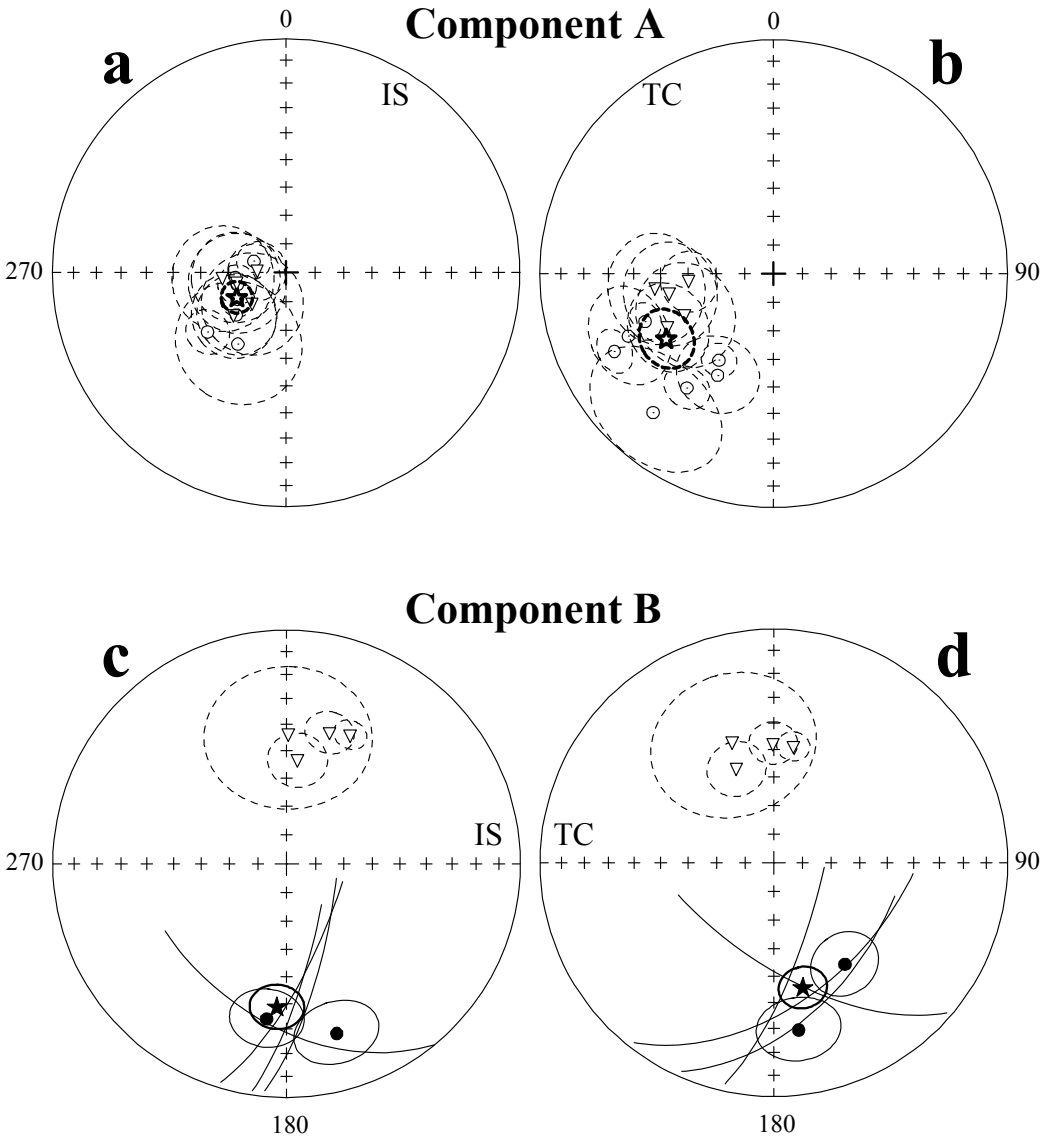

Figure 3-8. Site-mean directions of locality KU magnetizations. (a-b) Stereonets of component A site-mean directions. Triangles are the results from Levashova et al. (2003a) and open circles from this study, with associated confidence circles (thin lines) from the Givetian volcanics of locality KU. (a) in situ and (b) after tilt correction. Star with associated confidence circle (thick line) is the locality-mean direction of the secondary A-component. (c-d) Component B site-mean directions (triangles and filled circles as in (a-b) with associated confidence circles in the Givetian volcanics from locality KU in situ (c) and after tilt correction (d). Star with associated confidence circle (thick line) is the locality-mean HTC direction.

Table 3-3. Component B data from Lower-Middle Devonian rocks from localities KN and DG

		In Situ					Tilt corrected			
Site	N	A	D°	I°	k	α_{95}°	D°	I°	k	α_{95}°
A44	5/3	8/50	163.2	30.3	162	9.7	116.2	67.9	162	9.7
A81	6/4	297/24	157.4	47.6	55	17.0	186.0	61.9	55	17.0
M8019#	7/4	350/28	348.9	22.9	226	6.5	348.9	-5.1	226	6.5
M8037	6/4	338/40	349.0	-35.1	100	9.2	11.0	-73.0	100	9.2
M8044	6/6	143/15	102.0	63.5	125	6.1	115.2	50.9	125	6.1
M8050	5/2	168/20	303.3	-60.4	-	-	318.9	-44.1	-	-
M8056	5/3	168/20	309.8	-69.6	66	15.3	327.3	-51.9	66	15.3
M8062	5/4	168/20	297.9	-53.6	36	15.5	312.2	-38.7	36	15.5
P200	5/5	358/55	176.2	32.3	136	7.1	153.7	87.0	136	7.1
P206	5/5	348/50	158.0	15.5	237	5.0	146.1	64.1	237	5.0
P211	7/6	348/50	157.4	23.2	220	4.5	137.4	71.1	220	4.5
P218#	6/4	259/14	264.4	74.1	126	11.0	262.1	60.5	106	12.0
P266	6/2	294/29	318.8	-30.6	-	-	333.7	-55.4	-	-
A166	5/5	16/31	171.2	22.2	87	8.8	159.6	49.0	97	8.4
A172	6/6	16/23	163.9	16.3	118	6.3	157.1	35.4	118	6.3
A180	2/2	13/26	165.1	23.9	-	-	155.7	46.6	-	-
A190#	7/6	12/33	92.4	-41.8	159	5.4	121.7	-38.7	159	5.4
M8167	3/3	356/46	337.5	-40.4	50	20.6	274.2	-76.1	50	20.6
M8187	5/5	1/41	158.9	0.9	24	17.0	152.4	38.4	24	17.0
P362	9/5	263/47	107.3	38.2	35	14.1	166.7	70.7	35	14.1
P371	6/4	248/40	90.8	46.7	48	15.6	154.6	74.3	48	15.6
Reverse	(6)		322.8	-49.8	16	17.2	322.8	-58.2	18	16.4
Normal	(12)		152.6	32.5	9	15.7	150.4	61.1	20	10.0
Mean1	(44/18)		149.8	38.6	10	11.9	147.7	60.2	20	8.0
Mean2	(44/14)		150.0	38.2	8	14.8	149.1	61.2	19	9.4

Legend and explanation for Table 3-3.
– this anomalous site is excluded from computation of the overall mean.
Mean1(Mean2) is the overall mean direction of all sites (sites with more than two samples and $\alpha 95 < 20°$). Other notation is as in Table 3-1.

Table 3-4. Paleomagnetic data from Givetian (Middle Devonian) volcanics (locality KU)

			In Situ				Tilt corrected			
Site	N	A	D°	I°	k	α_{95}°	D°	I°	k	α_{95}°
Intermediate-temperature A component										
M9198	7/4	63/48	261.2	-72.5			249.0	-25.2	183	6.8
M9205	6/5	62/41	269.7	-72.2			251.7	-32.8	29	15.6
M9211	6/6	62/41	294.6	-78.1			254.6	-41.0	135	6.0
M9217#	6/6	269/16	276.5	-25.7			278.1	-41.5	11	21.2
M9223	6/4	54/38	219.1	-59.7			226.0	-22.4	19	21.8
N3858	7/7	9/22	246.3	-70.7			217.2	-53.9	102	6.0
N3865	6/6	9/22	238.0	-55.3			224.3	-38.5	84	7.7
N3871	6/6	9/22	234.6	-67.2			213.9	-48.9	24	13.9
N3883#	6/6	269/16	143.9	-47.1			132.9	-36.6	32	11.9
D7	7/6	85/20	278.0	-79.9			269.5	-60.1	44	10.2
D8	7/3	85/20	269.6	-67.6			267.6	-47.6	47	18.1
D9	7/6	85/20	235.6	-66.2			247.9	-47.7	22	14.8
D10	6/6	85/20	232.2	-73.8			249.6	-55.3	15	17.8
D11	7/6	85/20	262.7	-72.4			263.9	-52.4	16	17.2
Mean	(18/12)		248.5	-70.8	65	5.4	243.9	-45.3	20	9.9
High-temperature B component										
m9198	7/7	63/48	187.3	33.5			145.0	46.0	37	11.5
M9205-GC	*6/4*	*62/41*	*107.8*	*-20.5*			*130.5*	*-43.8*		*7.1*
M9211-GC	*6/4*	*62/41*	*99.2-*	*14.5*			*116.5*	*-44.1*		*29.2*
N3865-GC	*6/4*	*9/22*	*230.9*	*-49.3*			*219.7*	*-31.4*		*8.7*
N3871-GC	*6/3*	*9/22*	*96.5*	*-17.8*			*103.5*	*-17.5*		*25.9*
N3877	6/6	9/22	163.6	25.3			171.6	28.5	33	12.7
D7	7/4	85/20	0.7	-43.8			341.0	-44.4	12	27.1
D8	7/6	85/20	6.0	-53.1			338.3	-54.3	53	9.9
D9	7/7	85/20	18.1	-40.5			359.7	-47.4	63	7.9
D11	7/5	85/20	26.2	-38.3			9.5	-48.1	217	5.4
North	(4)		13.4 -	44.4	58	12.1	352.4	-49.3	58	12.1
South	(6)		178.2	30.7	64	9.4	162.3	40.0	38	12.3
Mean	(18/10)		183.9	38.4	34	8.5	167.0	44.3	41	7.8

Legend and explanation for Table 3-4.
- two anomalous sites were excluded from the computation of mean A-component directions; entries in italics represent great-circle poles rather than declinations and inclinations. North (South) are polarity-means for northward (southward) pointing directions, Other notations as in Tables 3-1 and 3-3.

Silurian rocks is confirmed by fold, reversal, and conglomerate tests (Levashova et al., 2003a). Our new Ludlovian AY result is also primary and reliable, as evidenced by adequate statistics and a positive conglomerate test.

A result from Lower-lower Middle Devonian volcanics (G1) and another one from Upper Silurian redbeds (G2) were reported by Grishin et al. (1997). Despite very limited statistics, the lack of the field tests and hence, rather low reliability (Table 3-5), these results are included in the analysis as "supporting" entries.

Burtman et al. (1998) studied Lower-lower Middle Devonian rocks and presented a mean direction based on principal component analysis, applied to stepwise demagnetization of 40 samples (out of 97 studied), of which 30 are reversed and 10 are of normal polarity. Although the sample directions are rather scattered, the mean appears statistically well defined, but this is only because unit weight was given to samples and not to sites (B1, Table 3-5); even so, the k-value is only 12. However, the fold and reversal tests are reported as positive. The most disturbing feature is the simple observation that Burtman et al. (1998) sampled the same locality KN as we did. Thus, the difference in declinations cannot be attributed to local tectonics. The in situ data (in figure 4 of Burtman et al. (1998)) display a cluster centered on our overall A-direction. We assume, therefore, that the mean direction represents the same late Paleozoic remagnetization as our secondary A-component. We assign the result of Burtman et al. (1998) to Permian remagnetization status, and exclude it from the discussion of Devonian paleogeography.

Upper Permian basalts from the southeastern part of the Chingiz Range are the youngest rocks that have been studied in the area. The Late Permian results (PA and PB, Table 5) are confirmed by a positive fold test and are reliable (Levashova et al., 2003b).

We consider these published and our new results together, resulting in a dataset consisting of inclinations (=paleolatitudes) as well as declinations from CL, SI, AY, KN&DG, KU, PA, and PB (Table 3-5), that can be used for tectonic analysis. The OE result can be used for paleolatitude analysis only. Finally, we will see that the supporting role of the G1 and G2 results will strengthen rather than diminish the conclusions.

Table 3-5. Summary of primary paleomagnetic results from northeastern Kazakhstan

Result	Age	Stat	Tests	D°	I°	k	α_{95}°	Plat °	REF
PA	P_l (260)	(8)	F	264.9	-50.2	107	4.8	+31±4	1
PB	P_l (260)	(8)	F	237.0	-47.9	216	3.4	+30±3	1
KU	D_m (388)	(10)	R	167.0	44.3	41	7.8	+26±6	TP
B1[#]	D_{e-m} (402)	40(?)	FR	52	41	12	6.4	+24±7	2
G1	D_{e-m} (402)	9(1)	NT	168	48	25	9.3	+29±12	3
KN&DG	D_{e-m} (402)	(18)	FR	147.7	60.2	20	8.0	+41±9	TP
G2	S_l (420)	12(2)	NT	144	11	-	13	+6±7	3
AY	S_{e-l} (425)	(12)	C	168.0	13.2	28	8.4	+7±4	TP
SI	S_e (433)	(12)	FCR	216.5	-2.8	12	13.3	-1±4	4
OE[##]	O_e (480)	(11)	F	*146.3*	-23.1	10	14.8	-12±4	5
CL	Cm_l (495)	(8)	F	109.1	-35.2	33	9.8	-19±6	5

Legend and exexplanation for Table 3-5.
- excluded (see text for detail);
- the elongated distribution of site-mean directions renders the mean declination (in italics) imprecise.
Directions are presented in stratigraphic coordinates. Age abbreviations: Cm, Cambrian, other period abbreviations are standard, subscripts e=early, m=middle and l=late; ages in Ma are from Gradstein and Ogg (2004). Stat = statistical treatment: numbers without parentheses represent samples, when given unit weight by the authors, whereas numbers in parentheses represent the number of sites. Tests, positive field tests: F, fold test; R, reversal test; C, conglomerate test; NT, no tests. Plat, paleolatitude, positive if in the northern hemisphere, with 95% confidence intervals. REF, reference: 1, Levashova et al. (2003b); 2, Burtman et al. (1998); 3, Grishin et al. (1997); 4, Levashova et al. (2003a); 5, Collins et al. (2003); TP, this paper. Other notation as in Table 3-1. Note that the G2 result is based on remagnetization circles only, so that the concentration parameter cannot be computed.

Overprint data

The locality-mean directions of postfolding magnetizations in Silurian and Devonian rocks of localities KU (this study) and from SI and GV (Levashova et al., 2003a) agree in situ within the size of the symbols (Fig. 3-9, Table 3-6). The KN&DG secondary component A after 35% unfolding is in close agreement with these three remagnetization directions (Fig. 3-9), despite the distance of about 200 km between the localities. Judging by the very tight grouping of overprint directions over a large area, we suggest that remagnetization was contemporaneous and of regional extent.

While the exclusively reversed polarity could be taken to suggest a remagnetization event during the reversed Kiaman superchron (ca. 315-265 Ma) (Opdyke and Channell, 1996), the mean overprint inclination of -70.4° ± 1.9° is steeper by about 20° than the mean inclination of -49° ± 4° of the prefolding and presumably primary remanence in the Upper Permian basalts from the PA and PB localities (Table 3-5; Levashova et al., 2003b). Similar very steep overprint inclinations were also found in other parts of the Chingiz area (Collins et al., 2003). It seems highly unlikely that the primary magnetization at localities PA and PB and the secondary magnetizations from the study area constitute an unbiased record of the same field. Hence one explanation is to assume that secondary components may have been distorted by subsequent tilting; in our particular case, that would amount to a tilt of about 20° to the northeast. Such a tilt might be compatible with the observed fault network (Fig. 3-2); however, any supportive geological evidence of such tilting, which must have been uniform and yet affecting a rather large area is absent.

A more likely solution is to assign somewhat younger ages to the remagnetization event. Latest Permian – Early Triassic magmatic rocks age are known in north Kazakhstan (Bekzhanov et al., 2000); one complex (Semeitau igneous suite), about 200 km to the north of our study area, has recently been dated as 248.2 ± 0.5 Ma by the $^{40}Ar/^{39}Ar$ method on sanidine (Lyons et al., 2002) and has given a paleopole that gives a direction (recalculated to our area; diamond in Fig. 3-9), which perfectly agrees with the overall mean of the secondary components. The Semeitau pole agrees well with a new mean pole on Siberian traps (Pavlov et al., 2007). Arguing against this earliest Triassic

age of the overprints, however, is that the reversal frequency close to the Permian-Triassic boundary was rather high (Opdyke and Channell, 1996), whereas normal polarity directions have not been observed in the Chingiz Range. We have difficulties imagining that the remagnetization event was of regional extent and yet very brief.

Thus it remains unclear whether overprint directions were of Kiaman age and distorted by younger deformation or whether they were acquired during a short remagnetization event near the Permian-Triassic boundary. Regardless, it is worth noting that all secondary directions from the Chingiz area concur both in declination and inclination with directions recalculated from the earliest Triassic APWP of Baltica (Torsvik et al., 2001), and thus, that they do not indicate any tilting, rotation, or relative displacements for such an age (Fig. 3-9).

Polarity choice

The declinations from the rocks ranging in age from Late Cambrian to Middle Devonian from the Chingiz area are generally to the southeast or south, while the inclinations change from older and moderate up to younger, moderate down values (Table 3-5). In contrast, Permian directions are southwest and up (or rarely, northeast and downwards). We know that by Permian time, when Siberia, Tarim, Baltica and the Kazakhstan areas were in the final stages of amalgamation, the study area must have been in the northern hemisphere, as uniformly agreed upon in the literature (e.g., Van der Voo, 1993; Didenko et al., 1994; Şengör and Natal'in, 1996; Smethurst et al., 1998a; Filippova et al., 2001; Stampfli and Borel, 2002; Kravchinsky et al., 2002a; Van der Voo et al., 2006; Cocks and Torsvik, 2007). Thus the NE/downwards Permian directions represent normal polarity.

Carboniferous data from the Chingiz area are absent, but a dual-polarity result from Upper Carboniferous-Lower Permian rocks from the central arm of the Balkhash-Ili volcanic belt (Abrajevitch et al., 2008) has an unambiguously normal polarity represented by NE and down directions. With respect to these late Paleozoic directions, and keeping the inclinations (and, hence, paleolatitudes) similar, the Early and Middle Devonian results display declinations that are rotated clockwise by more than 100° (Table 3-5).

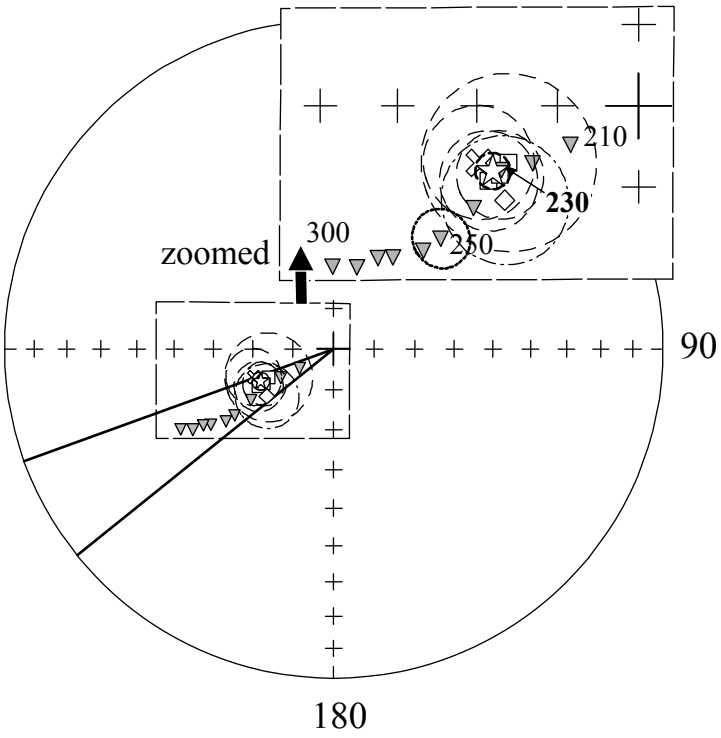

Figure 3-9. Stereonet of locality-mean overprint directions with confidence circles (thin lines): squares, locality-means in situ; oblique cross, the result for locality KN&DG after 35% unfolding. Star, the overall mean direction with associated confidence circle (thick line). Diamond, recalculated (see text) mean direction with confidence circle (dashed-dotted line) from the ca. 248 Ma old Semeitau igneous complex from north Kazakhstan (Lyons et al., 2002). Shaded triangles, reference directions recalculated from the APWP of Baltica with 10 m.y. increments (Torsvik et al., 2001). For clarity, the confidence circle is shown only for the 230 Ma direction. All data in (b) are upper hemisphere projections. Other notation as in Figure 3-4.

Table 3-6. Summary of overprint directions from northeastern Kazakhstan

		In Situ					Tilt corrected			
Site	N	A	D°	I°	k	α_{95}°	D°	I°	k	α_{95}°
KN&DG-A	(44/28)	35%	251.2	-68.2	16	7.2	220.3	-73.5	8	10.1
KU-comp. A	(18/12)	IS	243.5	-70.8	65	5.4	238.7	-45.3	20	9.9
GV	(6/6)	IS	243.4	-69.2	121	6.1	21.0	-62.4	25	13.7
SI	(18/5)	IS	246.4	-72.4	50	10.9	77.5	-56.6	<3	>60
Mean	[4/4]		246.2	-70.2	1304	2.5	249.5	-88.5	5	46.2

Legend and explanation for Table 3-6.
A is coordinate system: (35%) denotes the fact that the A-component at this locality is syn-tilting, estimated to have been acquired at 35% of the total tilting; IS denotes in situ data. Locality-mean overprint directions for Givetian (GV) and Lower Silurian (SI) rocks are from Levashova et al. (2003a). Mean is the overall mean overprint direction for KU, GV, and SI in situ, and KN&DG after 35% unfolding. N is the ratio of the number of (sites) [localities] studied/accepted. Other notation as in Table 3-1.

Devonian paleolatitudes were almost certainly in the northern hemisphere (see the above cited list of paleogeographic syntheses), implying that the Chingiz Range and vicinity suffered a large CW rotation in the interval between Middle Devonian and Early Permian time. The opposite polarity option would imply a highly unlikely motion through ca. 60° of latitude spanning the southern and the northern hemisphere during the above time interval while all the surrounding tectonic elements stayed in the northern hemisphere.

Silurian declinations generally agree with the Devonian ones (Table 3-5), except for the SI result, which is likely to have been deflected by local rotation because of abundant strike-slip faults (Levashova et al., 2003a). It is logical to assume normal polarity for the southeasterly and upward early Paleozoic directions (Table 3-5) of Collins et al. (2003), which then imply southern-hemisphere positions and a crossing of the equator by the Chingiz area in Silurian times. The opposite option would require a reversal of the steady northward motion of the Chingiz area, as indicated by the Silurian to Permian data, in addition to another rotation of ~180° in the Middle-Late Ordovician. Note also that all major cratons like Siberia, Baltica, and Tarim were steadily moving northward in the Paleozoic, so that a Kazakhstan unit bucking this trend seems improbable. All in all, we conclude that the Chingiz area was moving northward through the Paleozoic from low southern to moderate northern latitudes.

Declinations and rotations

The structural pattern of Kazakhstan is dominated by the strongly curved Devonian and late Paleozoic volcanic belts (Fig. 3-2), unconformably overlying older structures, which have been dismembered but still retain a suggestion of a horseshoe shape as well, e.g., for Ordovician subduction-related volcanics. Until the mid-Permian, the volcanics in the belts are of calc-alkaline affinity implying a continuous supra-subduction setting (Kurchavov, 1994; Tevelev, 2001). The horseshoe shape of the volcanic belts, marking the former subduction zone, has attracted attention of many geologists for a long time already. Some of them regarded the curvature of the volcanic belts as primary features (Zaytsev, 1984; Kurchavov, 2001), while others advocated oroclinal bending (Zonenshain et al., 1990; Şengör and Natal'in, 1996; Tevelev, 2001).

The proponents of oroclinal bending are not so unanimous, however, insofar as the timing of the rotations is concerned.

After a first attempt to test the hypothesis of oroclinal bending by Grishin et al. (1997), concluding that about half of the strike contrast was due to vertical-axis rotations, Levashova et al. (2003a) compared Ordovician and Silurian data from the Chingiz Range (OE and SI, Table 3-5) with results from the North Tien Shan that revealed a Late Ordovician paleolatitude of ~8ºS (Bazhenov et al., 2003). They observed that the two arms of the giant horseshoe had declinations that differed from each other by approximately 180°, provided that both areas were located in low southerly paleolatitudes during the Ordovician.

With new paleomagnetic data from the southern limb of the late Paleozoic volcanic belt, Van der Voo et al. (2006) re-analyzed the problem and concluded that rotations were ubiquitous but that the pattern and sequence of events are complex. The two limbs underwent at least two episodes of vertical-axis rotational movements with respect to each other. Up to some 90° of rotation could be attributed to large-scale east-west (present day coordinates) sinistral wrenching in an intracontinental setting during the Permo-Triassic between Siberia and Baltica, as envisioned earlier by Natal'in and Şengör (2005). Noteworthy is that these rotations are widespread, but not uniform: some areas near strike-slip faults have rotated, other areas have not (Van der Voo et al., 2006). The remaining (and equally large) component of the observed declination deviations was left available for an interpretation in terms of pre-Permian oroclinal bending.

Most recently, Abrajevitch et al. (2007) combined Silurian and Devonian data from the volcanic belts, and first corrected for the post-Middle Permian rotations due to the just-described local small-scale block motions within the larger-scale sinistral wrench zone (Van der Voo et al., 2006). They could carry out such corrections, wherever (fortunately) Permian primary or overprint directions showed through their declination deviation what the magnitude of Late Permian – Early Triassic rotations had been. The mid-Paleozoic declinations, so corrected, now showed a remarkably consistent pattern, all generally pointing to the north in the southern arm (Fig. 3-10). Using the then-available Silurian and Devonian results from the Chingiz Range, Abrajevitch et al. (2007)

could conclude that the strongly curved Devonian Volcanic Belt was originally a nearly rectilinear structure. Our current study puts the database from the northeastern arm on a much firmer footing and reconfirms the oroclinal rotations.

In the Chingiz area, there is no need for a correction for latest Paleozoic rotations, because the primary Permian and all Permo-Triassic remagnetization directions agree with each other and the reference paths of Baltica (Fig. 3-9). We can conclude that the primary Devonian and Silurian declinations reflect pre-Late Permian rotations only. As already noted, all these directions point to the southwest to (mostly) southeast (Fig. 3-10, Table 3-5), confirming the preliminary analysis of Abrajevitch et al. (2007) on oroclinal bending of the Devonian volcanic belt. The timing of this oroclinal bending remains constrained to the interval between Middle Devonian and Middle Permian in the absence of reliable Carboniferous paleomagnetic results from the northern and northeastern arms.

Paleolatitudes

In this section, we compare the paleolatitudes derived from the entire set of Paleozoic paleomagnetic data from the Chingiz with those of the major cratons around the Ural-Mongol mobile belt (UMB). Following paleomagnetic custom for such comparisons, we calculate reference paleolatitudes by extrapolation from an APWP for an optimal location in the area of interest; for this study we chose 48.5°N, 78.5°E within the Chingiz Range. Such a calculation is a prediction of the paleolatitude the Chingiz Range would have had, if it had stayed rigidly attached to the reference craton since the time of magnetization acquisition. Any deviation between prediction and an observed paleolatitude then becomes a measure of the relative displacements, in terms of latitudinal movements and relative rotations.

Only for Baltica does an adequately determined apparent polar wander path (APWP) exist for the entire interval of Early Ordovician through Late Permian. For Siberia, the data are unreliable for most of the middle and late Paleozoic (Cocks and Torsvik, 2007), with the exception of one good pole for ~360 Ma (Kravchinsky et al., 2002b), whereas the Tarim dataset is simply too limited for construction of an APWP before Carboniferous times.

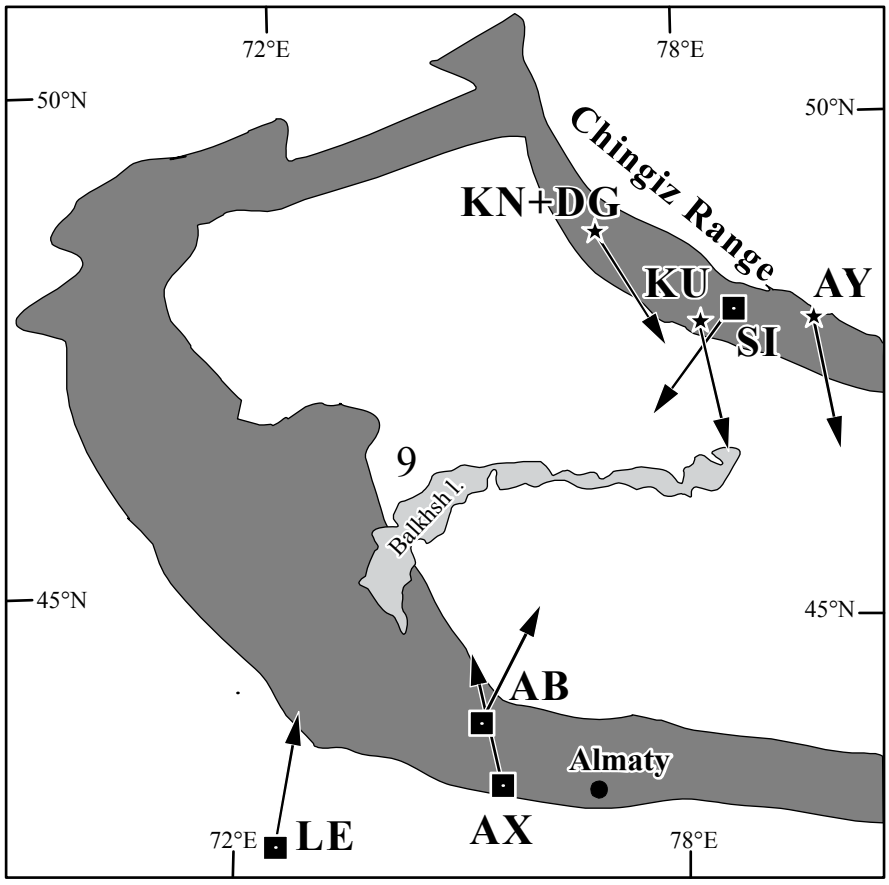

Figure 3-10. Schematic outline of the Devonian volcanic belt (gray; simplified from Figure 3-2) with Silurian and Devonian paleomagnetic declinations (arrows). Only the results are shown that are based on full demagnetization and confirmed by positive field tests. Stars are the results from this study labeled as in the text. Published data (squares) are from: SI, Levashova et al. (2003a); AX, Alexyutin et al. (2005); AB, Abrajevitch et al. (2007); LE, Levashova et al. (2007). The last two results are corrected for Late Paleozoic rotations as described in Abrajevitch et al. (2007).

For Baltica, we can compute two versions (Fig. 3-11a), using the reference APWP's of Van der Voo (1993) and Smethurst et al. (1998b). The two plots concur reasonably well, despite different selection criteria and smoothing approaches in constructing the APWP. To first approximation, the Chingiz observations show reasonable agreement with these plots for the Early Silurian – Late Permian interval. In contrast, the observed early Paleozoic paleolatitudes differ from the predicted ones, and show that there is much less poleward motion of Chingiz than what is extrapolated from Baltica for Cambrian and Ordovician time (Fig. 3-11a).

The reference APWP for Siberia became different after the ~360 Ma pole of Kravchinsky et al. (2002b) was published, as illustrated in Figure 11b. As our starting point, we used the APWP of Cocks and Torsvik (2007), who presented it in two options, CT1 and CT2, depending on whether the Early Permian pole of Pisarevsky et al. (2006) is included, or excluded, respectively (Fig. 3-11b). This result was presented as the first well-dated Early Permian pole for Siberia based on fully demagnetized data, but only five dykes could be studied, which is nowadays considered an inadequate quantity because it usually fails to average secular variation and other sources of noise. Our comparison of CT1 predictions with primary Late Permian PA and PB poles shows (Fig. 3-11b) that the pole of Pisarevsky et al. (2006) would imply that Kazakhstan and Siberia had to converge by more than 3000 km in the Late Permian, which contradicts most available geological data. Due to these reasons, we prefer the comparison involving CT-2.

The post-Ordovician APWP of Cocks and Torsvik (2007) is based on very limited data, and the path strongly depends on the degree of smoothing by spline-fitting, which may introduce artificial maxima and minima during intervals with few or no data. To check on such problems we also use individual poles from Siberia instead of Cocks and Torsvik's APWP (Table 3-7, Fig. 3-11c). Because the data are abundant for the early Paleozoic, we included only results based on detailed demagnetization and principal component analysis.

Recently Shatsillo et al. (2007) published a paleomagnetic result from Early Silurian sedimentary rocks in Siberia. They isolated high-temperature, presumably primary components (#6, Table 3-7) as well as intermediate-temperature secondary

components (#5, Table 3-7). The latter are inferred to be of Late Silurian – Early-Middle Devonian age. Their high temperature Early Silurian pole is drastically different from a roughly coeval pole (#7, Table 3-7) of Torsvik et al. (1995). As the latter result is based on only nine samples and coincides rather precisely with the remagnetization pole of Shatsillo et al. (2007), we have excluded #7 from Figure 3-11c.

A paleomagnetic pole of latest Silurian-earliest Devonian age was reported from the Tuva area to the south of the Siberian craton (see Fig. 3-1 for location) by Bachtadse et al. (2000). This area belongs to the mobile belt that borders the craton; geological data, however, indicate that the Tuva area docked to Siberia by Ordovician time (Mossakovsky et al., 1993; Dobretsov et al., 1995, Cocks and Torsvik, 2007). Of course, some rotations could occur and, moreover, Bachtadse et al. (2000) did document them. Our calculations show that the paleolatitude predicted for Chingiz from the Tuva result varied narrowly (±3º) unless the Tuva area underwent a later vertical-axis rotation >20º, which seems unlikely. Hence we used the Tuva result (#4) as a proxy for the cratonic pole and recalculated it to our study area. Additional confirmation of this comes from the fact that the Tuva pole of Bachtadse et al. (2000) and the overprint pole of Shatsillo et al. (2007) agree rather well, differing by about 7°.

With the comparison provided by the set of unit poles from Siberia (Fig. 3-11c) we find that the observed Cambrian, Ordovician, and Silurian paleolatitudes from Chingiz fall generally within its distribution, and the extrapolated Silurian – earliest Devonian paleolatitude from Tuva (#4) also agrees well with the average of our new KU and KN&DG results. Because the Silurian – Permian APWP for Siberia is still so sparsely populated, any comparison with Siberia's positions in this interval inevitably remains speculative. Nevertheless, the possibility is negligible that the data from Chingiz and Siberia show the good agreement of Figure 3-11c just by chance. This implies that these two units were moving for more than 100 My in such a way that they retained a certain paleolatitudinal relationship that precludes large-scale separations (>1500 km or so) unless followed quickly and dramatically by equally large re-approaches in what must be regarded as unlikely plate tectonic schemes for the 500 – 390 Ma interval. In other words, we cannot preclude, but find highly improbable, the notion that subsequent relative motions completely cancelled each other. To conclude this section, we favor the

Table 3-7. Paleozoic paleomagnetic poles of Siberia

Age			Poles				
N	ST	NU	Φ°	Λ°	A_{95}°	Plat	Reference
1[#]	P_l-T_e	251	57.2	151.1	4.0	47.5	Pavlov et al., 2007
2[##]	P_e	275	50.5	121.4	16.7	62.5	Pisarevsky et al., 2006
3	D_l-C_e	354	11.1	149.7	8.9	20.7	Kravchinsky et al., 2002b
4	S_l-D_e	410	-12	102	3	26	Bachtadse et al., 2000
5[§]	S_1-D_m	~400	-5.5	98.6	4.9	33.2	Shatsillo et al., 2007
6	S_e	433	-19.0	128.0	4.6	9.4	Shatsillo et al., 2007
7[##]	$O_l$as-S_e	439	3.1	118.1	14.8	33.4	Torsvik et al., 1995
8	$O_l$as-S_e	444	-13.9	124.1	5.9	15.7	Gallet and Pavlov, 1996
9	$O_l$as	450	-21	109	12.8	15.3	Torsvik et al., 1995
10	O_l	453	-31.6	140.5	6.9	-7.3	Pavlov et al., 2003
11	$O_m$ld	463	-24.1	152.4	3.3	-7.9	Pavlov et al., 2008
12	$O_m$ld	463	-22.7	157.6	2.8	-10.0	Gallet and Pavlov, 1996
13[§§]	O_m	464	-27.6	124.8	4.0	3.4	Iosifidi et al., 1999
14	O_m	468	-32	139	2.2	-6.9	Torsvik et al., 1995
15	$O_m$lv	469	-35.2	153.2	3.6	-16.8	Pavlov et al., 2003
16	$O_m$lv	469	-30.9	152.7	2.8	-13.3	Pavlov and Gallet, 1998
17	$O_m$lv	469	-29.8	156.6	3.1	-14.7	Gallet and Pavlov, 1996
18	$O_e$ar	478	-36.4	158.2	6.5	-20.4	Pavlov et al., 2003
19	$O_e$ar	478	-33.9	151.7	1.9	-15.0	Gallet and Pavlov, 1996
20	O_e	480	-42.2	128.1	5.8	-10.7	Surkis et al., 1999
21	$O_e$tr	483	-35.2	127.2	4.1	-4.3	Pavlov and Gallet, 1998
22	$O_e$tr	483	-40.3	137.5	6.9	-13.0	Gallet et Pavlov, 1996
23	Cm_l	495	-36.1	130.7	2.6	-6.5	Pavlov and Gallet, 1998
24	Cm_l	495	-37.0	138.4	4.8	-10.7	Gallet et Pavlov, 1996
25	Cm_m	501	-37.7	124.0	4.5	-5.2	Rodionov et al., 1998
26	Cm_m	507	-41.9	135.8	2.3	-13.5	Pavlov and Gallet, 2001
27	Cm_m	507	-43.7	140.5	2.6	-17	Gallet et al., 2003
28	Cm_m	507	-36.4	139.6	4.0	-10.8	Pisarevsky et al., 1997

Legend and explanation for Table 3-7.

[#] - the overall mean pole for the Siberian traps (NSP4 pole from Pavlov et al. (2007))

[##] - discarded from our analysis (see text)

[§] - Overprint combined mean pole from Shatsillo et al. (2007) of presumably Late Silurian-Middle Devonian age;

[§§] - We used one pole for combined normal and reversed data from the Middle Ordovician rocks (Iosifidi et al., 1999) in contrast to Cocks and Torsvik, (2007), who used two poles (for normal and reverse polarity separately) in their compilation.

Other explanations: Ages of the rocks (components) are as inferred by the authors of the data: ST, stratigraphic age (as, Ashgillian; ld, Llandeilian, lv, Llanvirnian, ar, Arenigian, tr, Tremadocian), NU, numerical age interpolated from Geologic Time Scale (Gradstein and Ogg, 2004). Poles are given as latitude (Φ) and longitude (Λ) of the north poles together with corresponding radii of the 95% confidence circle (A_{95}). Plat, paleolatitude of the reference point at 48.5°N, 78.5°E, calculated by extrapolation from the entry's paleopole.

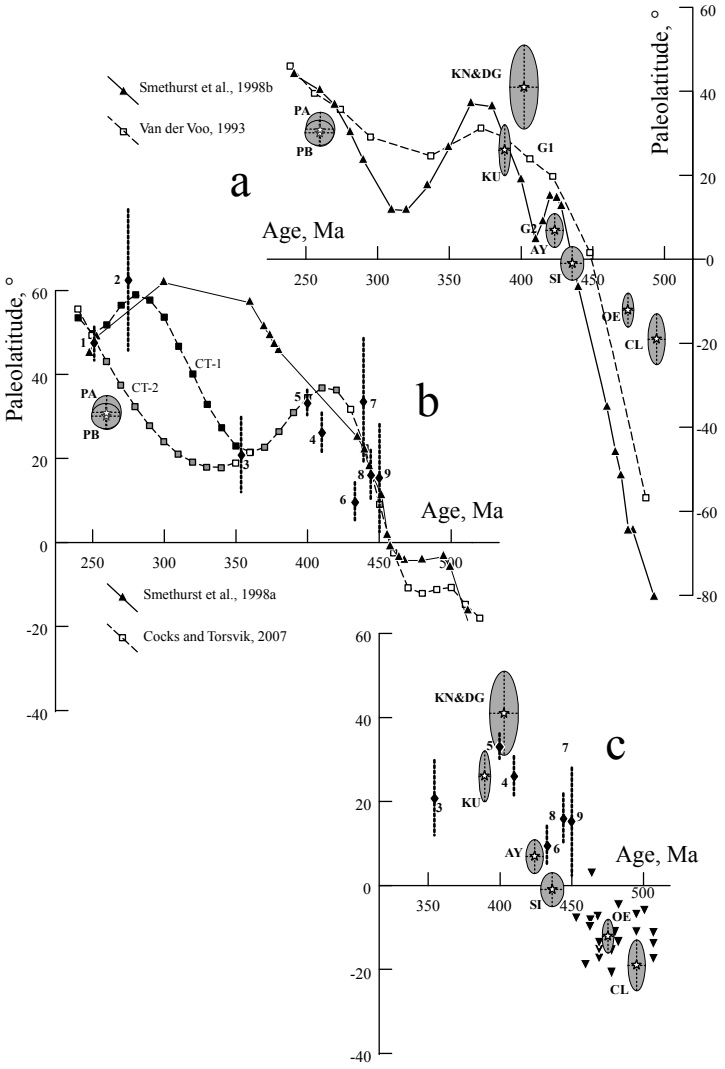

Figure 3-11. Plots of paleolatitude versus age for reference and observed data. (a) Comparison of the reference paleolatitudes extrapolated from Baltica's APWP to the Chingiz Range and the observed data. The observed data are those selected as more reliable, as discussed in the text, and have been plotted as stars with shaded ovals (95% confidence limits) with labels as in the text and Table 3-5. (b) Comparison between paleolatitudes extrapolated from two versions (CT1, CT2, see text) of the Siberian apparent polar wander path of Cocks and Torsvik (2007) and individual Siberian poles (numbered as in Table7) with ages <450 Ma (filled diamonds); latitudinal error bars are shown as thick dotted lines. Gray squares are for intervals devoid of data. Also shown, as stars with shaded error ellipses, are two Late Permian results from NE Kazakhstan (Levashova et al., 2003b). (c) Comparison between the reference paleolatitudes extrapolated from the individual Siberian poles (as in (b)) and the observed Chingiz data (as in (a)) for ~500 – 350 Ma. Selected reliable Siberian poles >450 Ma are shown as inverted triangles without error bars.

idea that Siberia and the Chingiz moved with a certain coherence after the Late Cambrian, similar to the conclusion we reached about the Baltica – NTS (= North Tien Shan) pair in an earlier report (Levashova et al., 2007).

Comparison with published paleogeographic models

Not surprisingly, most of the thus far published paleogeographic models do not assume any kinematic affiliation between Siberia and Chingiz. According to several Russian authors (Mossakovsky et al., 1993; Didenko et al., 1994; Filippova et al., 2001; Kheraskova et al., 2003), the UMB was formed by the closure of the Paleoasian Ocean, in which an archipelago of scattered Precambrian microcontinents, oceanic basins, and island arc segments existed in the Paleozoic. In their view, the most important role in the UMB amalgamation is played by diachronous opening and closing of the intervening oceans and, therefore, by similarly diachronous collisions of microcontinents and island arcs. The essential concepts of such models are similar, but they vary markedly in their details. For instance, Mossakovsky et al. (1993) and Didenko et al. (1994) assume that most microcontinents and island arcs docked to Siberia and formed a composite Kazakhstanian – Siberian continent in the Silurian, whereas Filippova et al. (2001) suggested that several of these units collided with each other first, thereby forming an independently moving mid-Paleozoic Kazakhstanian continent.

A different group of scenarios envisions the existence of a long and prominent volcanic arc system (Şengör and Natal'in, 1996; Yakubchuk et al., 2001; 2002; Stampfli and Borel, 2002). Şengör and Natal'in (1996), for instance, assumed that a continuous Kipchak Arc connected the Siberian and Baltica cratons in the early Paleozoic. In their views, arc motions are therefore linked to the kinematics of Siberia and Baltica, so that a certain coherence of the Siberian and Chingiz paleolatitudes, or those between Baltica and North Tien Shan, is to be expected. As is clear from our previous section, we see confirmation to some extent for these ideas in the paleomagnetic data (see also Levashova et al., 2007).

At the same time, much detail in the model of Şengör and Natal'in (1996) remains to be validated, as it assumes very specific kinematics of the major cratons. For example, from the Vendian until the end of the Devonian, Siberia would have to have been located

about 2000 km to the north from Baltica (Fig. 3-12 b). Such a configuration is necessary for the existence of a large ocean (called Khanty-Mansi) between Baltica and Siberia that is thought to have been bounded by the Kipchak Arc as a long-lived subduction feature. Further discussion of this topic is outside the scope of this paper, not because it is irrelevant, but because with the paleomagnetic contributions of our studies we cannot make inroads towards resolution or rejection of several such aspects.

The Early Silurian pole of Shatsillo et al. (2007) places Siberia closer to Baltica than most other paleogeographic portrayals for Silurian time, and also closer than is typically shown for Ordovician or Devonian times. Thus, it appears that the relative positions of Baltica and Siberia in the middle Paleozoic may have varied to some extent. We make an attempt to show schematically the paleogeography of Baltica, Kazakhstan and Siberia, while satisfying the following constraints: (1) The Chingiz is moving in accord with, and remains close to, Siberia (this study); (2) The Kokchetav-North Tien Shan domain (KNTD) is moving approximately in accord with Baltica (Levashova et al., 2007); (3) The original Devonian volcanic belt is rectilinear and trends about 135° (Abrajevitch et al., 2007), and (4) Baltica and Siberia are in the latitudinal positions mandated by their paleomagnetic data.

Note in particular, that 1) and 2) do not imply an absolutely rigid connection between the cratons and UMB units, but suggest rather that a limit should be placed on the possible relative motions between them to a value of 1000 km or less.

With this information and limits in mind, we propose a schematic reconstruction of Baltica, Kazakhstan and Siberia for mid-Silurian time (Fig. 3-12b). The reconstruction differs from previous paleogeographic configurations in a more westerly position of Siberia with respect to Baltica as well as a nearly rectilinear “ribbon” Kazakhstan continent, that is in sharp contrast to much more complicated predictions of other authors.

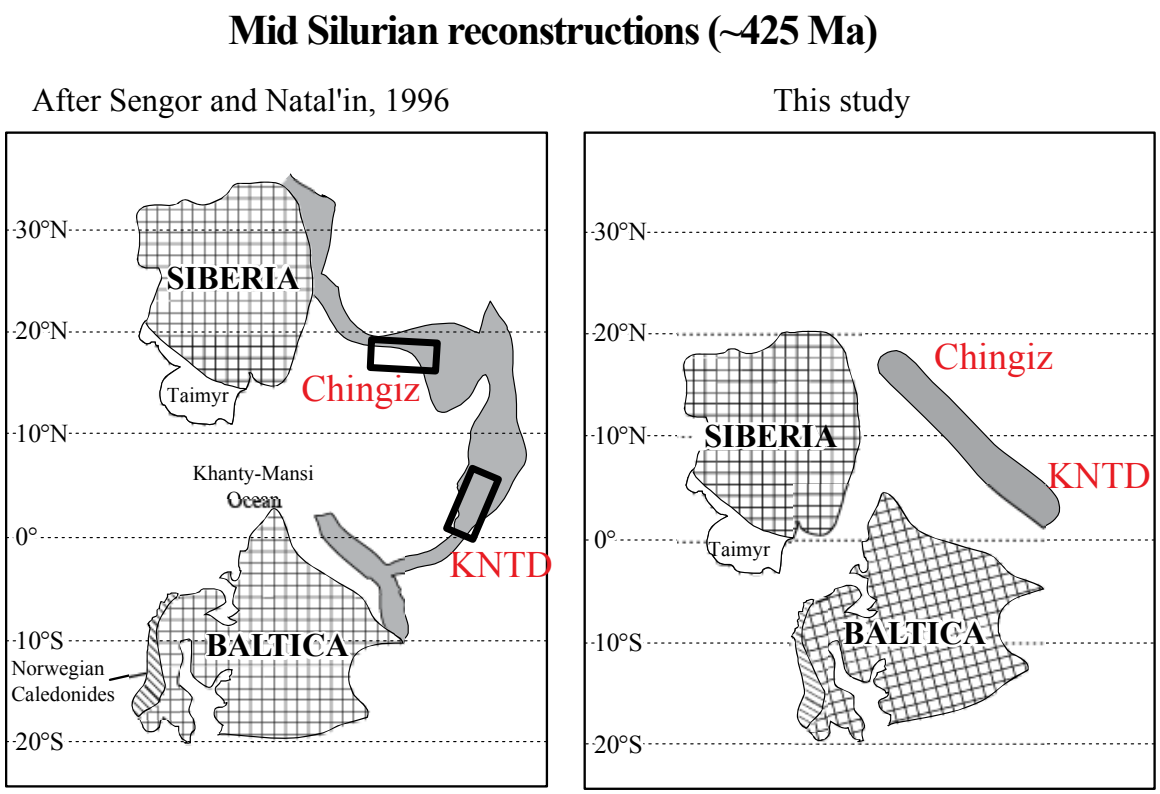

Figure 3-12. Reconstruction of the Ural-Mongol belt and the major cratons of Baltica and Siberia (cross-hatched) for mid-Silurian time. (a) Reconstruction after Şengör and Natal'in (1996). Note ca. 2000 km latitudinal separation of Baltica and Siberia and complicated form of external active margin of the Ural-Mongol belt (gray). (b) The position of Siberia is in accord with the new paleopole of Shatsillo et al. (2007); the Devonian volcanic belt and adjacent parts of Kazakhstan are shown as a rectilinear ribbon continent (shaded). See text for more detail.

Conclusions

Our paleomagnetic study of mid-Silurian to Middle Devonian volcanics from three localities in the Chingiz Range of NE Kazakhstan yields characteristic and likely primary magnetizations as well as overprint directions. The agreement of the latter data with extrapolated earliest Triassic predictions from Baltica or Siberia implies that strike-slip fault- related rotations are not present in the Chingiz Range, unlike the abundance of such rotations in the North Tien Shan branch of the Balkhash-Ili volcanic belt (Van der Voo et al., 2006). In contrast, presumed primary declinations indicate a very large rotation of the Chingiz area after the Middle Devonian, with respect to Baltica as well as the North Tien Shan. This rotation fits into a model that advocates oroclinal bending of up to 180º within the strongly curved Devonian volcanic belt of Kazakhstan (Abrajevitch et al., 2007).

We find, in contrast with most previous paleogeographic models, that the Chingiz block has not been far away from the Siberian craton during much of the Paleozoic. In turn, this requires a considerable revision of existing and rather disparate paleogeographic models for Central Asia. We do present a possible paleogeography of Baltica, Siberia and Kazakhstan for mid-Silurian time at ca. 425 Ma (Fig. 3-12b) but would like to stress that this very schematic reconstruction is just a passing stage on the road to improved understanding of the process of Eurasia amalgamation.

Acknowledgements

This study was supported by the Division of Earth Sciences and the Office of International Science and Engineering's Eastern and Central Europe Program of the U.S. National Science Foundation, grant EAR 0335882. Support was also derived from the Russian Foundation of Basic Research, grants 04-05-64050, 05-05-65105 and 07-05-00021 and Program No. 8 of the Earth Science Division, Russian Academy of Sciences. We thank many colleagues from the Scientific Station of the Russian Academy of Sciences in Bishkek (Kyrgyzstan) for logistic support of the fieldwork. We warmly acknowledge Phil McCausland's participation in the fieldwork. We are in debt to Andrei

Shatsillo and Vladimir Pavlov, who kindly provided us with unpublished results, and to Zhengxiang Li and Sergey Pisarevsky for helpful discussions.

References

Abrajevitch, A.V., Van der Voo, R., Levashova, N.M., Bazhenov, M.L. 2007. Paleomagnetism of the mid-Devonian Kurgasholak Formation, Southern Kazakhstan: Constraints on the Devonian paleogeography and oroclinal bending of the Kazakhstan volcanic arc. *Tectonophysics*, v. 441, 67–84.

Abrajevitch, A., Van der Voo, R., Bazhenov, M. L., Levashova, N. M., McCausland, P. J. A. 2008. The role of the Kazakhstan orocline in the late Paleozoic amalgamation of Eurasia, *Tectonophysics*, in review.

Alexyutin, M.V., Bachtadse, V., Alexeiev, D.V., and Nikitina, O.I. 2005. Paleomagnetism of Ordovician and Silurian rocks from the Chu-Yili and Kendyktas mountains, South Kazakhstan. *Geophysical Journal International*, 162, 321-331.

Bachtadse, V., Pavlov, V.E., Kazansky, A.Y., Tait, J.A. 2000. Siluro-Devonian paleomagnetic results from the Tuva Terrane (southern Siberia, Russia): implications for the paleogeography of Siberia. *Journal of Geophysical Research*, 105, 13509-13518.

Bazhenov, M.L., Collins, A.Q., Degtyarev, K.E., Levashova, N.M., Mikolaichuk, A.V., Pavlov, V.E., Van der Voo, R. 2003. Paleozoic northward drift of the North Tien Shan (Central Asia) as revealed by Ordovician and Carboniferous paleomagnetism. *Tectonophysics*, 366, 113-141.

Bekzhanov, G.R., Koshkin, V.Y., Nikitchenko, I.I., Skrinnik, L.I., Azizov, T.M., Timush, A.V. 2000. Geological structure of Kazakhstan. Almaty, Acad. Mineral Resources of Republic of Kazakhstan, 394 p. (in Russian).

Bogdanov, A.A. 1965. Tectonic setting of the Paleozoides of Central Kazakhstan and the Tien Shan. MOIP Bulletin, Geolog. Section, XL, no. 5, 40-68 (in Russian).

Burtman, V.S., Gurary, G.Z., Belenky, A.V., Kudasheva, I.A. 1998. Kazakhstan and the Altai in the Devonian: Paleomagnetic evidence. *Geotectonics*, 32, no. 6, 63-71.

Cocks, L.R.M., Torsvik, T.H. 2007. Siberia, the wandering northern terrane, and its changing geography through the Palaeozoic. *Earth-Science Reviews*, 82, 29-74.

Cogné, J.P. 2003. PaleoMac: a Macintosh application for treating paleomagnetic data and making plate reconstructions. *Geochemistry, Geophysics, Geosystems*, 4(1), 1007, doi:10.1029/2001GC000227.

Collins, A.Q., Degtyarev, K.E., Levashova, N.M., Bazhenov, M.L., Van der Voo, R. 2003. Early Paleozoic paleomagnetism of east Kazakhstan: implications for paleolatitudinal drift of tectonic elements within the Ural-Mongol belt: *Tectonophysics*, 377, 229-247.

Degtyarev, K.E., Ryazantsev, A.V. 1993. Geology of the orogenic Silurian and the structures with continuous sections in the Caledonides of Kazakhstan: *in* Milanovsky, E.E., ed., Geology and Metallogeny of Central Kazakhstan: Moscow, Nauka, 64-82 (in Russian).

Degtyarev, K.E. 1999. Tectonic evolution of the Early Paleozoic active margin in Kazakhstan: Moscow, Nauka, 123 p. (in Russian).

Degtyarev, K.E. 2003. The position of the Aktau-Junngar microcontinent in the Paleozoides of Central Kazakhstan. *Geotectonics*, 37(4), 14-34. (in Russian).

Degtyarev, K.E., Tolmacheva, T.Y. 2005. Oblique strike-slips and their role in disturbance of lateral structural row of the Early Paleozoic Chingiz island arc system, East Kazakhstan: *in* Ruzhentsev, S.V., et al., eds., Essays on regional tectonics, Book 2, Kazakhstan, Tien Shan, Polar Urals. Moscow, Nauka, 40-67 (in Russian).

Dercourt, J., et al. 1986. Geologic evolution of the Tethys belt from the Atlantic to the Pamirs since the Lias. *Tectonophysics*, 123, 241-315.

Didenko, A.N., Mossakovsky, A.A., Pechersky, D.M., Ruzhentsev, S.V., Samygin, S.G., Kheraskova, T.N. 1994. Geodynamics of Paleozoic oceans of Central Asia. *Geology and Geophysics*, 7-8, 59-75 (in Russian).

Dobretsov, N.L., Berzin, N.A., Buslov, M.M. 1995. Opening and tectonic evolution of the Paleoasian ocean. *International Geology Review*, 37, 335-360.

Filippova, I.B., Bush, V.A., Didenko, A.N. 2001. Middle Paleozoic subduction belts: The leading factor in the formation of the Central Asian fold-and-thrust belt. *Russian Journal of Earth Sciences*, 3(6) 405–426.

Fisher, R.A. 1953. Dispersion on a sphere. *Proceedings of Royal Society*, A217, p. 295-305.

Gallet, Y., Pavlov, V.E. 1996. Magnetostratigraphy of the Moyero river section (northwestern Siberia): a constraint on the geomagnetic reversal frequency during the Early Palaeozoic. *Geophysical Journal International*, 125, 95-105.

Gallet, Y., Pavlov, V.E., Courtillot, V. 2003. Magnetic reversal frequency and apparent polar wander of the Siberian platform in the earliest Palaeozoic, inferred from the Khorbusuonka river section (northeastern Siberia). *Geophysical Journal International*, 154, 829-840.

Gradstein, F.M., Ogg, J.G., Smith, A.G., eds. 2004. A geologic time scale 2004: Cambridge, Cambridge University Press, 589 p. (see www.stratigraphy.org) .

Grishin, D.V., Pechersky, D.M., Degtyarev, K.E. 1997. Paleomagnetism and reconstruction of Middle Paleozoic structure of Central Kazakhstan. *Geotectonics*, 31(1), 71-81. (in Russian).

Iosifidi, A.G., Khramov, A.N., Rodionov, V.P., Pisarevsky, S.A., Popov, V.V. 1999. Geomagnetic reversals in the Early Palaeozoic: 2. A nonsynchronous record of Middle Ordovician reversals in the Berezovskaya Section, southern Siberian Platform. *Physics of the Solid Earth*, 35(1), 24-32 (in Russian).

Kheraskova, T. N., Didenko, A.N., Bush, V.A., Volozh, Y.A. 2003. The Vendian-Early Paleozoic history of the continental margin of eastern Paleogondwana, Paleoasian Ocean, and Central Asian foldbelt: *Russian Journal of Earth Sciences*, 5(3), 165–184.

Kirschvink, J.L. 1980. The least-square line and plane and the analysis of palaeomagnetic data. *Geophysical Journal of the Royal Astronomical Society*, 62, 699-718.

Kravchinsky, V.A., Sorokin, A.A., Courtillot, V. 2002a. Paleomagnetism of Paleozoic and Mesozoic sediments of southern margin of Mongol-Okhotsk ocean, Far East of Russia. *Journal of Geophysical Research*, 107, B10, 2253, doi: 10.1029/2001JB000672.

Kravchinsky, V.A., Konstantinov, K.M., Courtillot, V., Savrasov, J.I., Valet, J.-P., Cherniy, S.D., Mishenin, S.G., Parasotka, B.S. 2002b. Palaeomagnetism of East Siberian traps and kimberlites: two new poles and palaeogeographic reconstructions at about 360 and 250 Ma. *Geophysical Journal International*, 148, 1-33.

Kurchavov, A.M. 1994. The lateral variability and evolution of orogenic volcanism in the fold belts. *Geotectonics*, 28(2), 3-18 (in Russian).

Kurchavov, A.M. 2001. Geodynamic setting of Devonian continental volcanism of Kazakhstan and southern West Siberia, *in* Milanovsky, E.E., et al., eds., Geology of Kazakhstan and the problems of the Ural-Mongol fold belt. Moscow, Moscow State University, 65-72 (in Russian) .

Levashova, N.M., Degtyarev, K.E., M.L. Bazhenov, M.L., Collins, A.Q., Van der Voo, R. 2003a. Middle Paleozoic paleomagnetism of east Kazakhstan: post-Middle Devonian rotations in a large-scale orocline in the central Ural-Mongol belt. *Tectonophysics*, 377, 249-268.

Levashova, N.M., Degtyarev, K.E., M.L. Bazhenov, M.L., Collins, A.Q., Van der Voo, R.. 2003b. Permian Paleomagnetism of East Kazakhstan and the Amalgamation of Eurasia. *Geophysical Journal International*, 152, 677-687.

Levashova, N.M., Mikolaichuk, A.V., McCausland, P.J.A., Bazhenov, M.L., Van der Voo, R. 2007. Devonian paleomagnetism of the North Tien Shan: implications for Middle-Late Paleozoic paleogeography during the assembly of Eurasia. *Earth and Planetary Science Letters*, 257, 104–120.

Lyons, J.J., Coe, R.S., Zhao, X., Renne, P.R., Kazansky, A.Y., Izokh, A.E., Kungurtsev, L.V., Mitrokhin, D.V. 2002. Paleomagnetism of the early Triassic Semeitau igneous series, eastern Kazakhstan. *Journal of Geophysical Research*, 107, no. B7, 10.1029/2001JB000521.

Mardia, K.V. 1972. Statistics of directional data. London, Academic Press, 357 p..

McElhinny, M.W. 1964. Statistical significance of the fold test in palaeomagnetism. *Geophysical Journal of the Royal Astronomical Society*, 8, 338-340.

McFadden, P.L., McElhinny, M.W. 1988. The combined analysis of remagnetization circles and direct observations in palaeomagnetism. Earth *and Planetary Science Letters*, 87, 161-172.

McFadden, P.L., Reid, A.B. 1982. Analysis of paleomagnetic inclination data. *Geophysical Journal of the Royal Astronomical Society*, 69, 307-319.

Merrill, R.T., McElhinny, M.W., McFadden, P.L. 1996. The magnetic field of the Earth: Acad. Press, San Diego, 527 p.

Mossakovsky, A.A., Ruzhentsev, S.V., Samygin, S.G., Kheraskova, T.N. 1993 Central Asian fold belt. Geodynamic evolution and formation: *Geotectonics*, 27(6), 3-32.

Natal'in, B.A., Şengör, A.M.C. 2005. Late Palaeozoic to Triassic evolution of the Turan and Scythian platforms: the pre-history of the palaeo-Tethyan closure. *Tectonophysics*, 404, 175-202.

Opdyke, N.D., Channell, J.E.T. 1996. Magnetic stratigraphy. International Geophysics Series, v. 64, London, New York, Academic Press, 346 p.

Pavlov, V.E., Gallet, Y. 1998. Upper Cambrian to Middle Ordovician magnetostratigraphy from the Kulumbe river section (northwestern Siberia). *Physics of the Earth and Planetary Interiors*, 108, 49-59.

Pavlov, V.E., Gallet, Y. 2001. Middle Cambrian high magnetic reversal frequency (Kulumbe River section, northwestern Siberia) and reversal behavior during the Early Palaeozoic. *Earth and Planetary Science Letters*, 185, 173-183.

Pavlov, V.E., Shatsillo, A.V., Veselovsky, R.V. 2003. Magnetostratigraphy of the Middle Angara Ordovician section: more evidence in support of the third Phanerozoic superchron, *in* Gapeev, A.K., ed., Paleomagnetism and rock magnetism: theory, practice and experiment: GEOS, Moscow, p. 57-60 (in Russian).

Pavlov, V.E., Courtillot, V., Bazhenov, M.L., Veselovsky, R.V. 2007. Paleomagnetism of the Siberian traps: new data and a new overall 250 Ma pole for Siberia. *Tectonophysics*, 443, 72–92.

Pavlov, V., Gallet, Y., Bachtadse, V., Mikhailov, V. 2008. New paleomagnetic data for the Middle Cambrian and Middle Ordovician of the Siberian platform: Llandeilian magnetostratigraphy and the hypothesis of relative rotation between the Aldan and Anabar-Angara blocks. *Earth and Planetary Science Letters*, (submitted).

Pisarevsky, S.A., Gurevich, E.L., Khramov, A.N. 1997. Paleomagnetism of Lower Cambrian sediments from the Olenek river section (northern Siberia): paleopoles and the problem of magnetic polarity in the Early Cambrian. *Geophysical Journal International*, 130, 746-756.

Pisarevsky, S. A., Gladkochub, D.P., Donskaya, T.A., De Waele, B., Mazukabzov, A.M. 2006. Palaeomagnetism and geochronology of mafic dykes in south Siberia, Russia: the first precisely dated Early Permian palaeomagnetic pole from the Siberian craton. *Geophysical Journal International*, 167, p. 649-658.

Puchkov, V.N. 1997. Tectonics of the Urals: modern conceptions. *Geotectonics*, 31, no 4, 30-45.

Puchkov, V.N. 2000. Paleogeodynamics of the Southern and Middle Urals. Ufa, Dauria, 146 p. (in Russian).

Rodionov, V.P., Dekkers, M.J., Khramov, A.N., Gurevich, E.L., Krijgsman, W., Duermeijer, C.E., Heslop, D. 2003. Paleomagnetism and cyclostratigraphy of the Middle Ordovician Krivolutsky Suite, Krivaya Luka section, Southern Siberian platform: record of non-synchronous NRM components or a non-axial geomagnetic field? *Studies in Geophysics and Geodesy*, 47, 255−274.

Sal'menova, K.Z., Koshkin, V.Y. 1990. Stratigraphy and flora of the Late Paleozoic in the North Balkhash area. Almaty, Nauka, 160 p. (in Russian).

Samygin, S.G. 1974. The Chingiz strike-slip fault and its position in the structure of Central Kazakhstan. Moscow, Nauka, 208 p. (in Russian).

Schegoleva, L.A., Belyaev, O.E., Bilenko, E.A., Zhuravlev, B.Y., Kabanov, Y.F., Malinovskaya, S.P., Yurina, A.L. 1993. New data on correlation of Lower and Middle Devonian volcanic sequences in the central and eastern segments of the Devonian volcanic belt and adjacent parts of Central Kazakhstan: *in* Milanovsky E.E., ed., Geology and Metallogeny of Central Kazakhstan. Moscow, Nauka, p. 82-99 (in Russian).

Şengör, A.M.C., Natal'in, B.A. 1996. Paleotectonics of Asia: fragments of a synthesis, *in* Yin, A. et al., eds., The tectonic evolution of Asia. Cambridge, Cambridge University Press, p. 486-640.

Schmidt, P.W. 1985. Bias in converging great circle methods. *Earth and Planetary Science Letters*, 72, 427-432.

Shatsillo, A.V., Pavlov, V.E., Paverman, V.I. 2007. The Middle Paleozoic segment of the Siberian APWP: Early Silurian paleomagnetic results from the Nyuya-Berezov area. *Fizika Zemli*, (in press; in Russian).

Smethurst, M.A., Khramov, A.N., Torsvik, T.H. 1998a. The Neoproterozoic and Paleozoic paleomagnetic data for the Siberian platform: from Rodinia to Pangea. *Earth-Science Reviews*, 43, 1-24.

Smethurst, M.A., Khramov, A.N., Pisarevsky, S.A. 1998b. Palaeomagnetism of the Lower Ordovician Orthoceras Limestone, St. Petersburg, and a revised drift history for Baltica in the Early Palaeozoic. *Geophysical Journal International*, 133, 44-56.

Stampfli, G.M., Borel, G.D. 2002. A plate tectonic model for the Paleozoic and Mesozoic constrained by dynamic plate boundaries and restored synthetic oceanic isochrones. *Earth and Planetary Science Letters*, 196, 17-33.

Surkis, Y.F., Westphal, M., Rodionov, V.P., Khramov, A.N., Gurevich, E.L. 1999. Geomagnetic reversals in Early Palaeozoic. 3 - Reversals recorded in Lower Ordovician Redbeds, Mandra section. *Fizika Zemli*, 5, 3-13 (in Russian).

Tectonics of Kazakhstan: Explanatory notes to Tectonic map of East Kazakhstan, 1:2 500 000. 1982. Moscow, Nauka, 139 p. (in Russian).

Tevelev, A.V. 2001. The evolution of the south-eastern margin of the Kazakhstan paleocontinent in the Late Paleozoic, *in* Milanovsky, E.E., et al., eds., Geology of Kazakhstan and the problems of the Ural-Mongol fold belt. Moscow, Moscow State University, p. 113-125 (in Russian).

Torsvik, T.H., Tait, J., Moralev, V.M., McKerrow, W.S., Sturt, B.A., Roberts, D. 1995. Ordovician paleogeography of Siberia and adjacent continents. *Journal of the Geological Society of London*, 152, 279-287.

Torsvik, T.H., Van der Voo, R., Meert, J.G., Mosar, J., Walderhaug, H.J. 2001. Reconstruction of the continents around the North Atlantic at about the 60th parallel. *Earth and Planetary Science Letters*, 187, 55-69.

Van der Voo, R. 1993. Paleomagnetism of the Atlantic, Tethys and Iapetus oceans. Cambridge, Cambridge University Press, 411 p.

Van der Voo, R., Levashova, N.M., Skrinnik, L.I., Kara, T.V., Bazhenov, M.L. 2006. Late orogenic, large-scale rotations in the Tien Shan and adjacent mobile belts in Kyrgyzstan and Kazakhstan. *Tectonophysics*, 426, 335-360.

Yakubchuk, A.S., Seltmann, R., Shatov, V.V., Cole, A.. 2001. The Altaids: tectonic evolution and metallogeny. *Society of Economic Geologists Newsletter*, 46, 7-14.

Yakubchuk, A., Cole, A., Seltmann, R., Shatov, V.V. 2002. Tectonic setting, characteristics, and regional exploration criteria for gold mineralization in the Altaid tectonic collage: the Tien Shan province as a key example. *Society of Economic Geologists, Special Publications*, 9, 177-201.

Zaytsev, Y.A. 1984 Evolution of Geosynclines: oval, concentrically zonal type. Moscow, Nedra, 208 p. (in Russian).

Zonenshain, L.P., Kuzmin, M.I., Natapov, L.M. 1990. Geology of the USSR: a plate-tectonic synthesis. American Geophysical Union, Washington, D.C., Geodynamics Series, v. 21, 242 p.

Zijderveld, J.D.A. 1967. AC demagnetization of rocks: analysis of results: *in* Collinson, D.W. et al., eds., Methods in Paleomagnetism. Elsevier, Amsterdam, p. 254-286.

Chapter 4

The role of the Kazakhstan orocline in the late Paleozoic amalgamation of Eurasia

Abstract

The Kazakhstan orocline, a pair of concentric horseshoe-shaped volcanic arcs of Devonian (external) and late Paleozoic (internal) age, is thought to have formed as a result of convergence between the cratons of Siberia, Baltica and Tarim leading to the amalgamation of Eurasia. Paleomagnetic and geologic data indicate that in the Middle Devonian the arc, which is now strongly curved, was nearly straight near the northwest-southeast trending volcanic margin of a Kazakhstania continent. To constrain the age of oroclinal bending we conducted a paleomagnetic study of Late Carboniferous to Late Permian subduction-related volcanics from the middle (NW) and north-eastern (NE) limbs of the orocline. Our new results indicate that the rotation of the middle arm of the orocline was essentially completed by the earliest Permian, while the NE arm probably was still ~ 30º short of it final orientation with respect to Baltica. The rotation of, or rotation within, the NE arm was completed by the Late Permian.

The paleomagnetic data constraining the timing and rotation patterns lead us to propose the following scenario for the bending of the Kazakhstan orocline. The orogenic deformation scenario began in the Late Devonian when an initial collision with Tarim pinned Kazakhstania's southern corner, while a dextral shear motion and a considerable clockwise rotation of Siberia dragged its northern end. Relative convergence between Siberia and Tarim caused initial buckling of the Kazakhstania continental element trapped between them, subdividing the belt into three (SW, NW, NE) segments. Continued subduction under the established limbs of the orocline with an estimated

outward-directed subduction velocity of well less than 1 cm/yr gradually led to closure of the intervening Junggar-Balkhash oceanic basin and tightening of the orocline.

Introduction

Oroclines, or map-view bends of curved tectonic elements, are common features of continental crust and may have played an important role in the making of continental lithosphere (Van der Voo, 2004). In its original definition by Carey (1955), the word orocline characterized an originally linear fold and thrust belt that became curved during subsequent deformations. The definition has since evolved for some authors to include any elongate lithospheric element, such as terranes, individual thrust sheets, magmatic arcs or sea-mount chains, as long as they have a significant degree of curvature (e.g., Johnston, 2004). Rotations within these elongated lithospheric elements have been found to develop in response to a variety of boundary conditions, ranging from local variations in the configuration of colliding terranes to regional changes in the stress-field (for a comprehensive review on mechanisms driving oroclinal bending see Weil and Sussman (2004)). A particular mechanism and its inherent boundary conditions for bending may be deduced from the kinematics of the curvature formation.

The Kazakhstan orocline – a pair of concentric horseshoe-shaped volcanic belts in Central Kazakhstan (Fig.4-1) – formed during the amalgamation of Eurasia; the ultimate cause of the bending is thought to be the convergence of the large cratonic blocks of Baltica, Siberia and Tarim (e.g. Zonenshain et al., 1990; Şengör et al., 1993; Van der Voo, 2004). Hence, the detailed record of the timing and pattern of rotations during the oroclinal orogeny could provide important kinematic constraints on the relative movements of these cratons prior to their amalgamation.

Previous paleomagnetic studies of the Kazakhstan orocline confined the timing of the oroclinal orogeny to an interval between the Middle Devonian (when the arc was still straight; Abrajevitch et al., 2007) to the Late Permian (the bending was essentially over; Levashova et al, 2003). To better understand the final stages of the bending and the geodynamic constraints this puts on the motion of the converging Baltica, Siberia and Tarim cratons, we studied a set of Upper Carboniferous to Upper Permian rocks at two localities from the middle (locality Tokrau) and northeastern (locality Ayaguz) arms of the curved structure (Fig. 4-1).

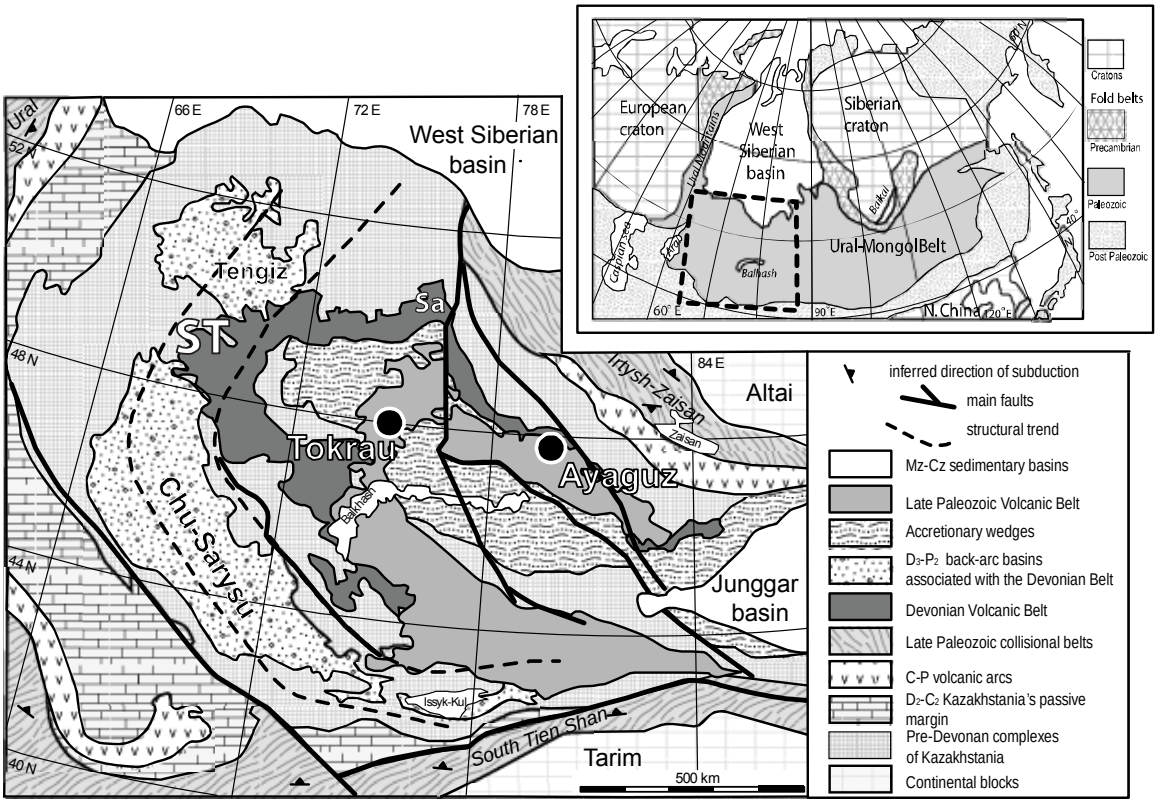

Figure 4-1. Location of the study area. Inset: Schematic map of Eurasia, showing the location of the Kazakhstan study area, wedged in between the European craton ("Baltica") and Siberia. The main map presents a tectonic sketch of the study area, modified from Windley et al. (2007). D = Devonian, C=Carboniferous, P=Permian, Mz =Mesozoic, Cz = Cenozoic. Subscripts 2, 3 refer to Middle, Late. Sampling localities at Ayaguz and Tokrau are shown by large filled circles. The hinge zones of the Devonian volcanic belt, as mentioned in the text, are labeled Sa (Spassk anticlinorium) and ST (Sarysu – Tengiz uplift).

The tectonics of Kazakhstan and adjacent areas

In the Early and Middle Devonian, the areas to the west and southwest of the Devonian volcanic belt (Fig. 4-1) were above sea level, as indicated by continental red beds and subaerial volcanics. Marine sedimentation started in the Late Devonian and continued for most of Early Carboniferous time. These sediments are represented by shallow-water limestones and clastic sediments; some marker horizons can sometimes be traced over hundreds of kilometers. From the end of the Early Carboniferous, clastic sedimentation, with rare shallow marine and lacustrine interbeds, continued in some basins until Late Permian time. On the whole, the Early Devonian through Late Permian geologic record is usually interpreted as resulting from accumulation under subaerial or shallow-marine conditions. The complete lack of deep-water sediments, ophiolites, or sutures led most geologists to conclude that this part of Kazakhstan was one large continental mass during the second half of the Paleozoic.

The situation is less clear to the north and northeast of the Devonian belt, where Devonian and younger rocks are less common and the record is less complete. Even there, however, the Devonian is represented by continental red beds of limited thickness, while deep-sea sediments are absent altogether. Despite numerous faults dissecting this area, none was ever regarded as a suture of Devonian or younger age.

Hence it looks very likely that the above territories formed a single continent (Kazakhstan block or microcontinent, also called Kazakhstania) at least since the Early Devonian. For instance, a single landmass is shown on such different reconstructions as those of Şengőr and Natal'in (1996) and Filipova et al. (2003). Rather strong and laterally variable late Paleozoic deformation is agreed to by all scientists discussing the tectonics of this micro-continent, so Kazakhstania was not a rigid block. The scale and character of the deformation within Kazakhstan, however, remain rather controversial.

Kazakhstania is located in the center of the Eurasian continent and is made of crust stabilized during the Paleozoic that is sandwiched between the old cratons of Siberia, Baltica and Tarim (Fig. 4-1). Kazakhstania was assembled by accretion of various blocks with Precambrian crust, island arc fragments, and accretionary complexes.

The mechanism of the early Paleozoic assembly and paleogeographic origin of the fragments comprising Kazakhstania are a matter of contention; proposed models range from collision of microcontinents that were originally separated by oceanic basins and multiple island arcs (Mossakovsky, et al., 1993; Didenko et al., 1994; Dobretsov et al., 1995; Filippova et al., 2001; Windley et al., 2007), to forearc accretion and oroclinal bending of a single, long-lived subduction system (Şengör and Natal'in, 1996). Many models agree, though, that by middle Paleozoic time, these fragments coalesced into a single continental block, although the shape and tectonic elements of this block remain contentious (see for example, Şengőr and Natal'in, 1996; Fillipova et al., 2001; Windley et al., 2007). From the early Devonian onward, significant subduction of oceanic ("Junggar-Balkhash") lithosphere occurred underneath this continental element and led to the Devonian and younger volcanic arcs of Figure 4-1. Carboniferous-Permian final collisions with the surrounding Baltica, Siberia and Tarim cratons were probably preceded by limited subduction in locations at the other three (exterior) sides of the orocline (Fig. 4-1).

Unlike any other continental interior, the central part of Kazakhstania displays a pair of concentric horseshoe-shaped volcanic belts (Fig. 4-1), which unconformably overlie older structures. The area internal to the strongly curved volcanic structures is dominated by rocks indicative of deeper marine environments, whereas the regions surrounding it were either non-depositional highlands or epicontinental shallow marine and non-marine basins (Zonenshain et al., 1990). The outer volcanic belt consists of a sequence of Upper Silurian to Middle Devonian extrusives. In the Frasnian, volcanic activity shifted to the more interior belt, about 150 km to the south, and continued there in the Famennian-Tournaisian. Further inward displacement of volcanic activity occurred in the Early Carboniferous and lasted until the Middle Permian (Tectonics of Kazakhstan, 1982). The composition of the volcanics, their calc-alkaline affinity and general progression from basalt to andesite and/or dacite and then to rhyolite in all belts, indicates that volcanics are subduction-related, and represent an Andean-type volcanic arc (Zonenshain et al., 1990; Bakhtiev, 1987, Kurchavov, 1994; Skrinnik and Horst, 1995).

Previous paleomagnetic studies have demonstrated that in the Middle Devonian the volcanic arc demarcated the eastern margin of Kazakhstania; the arc was nearly

straight and NW-SE trending (Abrajevitch et al., 2007; chapter 2 of this thesis). Today, the shape of this Devonian volcanic belt can be approximated by three linear segments: north-eastern (NE), middle (NW) and south-western (SW). Deviations of the Devonian paleomagnetic directions in different arms of the orocline show that the SW arm has experienced only a small net clockwise rotation (~20º) since the Middle Devonian, whereas the middle arm has rotated clockwise by ~110º, and the NE arm by ~ 160º (Abrajevitch et al., 2007; Levashova et al., 2008). The rotations are thought to have been largely completed by the Early Triassic (Van der Voo, 2004; Van der Voo et al., 2006); thus, the timing of the oroclinal orogeny can be considered as confined to the interval of about 385 Ma to 240 Ma. To characterize the final stages of the bending, and to constrain its age-span better, we have studied a set of Upper Carboniferous to Upper Permian rocks at two localities from the middle (locality Tokrau) and NE (locality Ayaguz) arms of the curved structure (Fig. 4-1).

Sampling and laboratory methods

At all localities we sampled stratified rocks with various bedding attitudes to permit a fold test. Geological sketches of the sampling areas and the locations of the sampling sites for individual collections are shown in Figures 4-2a, 4-3a, 4-5a and 4-6a.

At both Tokrau and Ayaguz localities the sampled sections consist of lava flows and tuffs of dacitic to rhyolitic composition, ignimbrites, and volcaniclastic breccia with some conglomerates, sandstone and mudstone layers (Myasnikov, 1971). In the Ayaguz area, this sequence is called the Koldar Formation. In the Tokrau area, we studied the upper part of the Kalmakemel Formation, which is thought to be of Late Carboniferous – Early Permian age (Tevelev, 2001; Tevelev, pers. comm. 2005).

The middle member of the Koldar Formation at Ayaguz is characterized by a thick, laterally persistent sequence of lithoclastic tuffs with sedimentary interbeds. The age assignment for this formation is based on relatively abundant flora (*Noeggerathiopsis theodori* Zal. et Tschirk., *Phyllotheca deliquescens* (Goepp.) Schm., *Paracalamites frigidus* Neub., etc.) found in the middle member (Myasnikov, 1971; Sal'menova and Koshkin, 1990). The Late Carboniferous-Early Permian Formation age so reported must

be evaluated today within the East European stratigraphic scale as previously in use. The age then corresponds to the Kasimovian-to mid-Kungurian stages (i.e., ~305 to 275 Ma) of the latest geological time scale (Gradstein et al., 2004; Menning et al., 2006).

At the Tokrau locality, in addition to the Kalmakemel Formation rocks, we sampled latest Early to Late Permian rocks of the Maitas Formation that overlies older formations with a dis- or un-conformity marked by a basal conglomerate (Fig. 4-3). The Maitas Formation consists of laterally varying volcanics of rhyolitic, andesitic and basaltic composition, associated tuffs and rare tuffaceous sediments. The age of the formation was determined based on lithologic-stratigraphic relationships and fossil flora content (*Paracalamites angustus* Such., *Noeggerathopsis concinna* Radcz. etc.) (Koshkin, 1974; Sal'menova and Koshkin, 1990). The previously reported age of the Upper Permian rocks (again following previous East European conventions) corresponds to the mid-Kungurian – Guadalupian – Lopingian (273-251 Ma) of the International stratigraphic scale (Gradstein et al., 2004).

Samples for this study were collected either as oriented blocks or with a gasoline-powered drill. Whenever weather permitted, both solar and magnetic compasses with an inclinometer were used for sample orientation. Both methods gave identical readings, indicating that magnetic intensities of the sampled rocks did not affect orientation measurements.

In the laboratory, standard specimens were prepared from the collected samples; cubes with ~20 mm side dimensions were cut from the block samples, and ~2.2 cm long cylinders from the 2.5 cm diameter drill cores. Measurements of natural remanent magnetization (NRM) were performed in the University of Michigan paleomagnetic laboratory. The remanent intensities and directions were measured with a three-axis 2G superconducting magnetometer. Alternating field demagnetization of a few pilot specimens failed to isolate components of magnetization successfully. The bulk of the specimens were therefore thermally demagnetized in an ASC TD-48 demagnetizer. Both demagnetization and measurement were done in a magnetically shielded room with a residual field < 200 nT. Results of the demagnetization treatments have been plotted in orthogonal vector endpoint diagrams (Zijderveld, 1967) and in stereonets. For calculation

of the magnetization directions, principal component analysis (PCA, Kirschvink, 1980) was used on linear segments of the Zijderveld plots; in cases where stable endpoints were not obtained, as indicated by successive endpoints that could be seen moving as trends along great circle paths, a combined analysis of remagnetization circles and direct observations (McFadden & McElhinny, 1988) was used.

Results

Tokrau-A

Rocks of the Kalmakemel Formation sampled at Tokrau-A show consistent demagnetization behavior (Fig 4-2). Apart from a viscous magnetization that is usually removed by 200-300ºC, all specimens show a well defined (Maximum Angular Deviation (MAD) angle < 3º) characteristic component which decays to the origin. The typical unblocking temperature range for this component is 550-675ºC, indicating hematite as the principal magnetization carrier, although in two sites (a464, m9382) ~80% of NRM intensity is lost between 533 and 566ºC, suggestive of fine-grained single-/pseudo-single domain (SD/PSD) magnetite as the main carrier of magnetization. Site-mean directions of the characteristic high temperature component pass the fold test (Fig. 4-4a; Table 4-1) as well as the reversal test of McFadden and McElhinny (1990) with observed γ=3.11 being smaller than the critical γ=9.26, strongly suggesting a pre-folding age of the magnetization.

In addition to the high temperature component, most of the samples reveal the presence of a second magnetization in the ~300-550ºC range. Some demagnetization diagrams show clear separation of the two components (e.g. Fig. 4-2h, i). For the others, the separation is incomplete due the overlapping temperature spectra of the high temperature (HTC) and the intermediate temperature component (ITC) components, and the ITC is revealed as a curved segment, or just a kink (Fig. 4-2f,j). Wherever the curved segments were long enough, great circles were calculated for these segments. In sites that had both direct observation of the ITC and the great circles, the McFadden and McElhinny (1988) technique was used to calculate the site-mean direction of the ITC. When only the great circles were available, a site-mean great circle was calculated. The

Figure 4-2. (a) Geologic sketch of the Tokrau-A sampling locality. (b-j) orthogonal demagnetization diagrams (Zijderveld, 1967) in tilt-corrected coordinates for representative samples of the Tokrau-A collection. Open (closed) symbols correspond to magnetization end-points projected onto the vertical (north-south horizontal) plane. Tick-marks denote intensities as labeled in mA/m.

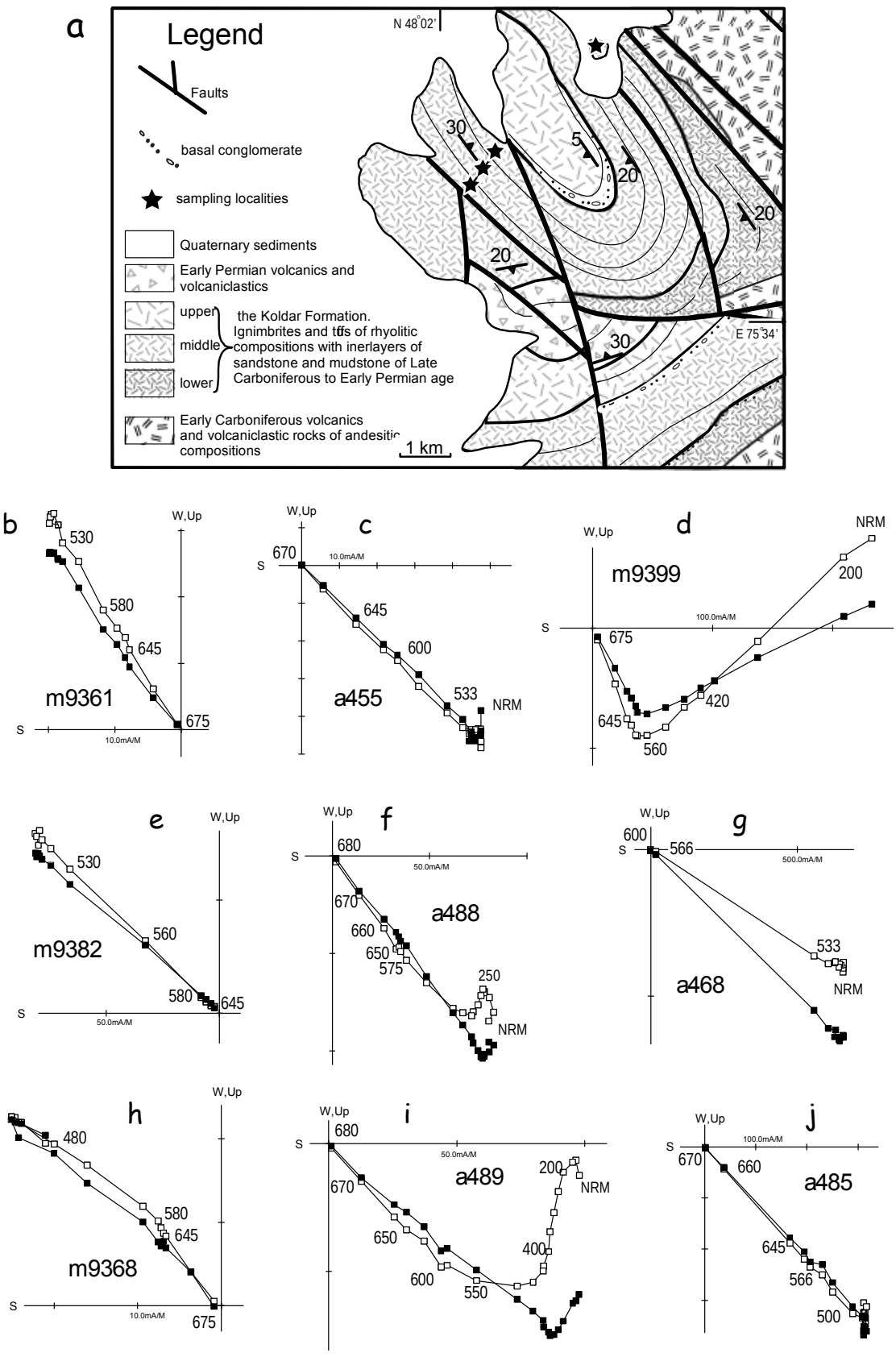
a
Legend
Faults
basal conglomerate
sampling localities
Quaternary sediments
Early Permian volcanics and volcaniclastics
upper
middle
lower
the Koldar Formation. Ignimbrites and tuffs of rhyolitic compositions with inerlayers of sandstone and mudstone of Late Carboniferous to Early Permian age
Early Carboniferous volcanics and volcaniclastic rocks of andesitic compositions
N 48°02'
E 75°34'
1 km
30
5
20
20
20
30
b
m9361
530
580
645
675
W,Up
S
10.0mA/M
c
a455
670
645
600
533
NRM
10.0mA/M
d
m9399
NRM
200
675
645
560
420
100.0mA/M
e
m9382
530
560
580
645
50.0mA/M
f
a488
680
670
660
650
575
250
NRM
50.0mA/M
g
a468
600
566
533
NRM
500.0mA/M
h
m9368
480
580
645
675
10.0mA/M
i
a489
680
670
650
600
550
400
200
NRM
50.0mA/M
j
a485
670
660
645
566
500
100.0mA/M

Table 4-1. High temperature component, Tokrau-A

site	N	bedding	In situ				Tilt corrected	
			D	I	k	α_{95}	D	I
m9392	6/6	327/28	65.7	79.0	82.9	7.4	59.6	51.1
m9398	5/6	327/28	15.1	80.7	46.0	11.4	46.3	54.6
m9350	5/6	327/28	92.3	68.0	206.5	5.3	74.1	42.5
m9356	5/6	327/28	218.0	-65.9	83.9	8.4	227.2	-38.7
m9362	5/6	327/28	226.1	-75.0	33.1	13.5	227.7	-55.0
m9368	6/6	319/20	247.6	-71.1	160.7	5.3	241.7	-43.3
m9374	5/6	327/28	237.0	-62.3	148.4	6.3	237.0	-34.3
m9380	6/6	327/28	237.8	-57.1	124.0	6.0	237.5	-29.1
m9386	6/6	327/28	226.5	-63.0	296.0	3.9	231.2	-35.3
a430	7/7	152/20	52.6	21.7	265.1	3.7	50.3	41.4
a437	6/6	152/20	52.0	21.2	89.0	7.1	49.8	40.8
a452	6/6	152/20	47.6	17.8	82.3	7.4	44.7	37.1
a458	5/5	152/20	50.4	22.4	26.7	15.1	47.5	41.9
a464	6/6	152/20	46.3	4.1	302.7	3.9	44.9	23.3
a470	5/6	152/20	45.0	15.7	83.4	7.7	42.0	34.7
a476	6/6	152/20	53.5	17.0	44.9	9.3	51.8	36.7
a482	6/6	152/20	51.4	19.7	44.7	10.1	49.1	39.3
a488	6/6	152/20	48.9	19.4	367.2	3.5	46.1	38.8
Mean IS	18		51.3	43.7	8.4	12.7		
Mean TC	18				66.5	4.3	51.5	40.0

Legend and explanation for Table 4-1: Bedding measurements are given as the strike and dip angle (down dip to the right (clockwise) of strike). N indicates the ratio of samples studied/used in the statistical analysis. Dec and Inc are the declination and inclination of the site-mean direction (in ˚); α95 is the radius of the 95% confidence cone about the mean direction (in ˚); k is Fisher's (1953) concentration parameter. IS – in situ, TC – tilt corrected directions.

site-mean directions of the ITC show better grouping *in situ* (Fig. 4-4c; Table 4-2), indicating a post-folding age of this magnetization.

Tokrau-B

The Upper Permian rocks sampled at Tokrau-B show variable demagnetization behavior. In all specimens a low temperature component whose *in situ* direction is often (but not always) close to the Present Day Field (PDF) direction at Tokrau is usually removed by ~200-300ºC, although it occasionally persists up to 550ºC (Fig. 4-3c). After removal of the low temperature component (LTC), sample magnetizations either show univectorial decay to the origin in the entire temperature range [300ºC-675ºC] or they have a change in direction between the magnetite [300-580ºC] and hematite [580-675ºC] unblocking temperature ranges (Fig. 4-3e, h, i). This directional change could be explained by two different magnetizations in the corresponding unblocking temperature ranges, or by the incomplete removal of a low-temperature overprint in the magnetite range. Great circles fitted through the "hematite" and "magnetite" mean directions for each of these three sites bypass the present day field direction (Fig. 4-3j), indicating that a magnetization in the "magnetite" temperature range is unlikely to be contaminated by a PDF-overprint, and it probably represents the true component of magnetization. The *in situ* directions and unblocking temperature range of this "magnetite" magnetization are similar to that of the ITC of the Tokrau-A collection, so the ITCs of these two collections were combined.

The highest temperature component that decays to the origin was designated as the characteristic remanent magnetization (ChRM; Table 4-3) component in the studied rocks. In two sites, the site-mean directions of the ChRM were found to be anomalous. In these anomalous sites the directions of individual samples show a good clustering on the site level (lightning induced magnetization is unlikely), site-mean directions differ from the PDF (recent weathering is unlikely), the sites were sampled in monoclinal sections with good structural control (unrecognized structural complications are unlikely), but the site-mean anomalous directions differ significantly from the mean directions of the neighboring sites with similar bedding attitudes. These anomalous site-mean directions are listed in italics in Table 4-3 (denoting outliers), and they are not

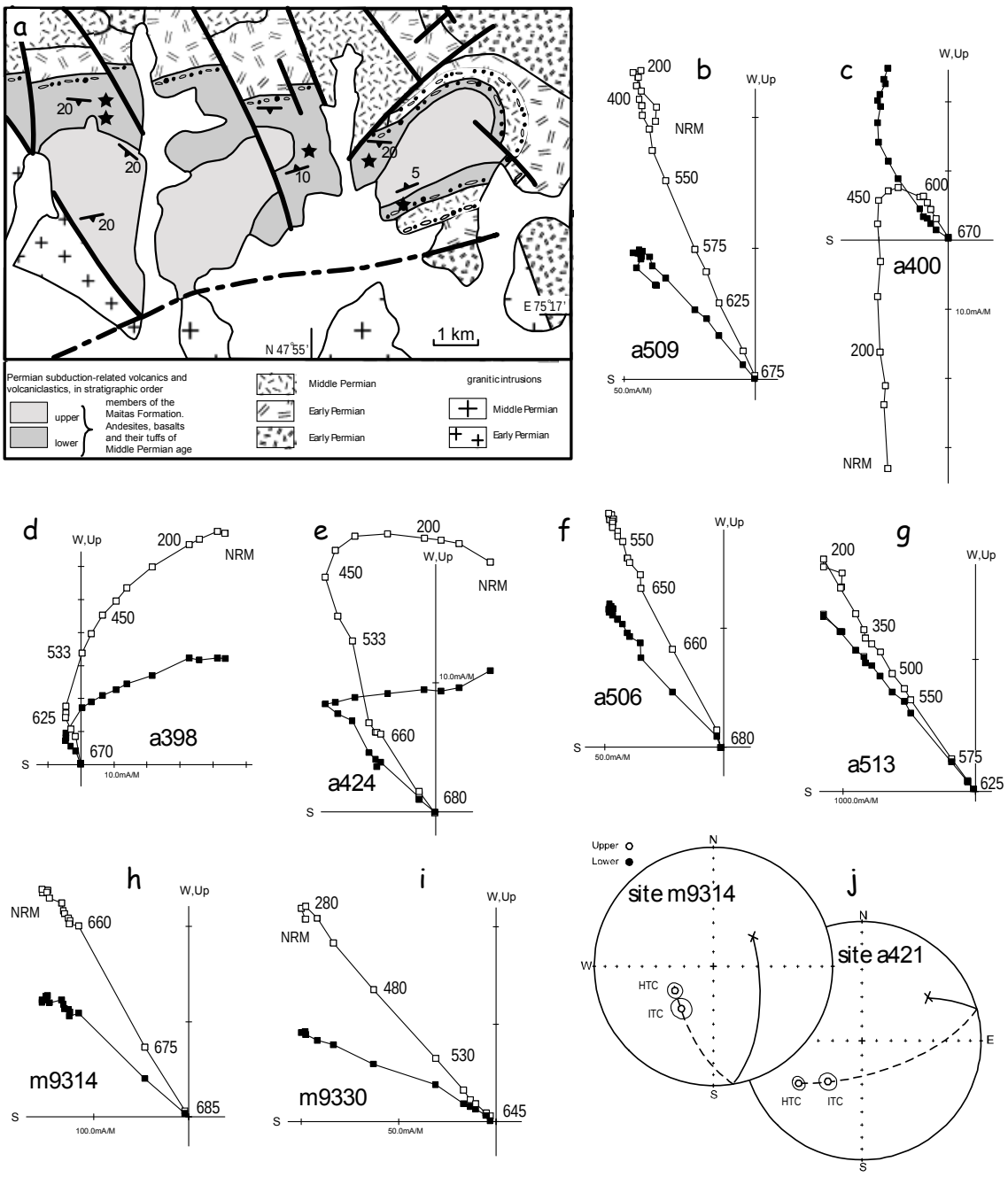

Figure 4-3. (a) Geologic sketch of the Tokrau-B sampling locality. (b-i) orthogonal demagnetization diagrams in tilt-corrected coordinates for representative samples of the Tokrau-B collection. Conventions as in Figure 4-2. (j) examples of angular separation between site-mean magnetizations defined by "hematite" (labeled HTC) and "magnetite" (ITC) unblocking temperature ranges. Great Circles fitted through HTC and ITC site-mean directions bypass the present-day field (PDF) direction, indicating that the ITC is not a composite HTC+PDF direction, but likely represents a meaningful ancient magnetization component.

Table 4-2. Intermediate temperature component, Tokrau

site	N	bedding	In situ				Tilt corrected	
			D	I	k	α_{95}	D	I
m9314	3/6	238/11	217.2	-53.4	305.4	7.1	211.2	-49.5
m9326	4/6	238/11	232.6	-49.4	42.0	14.3	220.4	-47.2
m9356	2/6	327/28	209.8	-60.8	32.9		221.3	-34.5
m9368	6/6	319/20	227.7	-62.1	173.5	5.1	231.7	-34.3
m9374	5/6	327/28	212.8	-59.0	187.6	5.6	222.5	-32.4
m9380	5/6	327/28	219.8	-61.9	167.6	5.9	227.3	-34.6
m9386	6/6	327/28	189.3	-65.0	367.2	3.5	212.2	-41.8
a421	6/6	190/16	223.1	-50.3	172.0	5.9	203.5	-58.6
a430	3GCs	152/20	323.0	-9.2			326.7	-11.7
a458	3GCs	152/20	321.0	-7.1			324.1	-10.4
a476	2GCs	152/20	320.2	-17.3			327.0	-20.3
a482	3GCs	152/20	328.0	-18.0			336.0	-18.2
a488	6/6	152/20	208.6	-68.3	21.7	17.3	144.2	-78.1
Mean IS			216.0	-59.0	85.6	4.6		
Mean TC					23.2	8.8	218.9	-46.8

Legend and explanation for Table 4-2.
GCs - indicates that the corresponding directions listed are site-mean directions representing the poles to great-circles rather than declinations and inclinations. Other notations are as in Table 4-1.

Table 4-3. High temperature, Tokrau-B

site	N	bedding	In situ				Tilt corrected	
			D	I	k	α_{95}	D	I
a391	5/6	98/18	209.0	-43.6	133.2	6.7	221.7	-58.6
a397	6/6	98/18	209.2	-44.6	73.7	7.9	222.6	-59.5
a403	6/6	98/18	213.5	-49.1	33.9	13.0	231.8	-63.4
a409	6/6	98/18	*143.1*	*-60.2*	*155.7*	*5.4*	*109.9*	*-71.2*
a415	6/6	190/16	225.9	-46.6	262.5	4.1	209.4	-55.8
a421	6/6	190/16	237.1	-38.0	223.6	4.5	226.9	-50.1
m9314	6/6	238/11	241.9	-57.3	167.5	5.2	224.0	-57.7
m9320	4/6	238/11	227.4	-41.8	89.0	9.8	218.3	-38.9
m9326	6/6	238/11	235.1	-41.5	32.1	12.0	225.7	-40.0
m9332	6/6	238/11	215.2	-50.3	130.9	5.9	204.5	-45.1
a500	6/6	100/22	218.4	-31.1	78.7	7.6	228.9	-49.6
a506	5/5	100/22	218.1	-40.7	194.4	5.5	233.5	-58.8
a512	4/6	100/22	196.6	-15.0	82.1	10.2	198.3	-36.8
a518	4/5	100/22	210.7	-20.5	159.3	7.3	215.9	-40.8
a524	4/4	100/22	*242.8*	*-68.8*	*251.8*	*5.8*	*307.0*	*-71.1*
m9404	3/6	100/22	209.6	-32.8	77.5	14.1	228.0	-53.0
m9410	6/6	100/22	215.6	-35.8	10.4	21.8	227.4	-54.7
m9416	6/6	100/22	208.7	-28.0	66.1	8.3	215.3	-48.5
m9422	6/6	100/22	206.3	-24.1	35.5	11.4	211.2	-45.0
m9428	5/6	100/22	207.7	-27.3	19.4	16.7	213.8	-47.9
m9434	6/6	100/22	208.9	-30.1	90.0	7.1	216.1	-50.5
Mean IS	19		215.5	-37.4	31.8	6.0		
Mean TC	19				67.5	4.1	218.8	-50.6

Legend and explanation for Table 4-3.
Site-mean directions in italics (sites a409, a524) indicate that they are considered outliers, not to be used in the calculation of the collection-mean. Other notations as in Table 4-1.

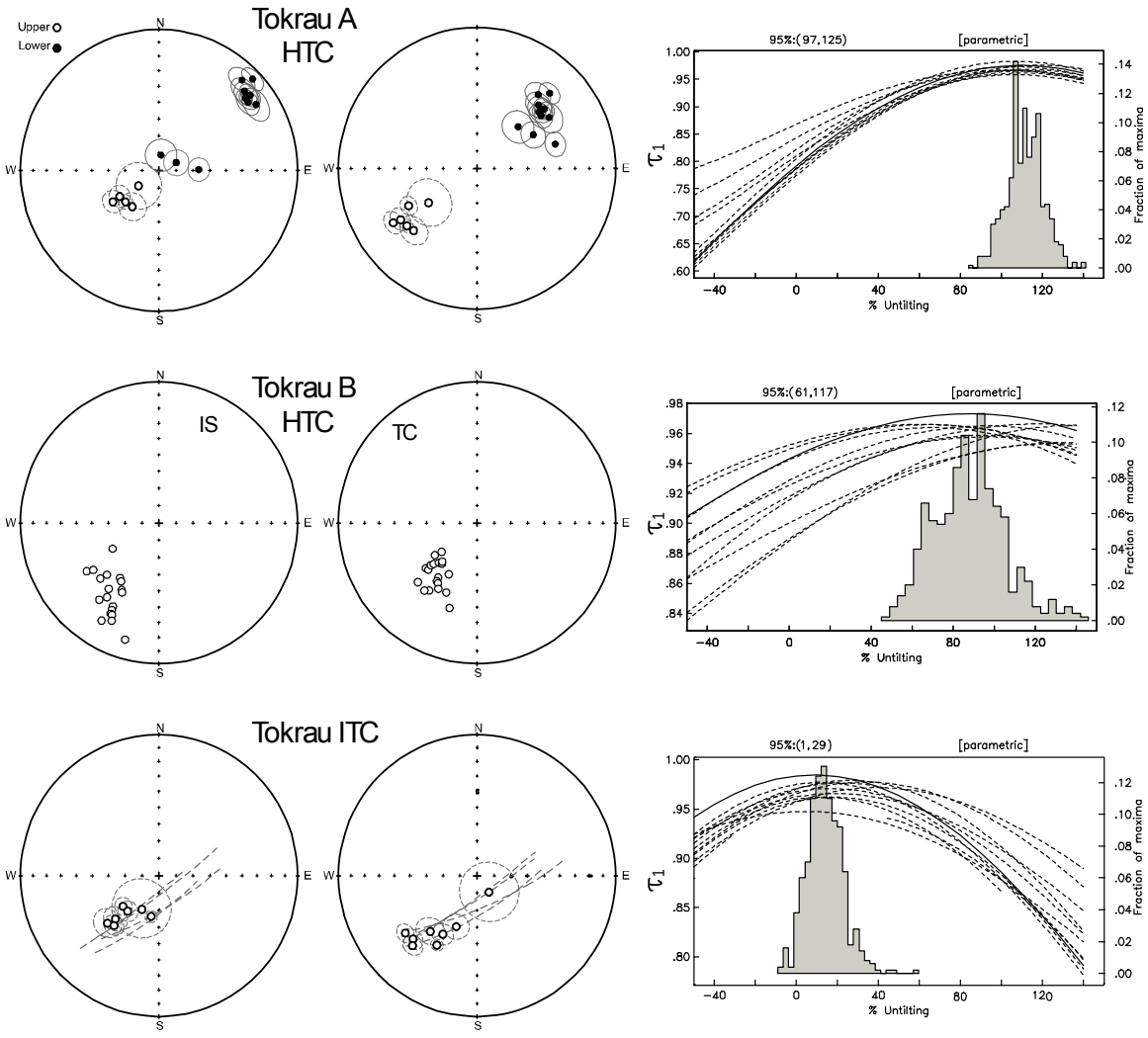

Figure 4-4. Equal-area stereoplots of site-mean magnetization directions of the Tokrau locality. The left plot is in situ (IS), middle is in tilt corrected coordinates. Open (closed) symbols represent upper (lower) hemisphere projections. The right column shows results of the parametric fold-tests (Tauxe and Watson, 1994) for the corresponding collections.

included in a calculation of the collection-mean. The ChRM directions of the remaining sites show better grouping upon tilt correction (Fig. 4b); a 95% confidence interval of the bootstrap fold test of Tauxe and Watson (1994), 61-117%, includes the 100% unfolding orientation, which indicates a pre-folding age of the magnetization.

Ayaguz-A

At Ayaguz-A, we sampled rocks of the Koldar Formation comprising tuffs of different grain-sizes and compositions and several volcanic flows. In addition, we sampled twenty clasts from an intra-formational conglomerate for a conglomerate test. Studied rocks show variable demagnetization behavior that usually corresponds to the lithology (Fig.4-4). In volcanic flows, welded tuffs and ignimbrites, after the removal of a viscous component at ~250-300ºC, a single component of magnetization unblocks up to 675ºC. In coarser-grained tuff varieties the viscous magnetization usually persists to higher temperatures, sometimes displaying a strong overlap in the unblocking temperature range with the high temperature component. Nevertheless, in all sites it was possible to isolate the high temperature component showing a linear decay to the origin.

In one of the studied sites, the directions of the HTC are widely scattered (α_{95} > 43º); this site (t1) was excluded from further consideration and is listed in Table 4-4 in italics. The HTC of the remaining sites passes the fold-test (Fig. 4-7), suggesting a pre-folding magnetization age.

Demagnetization behavior of the conglomerate clasts is generally different from that of the studied volcanics. Two specimens cut from the same clast (18 out of 20 studied clasts yielded two specimens) always show identical diagrams, but the behavior varies between the clasts. After removal at ~200ºC of the viscous magnetization whose direction is close to the PDF, the samples reveal two to three components of magnetization (Fig. 4-5f-i). Most of the samples display an upward pointing component unblocking between 250-520ºC, and eleven samples show a change of trend in the 540-580ºC temperature range (e.g. Fig. 5f-g). The presence of magnetization components in the hematite temperature range [580-660ºC] is evident in many samples (Fig. 4-5f-h), but only in seven samples could their directions be calculated with an acceptable precision,

Figure 4-5. (a) Geologic sketch of the Ayaguz-A sampling locality. (b-e) orthogonal demagnetization diagrams in tilt-corrected coordinates for representative samples of the Ayaguz-A collection. (f-i) Examples of demagnetization diagrams (in situ) of conglomerate clasts. Plotting conventions for (b-i) as in Figure 2. (j) Results of the randomness test for the clasts of an intraformational conglomerate. Plotting conventions as in Figure 4. The low temperature (250-520^{o}C) component is not random, whereas randomness could not be disproved at 95% confidence level for the intermediate (540-580^{o}C) and at 99% confidence level for the high temperature (580-660^{o}C) components. Thus, the conglomerate test is positive for the two higher-temperature components.

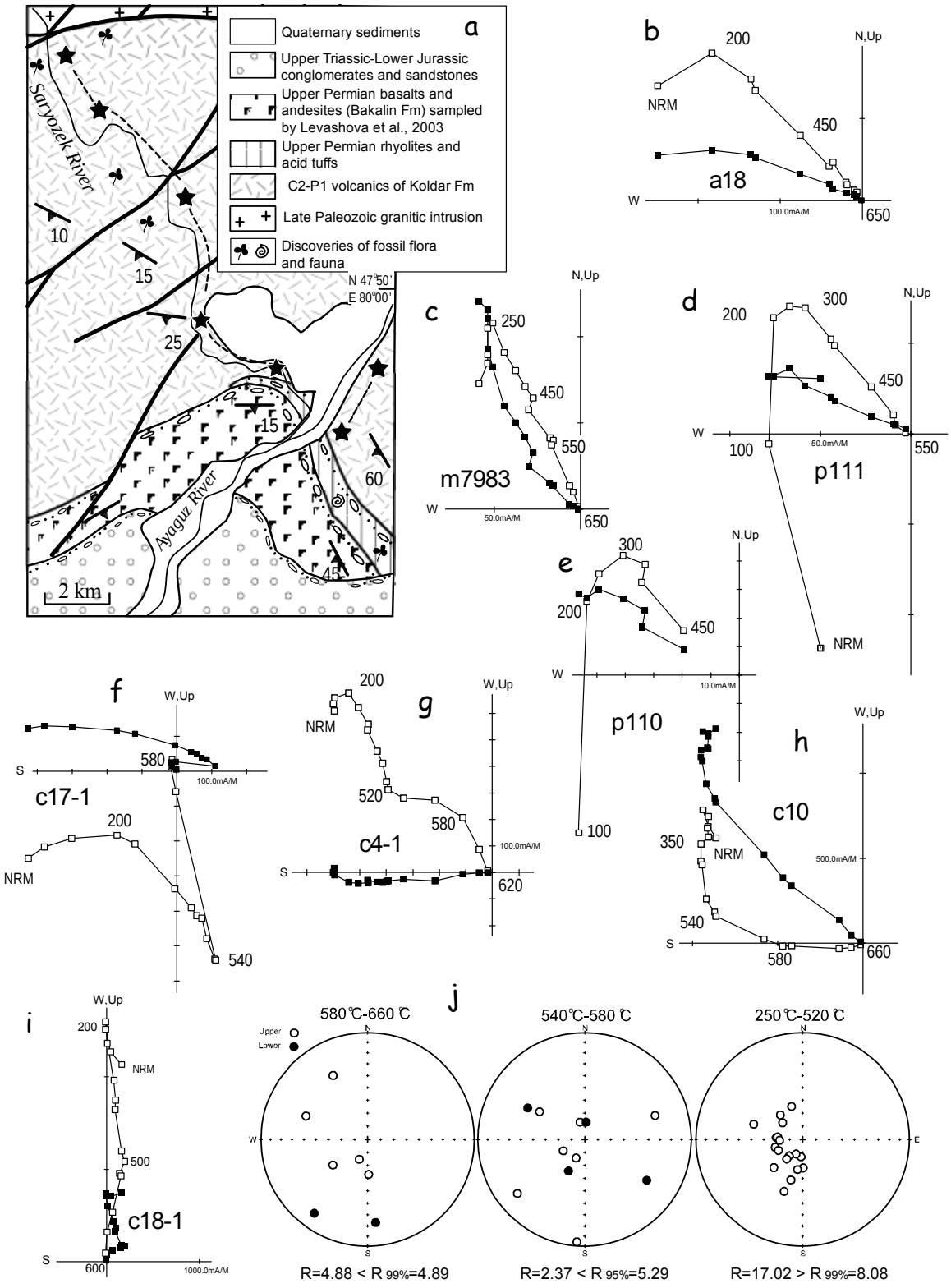
a
Quaternary sediments
Upper Triassic-Lower Jurassic conglomerates and sandstones
Upper Permian basalts and andesites (Bakalin Fm) sampled by Levashova et al., 2003
Upper Permian rhyolites and acid tuffs
C2-P1 volcanics of Koldar Fm
Late Paleozoic granitic intrusion
Discoveries of fossil flora and fauna
Saryozek River
Ayaguz River
N 47°50'
E 80°00'
2 km
10
15
25
15
60
45
b
a18
NRM
200
450
650
N,Up
W
100.0mA/M
c
m7983
250
450
550
650
N,Up
W
50.0mA/M
d
p111
200
300
450
550
N,Up
W
100
50.0mA/M
NRM
e
p110
300
200
450
100
N,Up
W
10.0mA/M
f
c17-1
W,Up
580
S
100.0mA/M
200
NRM
540
g
c4-1
200
NRM
520
580
620
W,Up
S
100.0mA/M
h
c10
W,Up
350
NRM
540
580
660
500.0mA/M
S
i
c18-1
W,Up
200
NRM
500
600
S
1000.0mA/M
j
580℃-660℃
540℃-580℃
250℃-520℃
Upper
Lower
N
W
E
S
R=4.88 < R 99%=4.89
R=2.37 < R 95%=5.29
R=17.02 > R 99%=8.08

Table 4-4. High temperature component, Ayaguz-A

site	N	bedding	In situ		Tilt corrected			
			D	I	k	α_{95}	D	I
a1	4/4	116/25	261.7	-31.1	113.5	8.7	278.8	-42.2
a7	5/5	157/66	277.0	-1.8	169.3	5.9	304.1	-53.5
a14	3/4	156/65	266.7	4.2	108.4	11.9	283.4	-54.5
a18	4/4	156/65	272.9	1.0	128.3	8.1	294.9	-53.2
m7962	4/4	75/36	229.1	-60.4	38.8	14.9	292.1	-56.1
m7969	5/5	76/28	217.9	-56.7	49.7	13.2	268.2	-63.8
m7975	6/6	156/33	261.5	-30.3	37.6	10	274.6	-61.2
m7982	6/6	151/60	279.8	-7.7	32.9	11.9	307.5	-47.4
m7988	5/5	142/60	260.0	4.7	87.7	8.2	274.5	-46.1
p109	6/6	101/25	273.4	-40.9	64.2	8.8	295.0	-39.5
p120	4/4	85/27	239.9	-52.1	21.5	20.5	277.8	-55.2
p124	4/4	63/13	260.4	-54.3	107.7	8.9	275.4	-48.8
p128	4/4	11/20	270.5	-54.7	41.5	14.4	273.6	-34.9
p132	4/4	11/20	277.6	-47.6	44.1	14.0	278.4	-27.6
t1	4/4	111/15	*204.4*	*-72.5*	*5.5*	*43.0*	*223.5*	*-87.3*
t7	3/4	111/20	266.6	-60.7	276.8	7.4	304.7	-62.7
Mean IS	15		263.8	-33.9	8.1	14.3		
Mean TC	15				38.3	6.3	285.2	-50.5

Notations as in previous Tables

(e.g., MAD ≤10º for a trajectory defined by at least 3 steps). To test for randomness (Watson, 1956), the components have been separated into three groups according to their unblocking temperature ranges. The low temperature component [250-520ºC] fails the randomness test; for the high temperature component [580-660ºC], the randomness cannot be disproved at 99% confidence level; and the intermediate temperature component [540-580ºC] is considered random at 95% confidence level. The co-occurrence of multiple magnetization components with different clustering indicates that although studied clasts did acquire a secondary magnetization during or after the conglomerate formation, re-magnetization was likely limited to the temperature range below 520ºC. The positive conglomerate test for the higher temperature components suggests that the clasts, and hence the studied volcanic rocks, in the area likely retained an ancient magnetization as characterized by unblocking > 520ºC.

Ayaguz-B

The Koldar Formation rocks sampled at this locality show consistent demagnetization behavior. After the removal by ~200-300ºC of a viscous overprint whose in situ direction is similar to the PDF, most of the samples reveal a single magnetization component decaying to the origin (Fig. 4-6b-g). The bootstrap fold test of Tauxe and Watson (1994) applied to the site-mean directions of this magnetization (Fig.4-7) shows that the best grouping is achieved between -34 and 14% unfolding, indicating a post-folding age of the magnetization.

Ages of magnetization

So far, in the studied collections, the age of magnetization has been determined relative to the folding, either as pre- or post-folding (see Table 4-6). The age of the folding itself, however, is often imprecisely defined, given that for both our sampling regions the deformation age is loosely described as “late Paleozoic” or “partly of early Mesozoic age” by, e.g., Sal’menova and Koshkin (1990) or Tevelev (2001). In such cases the magnetization age may be additionally constrained by a comparison of the observed magnetization direction with reference directions that are predicted for the sampling area

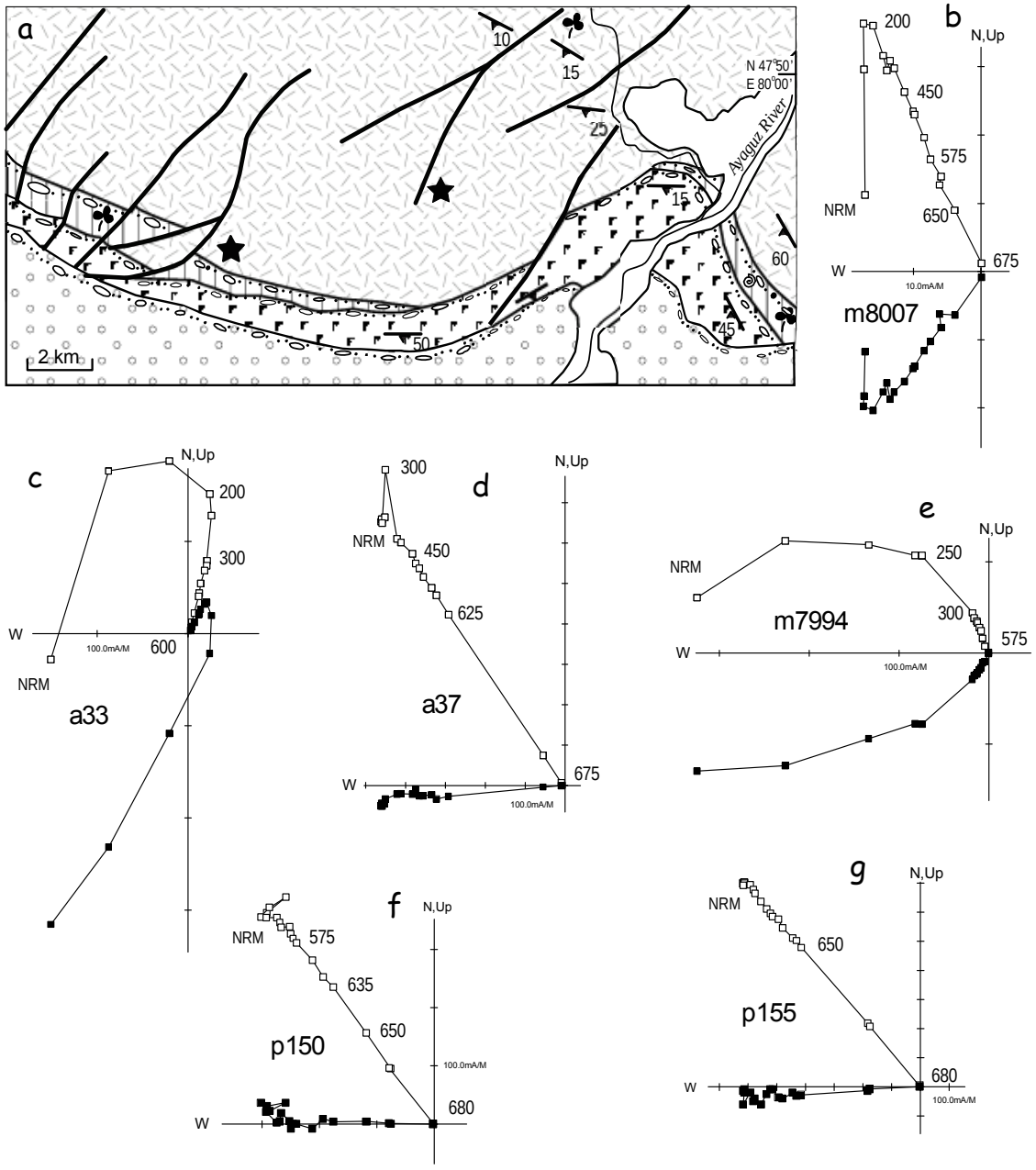

Figure 4-6. (a) Geologic sketch of the Ayaguz-B sampling locality, (b-g) orthogonal demagnetization diagrams (Zijderveld, 1967) in in situ coordinates for representative samples of the Ayaguz-B collection. For legend refer to Fig.4-5a; the boxes with stars inside outline sampling localities with multiple sites, which have varying bedding attitudes as listed in Table 4-4. Plotting conventions as in Figure 4-2.

Table 4-5. High temperature component, Ayaguz-B

site	N	bedding	In situ				Tilt corrected	
			D	I	k	α_{95}	D	I
a22	4/4	158/58	223.7	-52.4	141.8	7.7	101.6	-63.1
a30	4/5	115/44	217.6	-56.2	54.7	12.5	352.0	-77.1
a37	4/4	121/22	259.0	-52.8	142.3	7.7	291.3	-62.9
m7993	4/5	144/65	202.4	-50.2	205.0	6.4	89.8	-55.0
m7999	3/5	144/65	183.1	-57.6	16.9		87.7	-41.5
m8006	4/4	81/62	212.3	-50.8	316.8	5.2	308.9	-51.5
m8012	4/4	137/12	239.9	-33.5	56.3	12.4	242.3	-45.1
p136	3/2	161/16	227.9	-37.4	18.0		220.8	-51.7
p143	2/2	161/16	240.0	-50.3	872.9		233.7	-65.8
p149	5/5	116/15	265.4	-50.5	219.2	5.2	284.3	-56.0
p155	7/7	111/25	265.9	-50.6	369.2	3.1	299.2	-54.5
Mean IS	11		231.7	-51.9	21.0	10.2		
Mean TC	11				5.6	21.2	273.6	-80.1

Notations as in previous Tables

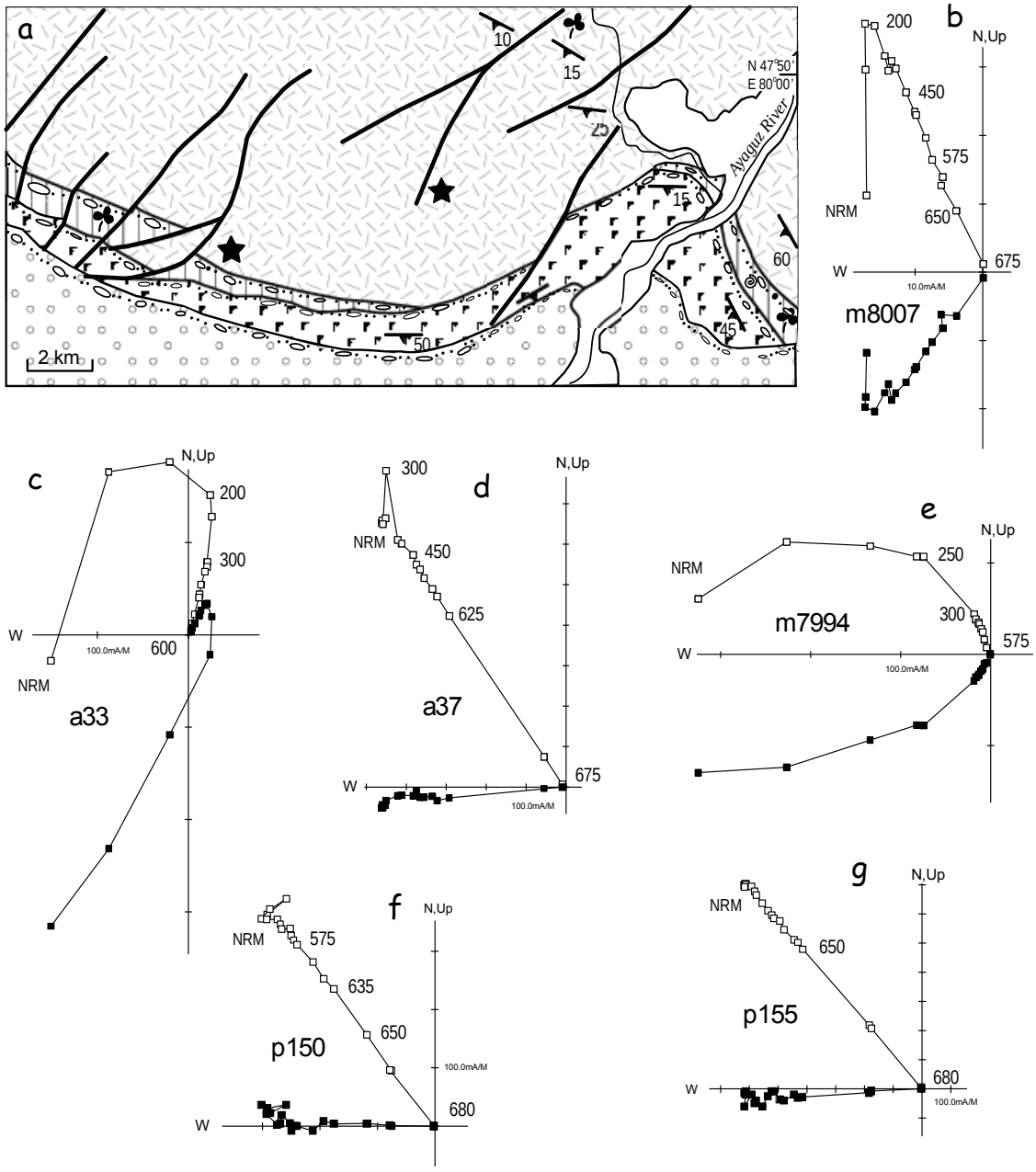

Figure 4-7. Equal-area stereoplots of site-means magnetization directions of the Ayaguz locality. The left plot is in situ, middle is in tilt-corrected coordinates. Plotting conventions as in Figure 4-4. The right column shows results of the parametric fold-tests for the corresponding collections.

for a given time interval (Irving, 1964; Van der Voo, 1993). An internal reference frame for Kazakhstania is very difficult to construct; large-scale deformations and shear-related block-rotations cause deviations in paleomagnetic declinations, resulting in an inconsistent apparent polar wander path (APWP). For the late Paleozoic, however, an external reference frame can be used. Geological evidence indicates that Kazakhstania and Baltica were not far away from each other in the late Carboniferous, and were certainly welded by the Late Permian (Zonenshain et al., 1990; Natal'in and Şengőr, 2005). Thus, the paleolatitudes of our study area should be in general agreement with those predicted by extrapolation from Baltica, and the degree of conformity should increase towards the Late Permian as the intervening Uralian Ocean progressively disappeared. A good agreement of paleolatitudes for Kazakhstan with those predicted from Baltica paleopoles has previously been demonstrated (Van der Voo et al., 2006). Thus, in this study we will use the Global APW path in Baltica co-ordinates of Torsvik et al. (2008) as a reference.

Tokrau

The rocks sampled at the Tokrau locality yielded three magnetization directions (Fig. 4-4): 1) a dual polarity pre-folding component was isolated in the Upper Carboniferous-Lower Permian rocks of the Tokrau-A collection; 2) an upward pointing pre-folding magnetization was observed in the Upper Permian rocks of the Tokrau-B collection; and 3) in addition, the two Tokrau collections yielded a post-folding magnetization. The results are summarized in Table 4-6.

The positive fold test and especially the presence of reversals in the Tokrau-A rocks suggest (but do not prove) that the magnetization is primary. However, the main carrier of magnetization in these rocks, hematite, is known to form as an alteration-oxidation product (Cornell and Schwertmann, 2003). Also, the presence of both normal and reversed polarities is rather surprising; the age of the Kalmakemel Formation (Late Carboniferous-Early Permian) overlaps the Kiaman, a well-known Long Reverse Polarity Interval of the geomagnetic field. Although the presence of short normal polarity intervals within the Kiaman has been reported before (Hounslow et. al., 2004; Khramov, 2000; Menning et al., 1988), their age and duration are poorly known. To refine the age

of formation for the rocks and define the timing of the normal polarity episode we attempted to use the ^{40}Ar-^{39}Ar technique to date three separate ignimbrite units containing normal polarity magnetization. For each unit, two samples of groundmass and seven individual plagioclase crystals were analyzed. However, our analyses did not yield fully consistent plateau ages (see Appendix A for results and explanations), although they did provide indications of the best estimate for the age of magnetization, as will be briefly summarized next.

^{40}Ar-^{39}Ar release spectra of the groundmass gave consistent Middle Triassic age estimates for all samples. The characteristic shapes of the spectra suggest clay minerals as a source of the radiogenic argon; in this case, the age of the groundmass likely reflects the age of clay formation, i.e. alteration due to devitrification or fluid migration. The expected geomagnetic inclination at an Early Triassic time of alteration (Fig. 4-8) fits the observed inclination of the post-folding magnetization (labeled as "secondary component" in Fig. 4-8), attesting that this overprint was acquired during the early Triassic alteration event.

The pre-folding dual polarity magnetization isolated in the same (Tokrau-A) rocks has a significantly lower inclination than that of the overprint (Fig. 4-8). The lower inclination, according to the reference curve extrapolated from Baltica, clearly corresponds to an older age for this magnetization. Thus, the hematite-carried remanence predates the alteration event. This suggests that hematite is not an alteration product; and, given the fact that it records the reversal, it most likely carries a primary magnetization that was acquired during the time of ignimbrite emplacement.

The age of the ignimbrite emplacement and magnetization acquisition, however, remains poorly constrained. ^{40}Ar-^{39}Ar apparent ages of individual plagioclase grains from the studied units show a wide scatter with a weak clustering at ~300-295 Ma (Fig.4-8). This wide age distribution likely reflects the combination of a significant xenocrystic contamination with a different degree of partial alteration of both xenocrysts and phenocrysts. An analysis of the presumably least contaminated grains suggests a 297-295 Ma time interval as the most likely eruption age. This best ^{40}Ar-^{39}Ar age estimate for the rock formation (and magnetization age) is, pleasingly, in agreement with the reported age

Figure 4-8. Age-correlation diagram for the Tokrau magnetizations. The nagnetostratigraphic scale has been compiled from Ogg (1995), Gialanella et al. (1997), and Hounslow et al. (2004). The reference inclination curve for the Tokrau locality is obtained by extrapolation from the Global APW path in Baltica co-ordinates (Torsvik et al., 2008). Description of the 40Ar-39Ar dating results can be found as "Background information" in the online version of this article. Horizontally elongated boxes illustrate the age ranges (horizontal dimension) of the Tokrau-A and Tokrau B collections that we consider most representative of the stratigraphic age-range of the studied rocks. Vertical dimensions are defined by the α95 of the corresponding collection-mean inclinations of Tokrau A and B. Good correlation between the 40Ar-39Ar age of alteration of the studied rocks, the observed inclination of the secondary component, and the early Triassic reference inclination for the study area suggests that the most likely age of acquisition for the secondary component is Early Triassic. The single-polarity (reversed) primary magnetization of Tokrau-B is likely to be Guadalupian-Lopingian ("middle" to Late Permian) in age. The dual-polarity primary magnetization of Tokrau-A is most likely of latest Carboniferous-Early Permian age, as indicated by the match between the reference and observed inclinations, the presence of reversals, and the most likely eruption age inferred from the 40Ar-39Ar analyses. See text for further discussion.

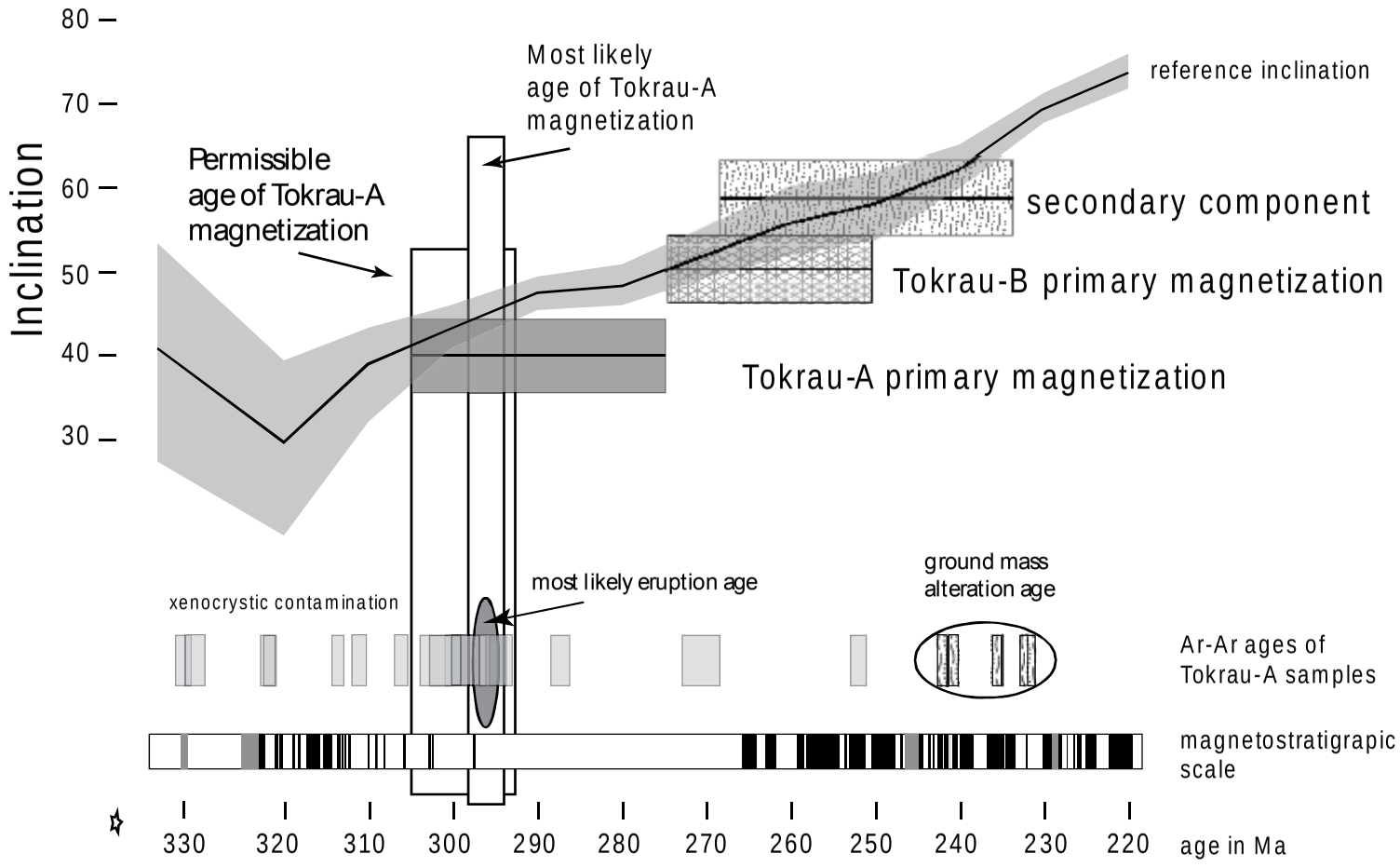
80
70
60
50
40
30
Inclination
Most likely
age of Tokrau-A
magnetization
reference inclination
Permissible
age of Tokrau-A
magnetization
secondary component
Tokrau-B primary magnetization
Tokrau-A primary magnetization
xenocrystic contamination
most likely eruption age
ground mass
alteration age
Ar-Ar ages of
Tokrau-A samples
magnetostratigrapic
scale
330
320
310
300
290
280
270
260
250
240
230
220
age in Ma

of the Kalmakemel Formation (Sal'menova and Koshkin, 1990; Tevelev, 2001). If an earliest Permian (~296 Ma) age of the magnetization is correct, it also agrees with the previously reported occurrences of a short normal polarity interval (Khramov et al., 1974; Khramov, 2000). The observed inclination, however, is slightly lower (i.e., "older looking", at ~307 Ma – see Figs. 4-8 and 4-9) than the reference one for this time. The difference is small, and may not be important given that some divergence between the predicted and observed inclinations may well arise from the use of the Baltica Early Permian reference poles when final convergence of Baltica and Kazakhstania is still a possibility.

At any rate, regardless whether the magnetization age is earliest Permian or whether it is latest Carboniferous, i.e., covering the entire permissible (i.e. biostratigraphically-defined) age range for this formation (~305-275 Ma), the reference declination changes very little (Fig. 4-9). Thus, the somewhat uncertain age estimate will not significantly affect our determination of the net tectonic rotation after magnetization acquisition. In further discussion we will consider the dual polarity pre-folding component isolated in the Kalmakemel Formation at Tokrau-A as a primary magnetization of latest Carboniferous-Early Permian age, and will use the ~300 Ma reference direction for the rotation estimate.

The pre-folding magnetization isolated in the Tokrau-B rocks is likely to be primary, dating to the time of the rock formation. Its inclination is shallower than that of the overprint (i.e. it is older than Early Triassic), but steeper than that of the Tokrau-A rocks (i.e. it is younger than Early Permian), and agrees well with the reference inclination for the Late Permian (stratigraphic) age of the rocks.

Ayaguz

The Ayaguz sampling locality yielded two magnetization components (Fig. 4-7; Table 4-6): 1) a pre-folding upward pointing magnetization isolated from the latest Carboniferous-Early Permian rocks at Ayaguz-A (Koldar Formation); 2) a post-folding magnetization in the Ayaguz-B collection. When corrected for tilt, the inclination of Ayaguz-A agrees well with the ~275-305 Ma age range deduced from the reference inclinations (Fig.4-9), which is the same as

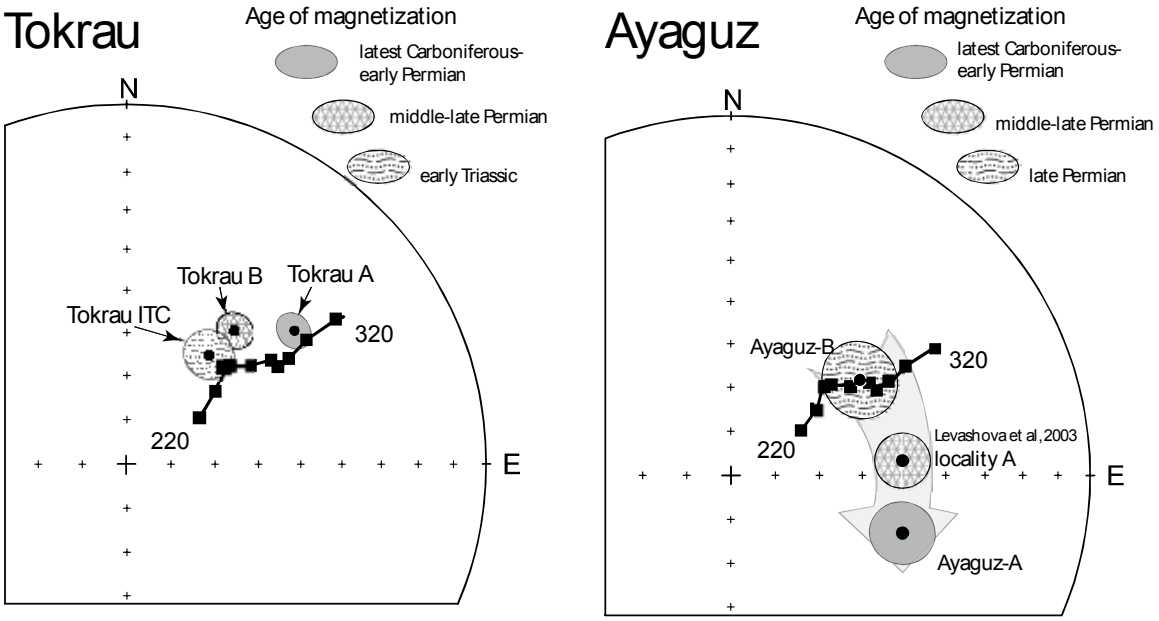

Figure 4-9. Baltica reference directions (black squares, plotted in 10 m.y. intervals, confidence limits are omitted for clarity) and directions of magnetization of the studied rocks. Filled circles are the mean magnetization direction, concentric ovals are cones of 95% confidence, and different shading signatures are representative of the inferred ages of magnetization. All directions are in the lower hemisphere, corresponding to normal-polarity field directions. The magnetization directions and their confidence circles from the Tokrau locality (middle arm of the orocline) overlap the error margins (not shown) of the coeval Baltica reference directions, indicating that any rotations with respect to Baltica cannot be considered significant. In Ayaguz (northeastern limb of the orocline), the distribution of the latest Carboniferous-Early Permian magnetization (Ayaguz-A, this study), middle-Late Permian (Locality-A of Levashova et al., 2003) and the Late Permian (this study; Ayaguz-B) magnetizations indicates progressive clockwise rotation of the study area with respect to Baltica, with a clockwise rotation of ~ 30º occurring between the latest Carboniferous and the Late Permian. For further discussion see text.

Table 4-6. Summary of paleomagnetic results

Result	age	tests	D	I	k	α_{95}	Plat	Plong	dp	dm
Tokrau-A	~305-275Ma	$F^+ R^+$	51.5	40.0	66.5	4.3	42.2	178.8	5.2	3.1
Tokrau-B	275-251Ma	F^+	218.8	-50.6	67.5	4.1	56.3	180.6	5.5	3.7
Tokrau-overprint	early Tr	F^-	216.0	-59.0	85.6	4.6	63.1	169.6	6.9	5.1
Ayaguz-A	~305-275Ma	$F^+ C^+$	285.2	-50.5	38.3	6.3	13.5	138.0	8.5	5.7
Ayaguz-B	late P	F^-	231.7	-51.9	21.0	10.2	48.5	172.1	13.9	9.5

Legend and explanation for Table 4-6.
Age: for pre-folding and presumably primary magnetizations it is indicated as a stratigraphic age of the sampled rocks according to the International stratigraphic scale (Menning et al., 2006); for post-folding magnetizations, the age is assigned based on a comparison with reference directions obtained by extrapolation from Baltica's APWP (Torsvik et al., 2008).
Tests: F fold; R reversals; C conglomerate; superscripts: T^- indicates negative; T^+ positive field test.
Directions and associated statistics are presented in stratigraphic coordinates for pre-folding magnetizations, and in geographic coordinates for post-folding remanence.
Pole coordinates are given for the north poles.

assigned to this Formation based on its fossil content and stratigraphic relationships. This good agreement indicates that the magnetization dates to the formation of the rocks and therefore may be considered primary. As is in the case of Tokrau-A, a somewhat broader age range does not affect estimates of post-Early Permian rotations of the Ayaguz area because the reference declination does not change perceptibly during this period.

The negative fold test for Ayaguz-B indicates that this remanence is post-folding. The in situ inclination of this magnetization best fits the 280-270 Ma reference directions, and the radius of the 95% confidence cone (α_{95}) about the mean suggests that, at the 95% probability level, this magnetization has been acquired before 250 Ma (Fig. 4-9). Consequently, although the magnetization is secondary, we can nevertheless be reasonably confident that the remanence is Permian in age.

Discussion

Rotations

Fig. 4-9 shows the distribution of the observed magnetization components relative to the reference directions calculated by extrapolation from Baltica's APWP (Torsvik et al., 2008) for the two sampling localities. As this plot clearly demonstrates, all three magnetization components isolated at the Tokrau locality are close to their coeval reference directions. A slight counterclockwise deflection of the observed directions could be explained by a post-Early Triassic rotation, but this deviation is statistically insignificant for the older Tokrau A and the younger Tokrau-overprint (i.e., the error limit (ΔR) about the rotation estimate overlaps a zero rotation value). Therefore we can only conclude that, for all practical purposes, no significant rotations occurred between the Tokrau area (i.e. the middle limb of the orocline) and Baltica since the Early Permian. Apparently, the middle limb of the orocline was in the same relative position with respect to Baltica in the Early Permian as it is today; the bending of this part of the curved structure was over by that time.

The older magnetization component observed in the Ayaguz locality by our study and the late Early to Late Permian result ("L-A") from the Bakalin Formation in the same area (see Fig. 4-5a) published by Levashova et al. (2003), differ in their declinations from

those extrapolated from Baltica. The younger (~275–250 Ma) magnetization is deflected clockwise by 19.8 ± 4.3º, and the older (~295–305 Ma) Ayaguz-A magnetization is deflected clockwise by 31.1 ± 6.2º relative to the reference directions (Fig. 4-9). On the other hand, the post-folding (likely Late Permian) declination of Ayaguz-B is statistically indistinguishable from the reference directions. The declination trend of the Ayaguz results (Fig. 4-9) suggests that since the latest Carboniferous-Early Permian (and very likely before the Early Triassic) the Ayaguz locality was undergoing a progressive clockwise rotation of about 30º with respect to Baltica.

It is tempting to interpret this rotation as evidence for the last rotation phase of the bending of the entire NE arm of the orocline. However, we do not have sufficient coverage of Permian paleomagnetic results in the Chingiz Range of the NE limb. The limited number of reliable Permian data allows another possibility, involving localized shear-related block-rotations, just as was argued for the SW limb (Van der Voo et al., 2006; see also Wang et al., 2007). In either case, the progressive rotations observed in the Ayaguz results suggest that the NE arm was still undergoing active deformation during the Late Permian. Levashova et al. (2003) reached a similar conclusion based on the more limited results from the Bakalin Formation alone for this area.

Combining these new data and conclusions with those of our other recent studies (Levashova et al., 2007, 2008; Abrajevitch et al., 2007), we can reconstruct a scenario of oroclinal bending in Kazakhstania. Table 4-7 lists the Devonian declinations, which strongly support oroclinal bending, because the structural trends today of the three limbs of the orocline (see also Fig. 4-1) correlate well with them (Abrajevitch et al., 2007; Levashova et al., 2008).

When the oroclinal bending was nearly completed, there was still further ongoing deformation in the area during the Late Permian – Early Triassic causing localized rotations in the vicinity of strike-slip faults, as documented for the North Tien Shan by Van der Voo et al. (2006) and Wang et al. (2007), and interpretable within the framework of left-lateral shear between Siberia and Baltica (Natal'in and Şengőr, 2005). This means that the Devonian declinations of areas affected by these localized rotations need to be restored to their pre-Permian configuration, as has been done by Abrajevitch et al. (2007).

Using Baltica's Late Permian paleopole as a reference, we can portray the structural trends with respect to the Late Permian meridian (when oroclinal bending had terminated). The correction to be applied to the present-day trends is about 44 to 48º for Kazakhstan's orocline. The resulting orientations are listed in Table 4-7, and are used to position the orocline at the end of the Paleozoic in Figure 4-10. Ideally, it would be useful in Table 4-7 to provide not just the declination and strike or orientation values that we have calculated, but also their error limits. However, for most of the information, listing any error ranges would be imprecise at best and unsubstantiated at worst, so we have refrained from entering these.

Geodynamic implications

The sequence of deformations that we can deduce from the middle to late Paleozoic paleomagnetic results, and the likely involvement of much of the crust and lithospheric mantle in the rotations of the volcanic arc complexes of Devonian through Permian ages, suggest that the mechanism that produced the strong curvature was buckling of Kazakhstania in response to the transmission of compressive stresses parallel to the long (i.e., trench-parallel) axis of this continental element. While such buckling has been proposed for some Alaskan terranes, the Olympic Mountains orocline in the State of Washington, and the Northland – Norfolk – New Caledonia–D'Entrecasteaux orocline near the Vanuatu-New Hebrides Arc of the southwest Pacific (Johnston, 2001, 2004; Johnston and Acton, 2007), there are limited or no paleomagnetic data that can be listed as evidence for such an oroclinal process involving much of the lithosphere. Thus, our recent and present studies may constitute some of the first evidence for oroclinal bending involving the entire crust, rather than the much better known and well-documented oroclinal rotations in just the upper crustal setting above a décollement zone.

It is clearly of interest to see whether the kinematics of the Kazakhstania oroclinal bending can be translated into a scenario of its dynamics. In this regard, the observations reveal the varying magnitude of the relative oroclinal rotations along the arc with respect to the Late Permian meridian, from small in the SW arm (~25º counterclockwise) to large

Table 4-7. Rotation angles deduced for the Devonian results from the three limbs of the Kazakhstan Orocline

Locality or Formation	Best age estimate	Decl.	Approximate strike of Devonian arc today	Declination w.r.t. Late Permian Meridian	Approximate strike of Devonian Arc in the Permian	Reference
Northeast Limb (48N, 76E)			120		72	
Kurbakanas (KU-L2)	392-385 Ma	167		119		Levashova et al. (2008)
G1	416-385 Ma	168		120		Grishin et al. (1997)
Kaynar-Dogolan	407-397 Ma	148		100		Levashova et al. (2008)
Northwest (Middle) Limb (48N, 80E)			70		24	
G2	416-385 Ma	111		65		Grishin et al. (1997)
Southwest (NTS) Limb (44N, 76E)			-55		-99	
Kurgasholak	398-385 Ma	27*		-17		Abrajevitch et al. (2007)
Aral (L1)	385-359 Ma	16*		-28		Levashova et al. (2007)
Redbeds K1	416-398 Ma	23*		-21		Klishevich and Khramov (1993)
K2	416-392 Ma	22*		-22		Klishevich and Khramov (1993)

* mean declinations corrected for Permotriassic shear-zone related rotations (see Abrajevitch et al., 2007)
Orientation angles and strikes are positive (negative) when striking east (west) of north.

Figure 4-10. Tectonic scenario for the bending of the Kazakhstan orocline. In the Late Devonian, Tarim and Kazakhstania collided, leading to a pinned situation of Kazakhstania's southern corner. A dextral shear motion and a considerable clockwise rotation of Siberia resulted in Kazakhstania's northern end being dragged clockwise with respect to its southern end held fixed by its backstop-pinning. Carboniferous continued convergence between Siberia and Tarim enhanced the buckling of Kazakhstania, trapped between them, leading to a subdivision of the belt into its three more or less orthogonal segments. The intervening Junggar-Balkhash Ocean was closed by Late Permian times after dual subduction at opposite zones. Reconstructions are based on APWP data for Baltica (Torsvik et al., 2008), Siberia (Kravchinsky et al., 2002; Pavlov et al., 2007), and Tarim (data averaged from the listing of Van der Voo, 1993 and those of Chen et al., 1999). The solid line denotes the Devonian Volcanic Belt above the pre-Late Permian subduction zone of the Junggar-Balkhash ocean basin.

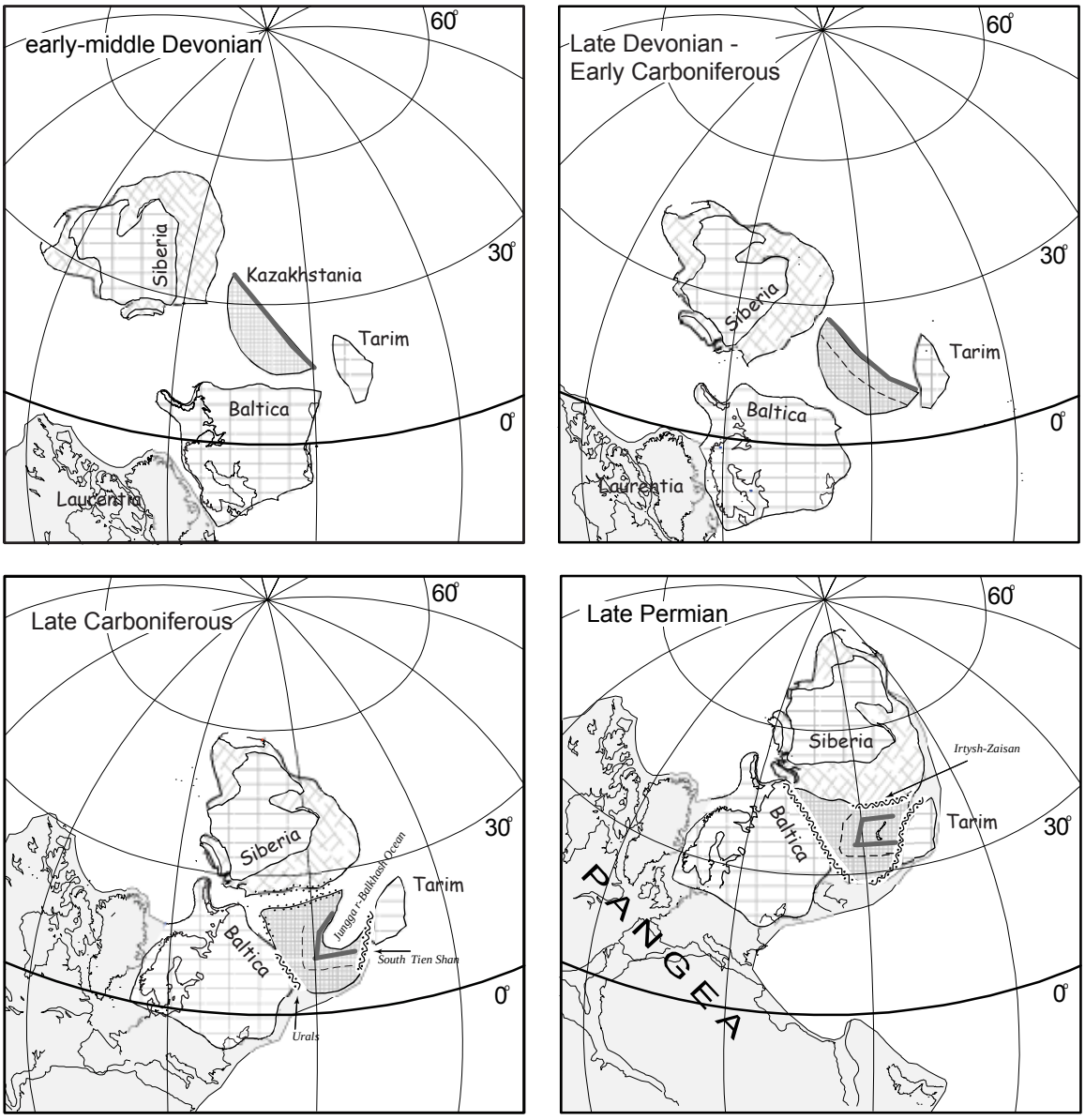
early-middle Devonian
60°
30°
0°
Siberia
Kazakhstania
Tarim
Baltica
Laurentia
Late Devonian -
Early Carboniferous
60°
30°
0°
Siberia
Tarim
Baltica
Laurentia
Late Carboniferous
60°
30°
0°
Siberia
Junggar - Balkhash Ocean
Tarim
Baltica
South Tien Shan
Urals
Late Permian
60°
30°
0°
Siberia
Irtysh-Zaisan
Tarim
Baltica
PANGEA

in the NE arm (~120º clockwise, Table 4-7). These values provide clues as to the mechanism. The large-scale movements of the surrounding Baltica, Siberia, and Tarim cratons are schematically shown in Figure 4-10. This figure illustrates how one might construct a plausible scenario involving dextral shear stress and drag applied by a clockwise-rotating Siberia to the northern end of the Kazakhstania structure, while its southern end was pinned down by a back-stop consisting of Tarim. This conceptual model, as based on paleomagnetic declination and paleolatitude data can also be tested with geological evidence.

The initiation of the collision between Kazakhstania and Tarim in the Late Devonian is documented by deformations and emplacement of granite in the Central Tien Shan (Cai et al., 1996); by an inferred change in Tarim's motion (Chen et al., 1999); and by extensive Late Devonian rifting in Kazakhstania itself (e.g. Veimarn and Milanovsky, 1990; Bukadorov et al., 2003), which possibly reflects back-arc extension within the overriding plate, and is elsewhere commonly associated with a switch in tectonic mode following an accretion event (Lister et. al., 2001).

The most likely candidate for imposing a shear stress on the northern end of Kazakhstania is clearly the Siberian craton. Although the late Paleozoic APWP for Siberia is rather poorly constrained (e.g., Cocks and Torsvik, 2007), reliable paleomagnetic poles for 360 and 250 Ma have been reported by Kravchinsky et al. (2002) and Pavlov et al. (2007). The difference in the pole positions indicates that Siberia underwent a significant clockwise rotation in this Permo-Carboniferous time interval. It is plausible that the Carboniferous movements of Siberia also had a dextral shear component with respect to Kazakhstania and Baltica (Fig. 4-10), although this sense of motion cannot be estimated from paleomagnetic data alone because latitude-parallel displacements cannot be uncovered. However, paleogeographic reconstructions for the Late Devonian (e.g. Kravchinsky et al., 2002), indicate that Siberia's then-southern (now-western) margin was located at ~20-30^{o}N, while similar Devonian paleolatitudes have been determined for the northern tip of Kazakhstania (Abrajevitch et al., 2007, Levashova et al., 2008; Grishin et al., 1997). Given the means (significant lateral displacement of Siberia between the Late Devonian and Permian) and the opportunity

(proximity of Kazakhstania and Siberia), it is likely that Siberia's movements imposed dextral shear stresses on Kazakhstania's then-northern margin, whereas relative convergence of Siberia and Tarim caused the Carboniferous buckling of the Kazakhstania microcontinent trapped between them.

To accommodate such large-scale oroclinal bending, crustal material must either be significantly shortened or be removed from between the converging arms. In the case of the Kazakhstan orocline, the crust of the Junggar-Balkhash Ocean between the converging arms was consumed at the surrounding subduction zones (Fig. 4-10). We obtain an approximate estimate of the average subduction velocity of ~ 6 mm/year from the calculation that ~1200 km of the oceanic crust must have been consumed in two concurrent subduction zones in the time interval between the Late Devonian and Late Permian (~ 360 - 260 Ma). This rate of subduction is geologically reasonable.

The buckling of the volcanic arc should also produce a specific deformation pattern, with contractional features inside the loop and extension on the outside, showing maximum contraction expected for the "hinges". In full agreement with these predictions, the hinge areas of the Devonian volcanic belt show evidence for significant contraction. For instance, in the northern part of the Spassk anticlinorium (a hinge zone between the middle (NW) and NE arms, labeled Sa in Fig. 4-1) isoclinal flow folds and strike-slip faults form "squeeze-out" structures that date to the early-middle Carboniferous (Suvorov 1963; Chitalin, 1983). Moreover, in the hinge zone between the SW and middle (NW) arms of the orocline, one finds compression in the Sarysu-Tengiz uplift in a ~150 km wide zone. This compression produced a system of closely spaced subparallel reverse faults that accommodated an estimated 150-200 km of shortening in this area (Tikhomirov, 1975; Zonenshain et al., 1990).

While compressional deformations dominated within the hinge zones of the volcanic belt, in the areas external to the belt large sedimentary basins had been forming. A Late Devonian-Permian sequence of intercalated continental clastics and shallow-marine deposits reaches huge thicknesses of over 6 km in the Chu-Sarysu Basin and over 7.5 km in the Tengiz Basin (Yakubchuk, 2001), suggesting syn-depositional formation of accommodation space for these sediments, likely by extension-driven subsidence.

We find that, all in all, the available paleomagnetic and geologic data are consistent with oroclinal bending of a thick-skinned lithospheric (continental) element as a result of buckling in the relative convergence trajectory between Siberia and Tarim.

Conclusions

Our paleomagnetic study of latest Carboniferous to Late Permian rocks from the middle and north-eastern limbs of Kazakhstan orocline has yielded several magnetization directions. At the Tokrau sampling locality (within the middle arm of the orocline), three components of magnetization have been isolated: 1) a pre-folding dual polarity primary magnetization of latest Carboniferous-Early Permian age at Tokrau-A; 2) a pre-folding primary magnetization of the Late Permian age at Tokrau-B; and 3) an overprint likely of early Triassic age. The directions are statistically similar to their coeval reference directions obtained by the extrapolation from Baltica's APWP. This correlation indicates that no significant rotations occurred between the middle limb of the orocline and Baltica since the latest Carboniferous-Early Permian and therefore, that the bending of this part of the curved structure was over by that time.

Two magnetization components have been isolated in the Ayaguz locality (within the NE limb of the orocline): 1) a pre-folding, likely primary magnetization of latest Carboniferous-Early Permian age at Ayaguz-A; and 2) a post-folding magnetization likely of Late Permian age at Ayaguz-B. These two directions differ in their position with respect to the reference directions. While the Late Permian magnetization of Ayaguz-B is statistically indistinguishable from both the coeval Tokrau-B magnetization and the reference direction, the latest Carboniferous-Early Permian Ayaguz-A magnetization is deflected clockwise by 31.1±6.2º relative to the reference. The deflection of this Ayaguz-A magnetization suggests that the studied area underwent a clockwise rotation of ~30º relative to Baltica sometime during the Permian.

The estimates of these rotation angles, combined with the data on the Middle Devonian configuration of the belt (see Abrajevitch et al., 2007) lead us to suggest the following scenario for the bending of the Kazakhstan orocline. A Late Devonian orogeny started when an initial collision occurred between Tarim and Kazakhstania (Fig. 4-10).

This pinned Kazakhstania's southern corner, while a dextral shear motion and a considerable clockwise rotation of Siberia dragged its northern end, forcing it to buckle with respect to its southern end (the modern North Tien Shan). Relative convergence between Siberia and Tarim during the Carboniferous enhanced this buckling and led to the subdivision of the belt into the three segments recognizable in modern maps (Fig. 4-1). Continued subduction under the opposing arc-limbs eventually led to closure of the intervening Junggar-Balkhash Ocean, in a process likely similar to the modern Molucca Sea dual-subduction system (Hafkenscheid et al., 2001), while tightening of the orocline continued. By the Late Permian the Junggar-Balkhash Ocean had ceased to exist.

Acknowledgements

This study was supported by the Division of Earth Sciences and the Office of International Science and Engineering's Eastern and Central Europe Program of the U.S. National Science Foundation, grant EAR 0335882. Support was also derived from the Russian Foundation of Basic Research, grants 04-05-64050, 05-05-65105 and 07-05-00021 and Program No. 8 of the Earth Science Division, Russian Academy of Sciences. We thank many colleagues from the Scientific Station of the Russian Academy of Sciences in Bishkek (Kyrgyzstan) for logistic support of the fieldwork. Chris Hall is greatfully acknowledged for conducting Ar-Ar dating of the rocks as well as for helpful discussion of the results.

References

Abrajevitch, A.V., Van der Voo, R., Levashova, N.M., Bazhenov, M.L. 2007. Paleomagnetism of the mid-Devonian Kurgasholak Formation, Southern Kazakhstan: Constraints on the Devonian paleogeography and oroclinal bending of the Kazakhstan volcanic arc. *Tectonophysics*, 441, p. 67–84.

Bakhtiev, M.K.. 1987. Paleozoic orogenic magmatic belts. Nauka, Moscow 168 p. (In Russian)

Bykadorov, V. A., Bush, V. A., Fedorenko, O. A., Filippova, I. B., Miletenko, N. V., Puchkov, V. N., Smirnov, A. V., Uzhkenov, B. S., Volozh, Y. A. 2003. Ordovician-Permian palaeogeography of central Eurasia; development of Palaeozoic petroleum-bearing basins. *Journal of Petroleum Geology*, 26, 325-350.

Cai D., Lu H., Jia D., Wu S., Chen C. 1996. $^{40}Ar/^{39}Ar$ dating of the ophiolite melange in the southern Tien Shan and the mylonite in the southern rim of central Tien Shan

and their tectonic significance. *Dizhi Kexue = Scientia Geologica Sinica*, 31, 384-390.

Carey, S.W. 1955. The orocline concept in geotectonics, part I. *Papers and Proceedings of the Royal Society of Tasmania*, 89, 255-288.

Chen C., Lu H., Jia D., Cai D., Wu S. 1999. Closing history of the southern Tianshan oceanic basin, western China; an oblique collisional orogeny. *Tectonophysics*, 302, 23-40.

Chitalin A.F. 1983. The upper Paleozoic structure of the eastern part of the Spassk Anticlinorium and its frame (Central Kazakhstan). *Moscow University Geology Bulletin,* 38(4), 26-34.

Cocks, L.R.M., Torsvik, T.H. 2005. Baltica from the late Precambrian to mid Palaeozoic: the gain and loss of a terranes's identity. *Eart- Science Reviews,* 72, 39-66.

Cocks, L.R.M., Torsvik, T.H. 2007. Siberia, the wandering northern terrane, and its changing geography through the Palaeozoic. *Earth-Science Reviews*, 82, 29-74.

Cornell, R.M., Schwertmann, U. 2003. The iron oxides. Structure, properties, reactions, occurrences and uses. Wiley-VCH Verlag GmbH & Co. KGaA, Weinheim, p. 664.

Didenko, A.L., Mossakovsky, A.A., Pechersky, D.M., Ruzhentsev, S.V., Samygin, S.G., Kheraskova, T.N. 1994. Geodynamics of Paleozoic oceans of Central Asia. *Geology and Geophysics*, 35, 118– 145 (in Russian).

Dobretsov N.L., Berzin N.A., Buslov M.M. 1995. Opening and tectonic evolution of the Paleo-Asian ocean. *International Geology Review*, 37, 335-360.

Filippova, I.B., Bush, V.A., Didenko, A.N. 2001. Middle Paleozoic subduction belts: The leading factor in the formation of the Central Asian fold-and-thrust belt. *Russian Journal of Earth Sciences,* 3 (6) 405–426.

Fisher, R.A., 1953. Dispersion on a sphere. *Proc. Roy. Soc. London*, A 217, 295– 305.

Gialanella, P R; Heller, F; Haag, M; Nurgaliev, D (Nurgaliyev, D); Borisov, A; Burov, B; Jasonov, P (Yasonov, P); Khasanov, D; Ibragimov, S; Zharkov, I. 1997. Late Permian magnetostratigraphy on the eastern Russian Platform. *Geologie en Mijnbouw*, 76(1-2), 145-154.

Gradstein, D. M., Ogg, J. G., Smith, A. G., and many others, 2004. A geologic time scale. Cambridge University Press.

Grishin, D.V., Pechersky, D.M., Degtyarev, K.E. 1997. Paleomagnetism and reconstruction of Middle Paleozoic structure of Central Kazakhstan. *Geotectonics*, 1, 71– 81.

Hafkenscheid, E., Buiter, S.J.H., Wortel, M.J.R., Spakman, W., Bijwaard, H. 2001. Modelling the seismic velocity structure beneath Indonesia: a comparison with tomography. *Tectonophysics*, 333, 35-46.

Hounslow, M.W., Davydov, V.I., Klootwijk, C.T., Turner, P. 2004. Magnetostratigraphy of the Carboniferous; a review and future prospects. *Newsletter on Carboniferous Stratigraphy*, 22, pp.35-41.

Irving, E. 1964. Paleomagnetism and its application to geological and geophysical problems. New York-London-Sydney, John Wiley & Sons, p. 399.

Johnston, S.T. 2001. The Great Alaskan Terrane Wreck: reconciliation of paleomagnetic and geological data in the northern Cordillera. *Earth and Planetary Science Letters*, 193, 259–272.

Johnston, S.T. 2004. The New Caledonia-D'Entrecasteaux orocline and its role in clockwise rotation of the Vanuatu-New Hebrides Arc and formation of the North Fiji Basin. *Special Paper - Geological Society of America*, 383, 225-236,

Johnston, S.T., Acton, S. 2007. The Eocene Southern Vancouver Island Orocline — a response to seamount accretion and the cause of fold-and-thrust belt and extensional basin formation. *Tectonophysics*, 365, 165-183.

Khramov, A.N. 2000. The general magnetostratigraphic scale of the Phanerozoic. In: A.I. Zhamoida (ed.) Supplement to the stratigraphic code of Russia. St.Petersburg, *Transactions of VSEGEI*, p. 24-45. (in Russian).

Khramov, A. N., Goncharov, G.I., Komissarova, R.A., Osipova, E.P., Pogarskaya, I.A., Rodionov, V.P., Stausilais, I.P., Smirnov, L.S. Forsh, N.N. 1974. Paleozoic Paleomagnetism. *Transaction of VNIGRI*, Leningrad, p.1-238. (in Russian).

Kirschvink, J.L. 1980. The least-square line and plane and the analysis of palaeomagnetic data. *Geophysical Journal of the Royal Astronomical Soc*iety, 62, 699– 718.

Koshkin, V. Ya. 1974. Upper Paleozoic stratigraphy of the northern part of the Balkhash-Ili Hercinian volcanic belt and the Sayak marine basin. In: Abdulin A.A. (ed.) Stratigraphy of Devonian, Carboniferous and Permian in Kazakhstan. Izdatel'stvo Nauka Kazahskoi SSR, Alma-Ata, p. 154-161. (in Russian).

Kravchinsky, V.A., Konstantinov, K.M., Courtillot, V., Savrasov, J.I., Valet, J.-P., Cherniy, S.D., Mishenin, S.G., Parasotka, B.S. 2002. Palaeomagnetism of East Siberian traps and kimberlites: two new poles and palaeogeographic reconstructions at about 360 and 250 Ma: *Geophysical Journal International*, 148, p. 1-33.

Kurchavov, A.M. 1994. The lateral variability and evolution of orogenic volcanism in the fold belts. *Geotectonics*, 28, 3-18.

Levashova, N.M., Degtyarev, K.E., M.L. Bazhenov, M.L., Collins, A.Q., Van der Voo, R. 2003. Permian Paleomagnetism of East Kazakhstan and the Amalgamation of Eurasia: *Geophysical Journal International*, 152, 677-687.

Levashova, N.M., Mikolaichuk, A.V., McCausland, P.J.A, Bazhenov, M.L., Van der Voo, R., 2007. Devonian paleomagnetism of the North Tien Shan: Implications for the middle-late Paleozoic paleogeography of Eurasia. *Earth and Planetary Science Letters*, 257(1-2), 104-120.

Levashova, N.M., Van der Voo, R., Abrajevitch, A.V., and Bazhenov, M.L. 2008. Paleomagnetism of mid-Paleozoic subduction-related volcanics from the Chingiz Range in NE Kazakhstan: The evolving paleogeography of an amalgamating Eurasian continent. *Geological Society of America Bulletin*, in revision.

Lister, G.S., Forster, M.A., Rawling, T.J. 2001. Episodicity during orogenesis. In: Miller, J A; Holdsworth, R E; Buick, Ian S; Hand, Martin (eds). Continental reactivation and reworking. *Geological Society Special Publications*, 184, 89-113.

McFadden, P.L., McElhinny, M.W. 1988. The combined analysis of remagnetization circles and direct observations in paleomagnetism. *Earth and Planetary Science Letters*, 87, 161– 172.

McFadden, P.L., and McElhinny, M.W. 1990. Classification of the reversal test in paleomagnetism. *Geophysical Journal International,* 103, 725– 729.

Menning, M., Alekseev, A.S., Chuvashov, B.I., Davydov, V.I., Devuyst, F.X., Forke, H.C., Grunt, T.A., Hance, L., Heckel, P.H., Izokh, N.G., Jin, Y.G., Jones, P.J., Kotlyar, G.V., Kozur, H.W., Nemyrovska, T.I., Schneider, J.W., Wang, X.D., Weddige, K., Weyer, D., Work, D.M. 2006. Global time scale and regional stratigraphic reference scales of central and west Europe, east Europe, Tethys, south China, and North America as used in the Devonian-Carboniferous-Permian Correlation Chart 2003 (DCP 2003). *Palaeogeography, Palaeoclimatology, Palaeoecology*, 240(1-2), 318-372.

Menning, M., Katzung, G.,Luetzner, H. 1988. Magnetostratigraphic investigations in the Rotliegendes (300-252 Ma) of Central Europe. *Zeitschrift fuer Geologische Wissenschaften*, 16(11-12), 1045-1063.

Miasnikov, A.K. 1974. Upper Paleozoic of Bakanas Synclinorium (North-East Balkhash area). In: Abdulin A.A. (ed) Stratigraphy of Devonian, Carboniferous and Permian in Kazakhstan. Izdatel'stvo Nauka Kazahskoi SSR, Alma-Ata, p. 154-161. (in Russian).

Mossakovsky, A.A., Ruzhentsev, S.V., Samygin, S.G., Kheraskova, T.N. 1993. Central Asian fold belt: geodynamic evolution and formation. *Geotectonics*, 27(6), 3– 32.

Natal'in, B. A., and Şengör, A. M. C. 2005. Late Palaeozoic to Triassic evolution of the Turan and Scythian platforms: the pre-history of the palaeo-Tethyan closure. *Tectonophysics,* 404, 175-202.

Ogg, J.G. 1995. Magnetic polarity time scale of the Phanerozoic. AGU Reference Shelf, 1, pp.240-270.

Pavlov, V.E., Courtillot, V., Bazhenov, M.L., Veselovsky, R.V. 2007. Paleomagnetism of the Siberian traps: new data and a new overall 250 Ma pole for Siberia: *Tectonophysics*, 443, 72–92.

Sal'menova, K.Z., Koshkin, V. Y. 1990. Stratigraphy and flora of the Late Paleozoic in the North Balkhash area. Nauka, Almaty, 160 p. (in Russian)

Şengör, A M C; Natal'in, B. A., Burtman, V. S. 1993. Evolution of the Altaid tectonic collage and Palaeozoic crustal growth in Eurasia. *Nature (London)*, 364, 299-307.

Şengör, A.M.C., Natal'in, B.A. 1996. Paleotectonics of Asia: fragments of a synthesis. In: Yin, A., Harrison, M. (Eds.), The Tectonic Evolution of Asia. Cambridge Univ. Press, Cambridge, pp. 486– 640.

Skrinnik, L.I., Horst, V.E. 1995. Devonian island arc volcanic complexes in the Junggar Alatau. *Geology and exploration of Kazakhstan*, 4, 6-10.

Suvorov, A.I., 1963. The Spassk Zone of Central Kazakhstan and some problems of its strike-slip tectonics. *Izvestiya of AN SSSR, seriya geologicheskaya*, 9, 46-50. (in Russian)

Tauxe, L., Watson, G.S., 1994. The fold test; an eigen analysis approach. *Earth and Planetary Science Letters,* 122(3-4), 331-341.

Tectonics of Kazakhstan: Explanatory notes to Tectonic map of East Kazakhstan, 1:2 500 000, 1982: Moscow, Nauka, 139 p. (in Russian).

Tevelev, A.V. 2001. The evolution of the south-eastern margin of the Kazakhstan paleocontinent in the Late Paleozoic, in: E.E. Milanovsky, A.B. Weinmar, Al.V. Tevelev, (eds.) Geology of Kazakhstan and the problems of the Ural-Mongol fold belt. Moscow State University Publications, Moscow, 113-125. (in Russian)

Tikhomirov, V.G., 1975. Paleozoic magmatism and tectonics of central Kazakhstan. Nedra, Moscow, USSR (SUN), 147 p. (in Russian)

Torsvik, T.H., Muller, R.D., Van der Voo, R., Steinberger, B., Gaina, C. 2008. Global plate motion frames: toward a unified model. *Reviews of Geophysics*, in revision.

Van der Voo, R. 1993. Paleomagnetism of the Atlantic, Tethys and Iapetus Oceans Cambridge Univ. Press, Cambridge. 411 pp.

Van der Voo, R. 2004. Paleomagnetism, oroclines and the growth of the continental crust, *GSA Today*, 14 (12), 4-9.

Van der Voo, R., Levashova, N.M., Skrinnik, L.I., Kara, T.V., Bazhenov, M.L. 2006. Late orogenic, large-scale rotations in the Tien Shan and adjacent mobile belts in Kyrgyzstan and Kazakhstan. *Tectonophysics*, 426, 335-360.

Veimarn, A.B. and Milanovsky, E.E. 1990. Framenian Rifting in Central Kazakhstan and some other areas, Paper 1. *Byullyuten' Moskovskogo Obschestva Ispatatelei Prirody, otd. geol*., 65, 34-47 (in Russian).

Wang, B., Chen, Y., Zhan, S., Shu, L.S., Faure, M., Cluzel, D., Charvet, J., Laurent-Charvet, S. 2007. Primary Carboniferous and Permian paleomagnetic results from the Yili Block (NW China) and their implications on the geodynamic evolution of Chinese Tianshan Belt. *Earth and Planetary Science Letters*, 263, 288-308.

Watson, G.S. 1956. A test for randomness. *Monthly Notes of the Royal Astronomical Society*, 7, 160-161.

Weil, A.B. and Sussman, A.J. (eds.) 2004. Orogenic curvature: Integrating paleomagnetic and structural analyses. *Geological Society of America Special Paper,* 383, p. 271.

Windley, B.F., Alexeiev, D., Xiao, W.J., Kröner, A., and Badarch, G. 2007. Tectonic models for accretion of the Central Asian Orogenic Belt, *Journal of the Geological Society of London*, 164, 31-47.

Yakubchuk, A. 1997. Kazakhstan. In: Moores and Fairbridge (Eds), Encyclopedia of European and Asian regional geology. Chapman and Hall, London, pp. 450-465.

Zijderveld, J.D.A. 1967. AC demagnetization of rocks: analysis of results. In: Collinson, D.W., Creer, K.M. (Eds.), Methods in Paleomagnetism. Elsevier, Amsterdam, pp. 254– 286.

Zonenshain, L.P., Kuzmin, M.I., Natapov, L.M. 1990. Geology of the USSR: a plate tectonic synthesis. Ed. Page, B.M. AGU, Geodynamic series, volume 21. Washington, D.C., 250p.

Chapter 5

Variations in relative abundances of goethite and hematite in the Bengal Fan sediments: climatic vs. diagenetic signal

Introduction

Growing realization that a warming climate is changing the globe contributed to the renewed interest in paleo-climate studies. One of the most important components of the climate system that profoundly affects humanity's livelihood is rain-fall patterns. Precipitation not only plays an important role in shaping the landscape on geologic (e.g., Etheredge et al., 2004; Grujic et al., 2006; Roe et al., 2002) and human time-scales (Hereford and Webb, 2001), it also brings moisture needed for agriculture and basic human necessities for the majority of the world's population. At present, more than a third of the world population lives in the areas of monsoonal climate; variations in the strength of the monsoon that are likely to result from modern global warming will affect the average amount of precipitation in these regions (e.g. Anderson et al., 2002). Understanding the factors influencing the monsoon system, as well as the range of variations in the average amount of rain-fall can provide a perspective for effective sustainable development planning.

In terrestrial environments, the average amount of precipitation can be estimated based on the response of iron-bearing minerals to climate induced changes in the soil-forming processes (e.g. Yapp, 2001; Evans and Heller, 2003). The ratio of two pedogenic minerals, goethite (G) and hematite (H), is climate sensitive and has been used by soil scientists to infer cold and humid versus warm climatic phases (e.g. Kampf and Schwertmann, 1983; Tardy and Roquin, 1992; Sangode and Bloemendal, 2004; and references therein). Detailed studies of soil sequences showed that the G/G+H ratio does

not depend on the parental rocks composition, and is influenced only by climatic factors. Higher average annual temperatures favor formation of hematite, whereas higher excess moisture and higher organic carbon promote goethite formation. As organic carbon content and moisture availability are generally joined in tropical and subtropical regions, a relative abundance of goethite (high G/(G+H)) can be used as an indicator of higher precipitation, whereas low values imply dryer/warmer conditions. The high sensitivity of the G/(G+H) ratio to precipitation is demonstrated by its correlation with topography on small (hundred meter) scales; soils with higher concentration of hematite occur on the drier slopes and grade into goethite-rich soils in the wetter depressions (Curi and Franzmeier, 1984a; Santana, 1984; da Motta and Kampf, 1992).

Similar climatic interpretation of relative abundances of goethite and hematite has been increasingly applied to marine sediments (e.g. Harris and Mix, 1999; 2002; Clift, 2006; Zhang at al., 2007). That is, goethite vs. hematite content in the detrital fraction reflects the precipitation regime in the source area of the sediments. Marine conditions, however, impose another variable on the ratio of pedogenic minerals. Diagenetic dissolution of iron (oxyhydr)oxides, goethite and hematite among them, have been documented in multiple studies of marine sediments (e.g., Tarduno and Wilkison, 1996; Giosan et al., 2002; Liu et al., 2004). In the studies cited at the beginning of this paragraph, the possibility of the diagenetic modification of the G/(G+H) ratio was either not considered (Clift, 2006), or inferred to be non-existent (Harris and Mix, 1999, 2002; Zhang et al., 2007). As strong evidence against dissolution, the last studies invoke an absence of a systematic down-core decline in amplitude of the variability, and the abundance, of the pedogenic oxides ratios.

To better understand the applicability of the G/(G+H) parameter as a precipitation proxy in the studies of marine sediments we conducted a rock-magnetic study of the Bengal Fan sediments. The Bengal Fan is the world's largest submarine fan; it is fed by the Ganges-Brahmaputra river system that carries sediments eroded from the Himalaya (Fig 5-1), including a share of sediments that had been temporarily stored on the Indo-Gangetic plain and were chemically altered during their residence there. Various proxy records indicate that

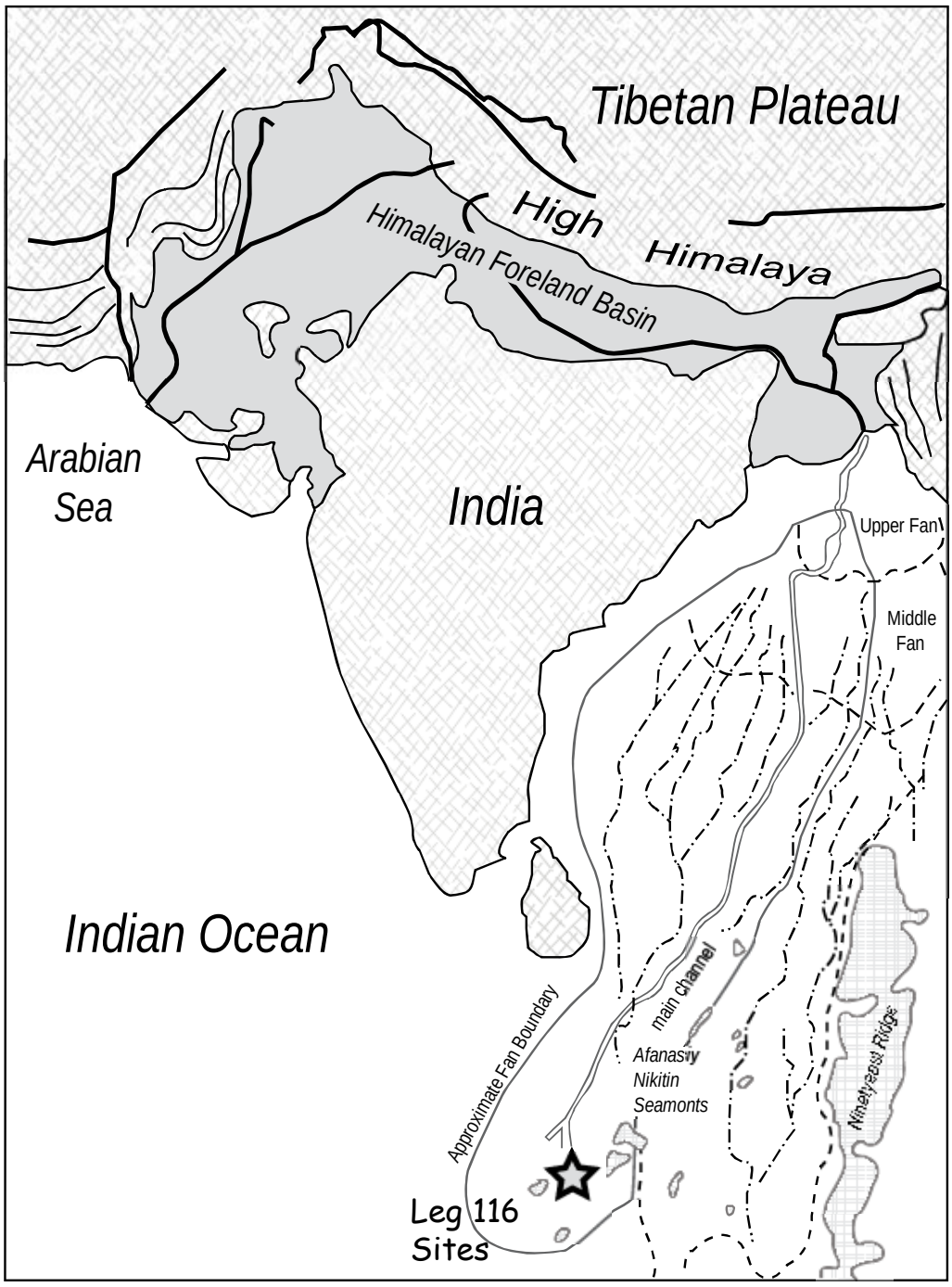

Figure 5-1. Location map of Himalayan foreland and Bengal Fan showing ODP leg 116 drill sites. Modified from Burbank et al. (1993) and Emmel and Curray (1984).

there was a significant climate change in the Himalaya-Indian Ocean region at ~ 7-8 Ma (see next section for details). The climatic turnover has been alternatively interpreted as an indication of the onset or marked strengthening of the monsoon (e.g., Prell et al., 1992; Quade et al., 1989; Ding et al., 2001), but also as marking increased aridity in the region (Gupta et al., 2004; Stern et al. 1997; Derry and France-Lanord, 1996). Both options imply a significant change, albeit of opposite sense, in the average amount of precipitation in the Himalayan Foreland. The mode of change in relative abundances of goethite and hematite in sediments derived from the foreland basin can help to discriminate between these end members, as the G/(G+H) parameter should increase with the intensification of the monsoon, and decrease with aridification.

Geological background

Climate change in the region

The modern precipitation regime in the Northern part of the Indian subcontinent is controlled by the South-Asian monsoon system. The monsoon itself is a progeny of the Tibetan Plateau. In summer, as the plateau heats, it generates a high-altitude region of low pressure; warm air rises from the plateau, pulling in moist air from the ocean and bringing heavy squally showers into the highlands. In winter, the cooling plateau generates a high pressure region; cold, dry air spills off the plateau bringing sunny, dry and dusty weather to the northern part of the Indian subcontinent. This distinctive alternation of wet and dry seasons implies the presence of a broad and high plateau (Hastenrath, 1991).

It is still debated when the Asian monsoon system was initiated. Estimates range from about 30 Ma to 7-8 Ma, based on the modeling of Paratethys retreat (Ramstein et al., 1997), sedimentary records in China (Guo et al., 2002; Wang 1990), oceanic microfossils (Chen et al., 2003; Kroon et al., 1991), or fossil flora (Quade et al., 1989; Spicer et al., 2003). Regadless whether the onset of monsoon was earlier, various proxy records indicate that there was a significant climate change in the region at ~ 7-8 Ma. At that time, accumulation of the aeolian loess deposits in Eastern China began (Ding et al., 2001), sedimentation rates in the Northern Indian Ocean increased (Rea 1992), biogenic productivity in the Arabian Sea rose (Prell et al., 1992; Kroon et al., 1991), and carbon

and oxygen isotopic ratios in soils in Northern Pakistan changed abruptly (Quade et al., 1989). These changes have often been interpreted as an indication of onset or marked strengthening of the monsoon, which in turn, may signal rapid uplift of the plateau possibly due to lithospheric delamination (Molnar et al., 1993).

However, the proxies for the intensified monsoon that were previously used allow for multiple and often conflicting interpretations. Thus, biotic changes in the Indian Ocean, especially abrupt increases in abundance of several foraminifera and radiolaria species (Prell et al., 1992; Kroon et al., 1991) have been interpreted as an indication of increased upwelling of cold, nutrient-rich water driven by the intensified monsoon. Yet, at the same time, a "biogenic bloom" also occurred in the Pacific and Atlantic oceans (Dickens and Owen, 1999; Hermoyian and Owen, 2001; Gupta et al., 2004), representing a much larger region than that affected by the monsoon. The regional high productivity event, according to Gupta et al. (2004), is not related to a strengthening of the monsoon, but rather reflects changes in ocean circulation due to high-southern-latitude cooling and increased glaciation of Antarctica.

Interpretation of the isotope data is also controversial. Stable isotope ratios of both carbon and oxygen are shown to have changed between 6 and 8 Ma in pedogenic sediments of northern Pakistan (Quade et al., 1989), Nepal (Harrison et al., 1993), and the Bengal Fan (France-Lanord and Derry, 1994), suggesting a strengthening of the monsoon at this time (Quade et al., 1989). However, a similar change in $\delta^{13}C$ occurred globally (Cerling et al., 1993; Cerling, 1994; Hay et al., 2002), and appears to be a worldwide trend related to evolutionary development of C4 plants. The variation in $\delta^{18}O$ in soil carbonates (Quade et al., 1989; Quade and Cerling, 1995), mammal teeth and freshwater bivalves (Dettman et al., 2001) in Siwalik Group sediments does indicate some kind of climate change. However, because $\delta^{18}O$ responds to numerous factors such as temperature, source region, rainfall amount, aridity and elevation, the $\delta^{18}O$ data have proven very difficult to be interpreted in a unique way. For example, in contrast to Quade et al. (1989), Stern et al. (1997) and Dettman et al. (2001) suggested that the sense of the $\delta^{18}O$ change is indicative of either a change in the source of precipitation or increased aridity of the region. Interpretations of the isotopic ratio of Sr are also confusing. Based

on the evolution curve of $^{87}Sr/^{86}Sr$ in seawater, Richter et al. (1992) suggested that the erosion rate of the Himalayan-Tibetan Plateau has been steadily increasing in the last 10 m.y. At the same time, the increased ratio of $^{87}Sr/^{86}Sr$ in pedogenic clay minerals in sediment of the Bengal Fan and in pedogenic carbonate of the Siwalik Group sediments has been interpreted to imply decreasing erosional fluxes (Derry and France-Lanord, 1996; Quade et al., 1997).

The sedimentary record from the Indian Ocean and Himalayan foreland is no less puzzling. There was a pulse of sedimentation in the northern Indian Ocean between 9 and 6 Ma (Rea, 1992), but the Indo-Gangetic foreland and the Bengal Fan experienced a decline in sediment accumulation rates at 8 Ma (Burbank et al., 1993). Sediments sampled from drill holes of ODP leg 116 in the Bay of Bengal show a change in grain size at ~ 7 Ma from coarser to fine material, and shifts in clay mineralogy from largely illite and chlorite to predominantly smectite and kaolinite, suggesting increased weathering (Cochran et al., 1989, France-Lanord et al., 1993; Bouquillon et al., 1989; Brass and Raman, 1990). These changes are more consistent with decreased runoff and equable climate in the Bengal Fan source area, rather than with seasonally stormy climate with the heavy rainfall and energetic erosion one might expect from an enhanced monsoon (Derry and France-Lanord, 1996; 1997).

Thus, different climatic proxies indicate that some kind of climate change did occur in Southern Asia and the neighboring Indian Ocean at ~7-8 Ma, but it is unclear whether those changes represent a global cooling trend or are related to the strengthening of the South Asian monsoon. The signatures of the South Asian monsoon are different in the eastern and the western part of the region. In the west (Arabian Sea), the monsoon manifests itself as a seasonal wind change, whereas in the east heavy summer rains occur (France-Lanord et al., 2000). Thus, a precipitation increase in the eastern (Siwalik) foreland basin can serve as an indication of the strengthening of the monsoon.

Himalayan foreland basin

In northeast India, the surface runoff of precipitation is collected by the Ganges/Brahmaputra river system that currently drains both the northern and southern slopes of the Himalayas. The erosion products have been stored in a foreland basin (Burbank et al., 1996), starting in the middle Miocene or earlier, and consist of fluvial and flood-plain deposits laid down by the ancestral Ganges and Brahmaputra as the

Siwalik Group. Overall, the strata are characterized by alternating overbank mudstones, channel sandstones and conglomerates. Overbank deposits typically display extensive pedogenic alteration. Paleosols of the foreland basin are of various pedogenic types, mainly developed under alternating wet and dry seasons (Johnson, 1977; Retallack, 1995).

A rock-magnetic study of paleosols in the Pliocene-Pleistocene fluvial Siwalik Group (Sangode and Bloemendal, 2004) showed a predominance of hematite (H) and goethite (G) as magnetic carriers, with a high G/(G+H) in selected intervals. This ratio and the presence of low-coercivity ferromagnetic minerals were used to infer climate-sensitive processes of oxidation-reduction, hydration-dehydration, or hydroxylation-dehydroxylation; intervals of high G/(G+H) were inferred to correspond to wetter conditions, consistent with the previous studies.

However, soil development in an alluvial landscape, like that of the Ganges basin, is extremely variable. Soils develop on parent material that is not static, but instead is undergoing a process of incremental addition of new parent material to the profile (Johnson, 1977). Pedogenic factors such as moisture availability and rate of new material addition are commonly affected by microtopography and distances from active channels (Kraus, 1999), which modifies the distribution of water and suspended sediments across the landscape (Sharma et al., 1998). These variations cause adjacent landforms on the alluvial plain to have grossly different histories in terms of their sedimentation and pedogenic record (Johnson, 1977). Thus, rock magnetic studies of isolated terrestrial sections are likely to be representative of local conditions only, and may be inadequate to generate high-resolution records of magnetic-climatic relationships. The integrated basin-wide record of climatic changes can be obtained from the Bengal Fan sediments that are derived from the Himalayan Foreland Basin.

The Bengal Fan

The Bengal Fan is the world's largest submarine fan; it is fed by the Ganges-Brahmaputra river system that carries sediments eroded from the Himalaya, including a share of sediments that had been temporarily stored on the Indo-Gangetic plain and were chemically altered during their residence there. The Fan has been sampled by DSDP leg 22 and ODP leg 116 (Shipboard scientific party, 1989). ODP sites 717, 718, and 719 (Leg 116) are located in the distal portion of the Bengal Fan (Fig. 5-1.). The holes are approximately 8

km apart. Holes 717C and 719B reached upper Miocene sediments, whereas Hole 718C reached lower Miocene strata at depth 935 mbsf. The principal lithologies encountered in all holes were silt and mud turbidites, with lesser amounts of biogenic mud. Dating of the sediments and correlations between holes are based on lithostratigraphy and nanofossil biostratigraphy (Stow et al., 1990; Gartner, 1990). Based on biogenic components, grain size, and clay mineralogy (relative abundance chlorite+illite vs. smectite+kaolinite), the sediments were divided into 7 facies. Clay mineral abundances and characteristic Sr- and Nd-isotope ratios in clays are consistent with the Ganges-Brahmaputra watershed being the main source of the detrital sediments in the Bengal Fan, with material derived from S. India, Sri Lanka or the Deccan traps being of minor volumetric importance (France-Lanord et al., 1993). Pedogenic hematite or goethite in the Bengal Fan sediments, like the other major parts of clastic input, are therefore also representative of the Ganges and Brahmaputra drainage area.

Sampling

For this study we have sampled ODP leg 116 drill cores, covering the age interval of ~4.0–10.8 Ma. The age of the strata was determined by nannofossil stratigraphy by Gartner (1990) and we used his biostratigraphic zonations and reassigned ages according to the Berggren et al. (1995) timescale now in general use. The age assignments, however, should be treated with caution. Sparse and sporadic occurrences of marker species, poor fossil preservation and evidence for their re-deposition led to suspicion that the entire biostratigraphy may be based on re-deposited fossils, thus every age assignment may be too old (Gartner 1990).

Sediment recovery at the ODP leg 116 sites, while normal for turbidite sections, is far from complete. This low recovery is somewhat compensated for by the very high overall sedimentation rates, roughly 100 m/m.y. at Site 717 and 65 m/m.y. at Site 718. Hence, in the intervals where recovery is limited to short sections or core-catchers, samples are expected to provide information on a temporal spacing of ~100 k.y. In an attempt to minimize the bias in recovery, to estimate the variability of the G/(G+H) parameter, and to obtain a representative record for the given time-interval we sampled two holes (Fig. 5-2.):

site 717, hole C, interval ~5.5 Ma (416.5 mbsf) to 9.4 Ma (828.2 mbsf), taking a sample every 30 cm;

site 718, hole C, interval ~4.0 Ma (132.8 mbsf) to 10.8 Ma (561.3 mbsf), taking a sample every 20 cm,

A sample in this study comprises ~1.8 cm^3 volume of sediment packed into a standard cylindrical holder (outer dimensions of $^7/_{16}$" diameter and ¾" length).

Methods for identification of magnetic minerals in samples

In this study magnetic minerals have been identified and their amount in the samples estimated based on their magnetic properties, such as coercivity (IRM acquisition analysis), the Curie or Neel temperature, and low temperature transitions (thermomagnetic runs). In addition, we performed a transmisson electron microscopy study on magnetic separates from two samples. A brief description of the methods and results from the Bengal Fan sediments are given below.

IRM acquisition analysis

We used the analysis of isothermal remanent magnetization (IRM) acquisition curves as the main method of identification/quantification of magnetic phases present in a sample. The samples were stepwise magnetized in 30 steps to the highest field of 4.5 Tesla with an impulse magnetizer. After each step the remanent magnetization of the sample was measured. The IRM acquisition curve then is statistically analyzed to find the number of different coercivity components that best fit the curve. We used the IRM fitting program of Kruiver et al. (2001) that is limited to symmetric distribution in log-space, which is also referred to as the cumulative log-Gaussian approach (Fig. 5-3). In this method, an assemblage of grains of a single magnetic mineral is characterized by: 1) its saturation IRM (SIRM), a parameter that is proportional to the content of the mineral in a sample, 2) mean coercivity, the field at which half of the SIRM is reached, $B_{1/2}$;

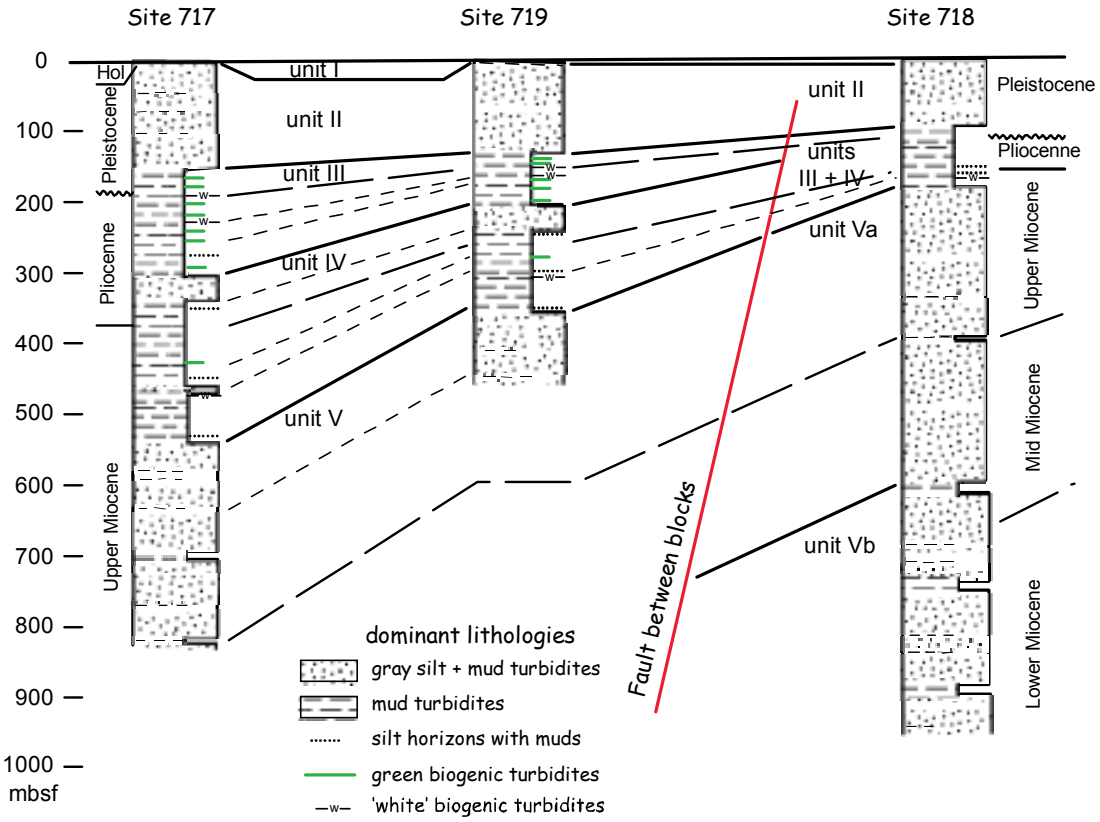

Figure 5-2. Summary of sites 717,718,719 (leg 116), showing lithostratigraphic units and correlations. From Stow et al., 1990.

3) the width of the distribution, the dispersion parameter DP, given by one standard deviation of the logarithmic distribution. If more than one magnetic mineral is present, their IRM acquisition curves add linearly.

Thermomagnetic runs

Magnetization (the IRM given at 0.5 T of a sample) was measured as a function of temperature for two representative samples, 7-75-2-30 and 7-64-2-90. Measurements were done with the high-temperature Vibrating Sample Magnetometer at the Institute for Rock Magnetism. Samples were heated from room temperature (25 ^{o}C) up to 700 ^{o}C in air, and then cooled back to room temperature; heating and cooling rates were ~ 10 ^{o}C/min. Stepwise thermomagnetic runs were performed for sample 7-54-7-0; the sample was warmed to increasingly elevated temperature with intermittent cooling between successive heatings. The peak heating temperatures of the steps ranged from 200^{o}C to 700^{o}C with 100^{o}C increments.

Low Temperature cycling

We conducted experiments described in Carter-Stiglitz et al. (2006) on a set of samples with variable relative contributions of hematite and goethite components as estimated by the technique of Kruiver et al. (2001). During the experiments, remanence acquired in 5T field and then partially AF demagnetized with a maximum field of 0.2T was measured on cooling from 300-20K, warming 20-400K, and cooling 400-20K. The Carter-Stiglitz et al. (2006) method allows evaluation of the contribution of goethite and hematite in the high coercivity fraction based on differences in temperature-dependent behavior of these minerals. On cooling from room temperature (300K) to 20K and then heating back to room temperature in zero field (i.e. low temperature loop of the thermomagnetic run), hematite can lose a part of the initial NRM intensity at the Morin Transition (at ~ 250K). Fig. 5-4a shows an example of the Morin transition in synthetic (stoichiometric) hematite with a large drop in intensity on cooling and a partial recovery on warming trough the transition temperature. The Morin transition, however, is very sensitive to crystallinity and substitution content; in pedogenic hematite, which is poorly crystalline and often incorporates significant amounts of aluminum into the structure, the Morin transition can be partially or completely suppressed (e.g. De Grave et al., 2002;

Cornell and Schwertmann, 2003, Dunlop and Ozdemir, 1997). Thus, the low temperature thermomagnetic runs for hematite can be either non-reversible if the Morin transition is present, or nearly reversible if it is suppressed. On heating from room temperature to 400K and cooling back to the room temperature (the high temperature part of the thermomagnetic run), the hematite's NRM does not change (Fig.5-4a).

Goethite's properties are opposite to those of hematite; the low temperature loop of the termomagnetic run is always reversible. However, upon heating from room temperature to 400 K (≥ the Neel temperature of goethite) goethite loses all NRM intensity, and there is no recovery of intensity upon cooling in a zero-field back to room temperature (Fig.5-4b). Accordingly, the contribution of goethite to the total IRM of the high coercivity fraction can be measured as a loss of $IRM^{5T-0.2T}$ (remanence acquired in 5T field and then partially AF demagnetized with a maximum field of 0.2T to eliminate low coercivity fraction of the magnetic assemblage) upon heating from 300K to 400K and cooling back to 300K in zero field after the low temperature loop of the termomagnetic run (Fig.5-4c).

Low temperature cycling (LowTC) experiments were performed on 51 representative samples from the Bengal Fan core 717. The samples were measured continuously during zero-field cooling to 20K, warming to 400K and cooling to 300K with an MPMS SQUID magnetometer at the Institute for Rock Magnetism in Minneapolis.

TEM observations

The magnetic separates from two samples, 7-68-cc-32 and 7-68-2-88, were prepared in order to validate the identification of magnetosomes in our samples. Distilled water was added to the samples, and the samples were put into ultra-sonic bath to form a suspension. A hand-held, rare-earth magnet then was used to separate magnetic grains. Magnetic separates were transferred from the magnet onto a copper grid for analysis in a Philips CM12 Analytical Electron Microscope. Elemental spectra for selected grains were determined using energy dispersive spectroscopy (EDS).

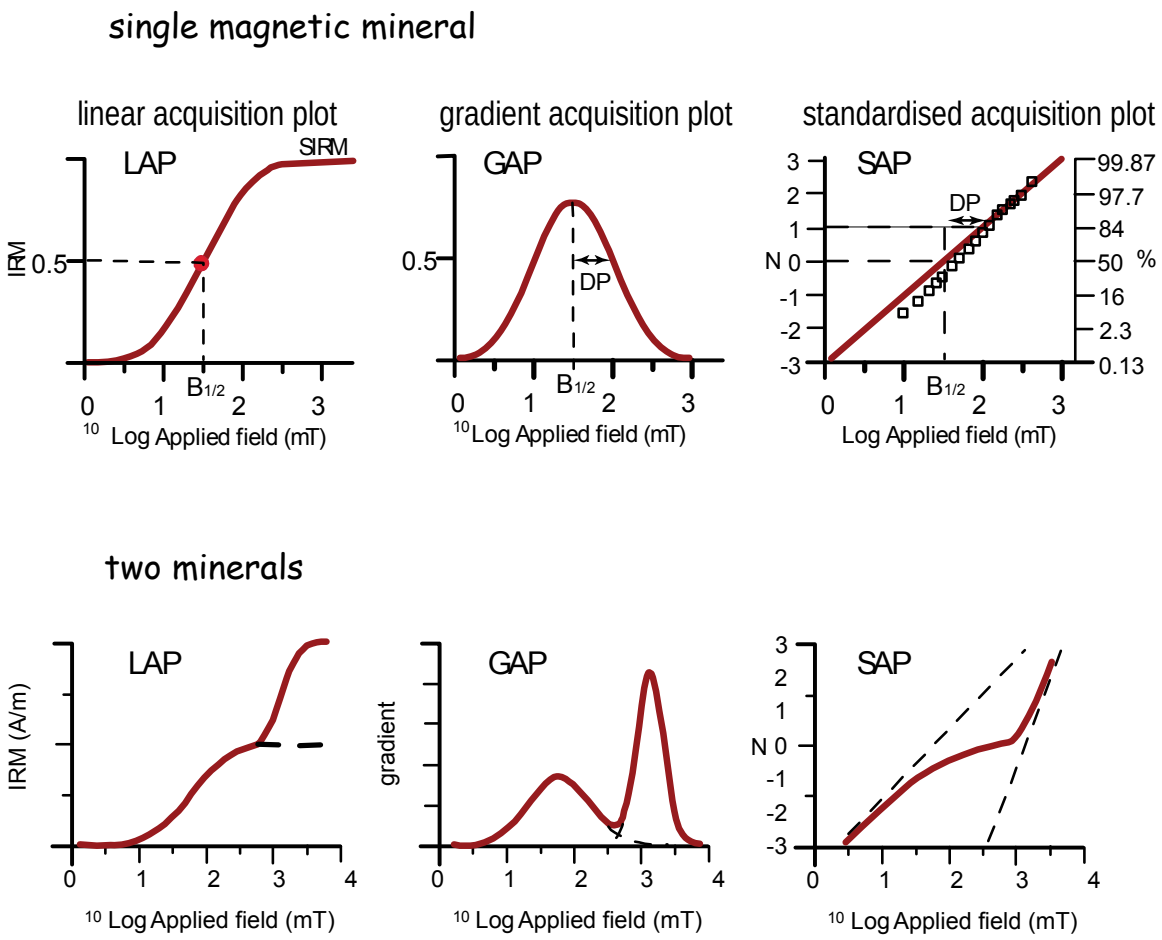

Figure 5-3. Basic principles of the IRM acquisition curves analysis, from Kruiver et al. (2001). IRM acquisition curves of individual minerals conform to a cumulative log-Gaussian curve. An assemblage of grains of a single magnetic mineral can be characterised by:

1) its saturation IRM (SIRM),

2) mean coercivity: the feld at which half of the SIRM is reached: $B_{1/2}$;

3) the width of the distribution: the dispersion parameter DP, given by one standard deviation of the logarithmic distribution

If more than one magnetic mineral is present, their IRM acquisition curves add linearly.

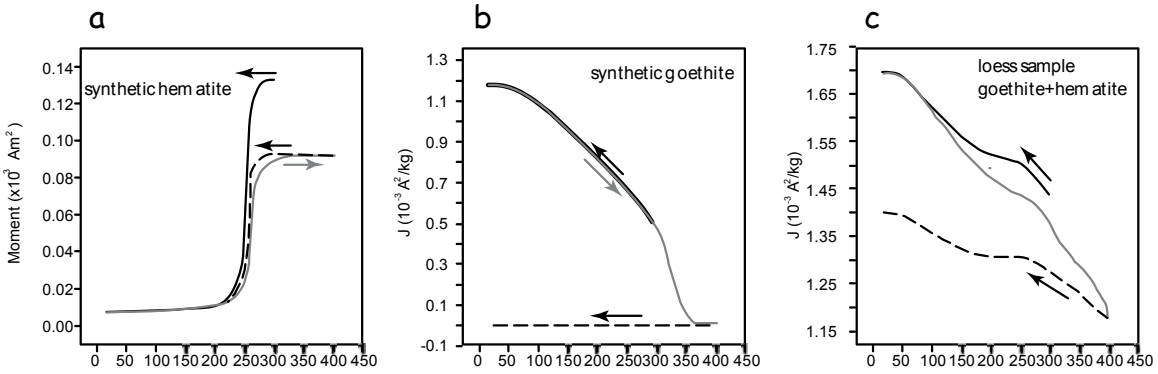

Figure 5-4. Low-temperature behavior of pedogenic iron oxides. Partial remanence acquired in 5T field and then partially demagnetized with a maximum field of 0.2T (5.0-0.2 TIRM) measured on cooling from 300-20 K, warming 20-400 K, and cooling 400 -20 K for a) a hematite standard, b) goethite standard, and c) a natural loess sample. From Carter-Stiglitz et al. (2006).

Results

Typical examples of the IRM acquisition plots for the studied samples are shown in Fig. 5-5. There are four distinctive magnetic components with variable contribution to the total IRM: 1) the low coercivity component with $\log B_{1/2}$ ~1.5-1.75 and DP ~3.0-3.5 (grey bar in Fig. 5-5) is present in all samples; 2) an additional component in the low coercivity range; the $\log B_{1/2}$ is ~1.85-1.9 and a very narrow distribution, DP ~ 0.7-1.2 (green bar) is present in a majority of the samples; 3) an intermediate coercivity component with $\log B_{1/2}$ ~ 2.4-2.7 and DP ~2.7-3.5 (orange bar); and 4) a high coercivity component with $\log B_{1/2}$ ~3.2-3.4 and DP ~ 2.2-2.7 (yellow bar in Fig. 5-5).

Identity of the components

The component with the lowest coercivity likely represents a mixture of several magnetic phases. Previous rock-magnetic study of the ODP Leg 116 cores (Hall and Sager, 1990) identified (titano-)magnetite and maghemite as dominant carries of magnetization in the sediments; mean coercivities of these minerals (e.g. Dunlop and Ozdemir, 1997) fall within our "first component" range. Thermomagnetic runs on representative samples (Fig. 5-6) indicate that the dominant carrier of magnetization has Curie temperature ~ 580 ^{o}C, typical of magnetite. The inflection at ~ 300-350 ^{o}C on the heating branch of the curve (sample 7-64-2-90) suggests the presence of another magnetic phase, likely iron sulfide, greigite or phyrrotite. The stepwise thermomagnetic runs on sample 7-54-7-0 (Fig. 5-7) shows non-reversible behavior during heating-cooling at temperatures up to 400 ^{o}C. In this temperature range, the cooling limb is lower than the heating one, indicating the ongoing destruction of a magnetic phase. The Curie temperature of this phase lies in the interval between 300 and 400 ^{o}C, consistent with iron sulfides. The 500 ^{o}C run is reversible, with no mineralogical changes occurring in this 400-500 ^{o}C range. The 600 and 700 ^{o}C runs are non-reversible again; this time the cooling limb is higher than the heating one, indicating that a formation of a new magnetic phase (with the Curie temperature of ~ 580 ^{o}C- magnetite) is occurring at temperatures higher than 500 ^{o}C. The oxidation of iron sulfide (either magnetic or non-magnetic) or a

Figure 5-5. Examples of IRM acquisition plotted as GAP (gradient acquisition plot) and SAP (standardized acquisition plot). Samples show variable contributions of four distinct components into the total IRM. The components are identified as hematite (orange bar), goethite (yellow bar), detrital magnetite/maghemite (grey) and biogenic magnetite (green).

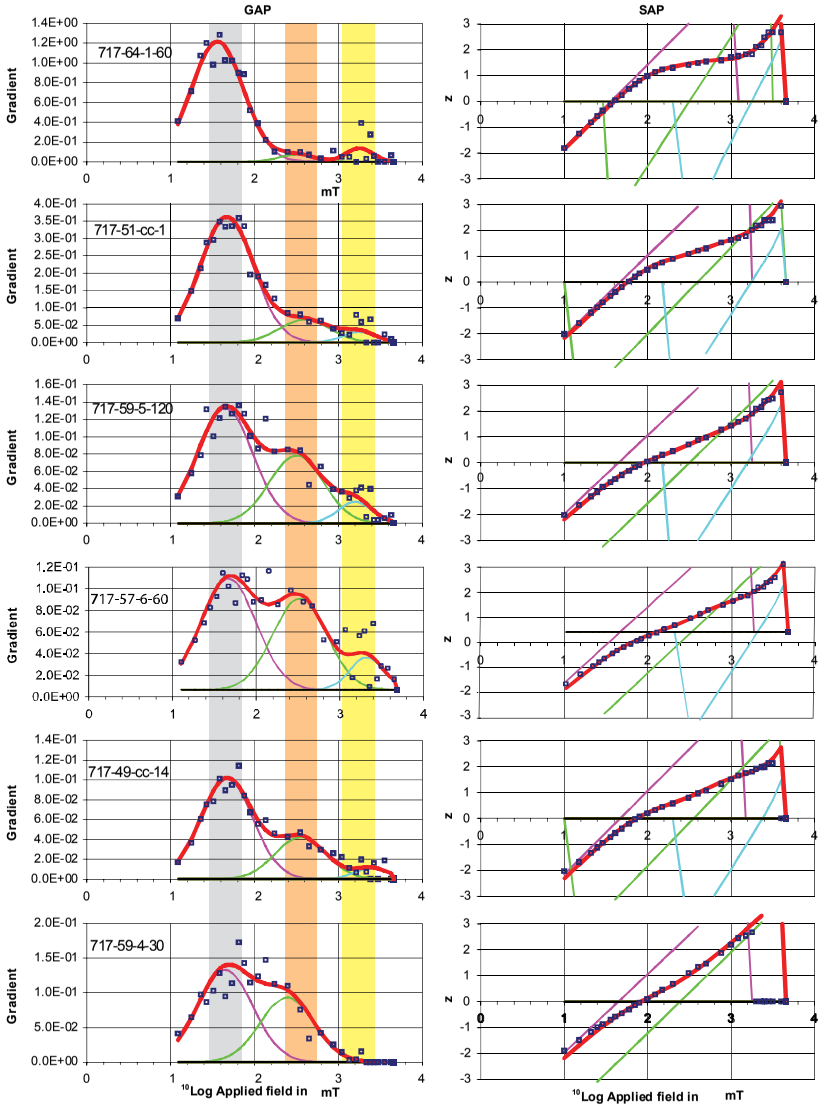
GAP
SAP
717-64-1-60
717-51-cc-1
717-59-5-120
717-57-6-60
717-49-cc-14
717-59-4-30
Gradient
z
mT
Log Applied field in mT

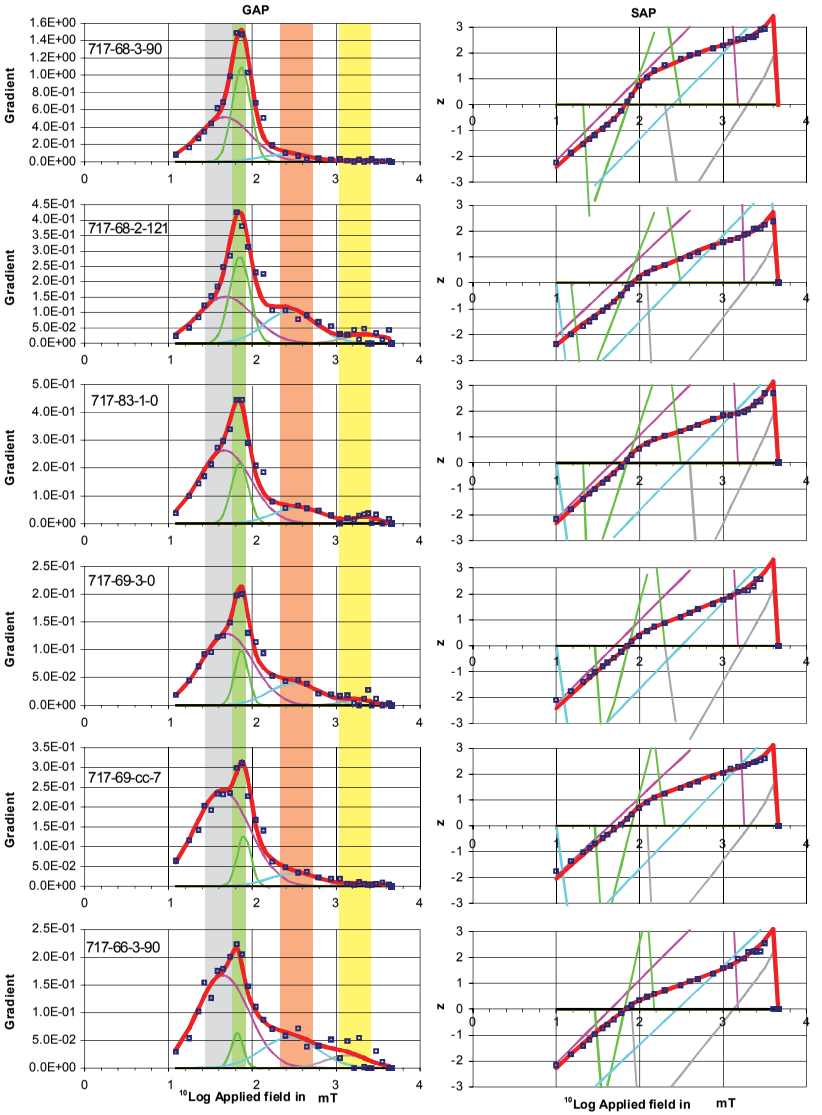
GAP
SAP
717-68-3-90
717-68-2-121
717-83-1-0
717-69-3-0
717-69-cc-7
717-66-3-90
Gradient
z
mT
Log Applied field in mT

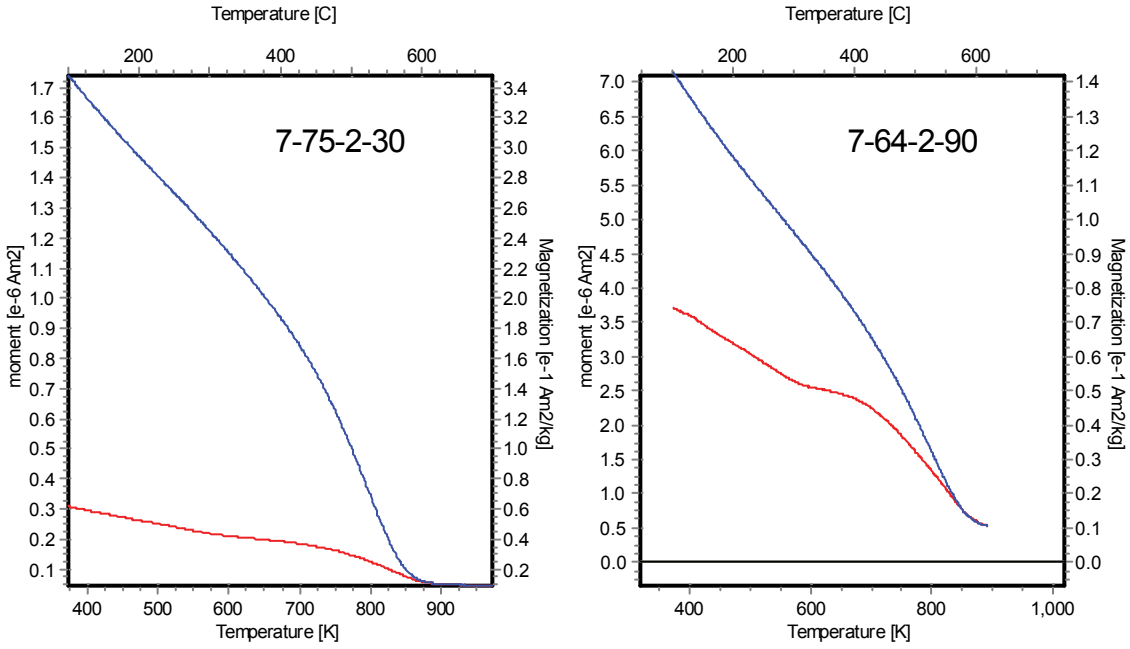

Figure 5-6. Thermomagnetic runs for representative samples. Curie temperature of ~ 580 ^{o}C indicates magnetite as a dominant carrier of magnetization. A slight inflection on a heating curve (sample 7-64-2-90) at ~ 300 ^{o}C, suggests presence of an iron sulfide (pyrrhotite or greigite).

Figure 5-7. The stepwise thermomagnetic runs on the sample 7-54-7-0. Non-reversible behavior during heating-cooling at temperatures up to 400^{o}C indicates the ongoing destruction of a magnetic (likely iron sulfide) phase. Non-reversible 600^{o}C and 700^{o}C runs with the cooling branch being higher than the heating branch suggest that a new magnetic phase (with a Curie temperature of ~ 580^{o}C, plausibly magnetite) is growing at temperatures higher than 500 ^{o}C.

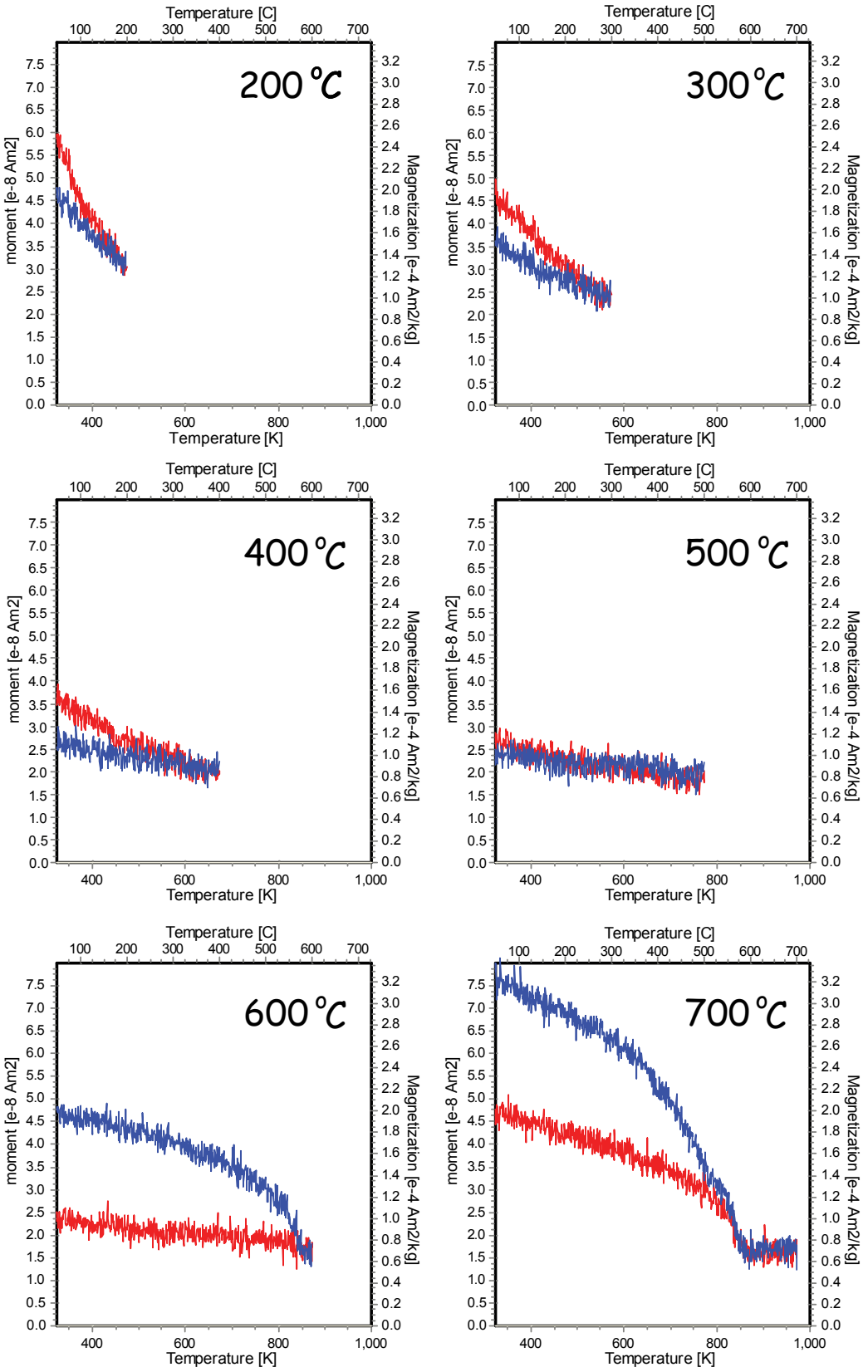
200 ℃
300 ℃
400 ℃
500 ℃
600 ℃
700 ℃
Temperature [C]
Temperature [K]
moment [e-8 Am2]
Magnetization [e-4 Am2/kg]

conversion of maghemite previously identified in the Bengal Fan samples by Hall and Sager (1990) can be the source of this neo-forming magnetite.

The second low coercivity component present in some samples is characterized by a very distinctive, narrow (DP=0.8-1.2) peak with $\log(B_{1/2})$=1.87-1.9 (green color in Fig. 5-5). The narrow shape of this peak indicates that the corresponding population of magnetic grains has a restricted coercivity range, which is a sign of uniform grain-size and/or composition. The field at which this assemblage of grains reaches saturation, at ~180 mT, is consistent with this mineral being single-domain size magnetite (Dunlop and Ozdemir, 1997). In previous studies, similar components with very narrow dispersion are believed to be of biogenic origin (e.g. Kruiver and Passier, 2001; Egli, 2004; Kawamura et al., 2007), e.g. related to magnetic grains (magnetosomes) produced by magnetotactic bacteria. Magnetosomes are well ordered, chemically pure, morphologically distinct crystals, with sizes (35-120 nm) that fall within the stable single magnetic-domain range (Bazylinski and Moskowitz, 1997; Cornell and Schwertmann, 2003). Our TEM investigation of magnetic separates from two samples that show prominent "biogenic" peaks revealed the presence of small chemically pure (e.g. Ti-free) iron oxide grains with morphologies unique to the magnetosomes (Fig. 5-8). High resolution TEM micrographs show well-ordered cubic structure (Fig. 5-8) with unit-cell dimensions typical of magnetite.

A six-criteria scoring scheme has been proposed for the identification of magnetofossils (Kopp and Kirschvink, 2007), i.e., 1) well-constrained geological context; 2) presence of significant single-domain magnetite; 3) narrow size and shape distributions, microscopic evidence reveals single-domain particles with truncated edges, elongate single-domain particles, and/or narrow size and shape distributions; 4) presence of chains; 5) near-stochiometry of the particles; 6) near-absence of crystallographic defects. Our identification failed to satisfy only one criterion; we did not observe chain alignment of the grains. The chain alignment is easily detected in living bacteria; however, it is rarely observed in magnetic separates (e.g. Maloof et al., 2007). The simple technique for the extraction of the magnetic fraction that we used is not likely to preserve the original spatial arrangement of the magnetic grains. All in all, the combination of

magnetic properties and TEM observations is definitely supportive of the interpretation of the second low coercivity component as of biogenic origin.

The two remaining high coercivity components we identified as hematite and goethite. The mean coercivities of these components ($logB_{1/2}$~ 2.4-2.7 and ~3.2-3.4) are similar to coercivities generally reported for hematite and goethite, respectively (e.g. Kruiver et al., 2001; France and Oldfield, 2000; Heller, 1978; Rochette and Fillion 1989). Low-temperature cycling runs (Fig. 5-9) also indicate hematite and goethite as the main contributors to the high coercivity (i.e. > 200 mT) fraction of the total IRM. Most of the low-temperature cycling runs display behavior typical of a hematite and goethite mixture such as the non-reversible low-temperature loop with a slight inflection on the cooling curve at ~ 200-250K (the weak Morin transition in hematite) as well as the non-reversible loss of intensity upon heating due to demagnetization of goethite (Fig. 5-9a,b). In some samples (e.g., Fig. 5-9c,d,e), the Morin transition is suppressed, which is typical of poorly crystalline hematite; yet the loss of intensity in the high temperature loop allows us to identify goethite with confidence. Out of fifty one samples that were studied, only five produced anomalous thermomagnetic runs with both the low-temperature and the high-temperature loops being practically reversible (Fig. 5-9f). These five samples display a significant rise in intensity upon cooling to 20K (a feature typical of goethite) and there is an indication of an intensity drop at ~ 390K (~ Neel temperature of goethite), yet the intensity recovers upon cooling in zero-field to 300K. This atypical behavior might represent an unusual magnetic mineralogy in these samples, but this "unusual mineralogy" explanation seems unlikely. The IRM acquisition plots for the samples with the anomalous thermomagnetic behavior indicate the presence of magnetization components that are identical to those in samples with normal behavior, including the prominent goethite component in some cases.

An alternative explanation for the unusual thermomagnetic curves is that the atypical behavior might be the result of spin-coupling between hematite and goethite. The spin-coupling mechanism of intensity recovery is postulated for hematite on warming through the Morin transition (Ozdemir and Dunlop, 2002). In the case of hematite, a small "defect ferromagnetism" preserved at temperatures below the Morin transition, serves as a catalyst in regenerating the anti-ferromagnetic moment upon warming (in zero

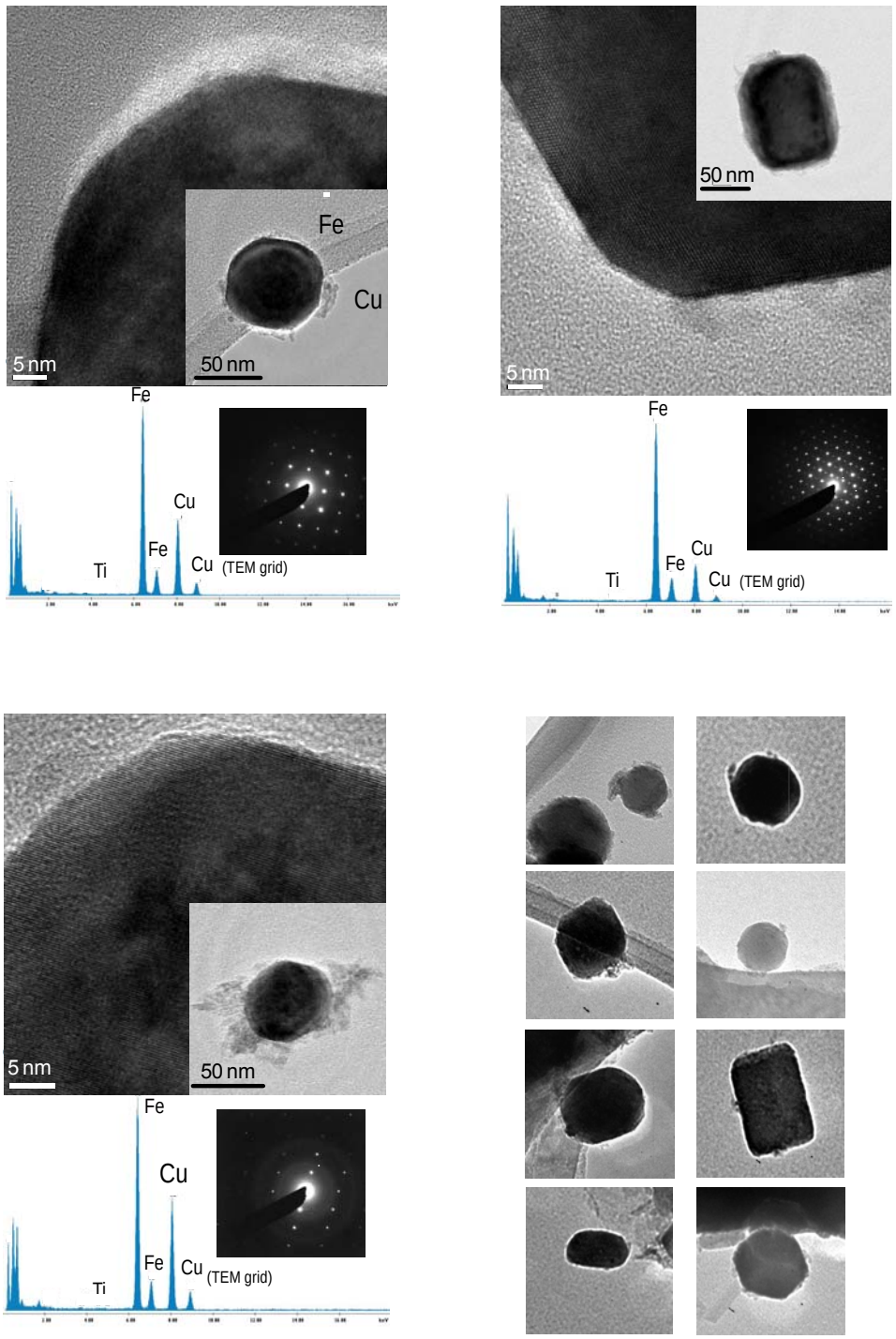

Figure 5-8. TEM micrographs of small grains from magnetic extract of sample 7-68-2-88, which shows a prominent "biogenic magnetite" peak. The size range of the grains (50-120 nm long dimensions), their rectangular prismatic to cubo-octahedral shapes and absence of Ti are typical for magnetosomes. Cu peaks on the energy dispersive X-ray spectra are from the TEM grid.

Figure 5-9. Low temperature cycling runs (Carter-Stiglitz et al., 2006) for representative samples. Partial remanence acquired in 5T field and then partially demagnetized with a maximum field of 0.2T (5.0-0.2 T IRM) measured on cooling from 300-20 K, warming 20-400 K, and cooling 400 -300 K. a) and b). Non-reversible low temperature loops with a slight inflection on the cooling curve at ~ 200-250K (the weak Morin transition) indicate the presence of hematite in the samples; non-reversible loss of intensity on heating 300 to 400 K and cooling back to 300 oC indicates the presence of goethite. c), d) and e). The Morin transition is suppressed in these samples, but the goethite contribution is evident by the loss of intensity on the high temperature loop. f). Example of an anomalous sample with both the low and high temperature loops being practically reversible.

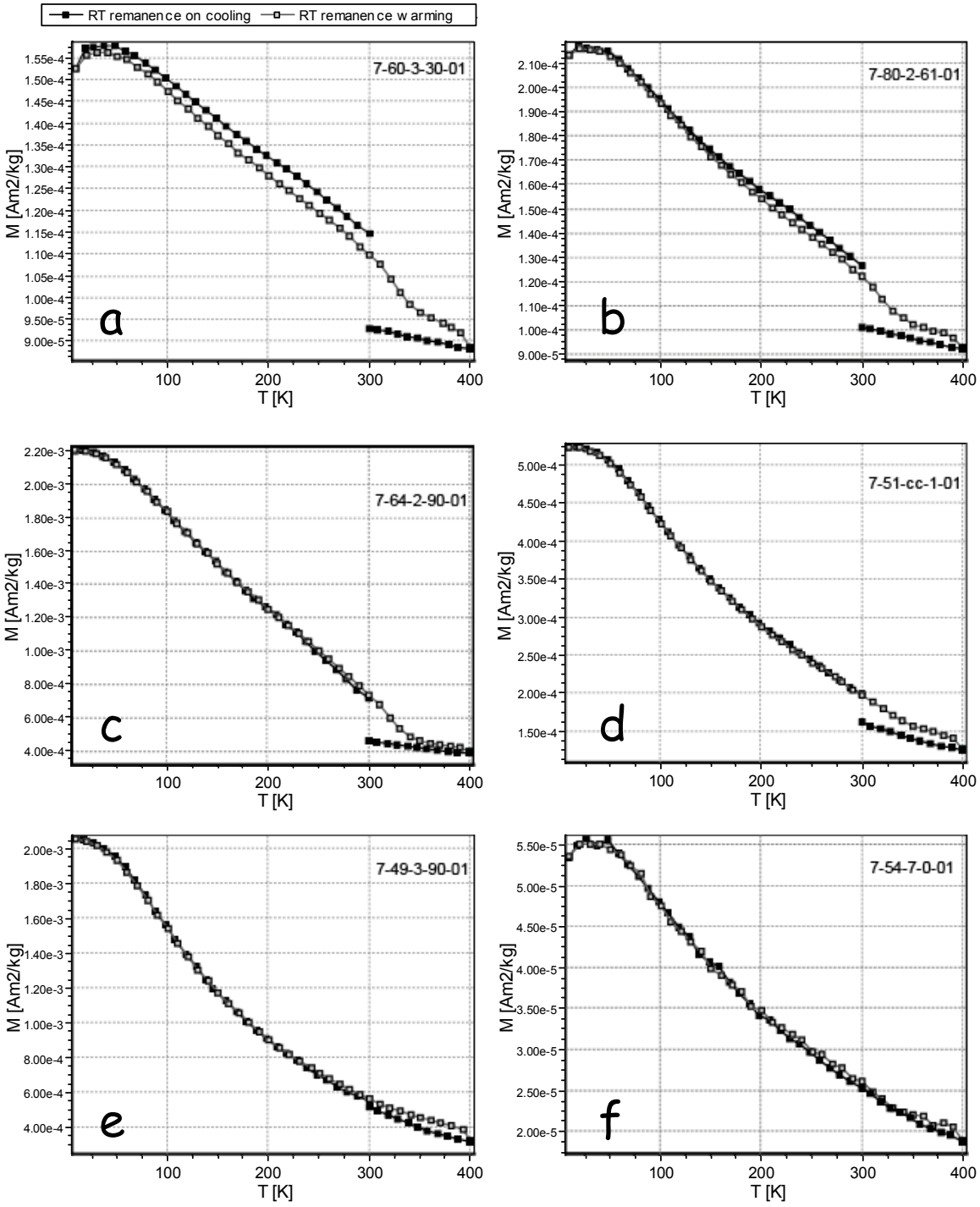
RT remanence on cooling
RT remanence warming
7-60-3-30-01
a
7-80-2-61-01
b
7-64-2-90-01
c
7-51-cc-1-01
d
7-49-3-90-01
e
7-54-7-0-01
f
M [Am2/kg]
T [K]

external field) through the transition. Similarly, in our samples, the magnetic moment of hematite might serve as a template in regenerating magnetic moments of the goethite grains as they cool through the Neel temperature.

Reliability of the IRM acquisition analysis in quantifying goethite and hematite

To further strengthen our interpretation of the two high coercivity components as hematite and goethite, as well as to evaluate the reliability of the Kruiver et al. (2001) technique in estimating relative contributions of these minerals, we compared the results of the IRM analyses with the results of the LowTC for the set of samples. In order to accommodate the different sample size employed by these two techniques, we used the ratio of goethite to hematite as a comparison parameter. The two techniques also define the "high coercivity fraction" (and thus the contributions of goethite and hematite into the high coercivity fraction) differently; Fig. 5-10 illustrates the difference in definition. In the IRM analysis, the high coercivity fraction is considered simply as the sum of the hematite and goethite SIRMs, while in the low-temperature cycling, high coercivity is defined as coercivity above 200 mT. According to the analysis of the IRM acquisition curves, the high coercivity part of the IRM used in the LowT cycling would include a contribution of the high coercivity end of the "magnetite" distribution and exclude the low coercivity portion of the "hematite" component. In our estimates of the goethite contribution and G/H ratios, we corrected for the differences in the IRM intensity estimates arising from variations in definition of the high coercivity fraction. Resulting estimates of the G/H ratio by both methods (Fig. 5-11) agree well (data-points lie close to 1:1 slope line) for all of the observed range of goethite contents, including samples with small contributions (<10%). The good fit suggests that 1) our interpretation of the highest coercivity peak in the IRM curve as goethite is correct; 2) the IRM analysis gives an adequate estimate for contribution of goethite and hematite into the total IRM.

Results summary

Analysis of the IRM acquisition curves (Kruiver et al., 2001) shows the presence of four magnetic components in the studied samples (Fig. 5-5). The lowest coercivity

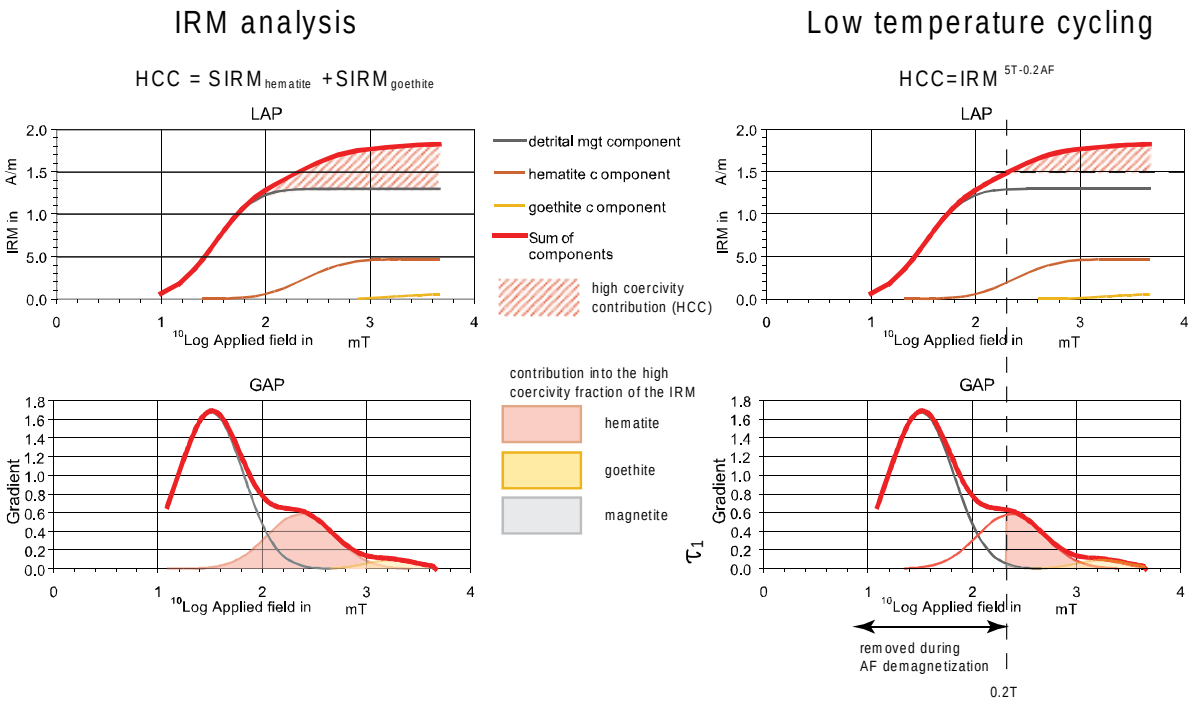

Figure 5-10. The difference in definition of the "high coercivity fraction" employed in the IRM analysis and in the low temperature cycling. According to the analysis of IRM acquisition curves, the high coercivity part of the IRM used in the low temperature cycling would include a contribution of a high coercivity end of the "magnetite" distribution and exclude the low coercivity portion of the "hematite" component.

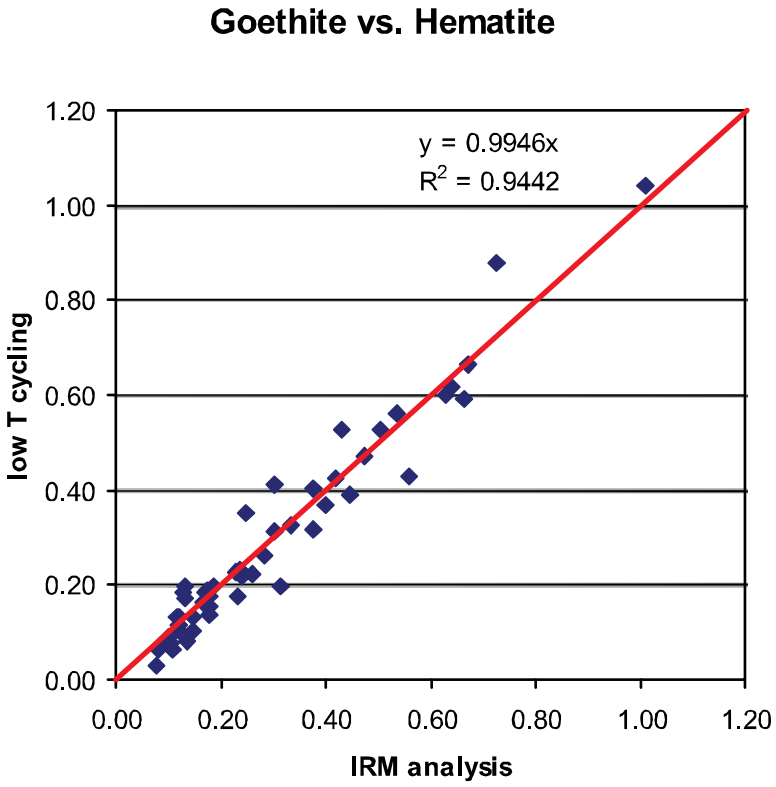

Figure 5-11. Values of the goethite to hematite ratio identified by two methods based on different physical principles. Results of both methods agree, suggesting that the IRM analysis gives an adequate estimate of the content of these minerals.

component is likely to represent a mixture of several phases, (titano)magnetite, ± maghemite and iron sulfides. The second low coercivity component with a characteristic narrow dispersion parameter is likely to be magnetite of biogenic origin. For simplicity sake, in further discussion, the first low coercivity component will be referred to as "detrital" as opposed to the "biogenic" second component. The third and fourth components are identified as hematite and goethite, respectively. The estimates for hematite and goethite contributions to the total IRM based on the analysis of the IRM acquisition curves (Kruiver et al., 2001) are consistent with similar estimates obtained from LowT cycling (Carter-Stiglitz et al., 2006), indicating that the Kruiver et al. (2001) technique provides adequate assessment of these two mineral contents in the samples.

The variations in the relative abundance of goethite and the presence of the biogenic component in the studied sections of the Holes 717 and 718 are plotted in Fig. 5-12. The relative abundance of goethite is shown as the G/(G+H) parameter, where the amount of goethite (G) and hematite (H) was estimated as the SIRM of the component divided by the saturation magnetization. The value of saturation magnetization of a magnetic mineral may vary depending on grain-size and stoichiometry (Dunlop and Ozdemir, 1997); in this study we used the values of ~ 2.5 kA/m for hematite and ~2kA/m for goethite estimated for pedogenic minerals in an Argentinian paleosol sequence (Carter-Stiglitz et al., 2006). We should note here, that the choice of different saturation magnetization values will change the absolute value of the G/(G+H) parameter but will not affect the overall trend of variations.

The biogenic magnetite content is plotted as the SIRM values (A/m). As the sample volume and mass in the IRM acquisition experiments were not strictly monitored, the absolute values of the biogenic contribution to the magnetization of the samples cannot be given much significance. The presence or absence of this component in a sample, however, is meaningful, and will be discussed below.

In the studied interval of Hole 717, where better recovery allowed for a more detailed record, the G/(G+H) ratio displays quasi-periodic variations in the lower part of the section, up to ~545 mbsf (~7 Ma). In the interval of ~545 to ~470 mbsf (or ~7 to 6.25 Ma) the ratio stays very low on average, then it shows gradual recovery in the upper part

of the interval, although the ratio does not reach the median value or the variability of the pre-7Ma portion. The drop in the G/(G+H) ratio at ~ 7 Ma coincides with the virtual disappearance of biogenic magnetite from the sediments. In the lower part of the section, the majority of the samples contain the biogenic component, but in the upper part, the biogenic component is rare and restricted to narrow horizons.

While data coverage of Hole 718 is limited due to very poor sediment recovery, the general trends are rather similar to those observed in Hole 717. The G/(G+H) parameter shows some variation prior to ~ 7 Ma. Although the scale and periodicity of the variations appears muted compared to the Hole 717, the median value of the parameter, ~0.25, is similar in both holes. Unfortunately, no sediments were recovered from the section that corresponds to the low G/(G+H) interval of Hole 717 (Fig. 5-12); yet, the decrease in the G/(G+H) ratio at ~ 7 Ma, and its gradual recovery after 6.2 Ma resemble the Hole 717 trend. Distribution of the biogenic component is also similar in two holes; while ubiquitous prior to ~ 7 Ma, biogenic magnetite becomes much rarer afterwards.

Discussion

Climatic signal vs. diagenetic changes

A straightforward interpretation, considering the variations in the G/(G+H) parameter in the studied sections as a proxy for the strength of the Indian monsoon, would suggest that between ~10 and 7 Ma, monsoonal precipitation varied quasi-periodically, with no net increase or decrease in the average intensity. The drop in goethite abundance at ~ 7 Ma, would imply the onset of an arid period in the Himalayan Foreland that lasted for ~ 700,000 yr; then the monsoon began gradual recovery. However, the drastic change in biogenic magnetite content of the sediments, which coincides with the decline in G/(G+H) ratio, hints at another possibility. The observed variations in the relative abundances of goethite and hematite could be in part related to post-depositional diagenetic processes.

Figure 5-12. The variation in relative abundance of goethite vs. hematite and presence of the biogenic component in the studied sections of Holes 717 and 718. The age of the strata was determined by nannofossil stratigraphy by Gartner (1990); the ages of the biostratigraphic zonations were reassigned according to the Berggren et al. (1995) timescale now in general use. Only a few horizons in each of the two studied sections (highlighted by large dots on a time scale) gave age estimates. The sedimentation rate is assumed to be constant between the dated horizons. The age assignments, however, should be treated with caution; there is a suspicion that the entire biostratigraphy may be based on re-deposited fossils, in which case every age assignment would be too old (Gartner 1990).

The inset figure shows variations in the estimated sedimentation rate for the two studied sections. Note, that at ~ 7 Ma, the sedimentation rate in Hole 718 decreased dramatically, while in Hole 717, the rate presumably did not change.

The relative abundance of goethite is shown as the G/(G+H) parameter; content of goethite and hematite is estimated based on the SIRM values obtained by the IRM acquisition analyses. The biogenic magnetite content is plotted as the SIRM values (A/m). As the sample volume and mass in the IRM acquisition experiments were not strictly monitored, the presence or absence of the biogenic component in a sample rather than the absolute values of the biogenic contribution should be considered.

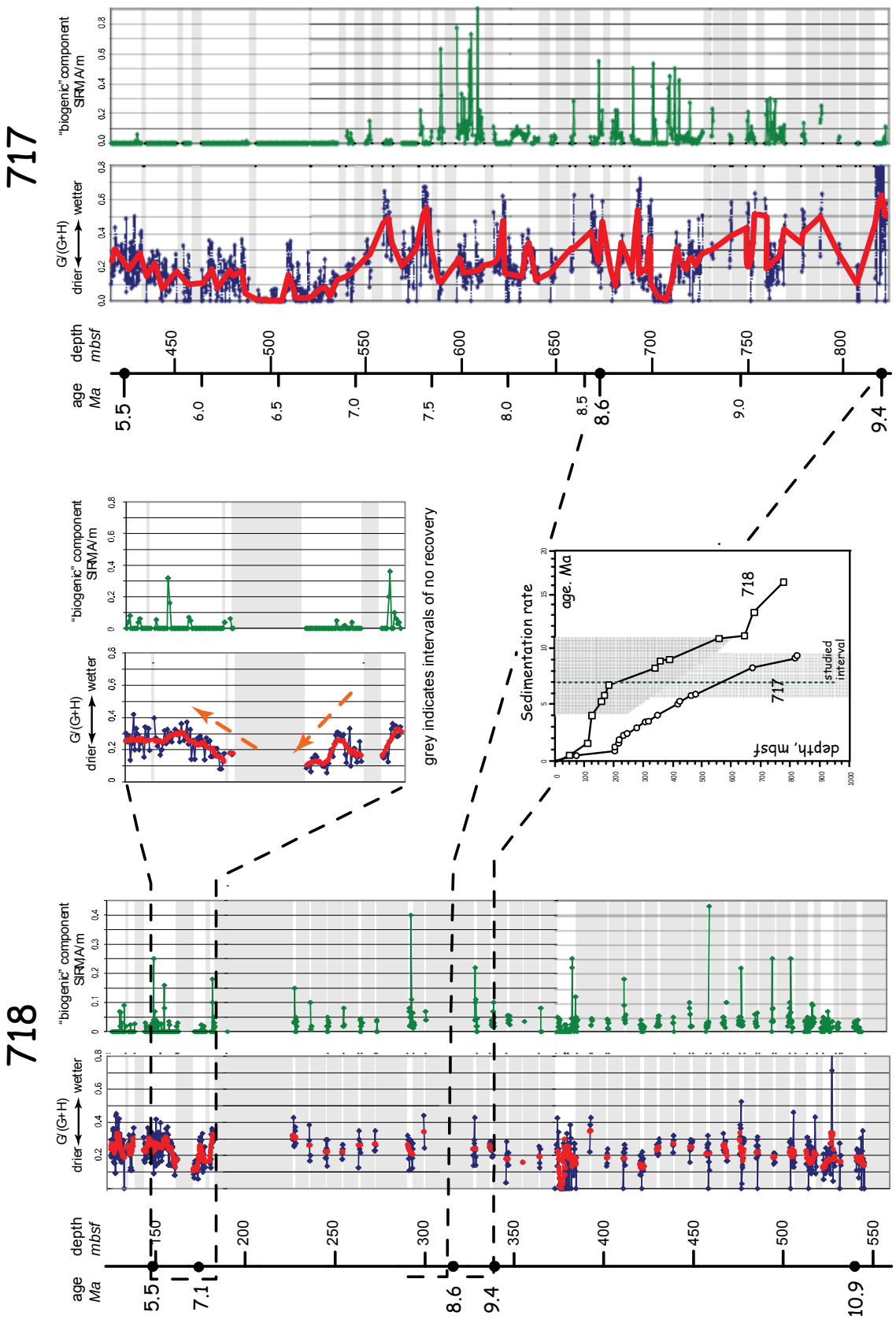
718
717
"biogenic" component SIRM A/m
G'(G+H)
drier
wetter
depth mbsf
age Ma
5.5
7.1
8.6
9.4
10.9
grey indicates intervals of no recovery
Sedimentation rate
age, Ma
depth, mbsf
718
717
studied interval

Stability of the iron (oxyhydr)oxides in marine environments

Burial of unoxidized organic detritus in deep-marine environments promotes bacterially-mediated processes of suboxic diagenesis (Froelich et al., 1979). To decompose organic matter, bacteria require an oxidant. Different populations of bacteria initially use O_2 dissolved in pore-water, followed by secondary oxidants obtained by the reduction of available oxides in the sediments (Curtis, 1983). The sequence of alternative oxidants is predictable and depends on the energy yield of the oxidation reaction. Nitrate and phosphate are utilized first, followed by Mn^{4+}-oxides, and then Fe^{3+}-oxides. In general, the more energetic oxidants are completely exhausted before less energetic ones are used. If the amount of organic matter in the sediments is high enough, such that suboxic diagenesis involves Fe-reducing bacteria, then reductive dissolution of detrital ferromagnetic iron oxides may occur (Bloemendal et al., 1992, Karlin, 1990, Leslie et al., 1990). The early stage of suboxic diagenesis is usually followed by a late stage of oxidative diagenesis associated with the progressive descent of the oxidation front, which is related to diffusion of O_2 from the overlying, oxygen-rich waters. Transition metal cations, including Fe^{2+} dissociated from detrital oxides during the diagenesis, migrate interstitially, following an Eh/pH gradient, to positions in the section where oxygen is available in pore-waters (Colley et al., 1984; Jarvis and Higgs, 1987). There, in the oxidized zone of the sediment, the biogenic or authigenic precipitation of secondary oxides and hydroxides (including magnetic Fe-compounds) could occur (e.g. Lowrie and Heller, 1982, Karlin et al., 1987).

Diagenetic modification of the iron oxide content of marine sediments is well documented in regions of high organic flux, e.g., continental shelf (e.g. Liu et al., 2004; Kawamura et al., 2007; Richter et al., 1999) or areas of high-productivity (e.g. Tarduno and Wilkison, 1996). In slowly accumulating pelagic sediments, the stage of Fe-oxide reduction is seldom reached (Canfield et al., 1992), except in some specific environmental contexts; for example, in turbidite-dominated sediments of abyssal plains. A study of late Cenozoic turbiditic sediments in the North Atlantic (Robinson et al., 2000), which are similar in lithology and organic carbon content to sediments of the distal part of the Bengal Fan, showed that reductive/oxidative processes are important

only in organic-rich (>0.5% organic carbon content) turbidite horizons. In these horizons, significant depletion of detrital (titano)magnetite/maghemite occurs during the initial stage of reductive diagenesis. Reductive dissolution of ferromagnetic grains is a grain-size selective process, that preferentially depletes finer detrital grains. However, the presence of ultrafine ferromagnetic grains has been noted by Robinson et al. (2000) at depths within the suboxic zone of the organic-rich turbidites; these grains were thought to be associated with populations of live magnetotactic bacteria. The high coercivity detrital fraction (hematite or goethite) appeared not to have been affected much, if at all, in the sediments of the organic-rich horizons (Robinson et al., 2000). No secondary, authigenic precipitation of these minerals has been detected in their studied rocks, either.

In modern sediments, the stage of diagenesis at a certain depth is identified by the presence of characteristic ions in the pore-waters. Whether the detrital iron oxides in the sediments have been modified by diagenesis in the paleo-environment has to be deduced from often imperfect clues, e.g., high organic carbon content in the samples, presence of pyrite or evidence for dissolution of ferromagnetic grains. A commonly used sign for alteration is the presence of framboidal pyrite in sediments, which is indicative of sulfate reduction with the replacement of magnetite (e.g., Berner, 1980; Passier and Dekkers, 2002). Pyrite is non-magnetic and often occurs as disseminated grains that require microscopic investigations to detect their existence in the studied rocks. For example, in a spectral reflectance study of ODP site 1143, South China Sea, Zhang et al. (2007) cited the absence of pyrite as evidence for the lack of post-depositional alteration of the sediments. The lithostratigraphic description of Site 1143, however, states that disseminated pyrite as well as pyritized burrows were observed throughout much of the core (Shipboard Scientific party, 2000).

Availability of organic matter, usually assessed as the total organic carbon (TOC) content, was found to correlate with the degree of reductive dissolution in a sequence of late Cenozoic turbiditic sediments in the North Atlantic (Robinson et al., 2000). The dissolution has been detected only in organic-rich (>0.5% organic carbon content) turbidite horizons. The TOC of ancient sediments by itself might not be a definitive indicator for the organic matter initially available for early diagenesis. Bio-available organic matter is consumed early, and only non-reactive organics, e.g. wood debris, tend

to be preserved. For example, in the sediments of ODP site 1143, so-called green layers have low (<0.5%) TOC while also showing evidence for significant selective dissolution of the original sedimentary matrix (Tamburini et al., 2003). The matrix dissolution as well as the presence of disseminated pyrite (Shipboard Scientific party, 2000) implies reducing conditions, perhaps caused by periods of intensive primary productivity in the region (Tamburini et al., 2003).

Early diagenetic dissolution of ferromagnetic grains (titano-magnetite and maghemite) and its grain-size selective character (preferential depletion of finer ferromagnetic grains) has been documented in multiple studies (e.g., Haese et al., 1998, Robinson et al., 2000; Kawamura et al., 2007). Thus, the loss of detrital magnetite and an increase in the mean grain-size can potentially be used to identify sedimentary horizons affected by diagenetic alteration, but only if the initial content and grain-size distribution of the detrital fraction is known. In turbidite sequences, the depositional processes and differential settling of ferromagnetic grains leads to large variations in the detrital ferromagnetic fraction even within a single turbidite-emplacement layer (Hall and Sager 1990). On the other hand, the preservation of the fine-grained ferromagnetic fraction in the sediments, for example, biogenic magnetite, can be used as a clue to estimating the degree of diagenetic alteration.

Environmental significance of biogenic magnetite

Biogenic magnetite, fine-grained crystals of magnetite (magnetosomes), is produced by magnetotactic bacteria. Magnetotactic bacteria are ubiquitous in aqueous habitats and are generally found in the highest numbers at the oxic-anoxic transition zone (also referred to as microaerobic zone or redoxcline). The bacteria usually inhabit zones within the sediment where only trace concentrations of oxygen exist, at a level where nitrate reduction is the dominant source of secondary oxidant (Rhoads et al. 1991). The majority of live (swimming) magnetotactic bacteria occupy a well-defined, narrow subsurface layer at a fixed distance below the oxidation front (Petermann and Bleil, 1993).

Upon the death of a magnetotactic bacterium, the protective organic membrane of the cell-wall disintegrates, and magnetosomes are released into the sediment. In suboxic

conditions that are optimal to the living bacteria, magnetofossils (SD magnetite) are unstable and may eventually dissolve. Gradual dissolution of biogenic magnetite was documented in sediments from a subarctic Swedish lake (Snowball, 1994) and in marine sediments (e.g. Tarduno and Wilkison, 1996; Vali and Kirschvink, 1989; Robinson et al., 2000). Thus, in a steady-state system of coupled sediment accumulation and reductive diagenesis, fossil magnetosomes are not likely to be preserved.

In turbidite sequences, such as those of the Bengal Fan, the pulse-like sedimentation nature promotes diagenesis to occur in two stages. An initial rapid phase of reductive diagenesis in organic-rich turbidites is followed by a later stage of oxidative diagenesis, associated with the slow descent of the oxidation front due to diffusion of oxygen from the overlying bottom waters (Robinson et al. 2000). As the oxidation front passes down within the turbidite, the zone of bacterial magnetite proliferation migrates accordingly, leaving fossil magnetosomes behind in the interval between the migrating colony of living bacteria and the descending oxidation front. Under these conditions, magnetofossils could be preserved if suboxic conditions are quickly transformed into an oxic (or post-oxic) state, either by rapid sediment accumulation or by the passage of the oxidation front (Robinson et al., 2000).

Accordingly, preservation of the magnetosomes in turbidite sequences indicates that diagenesis did not reach the iron reduction stage since in the iron reduction zone, fine-grained magnetosomes (having low preservation potential because of a large surface to volume ratio) would dissolve quickly. The ubiquitous presence of biogenic magnetite in the lower part of the studied sections of the Bengal Fan sediments demonstrates that diagenetic processes there are not likely to have reached the iron reduction stage, and, therefore, are not likely to modify the relative abundances of the derital components.

Disappearance of the biogenic component from the upper part of the studied sections, on the other hand, suggests that some kind of environmental change had taken place there. For example, the change in oxidation state of bottom waters could have modified the bacterial colonies and limited the production of magnetosomes, or alternatively, the change in diagenetic conditions could have led to dissolution of the magnetosomes.

Evidence for reductive dissolution

The content of the TOC, fine-grained (biogenic) and coarser-grained (detrital) ferromagnetic components, as well as the identified presence of pyrite in the sedimentary column and the G/(G+H) ratio for the studied section of Hole 717 are plotted side-by-side in Fig. 5-13. Based on the combination of these parameters, the sediments can be roughly subdivided into three categories. The first category (lower part of the section, no highlight) is characterized by the presence of the biogenic component (i.e. fine ferromagnetic grains), variable contributions of the detrital component and a TOC content genereally below 0.5%. The ubiquitous biogenic component testifies that the diagenesis there did not reach the iron reduction stage; thus, relative abundances of iron oxides of the initial detrital assemblage are not likely to be modified.

The second type (highlighted by green bars) is distinguished by the disappearance of the biogenic component, as well as extremely low content of the detrital component. These intervals usually have high (>0.5%) TOC, and multiple occurrences of pyrite. This combination strongly suggests that these sedimentary horizons have been affected by diagenesis to a significant degree.

The third type (the upper part of the section, blue higlight) essentially lacks biogenic component, yet it has a significant content of the detrital fraction. It also contains high TOC, as well as some pyrite. The absence of the fine-grained (biogenic) fraction in association with some occurrence of pyrite, indicates that diagenetic dissolution has affected this horizon, although the degree of alteration was not likely to have been as severe as in the second type.

The measured G/(G+H) ratio in the sedimentary column seems to correlate strongly with the dissolution-based type of the sediments, with an increased degree of alteration accompanied by lowering of the ratio. Whether this decrease in the ratio is an artifact of a diagenetic modification or a meaningful climatic signal is impossible to determine at present, as relative stabilities of goethite and hematite with the respect to the reductive dissolution are poorly known (for a brief overview of the previous studies on stability of iron oxides see Appendix B).

Figure 5-13. Variations in biogenic and detrital magnetite, hematite and goethite components obtained in present study as well as the total organic carbon (TOC) and documented presence of pyrite (purple stars) in the sediments of the studied interval of Hole 717 (Shipboard scientific party, 1989. ODP Leg 116 initial report). Based on a combination of these parameters the sediments can be subdivided into three types. The first type (no highlight) is characterized by the ubiquitous presence of the biogenic (fine-grained) magnetite component and low (<0.5 %) TOC. The second type (pale green highlight) is defined by the extremely low detrital (coarse-grained) content, absence of biogenic (fine-grained) magnetite, high TOC and multiple occurrences of pyrite. The third type (blue highlight) is similar to the second type in the high TOC, presence of pyrite and the absence of biogenic magnetite, yet differs from the second type by a higher content of the detrital (coarse-grained) component. These three categories likely reflect the variable degree of diagenetic alteration at different depth intervals; low in the first type, intermediate in the third, and the severe in the second (see text for explanation).
The G/(G+H) parameter exhibits a broad correlation with the diagenetic subdivision of the sediments. The first type (no significant alteration) displays a higher mean value as well as larger amplitude variability in the parameter. In the third type of the sediments (intermediate stage of alteration), both the mean value and variability of the parameter are lower compared to the first type. The second type (severe alteration) corresponds to the lowest values of the G/(G+H) parameter.

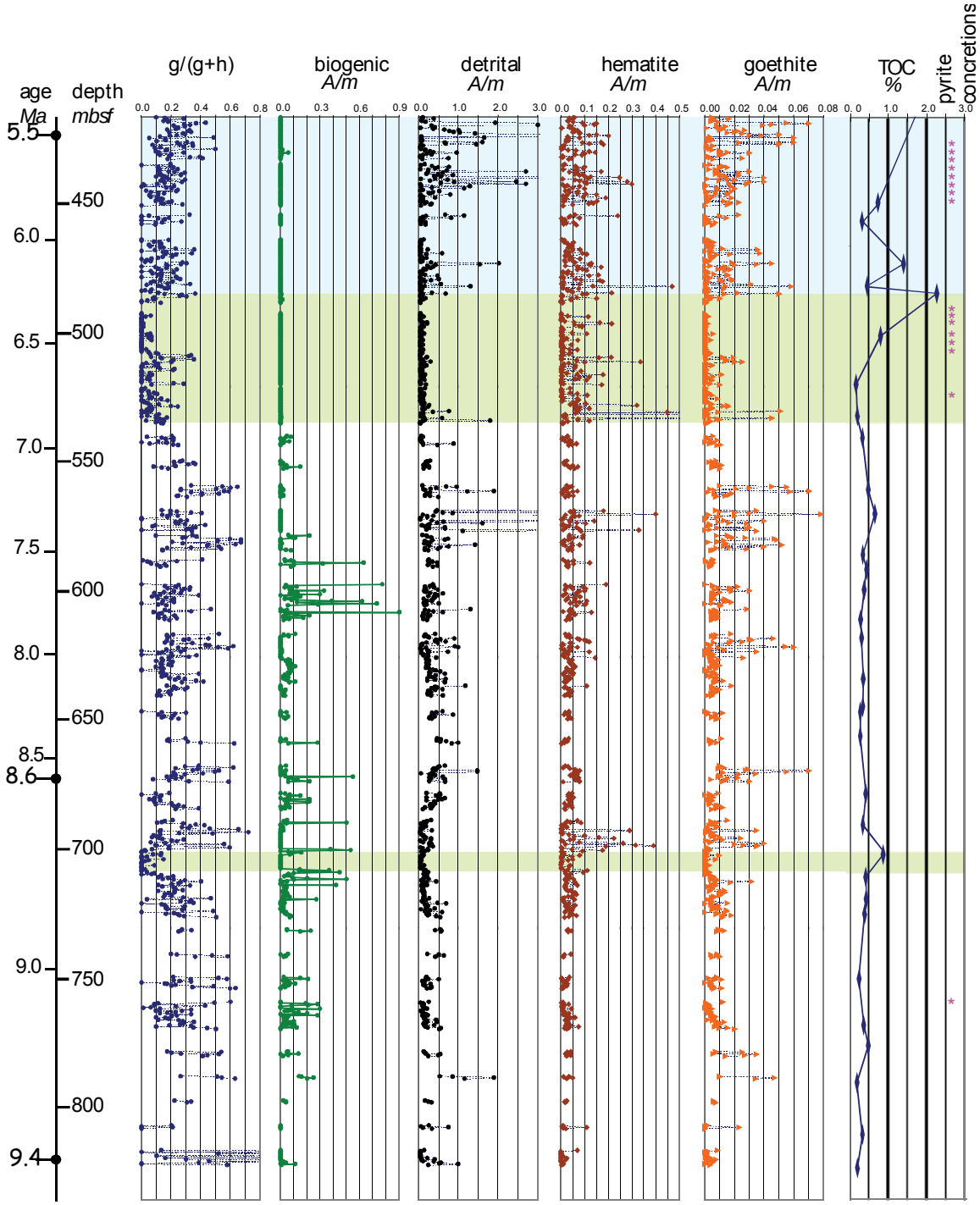
age
Ma
depth
mbsf
g/(g+h)
biogenic
A/m
detrital
A/m
hematite
A/m
goethite
A/m
TOC
%
pyrite
concretions
5.5
6.0
6.5
7.0
7.5
8.0
8.5
8.6
9.0
9.4
450
500
550
600
650
700
750
800

Summary and Conclusions

Our rock-magnetic study of the ~10.5~4.0 Ma Bengal Fan sedimentary sequence indicates the presence of four distinct magnetic components, including "detrital" and "biogenic" magnetite, hematite and goethite. Statistical analysis of the Isothermal Remanent Magnetization provides an adequate estimate for the content of goethite and hematite in the samples. Relative abundances of goethite and hematite vary with depth. In the lower part of the studied interval of Hole 717, up to 545 mbsf or ~ 7 Ma, the G/(G+H) ratio show quasi-periodic fluctuation, with local maximum at ~ 7.5-7.2 Ma. The biogenic magnetite component ubiquitously present in this part of the section testifies that iron-reduction diagenesis has not affected the studied rocks. Thus, the relative abundances of goethite and hematite reflect weathering conditions in the source area of the sediments. Accordingly, in the ~ 9.4-7.0 Ma time interval the Indian monsoon shows periodic variations in its intensity. Although poor sediment recovery, combined with largely uncertain age dating, does not allow for spectral analysis, a rather low-frequency cycle of ~ 400,000 yr seems to dominate the signal.

In the depth interval of ~ 545-480 mbsf (~7.0-6.3 Ma) the goethite content of the sediments is very low, above which, the G/(G+H) ratio shows gradual recovery, though it does not reach the mean value or variability of the pre-7 Ma part of the section. This part of the section is also characterized by the disappearance of the biogenic magnetite component and an extremely low detrital magnetite content coinciding with the lowest values of G/(G+H) ratios. Evidence for dissolution of the ferromagnetic detrital fraction, the higher organic carbon content and the presence of disseminated pyrite in this part of the section strongly suggests diagenetic alteration of the sediments, likely as advanced as the sulfite-reducing stage. This advanced stage of diagenesis is likely to affect the high coercivity minerals as well; but how exactly the original ratio of goethite and hematite has been modified cannot be determined, as relative stability of these two minerals with respect to reductive diagenesis is poorly known. As a result, no reliable climatic interpretation can be given to the G/(G+H) data from the upper part of the studied section.

The recognition of diagenetic alteration, however, brings out an important concern. Relative abundances of goethite and hematite in marine sediments have been increasingly used as a precipitation proxy for the source area of the sediments. Reflectance spectrometry, the method of choice in these studies, while quick and efficient in estimating the amount of goethite and hematite in the samples, might overlook the evidence for the post-depositional diagenetic alteration that can potentially modify the initial ratio of these minerals. The absence of a down-hole decrease in content of the high coercivity fraction, often cited as evidence that the G/H ratio has not been diagenetically modified (Harris and Mix, 1999, 2002, Zhang et al., 2007), is an unreliable criterion. As our study has shown, there is no simple correlation between the stage of diagenesis and the depth of the sediments. The diagenetic alteration, rather, is a stratigraphic feature that developed under the influence of several factors. In our case, the stage of diagenesis seems to be regulated by the availability of organic matter; variations in sedimentation rate or oxygen content of bottom waters similarly could result in a layer-parallel difference in the reductive dissolution.

Reflectance spectroscopy studies should be supplemented with other methods, such as rock-magnetic techniques, that allow for monitoring of diagenetic alteration. With rock magnetic methods, alteration in the ancient sediments can be detected, and its severity can be evaluated based on the presence and grain-size variation of the ferrimagnetic fraction (magnetite/maghemite), which is more sensitive to early reductive dissolution than the high coercivity minerals, goethite and hematite. There is also a need for further studies of dissolution behavior of various iron oxides. Better understanding of how fast and in what way reductive dissolution modifies the initial ratios of various iron oxide phases would improve our ability to detect and correct for the diagenetic changes, and consequently, to extract a reliable climatic signal in studies of marine sediments.

Acknowledgements

This study was supported by an ODP Schlanger fellowship. This research used samples and/or data provided by the Ocean Drilling Program (ODP). ODP is sponsored by U.S. National Science Foundation (NSF) and participating countries under management of Joint Oceanographic Institutions (JOI), Inc. I gratefully acknowledge

David Rea for his help in collecting the samples and for fruitful scientific discussions. I wish to thank the Institute of Rock Magnetism in Minneapolis for use of its facilities. The technical assistance of Mike Jackson, Thelma Berguo, and Peat Solheid at the IRM is greatly appreciated.

References

Anderson, D.M., Overpeck, J.T., Gupta, A.K. 2002. Increase in the Asian Southwest monsoon during the past four centuries. *Science*, 297, 596-599.

Bazylinski, D.A., Moskowitz, B.M. 1997. Microbial biomineralization of magnetic iron minerals; microbiology, magnetism and environmental significance. *Reviews in Mineralogy*, 35, 181-223.

Berggren W. A., Kent D. V., Aubry M. P., and Hardenbol J. (eds.) 1995. Geochronology, time scales and global stratigraphic correlation. SEPM Special Publication 54.

Berner, R.A. 1980. Early diagenesis: A theoretical approach. Prinston, New Jersey, Prinston University Press, 241 pp.

Bloemendal, J; King, J.W; Hall, F.R; Doh, S.J. 1992. Rock magnetism of late Neogene and Pleistocene deep-sea sediments; relationship to sediment source, diagenetic processes, and sediment lithology. *Journal of Geophysical Research*, B, Solid Earth and Planets, 97 (4), 4361-4375.

Bouquillon, A; Chamley, H; Frohlich, F. 1989. Upper Cenozoic clay sedimentation in the northeastern Indian Ocean. *Oceanologica Acta*, 12, 133-147.

Brass, G.W., Raman, C.V. 1990. Clay mineralogy of sediments from the Bengal Fan. *Proceedings of the Ocean Drilling Program, Scientific Results*, 116, 34-41.

Burbank D.W., Beck, A.R., Mulder, T. 1996. The Himalayan foreland basin. In: Yin, A., and Harrison, M. (eds) The tectonic evolution of Asia. Cambridge University Press, 149-188.

Burbank, D.W., Derry, L.A., France-Lanord, C. 1993. Reduced Himalayan sediment production 8 Myr ago despite an intensified monsoon. *Nature*, 364, (6432), 48-50.

Canfield, D. E., Raiswell, R., Bottrell, S.H. 1992. The reactivity of sedimentary iron minerals toward sulfide. *American Journal of Science*, 292, 659-683.

Carter-Stiglitz, B., Banerjee, S.K., Gourlan, A., Oches, E. 2006. A multi-proxy study of Argentina loess: Marine oxygen isotope stage 4 and 5 environmental record from pedogenic hematite. Palaeogeography, Palaeoclimatology, Palaeoecology, 239, 45-62.

Cerling, T.E. 1994. Global change in the late Miocene; terrestrial effects on the ocean carbon isotopic record. *Mineralogical Magazine*, 58A, 160.

Cerling, T.E., Wang, Y., Quade, J. 1993. Expansion of C4 ecosystems as an indicator of global ecological change in the late Miocene. *Nature*, 361(6410), 344-345.

Chen M., Wang R., Yang L., Han J., Lu J. 2003. Development of East Asian summer monsoon environments in the late Miocene; radiolarian evidence from Site 1143 of ODP Leg 184. *Marine Geology*, 201(1-3), 169-177.

Clift, P.D. 2006. Controls on the erosion of Cenozoic Asia and the flux of clastic sediment to the ocean. *Earth and Planetary Science Letters*, 241, 571-580.

Cochran, J.R., Stow, D.A.V., Auroux, C., Amano, K., Balson, P.S., Boulegue, J.J., Brass, G.W., Corrigan, J., Gartner, S., Hall, S., Iaccarino, S.M., Ishizuka, T., Kaczmarska, I., Kassens, H., Leger, G., Proto Decima, F., Raman, C.V., Sager, W.W., Takahashi, K., Thompson, T.L., Tiercelin, J-Ja., Townsend, M.R., Wetzel, A., Wijayananda, N.P., Williams, C. 1989. Proceedings of the Ocean Drilling Program, distal Bengal Fan, covering Leg 116 of the cruises of the drilling vessel JOIDES Resolution, Colombo, Sri Lanka, to Colombo, Sir Lanka, sites 717-719, 2 July 1987-19 August 1987. *Proceedings of the Ocean Drilling Program, Part A: Initial Reports,* 116, 388 pp.

Colley, S., Thomson, J., Wilson, T.R.S., Higgs, N.C. 1984. Post-depositional migration of elements during diagenesis in brown clay and turbidite sequences in the North East Atlantic. *Geochimica et Cosmochimica Acta*, 48 (6), 1223-1235.

Cornell, R. M., Schwertmann, U. 2003. The iron oxides : structure, properties, reactions, occurrences, and uses. Weinheim : Wiley-VCH, 664 pp.

Curi, N., . Franzmeier, D.P. 1984. Toposequence of Oxisols from the Central Plateau of Brazil, *Soil Scientists Society America Journal,* 48(2), 341–346.

Curtis, C. D. 1983. Microorganisms and diagenesis of sediments. Blackwell Scientific Publisher, Oxford, United Kingdom (GBR), 263-286.

da Motta, P.E.F., Kampf, N. 1992. Iron oxide properties as support to soil morphological features for prediction of moisture regimes in oxisols of central Brazil. *Pflanzenernahrung und Bodenkunde* 155, 385-90.

Derry, L.A., France-Lanord, C. 1996. Neogene Himalayan weathering history and river (super 87) Sr/ (super 86) Sr; impact on the marine Sr record. *Earth and Planetary Science Letters*, 142(1-2), 59-74.

Derry, L.A., France-Lanord, C. 1997. Himalayan weathering and erosion fluxes; climate and tectonic controls. In Ruddiman, W.F.(ed) Tectonic uplift and climate change. Press, New York, NY, United States (USA), 289-312.

Dettman, D.L., Kohn, M.J., Quade, J., Ryerson, F.J., Ojha, T.P., Hamidullah, S. 2001. Seasonal stable isotope evidence for a strong Asian monsoon throughout the past 10.7 m.y. *Geology*, 29(1), 31-34.

Dickens, G.R., Owen, R.M. 1999. The latest Miocene-early Pliocene biogenic bloom; a revised Indian Ocean perspective. *Marine Geology*, 161(1), 75-91.

Ding, Z.L., Yang, S.L., Sun, J.M., Liu, T.S. 2001. Iron geochemistry of loess and red clay deposits in the Chinese Loess Plateau and implications for long-term Asian monsoon evolution in the last 7.0 Ma. *Earth and Planetary Science Letters*, 185(1-2), 99-109.

Dunlop, D.J., Ozdemir, O. 1997. Rock magnetism; fundamentals and frontiers. Cambridge Studies in Magnetism, vol.3, 573 pp.

de Grave, E., Barrero, C.A., da Costa, G.M., Vandenberghe, R. E., van San, E. 2002. Moessbauer spectra of alpha - and gamma -polymorphs of FeOOH and Fe_2O_3; effects of poor crystallinity and of Al-for-Fe substitution. *Clay Minerals*, 37, 591-606.

Egli, R. 2004. Characterization of individual rock magnetic components by analysis of remanence curves. 3. Bacterial magnetite and natural processes in lakes. *Physics and Chemistry of the Earth*, 29, 869-884.

Emmel, F.J., Curray, J.R. 1984. The Bengal submarine fan, northeastern Indian Ocean, *Geo-Marine Letters* 3, 119–124.

Etheredge, D., Gutzler, D.S., Pazzaglia, F.J. 2004. Geomorphic response to seasonal variations in rainfall in the Southwest United States. *Geological Society of America Bulletin*, 116, 606-618.

Evans, M.E., Heller, F. 2003. Environmental magnetism; principles and applications of enviromagnetics. Academic Press, San Diego, CA, (USA). 299 pp.

France, D.E., Oldfield, F. 2000. Identifying goethite and hematite from rock magnetic measurements of soils and sediments. *Journal of Geophysical Research*, B, Solid Earth and Planets, 105(2), 2781-2796.

France-Lanord, C., Derry, L., Michard, A. 1993. Evolution of the Himalaya since Miocene time; isotopic and sedimentological evidence from the Bengal Fan. *Geological Society of London Special Publications*, 74, 603-621.

France-Lanord, C., Derry, L.A. 1994. delta (super 13) of organic carbon in the Bengal Fan; source evolution and transport of C3 and C4 plant carbon to marine sediments. *Geochimica et Cosmochimica Acta*, 58(21), 4809-4814.

France-Lanord, C., Spiess, V., Molnar, P., Curray, J.P. 2000. Summary on the Bengal Fan, An introduction to a drilling proposal, March 2000. available at http://www.whoi.edu/pclift/BengalSummary.pdf

Froelich, P N; Klinkhammer, G P; Bender, M L; Luedtke, N; Heath, G R; Cullen, D; Dauphin, P; Hammond, D; Hartman, B; Maynard, V, 1979. Early oxidation of organic matter in pelagic sediments of the eastern equatorial Atlantic; suboxic diagenesis. *Geochimica et Cosmochimica Acta*, 43 (7)1075-1090.

Gartner, S. 1990. Neogene calcareous nannofossil biostratigraphy, Leg 116 (central Indian Ocean). Proceedings of the Ocean Drilling Program, Scientific Results, 116, 165-187.

Giosan, L., Flood, R.D., Aller, R.C. 2002. Paleoceanographic significance of sediment color on western North Atlantic drifts; I, Origin of color. *Marine Geology*, 189, 25-41.

Grujic, D., Coutand, I., Bookhagen, B., Bonnet, S., Blythe, A., Duncan, C. 2006. Climatic forcing of erosion, landscape, and tectonics in the Bhutan Himalayas. *Geology*, 34, 801-804.

Guo, Z.T., Ruddiman, W.F., Hao, Q.Z., Wu, H.B., Qiao, Y. S., Zhu, R.X., Peng, S.Z., Wei, J.J., Yuan, B.Y., Liu, T.S. 2002. Onset of Asian desertification by 22 Myr ago inferred from loess deposits in China. *Nature*, 416(6877), 159-163.

Gupta, A.K., Singh, R.K., Joseph, S., Thomas, E. 2004. Indian Ocean high-productivity event (10-8 Ma); linked to global cooling or to the initiation of the Indian monsoons? *Geology*, 32(9), 753-756.

Haese, R.R., Petermann, H., Dittert, L., Schulz, H.D. 1998. The early diagenesis of iron in pelagic sediments; a multidisciplinary approach. *Earth and Planetary Science Letters*, 157(3-4),233-248.

Hall, S. A., Sager, W. W. 1990. Paleomagnetic and rock magnetic properties of sediment samples from Ocean Drilling Program Leg 116, central Indian Ocean. Proceedings of the Ocean Drilling Program, Scientific Results, vol.116, 337-344.

Harris, S.E., Mix, A.C. 1999. Pleistocene precipitation balance in the Amazon Basin recorded in deep sea sediments. *Quaternary Research*, 51, 14-26.

Harris, S.E., Mix, A.C. 2002. Climate and tectonic influences on continental erosion of tropical South America, 0-13 Ma. *Geology*, 30(5), 447-450.

Harrison, T.M., Copeland, P., Hall, S.A., Quade, J., Burner, S., Ojha, T. P. Kidd, W.S.F. 1993. Isotopic preservation of Himalayan/Tibetan uplift, denudation, and climatic histories of two molasse deposits. *Journal of Geology*, 101(2), 157-175.

Hastenrath, S., 1991, Climate dynamics of the tropics: Dordrecht, Kluwer Academic Publishers 488 p.

Hay, W.W., Soeding, E., DeConto, R.M., Wold, C.N. 2002. The late Cenozoic uplift; climate change paradox. *International Journal of Earth Sciences*, 91(5), 746-774.

Heller, F. 1978. The magnetic properties of Upper Jurassic limestones from southern Germany. *Eos, Transactions, American Geophysical Union*, 59 (12), 1035.

Hereford, R. and Webb, R. H. 2001. Climate variation since 1900 affects geomorphic processes and raises issues for land management. In: Reynolds, R.E. (ed.) The changing face of the east Mojave Desert. California State University, Desert Studies Consortium, p. 54-55.

Hermoyian, C.S., Owen, R.M. 2001. Late Miocene-early Pliocene biogenic bloom; evidence from low-productivity regions of the Indian and Atlantic Oceans. *Paleoceanography*, 16(1), 95-100.

Jarvis, I., Higgs, N. 1987. Trace-element mobility during early diagenesis in distal turbidites; late Quaternary of the Madeira Abyssal Plain, N Atlantic. *Geological Society of London Special Publications*, 31, 179-214.

Johnson, G D. 1977. Paleopedology of Ramapithecus-bearing sediments, North India. *Geologische Rundschau*, 66(1), 192-216.

Kampf, N., and Schwertmann, U. 1983. Goethite and hematite in a climosequence in southern Brazil and their application in classification of kaolinitic soils. *Geoderma*, 29, 27-39.

Karlin, R. 1990. Magnetic mineral diagenesis in suboxic sediments at Bettis Site W-N, NE Pacific Ocean. *Journal of Geophysical Research*, B, Solid Earth and Planets, 95 (4), 4421-4436.

Karlin, R., Lyle, M., Heath, G.R. 1987. Authigenic magnetite formation in suboxic marine sediments. *Nature,* 326(6112), 490-493.

Kawamura, N.,; Oda, H.,; Ikehara, K., Yamazaki, T., Shioi, K., Taga, S., Hatakeyama, S., Torii, M. 2007. Diagenetic effect on magnetic properties of marine core sediments from the southern Okhotsk Sea. *Earth, Planets and Space*, 59, 83-93.

Kopp, R. E., Kirschvink, J.L. 2007. A scoring scheme for evaluating magnetofossil identifications. AGU Fall 2007, abstract GP43B-1218.

Kraus, M.J. 1999. Paleosols in clastic sedimentary rocks; their geologic applications. *Earth-Science Reviews*, 47(1-2), 41-70.

Kroon, D., Steens, T.N.F., Troelstra, S.R. 1991. Onset of monsoonal related upwelling in the western Arabian Sea as revealed by planktonic foraminifers. *Proceedings of the Ocean Drilling Program, Scientific Results*, 117, 257-263.

Kruiver, P. P., Dekkers, M. J., Heslop, D. 2001. Quantification of magnetic coercivity components by the analysis of acquisition curves of isothermal remanent magnetisation. *Earth and Planetary Science Letters*, 189(3-4), 269-276.

Kruiver, P.P., Passier, H.F. 2001. Coercivity analysis of magnetic phases in sapropel S1 related to variations in redox conditions, including an investigation of the S ratio. *Geochemistry, Geophysics, Geosystems - G^3*, 2, paper number 2001GC000181.

Leslie, B. W., Hammond, D.E., Berelson, W.M., Lund, S.P. 1990. Diagenesis in anoxic sediments from the California continental borderland and its influence on iron, sulfur, and magnetite behavior. *Journal of Geophysical Research*, B, Solid Earth and Planets, 95 (4), 4453-4470.

Liu J., Zhu R., Roberts, A.P., Li S., Chang, J.-H. 2004. High-resolution analysis of early diagenetic effects on magnetic minerals in post-middle-Holocene continental shelf sediments from the Korea Strait. *Journal of Geophysical Research, B,* 109, 15.

Lowrie, W., Heller, F. 1982. Magnetic properties of marine limestones. *Reviews of Geophysics and Space Physics*, 20(2), 171-192.

Maloof, A.C, Kopp, R.E., Grotzinger, J.P., Fike, D.A., Bosak, T., Vali, H., Poussart, P.M., Weiss, B.P., Kirschvink, J.L. 2007. Sedimentary iron cycling and the origin and preservation of magnetization in platform carbonate muds, Andros Island, Bahamas. *Earth and Planetary Science Letters*, 259, 581-598.

Molnar, P., England, P., Martinod, J. 1993. Mantle dynamics, uplift of the Tibetan Plateau, and the Indian monsoon. *Reviews of Geophysics*, 31(4), 357-396.

Ozdemir, O., Dunlop, D.J. 2002. Thermoremanence and stable memory of single-domain hematites. *Geophysical Research Letters*, 29 (18), 4.

Passier, H.F., Dekkers, M.J. 2002. Iron oxide formation in the active oxidation front above sapropel S1 in the eastern Mediterranean Sea as derived from low-temperature magnetism. *Geophysical Journal International*, 150(1), 230-240.

Petermann, H., Bleil, U. 1993. Detection of live magnetotactic bacteria in South Atlantic deep-sea sediments. *Earth and Planetary Science Letters*, 117(1-2), 223-228.

Prell, W.L., Murray, D.W., Clemens, S.C., and Anderson, D.M. 1992. Evolution and variability of the Indian Ocean summer monsoon: Evidence from the western Arabian Sea drilling program, In Duncan, R.A., Rea, D.K., Kidd, R.B., von Rad, U., and Weissel, J.K. (eds.), Synthesis of Results from Scientific Drilling in the Indian Ocean, American Geophysical Union Geophysical Monograph 70, Washington, D.C., 447-469.

Quade, J., Cerling, T.E. 1995. Expansion of C (sub 4) grasses in the late Miocene of northern Pakistan: evidence from stable isotopes in Paleosols. *Palaeogeography, Palaeoclimatology, Palaeoecology*, 115(1-4), 91-116.

Quade, J., Cerling, T.E., Bowman, J.R. 1989. Development of Asian monsoon revealed by marked ecological shift during the latest Miocene in northern Pakistan. *Nature*, 342(6246), 163-166.

Quade, J., Roe, L., DeCelles, P.G., Ojha, T.P. 1997. The late Neogene $^{87}Sr/^{86}Sr$ record of lowland Himalayan rivers. *Science*, 276(5320), 1828-1831.

Ramstein, G., Fluteau, F., Besse, J., Joussaume, S. 1997. Effect of orogeny, plate motion and land-sea distribution on Eurasian climate change over the past 30 million years. *Nature*, 386(6627), 788-795.

Rea, D.K. 1992. Delivery of Himalayan sediment to the northern Indian Ocean and its relation to global climate, sea level, uplift, and seawater strontium. In: Duncan, R.A., D.K. Rea, R.B. Kidd, U. von Rad, and J.K. Weissel (eds.), Synthesis of Results from Scientific Drilling in the Indian Ocean, American Geophysical Union Geophysical Monograph 70, Washington, D.C., 387-402.

Retallack, G.J. 1995. Palaeosols of the Siwalik Group as a 15 Myr record of South Asian palaeoclimate. *Memoir - Geological Society of India*, 32, 36-51.

Rhoads, B.L. 1991. Impact of agricultural development on regional drainage in the lower Santa Cruz Valley, Arizona, U.S.A. *Environmental Geology and Water Sciences*, 18, 119-135.

Richter, C., Hayashida, A.,; Guyodo, Y.,; Valet, J.-P.,; Verosub, K.L. 1999. Magnetic intensity loss and core diagenesis in long-core samples from the East Cortez Basin and the San Nicholas Basin (California Borderland). *Earth, Planets and Space*, 51(5), 329-336.

Richter, F.M., Rowley, D.B., Depaolo, D.J. 1992. Sr isotope evolution of seawater - The role of tectonics. *Earth and Planetary Science Letters*, 109, 11-23.

Robinson, S.G., Sahota, J.T.S., Oldfield, F. 2000. Early diagenesis in North Atlantic abyssal plain sediments characterized by rock-magnetic and geochemical indices. *Marine Geology*, 163 (1-4), 77-107.

Rochette, P; Fillion, G, 1989. Field and temperature behavior of remanence in synthetic goethite; paleomagnetic implications. *Geophysical Research Letters*, 16 (8), 851-854.

Roden, E.E., Zachara, J.M. 1996. Microbial reduction of crystalline Fe(lll) oxides: role of oxide surface area and potential for cell growth. *Environmental Science and Technology,* 30, 1618-1628.

Roe, G.H., Montgomery, D.R., Hallet, B. 2002. Effects of orographic precipitation variations on the concavity of steady-state river profiles. *Geology*, 30, 143-146.

Sangode, S.J., Bloemendal, J. 2004. Pedogenic transformation of magnetic minerals in Pliocene-Pleistocene Palaeosols of the Siwalik Group, NW Himalaya, India. *Palaeogeography, Palaeoclimatology, Palaeoecology*, 212(1-2), 95-118.

Santana, D.P. 1984. Soil formation in a toposequence of oxisols from Patos de Minas region, Minas Gerais, State, Brasil. Ph. D. Thesis. Purdue University, West Lafayette, 129 pp.

Sharma, B D; Mukhopadhyay, S S; Sidhu, P S. 1998. Microtopographic controls on soil formation in the Punjab region, India. *Geoderma*, 81(3-4), 357-368.

Shipboard Scientific Party. 1989. Initial reports, sites 717-718-719 Distal Bengal Fan. *Proceedings of the Ocean Drilling Program, Initial Reports*, 116.

Shipboard Scientific Party. 2000. Initial reports, volume 184, South China Sea. *Proceedings of the Ocean Drilling Program, Initial Reports*, 184.

Snowball, I.F. Bacterial magnetite and the magnetic properties of sediments in a Swedish lake. *Earth and Planetary Science Letters*, 126(1-3), 129-142.

Spicer, R.A., Harris, N.B.W., Widdowson, M., Herman, A.B., Guo S., Valdes, P.J., Wolfe, J.A., Kelley, S.P. 2003. Constant elevation of southern Tibet over the past 15 million years. *Nature*, 421(6923), 622-624.

Stern, L.A., Chamberlain, C.P., Reynolds, R.C., Johnson, G.D. 1997. Oxygen isotope evidence of climate change from pedogenic clay minerals in the Himalayan molasse. *Geochimica et Cosmochimica Acta*, 61(4), 731-744.

Stow, D.A.V., Amano, K., Balson, P.S., Brass, G.W., Corrigan, J.D., Raman, C.V., Tiercelin, J-J., Townsend, M., Wijayananda, N P. 1990. Sediment facies and processes on the distal Bengal Fan, Leg 116. Proceedings of the Ocean Drilling Program, Scientific Results, 116, 377-396.

Tamburini, F., Adatte, T., Föllmi, K.B. 2003. Origin and Nature of Green Clay Layers, ODP Leg 184, South China Sea . Proceedings of the Ocean Drilling Program, Scientific Results, vol.184. doi:10.2973/odp.proc.sr.184.206.2003

Tarduno, J.A., Wilkison, S.L. 1996. Non-steady state magnetic mineral reduction, chemical lock-in, and delayed remanence acquisition in pelagic sediments. *Earth and Planetary Science Letters*, 144(3-4), 315-326.

Tardy, Y., Roquin, C. 1992. Geochemistry and evolution of lateritic landscapes. In: Martini, I P; Chesworth, W (eds). Developments in Earth Surface Processes,

vol.2. Elsevier, Amsterdam-Oxford-New York-Tokyo, Netherlands (NLD); pp. 407-443.

Vali, H., Kirschvink, J.L. 1989. Magnetofossil dissolution in a palaeomagnetically unstable deep-sea sediment. *Nature*, 339(6221), 203-206.

Wang, P. 1990. Neogene stratigraphy and paleoenvironments of China. *Palaeogeography, Palaeoclimatology, Palaeoecology*, 77, 315-334.

Yapp, C. 2001. Rusty relics of Earth history; iron (III) oxides, isotopes, and surficial environments. *Annual Review of Earth and Planetary Sciences*, 29, 165-199.

Zhang., Y.G., Ji, J., Balsam, W., Liu, L., Chen, J. 2007. High resolution hematite and goethite records from ODP 1143, South China Sea: Co-evolution of monsoonal precipitation and El-Nino over the past 600,000 years. *Earth and Planetary Science Letters*, 264, 136-150.

Chapter 6

Conclusions

Kazakhstan orocline

Two subduction-related volcanic belts in Central Kazakhstan (Fig. 1-1a) represent remains of an Andean type volcanic arc (e.g., Zonenshain et al., 1990; Bakhtiev, 1987, Kurchavov, 1994), with a Devonian outer belt and a late Paleozoic inner belt. In their present configuration, the belts are strongly curved. The overall shape of the structure can be described as having three limbs; a northeastern limb (Chingiz Range), a middle limb and a southwestern limb (North Tien Shan), with the NE and SW arms being roughly parallel. Such a strongly curved shape is an unusual feature for a plate boundary; hence, the oroclinal bending of an originally straighter arc has been proposed as a mechanism for the formation of the structure (e.g., Zonenshain et al., 1990; Sengor and Natal'in, 1996). To prove the oroclinal nature of the curvature, the following questions had to be addressed:

What was the initial configuration of the belts?

When did the bending occur?

How was the bending accommodated?

What caused the bending?

A paleomagnetic study, results of which are described in the Chapters 2, 3 and 4 of this thesis, provided the following answers to these questions.

1) Our investigation of a middle Devonian volcanic formation from the SW arm of the orocline (Chapter 2) revealed two meaningful components of magnetization, one being primary (of middle Devonian age) and the other being secondary (late Paleozoic in

age). The declination of the secondary magnetization is deflected counterclockwise by ~ 100^{o} relative to the reference direction. The deflection of this overprint is likely related to the Late Permian-Triassic episode of strike-slip faulting in the area that occurred after the oroclinal orogeny had ended (Van der Voo et al., 2006). Using the deflection of the overprint, we corrected for these post-Permian rotations and restored the declination of the primary Devonian magnetization to its initial orientation. Applying a similar correction to other published and newly obtained (Chapter 3) results from the different arms of the curved structure, we compiled a set of primary declinations. The corrected Devonian declinations vary systematically from southerly in the northern limb to northerly in the southern limb, closely following the change in the overall strike of the structure. Using the corrected declinations as passive markers (when the studied rocks formed, declination pointed to the north), we restored the volcanic belt to its Devonian configuration. Our analysis showed that ***in the Devonian, the volcanic margin was nearly straight and northwest-southeast trending***.

2) Our paleomagnetic study of late Paleozoic volcanic sequences (Chapter 4) from the middle and NE limbs of the curved structure produced a set of three magnetizations; one of latest Carboniferous-Early Permian age, one of middle Permian age and one of Late Permian or Early Triassic in age in each of the studied localities. In the middle arm of the structure, all three magnetizations are statistically indistinguishable from the coeval reference directions (obtained by extrapolation from Baltica), indicating that ***oroclinal rotation of the middle arm was completed by the latest Carboniferous-Early Permian***. In the NE arm, the three magnetization directions form a trend that indicates progressive clockwise rotation of the study area with respect to Baltica, spanning from the latest Carboniferous to the Late Permian. Approximately 30^{o} of clockwise rotation has been accommodated during this time and by the Late Permian, the study area had reached its present day position relative to Baltica. Although limited data coverage does not allow us to assert whether the rotation of the study area within the NE arm reflects the latest stages of the oroclinal bending or is related to strike-slip associated block-rotations, the protracted rotations in this area indicate that ***the deformation in the NE arm of the curved structure continued up to the Late Permian.***

Thus, ***the oroclinal orogeny in Kazakhstan can be constrained to the interval between the middle Devonian (the nearly straight belt) and the Late Permian (oroclinal rotations are over in all parts of the structure)***.

3) Combining information on the initial configuration of the belt (Chapters 2 and 3) with the data on position of the orocline arms at the end of the orogeny (Chapter 4), we obtained the following estimates for the amount of rotation experienced by each of the three arms during the oroclinal orogeny.

The NE arm rotated ~ 120^o clockwise

The middle arm rotated ~ 60^o clockwise

The SW arm rotated ~ 25^o counterclockwise

4) The varying magnitude of the relative oroclinal rotations along the Devonian volcanic arc provides clues as to the mechanism of bending. A plausible scenario involves ***dextral shear stress and drag applied to the northern end of the Kazakhstania structure, while its southern end was pinned down by a back-stop*** consisting of Tarim.

5) The most likely candidate for imposing a shear stress on the northern end of Kazakhstania is the Siberian craton. Paleogeographic reconstructions for the Late Devonian (Kravchinsky et al., 2002) indicate that Siberia's paleo-southern (present western) margin was located at ~20-30^{o}N, while similar Devonian paleolatitudes have been determined for the northern tip of Kazakhstania (Chapters 2 and 3). Available paleomagnetic data (Kravchinsky et al., 2002, Pavlov et al., 2007) also indicate that Siberia underwent a significant clockwise rotation in the Permo-Carboniferous time interval. It is plausible that the Carboniferous movements of Siberia also had a dextral shear component with respect to Kazakhstania and Baltica, although this sense of motion cannot be estimated from paleomagnetic data alone because latitude-parallel displacements cannot be uncovered. Given the means (significant lateral displacement of Siberia between the Late Devonian and Permian) and the opportunity (proximity of

Kazakhstania and Siberia), it is likely that ***Siberia's movements imposed dextral shear stresses on Kazakhstania's then-northern margin.***

6) Bending of a large-scale structure such as the Kazakhstan orocline requires removal of ~ 1200 km of crustal material from between the converging arms. The crust (of the Junggar-Balkhash Ocean) must have been consumed in two concurrent subduction zones (see Figure 4-10). An estimate for the average subduction velocity for this model gives a geologically reasonable value of ~6mm/yr. Thus, ***the Kazakhstan orocline is an example of thick-skinned tectonics, where the entire crust, and perhaps even the lithospheric mantle, was involved in deformation***.

The main findings of our study of the Kazakhstan orocline are briefly summarized in the following scenario, which is also depicted in Fig. 4-10. In the middle Devonian, a nearly straight, northwest-southeast trending volcanic arc delineated the northeastern margin of Kazakhstania landmass. In the Late Devonian, an initial collision with Tarim pinned Kazakhstania's southern corner, while a dextral shear motion and a considerable clockwise rotation of Siberia dragged its northern end. Relative convergence between Siberia and Tarim caused initial buckling of the Kazakhstania microcontinent trapped between them, subdividing the volcanic arc into three (SW, middle, and NE) segments. Continued subduction under the established limbs of the orocline, with an estimated outward-directed subduction velocity of ~6mm/yr, gradually led to closure of the intervening Junggar-Balkhash Ocean and tightening of the orocline. By the Late Permian, the Junggar-Balkhash Ocean no longer existed and the Kazakhstan orocline had obtained its present-day strongly curved shape.

Rock magnetic study of the Bengal Fan sediments

Relative abundance of two pedogenic iron oxides (goethite and hematite) is controlled by moisture availability during soil formation (e.g., Cornell and Schwertmann, 2003). Consequently, the ratio between the two has been used as a proxy for precipitation

in soil-forming (terrestrial) environments. A similar interpretation of the mineral ratio has been increasingly applied in studies of marine sediments, in which the variation in the relative abundances of goethite and hematite is thought to reflect the variation in precipitation regime at the source area of the sediments. The applicability of this parameter to the studies of marine sediments is contingent on the unconfirmed assumption that the ratio of these minerals is not modified by diagenetic processes.

A method of choice for the identification of goethite and hematite in the previous studies was reflectance spectrometry. While this method is quick and efficient in identifying these minerals, it is not sensitive to other iron oxides usually present in rocks. Our rock-magnetic study of the ~10.5~4.0 Ma interval of the Bengal Fan sedimentary sequence (Chapter 5) indicates that ***a statistical analysis of the Isothermal Remanent Magnetization (Kruiver et al., 2001) and low-temperature cycling (Carter-Stiglitz et al., 2006), also provide adequate estimates for the content of goethite and hematite in the samples***. In addition to goethite and hematite, the IRM analysis also indicates the presence of distinctive "detrital" and biogenic components in the studied samples.

We observed in our samples that ***relative abundances of goethite and hematite vary with age***. At ~ 7 Ma, the sediments show a significant change in magnetic parameters. The goethite content decreases at this time, and the biogenic component, ubiquitous in the lower part of the sequence, practically disappears. This change is approximately coeval with climatic turnover in the source area of the studied sediments, as postulated by multiple studies (e.g., Gupta et al., 2004; Stern et al. 1997; Prell et al., 1992; Quade et al., 1989; Ding et al., 2001). However, the variations in the content of other magnetic components, both "detrital" and biogenic, as well as an increase in a total organic carbon content of the samples and the appearance of pyrite concretions at the same stratigraphic level, suggest that this ***change in magnetic content reflects a change in the degree of diagenetic alteration of the initial detrital assemblage rather than a climatic signal***.

Our rock magnetic study also demonstrates that ***diagenetic alteration does not show a simple correlation with depth, but rather is a stratigraphic feature,*** the development of which can be controlled by several factors. While the stage of diagenesis

seems to be regulated by the availability of organic matter in the Bengal Fan sediments, variations in sedimentation rate or oxygen content of bottom waters similarly could result in a layer-parallel difference in the reductive dissolution. Thus, ***the absence of a systematic down-hole decrease in the content of the high coercivity fraction should not be taken as evidence for absence of diagenetic modification***.

In assigning climatic interpretation to changes in the relative abundance of goethite and hematite in marine sediments, the possibility of diagenetic modification should be evaluated. Reflectance spectroscopy studies should be supplemented with other methods, such as rock-magnetic techniques, that allow for monitoring of diagenetic alteration. ***With rock magnetic methods, alteration in ancient sediments can be detected and the severity of alteration can be evaluated based on the presence and grain-size variation of the ferrimagnetic fraction (magnetite/maghemite), which is more sensitive to early reductive dissolution than high coercivity minerals (goethite and hematite)***. There is also a need for further studies of dissolution behavior of various iron oxides. Better understanding of the rate and the manner in which reductive dissolution modifies the initial ratios of various iron oxide phases would improve our ability to detect and correct for diagenetic changes, and consequently, to extract a reliable climatic signal in studies of marine sediments.

References

Bakhtiev, M.K. 1987. Paleozoic orogenic magmatic belts. Nauka, Moscow 168 p. (In Russian).

Carter-Stiglitz, B., Banerjee, S.K., Gourlan, A., Oches, E. 2006. A multi-proxy study of Argentina loess: Marine oxygen isotope stage 4 and 5 environmental record from pedogenic hematite. *Palaeogeography, Palaeoclimatology, Palaeoecology*, 239, 45-62.

Cornell, R. M., Schwertmann, U. 2003. The iron oxides : structure, properties, reactions, occurrences, and uses. Weinheim : Wiley-VCH, 664 pp.

Ding, Z.L., Yang, S.L., Sun, J.M., Liu, T.S. 2001. Iron geochemistry of loess and red clay deposits in the Chinese Loess Plateau and implications for long-term Asian monsoon evolution in the last 7.0 Ma. *Earth and Planetary Science Letters*, 185(1-2), 99-109.

Gupta, A.K., Singh, R.K., Joseph, S., Thomas, E. 2004. Indian Ocean high-productivity event (10-8 Ma); linked to global cooling or to the initiation of the Indian monsoons? *Geology*, 32(9), 753-756.

Kravchinsky, V.A., Konstantinov, K.M., Courtillot, V., Savrasov, J.I., Valet, J.-P., Cherniy, S.D., Mishenin, S.G., and Parasotka, B.S. 2002. Palaeomagnetism of East Siberian traps and kimberlites: two new poles and palaeogeographic reconstructions at about 360 and 250Ma: *Geophysical Journal International*, 148, p. 1-33.

Kruiver, P.P., Dekkers, M..J., Heslop, D. 2001. Quantification of magnetic coercivity components by the analysis of acquisition curves of isothermal remanent magnetisation. *Earth and Planetary Science Letters*, 189(3-4), 269-276.

Kurchavov, A.M. 1994. The lateral variability and evolution of orogenic volcanism in the fold belts. *Geotectonics*, 28, 3-18.

Pavlov, V.E., Courtillot, V., Bazhenov, M.L., Veselovsky, R.V. 2007. Paleomagnetism of the Siberian traps: new data and a new overall 250 Ma pole for Siberia: *Tectonophysics*, 443, 72–92.

Prell, W.L., Murray, D.W., Clemens, S.C., Anderson, D.M. 1992. Evolution and variability of the Indian Ocean summer monsoon: Evidence from the western Arabian Sea drilling program, In Duncan, R.A., Rea, D.K., Kidd, R.B., von Rad, U., and Weissel, J.K. (eds.), Synthesis of Results from Scientific Drilling in the Indian Ocean, American Geophysical Union Geophysical Monograph 70, Washington, D.C., 447-469.

Quade, J., Cerling, T.E., Bowman, J.R. 1989. Development of Asian monsoon revealed by marked ecological shift during the latest Miocene in northern Pakistan. *Nature*, 342(6246), 163-166.

Şengör, A.M.C., Natal'in, B.A., 1996. Paleotectonics of Asia: fragments of a synthesis. In: Yin, A., Harrison, M. (Eds.), The Tectonic Evolution of Asia. Cambridge Univ. Press, Cambridge, pp. 486– 640.

Stern, L.A., Chamberlain, C.P., Reynolds, R.C., Johnson, G.D. 1997. Oxygen isotope evidence of climate change from pedogenic clay minerals in the Himalayan molasse. *Geochimica et Cosmochimica Acta*, 61(4), 731-744.

Van der Voo, R., Levashova, N. M., Skrinnik, L. I., Kara, T. V., Bazhenov, M. L. 2006. Late orogenic, large-scale rotations in the Tien Shan and adjacent mobile belts in Kyrgyzstan and Kazakhstan, *Tectonophysics*, 426, 335-360.

Zonenshain, L.P., Kuzmin, M.I., Natapov, L.M., 1990. Geology of the USSR: a plate tectonic synthesis. Ed. Page, B.M. AGU, Geodynamic series, volume 21. Washington, D.C., 250p.

Appendices

Appendix A

Ar-Ar dating of the Tokrau-A rocks

Ar-Ar analytical method

We attempted to date the Tokrau-A ignimbrites, sampled for paleomagnetism, because of their interesting magnetic polarity characteristics, where Normal (N) polarity is observed presumably ***within*** the long Reversed (R) Kiaman superchron. For dating we selected three cooling units containing this normal-polarity magnetization. Samples were crushed using a jaw crusher. For each of the three cooling units, plagioclase grains and samples of ground mass were carefully hand picked from the separates to avoid grains containing any visible glass or mineral inclusions. Seven individual plagioclase grains, plus two groundmass samples, were dated for each of the three units, twenty seven samples in total, by the $^{40}Ar/^{39}Ar$ laser ablation method at the University of Michigan.

Neutron-fluence monitor MMhb-1 was used with an assumed K-Ar age of 520.4 Ma (Samson and Alexander, 1987) as a calibration standard. Irradiation was done at the McMaster Nuclear Reactor in Hamilton, Ontario. For groundmass separates, a total mass of ~2 mg from each sample was step-heated at increasing levels of laser power until complete fusion was achieved, using a defocused beam from a Coherent Innova 5 W continuous argon-ion laser. For plagioclase separates, a step-heating was performed on individual grains. Fusion-system blanks were run after every five steps of analysis and subtracted from all gas fractions. The data were corrected for interference reactions due to Ca, K, and Cl, and for ^{37}Ar and ^{39}Ar decay. A summary of analytical data is included in Table A1.

Results of Ar-Ar dating

All groundmass samples have a characteristic $^{40}Ar/^{39}Ar$ release spectrum showing an initial peak followed by an asymptotic decay to a plateau with the total gas ages of the sample being equal to the plateau ages (Fig. A1-a). This type of spectra is typical of many age spectra from clay samples (e.g. Hall et al., 2000), suggesting that the Ar-Ar ages of the groundmass (232-242 Ma) likely reflect the age of alteration.

Single crystals of plagioclase show a wide range in their apparent Ar-Ar ages, spanning from ~360 to ~250 Ma with a weak clustering of dates between 305 to 295 Ma (Fig. 4-9). Single-crystal ages that are older, sometimes significantly older, than the eruption age are often reported from explosively emplaced volcanic rocks (e.g. Smith et al., 2003; Spell et al., 2001; Miller et al., 1998; Ganeski et al., 1996; Fleck et al., 1994). These older ages are obtained from xenocrystic grains that were incorporated in the magma during the eruption, and have not been completely reset. Calculations of ^{40}Ar diffusion rate in plagioclase at ~900°C magma temperature (typical for rhyolitic magmas) have shown that complete degassing of larger grains takes at least several months (Ganeski et al., 1996). The extent to which contaminating grains might have degassed in magma prior to the eruption is impossible to determine from their total-fusion ages, and it is notoriously difficult to distinguish xenocrysts from true phenocrysts while hand picking and even chemically (see the references given above). It is very likely that the older plagioclase ages in our samples represent xenocrystic contamination; large lithic clasts with plagioclase grains are visible in hand samples (Fig. A2-a), and a rapid cooling indicated by the glassy groundmass can account for incomplete resetting of the Ar system.

Relatively younger ages, in the ~290 to 250 Ma interval, likely reflect partial alteration of plagioclase phenocrysts. Although hand-picked grains appeared to be fairly fresh, alteration of plagioclase to clay minerals is evident petrographically (Fig A2-b-d).

To estimate the most likely eruption age we calculated $^{39}Ar/^{40}Ar$ versus $^{36}Ar/^{40}Ar$ isochron ages for the three best samples with uniform high Ca/K ratios that produced well defined plateaus on the Ar release spectra (samples 493-15a, e and g, Fig. A1-c,d). In calculating a regression line, we omitted points lying above the line by more than 3 sigma

as these points likely indicate alteration-related Ar loss. We also plot up the goodness of fit (as the mean square weighted deviation -MSWD) on a contour plot (Fig. A1-f). Although there is always some non-uniqueness to a solution, the best fits are achieved for the range from t=~295 and initial $^{40}Ar/^{36}Ar$ ratio =~575 to t=~297.5, $^{40}Ar/^{36}Ar$=~540. Thus, we accepted this range, 297.5 to 295 Ma, as the most likely eruption age.

Table A1. $^{40}Ar/^{39}Ar$ analytical data (following pages)

F39	LasPowm	Vol36	Err36	Vol37	Err37	Vol38	Err38	Vol39	Err39	Vol40	Err40	Age(Ma)	AgeErr
MC14-x14a A435-i Plagioclase													
mass=1		J= 0.00353724+/- 0.00000743162				tot.gas.age= 311.245 +/- 0.755							
0.00790	100	1.88963	0.05670	9.83608	0.14553	4.26224	0.09382	12.44545	0.20268	1164.930	1.15598	286.931	8.524
0.02017	150	1.88978	0.06475	14.33580	0.30287	2.86273	0.09022	19.35117	0.18231	1485.352	2.63400	282.374	5.978
0.04211	200	1.30057	0.09279	21.10067	0.25587	1.37585	0.10104	34.57577	0.22828	1917.678	1.39751	262.885	4.669
0.07870	250	0.71206	0.10620	28.78842	0.37947	0.48781	0.12033	57.66669	0.39622	3149.617	2.64998	299.043	3.509
0.13196	300	0.60508	0.06528	40.02277	0.29490	0.59608	0.09052	83.95340	0.15312	4500.920	2.38627	301.817	1.349
0.22111	400	1.16313	0.09342	81.98226	0.57876	0.98282	0.10339	140.50845	0.49297	7857.761	4.02373	312.556	1.467
0.29851	500	0.78944	0.09476	93.15446	0.62718	0.85345	0.12943	122.00154	0.73981	6728.035	5.14618	311.254	2.140
0.36282	600	0.32542	0.06860	92.49691	0.43065	0.14266	0.10569	101.35377	0.53954	5310.382	3.84630	301.619	1.843
0.45013	800	1.02680	0.07900	144.00306	0.61582	0.93863	0.13493	137.61667	0.44707	7263.620	6.45787	296.921	1.304
0.51407	1000	0.39496	0.08611	110.05240	0.59858	0.16859	0.11928	100.76817	0.28618	5115.239	4.01856	291.650	1.585
0.55012	1200	0.20578	0.08326	74.43050	0.27114	0.20000	0.11803	56.82223	0.38927	2815.121	2.61934	285.495	2.984
0.59629	1600	0.45856	0.07342	96.40205	0.47136	0.47911	0.08373	72.76878	0.27353	3684.023	2.09672	287.084	1.912
0.62300	2000	0.47372	0.06134	51.88184	0.48827	0.41918	0.07836	42.10087	0.25287	2204.969	2.22779	288.630	2.852
0.68772	2600	1.19921	0.11468	93.15110	0.57786	1.66771	0.08873	102.01421	0.40953	5724.443	4.90562	308.058	2.134
0.83781	3200	5.64284	0.10664	516.94717	1.92350	8.63381	0.18023	236.56383	0.17114	15121.759	8.90858	330.690	0.767
1.00000	4000	8.30938	0.12354	751.91950	1.36258	12.79082	0.10403	255.63435	0.52052	17656.915	8.74071	344.408	1.004
MC14-x14b A435-i Plagioclase													
mass=1		J= 0.00353724 +/- 0.00000743162				tot.gas.age= 306.498 +/- 0.72							
-0.00002	100	0.25528	0.07346	0.55129	0.15687	0.10232	0.07133	-0.05247	0.07943	81.436	0.65673	-934.669	4808.378
0.00017	150	0.89365	0.05772	0.87095	0.18120	0.64165	0.08585	0.57760	0.09498	469.368	1.35609	1468.766	185.266
0.00050	200	0.86207	0.07599	1.51469	0.18182	0.92920	0.07963	1.06728	0.10502	735.349	1.10096	1718.856	120.762
0.00105	250	3.23637	0.08601	3.31328	0.14593	1.81715	0.04646	1.72572	0.11482	1853.510	0.82985	1882.426	84.520
0.00161	300	3.90819	0.14943	3.08891	0.20612	1.91709	0.09161	1.77334	0.09506	1921.909	1.95965	1674.576	85.869
0.00272	400	7.23579	0.13425	6.52750	0.20674	3.40910	0.15024	3.48881	0.13928	3468.203	1.92716	1540.270	51.648
0.00476	500	11.43360	0.13406	12.77656	0.28982	5.16432	0.09751	6.43057	0.11792	5024.635	2.74045	1163.086	25.980
0.00788	600	19.63275	0.17932	20.11655	0.21066	6.24345	0.13614	9.85774	0.18053	7077.317	4.26371	680.018	25.787
0.01918	800	56.33678	0.21387	78.12573	0.50547	16.59528	0.18580	35.62020	0.18484	20411.384	9.21409	572.898	8.710
0.04118	1000	53.33671	0.28525	170.10549	0.85058	15.41914	0.16524	69.41783	0.32454	20367.339	5.71925	380.379	6.492
0.07771	1200	38.62746	0.15256	376.86384	1.36887	12.81240	0.18412	115.21688	0.40808	19082.468	5.45026	381.394	2.373
0.15563	1600	27.11932	0.18729	724.04569	1.74038	10.09485	0.17443	245.78159	0.60245	21645.811	7.80202	323.185	1.414
0.34248	2000	67.27530	0.28273	1260.01986	1.83949	22.73685	0.16824	589.36575	0.99545	51570.831	4.98212	314.132	0.904
0.69873	2600	38.39894	0.18799	1265.91597	0.96165	13.40146	0.24707	1123.68429	1.44888	64342.876	12.95993	278.346	0.433
0.89426	3200	14.95421	0.18001	797.45415	2.17749	5.44125	0.18356	616.75112	1.09880	32988.720	7.38061	273.747	0.658
1.00000	4000	11.65207	0.18140	621.29198	1.14222	4.78543	0.13715	333.53945	0.68401	19034.867	6.93776	276.066	1.031
MC14-x14c A435-i Plagioclase													
mass=1		J= 0.00353724 +/- 0.00000743162				tot.gas.age= 18.556 +/- 0.208							
0.00440	150	1.71202	0.07349	2.43424	0.54781	4.67907	0.08932	16.41829	0.14641	1004.999	1.69885	184.252	7.803
0.00962	200	0.38763	0.05453	3.62276	0.47621	1.24958	0.09067	19.46157	0.27203	247.493	0.93376	43.076	5.202
0.02701	300	1.55735	0.12145	15.46797	0.63590	3.18143	0.09916	64.89632	0.26832	789.836	1.09115	32.127	3.471
0.04825	400	0.59623	0.06626	18.71992	0.63823	1.54025	0.09149	79.26109	0.21202	457.928	0.96573	22.542	1.560
0.07454	500	0.90477	0.06938	16.87546	0.84734	1.27638	0.08617	98.10495	0.38562	547.322	0.77590	18.119	1.323
0.11208	600	1.06796	0.09346	20.37606	1.06819	1.56583	0.09183	140.04001	0.49745	726.173	2.09029	18.614	1.251
0.23908	800	3.47893	0.10390	68.82532	1.30648	5.53311	0.12852	473.88293	0.53892	2343.425	3.17911	17.627	0.412
0.57523	1000	3.24810	0.09171	164.26679	0.74216	5.90748	0.32082	1254.25756	2.15303	3881.615	3.70076	14.805	0.140
0.79410	1200	1.84757	0.07157	127.05694	0.88606	5.42649	0.14308	816.65851	1.61541	2324.317	1.99617	13.843	0.167
0.84530	1600	1.76864	0.16605	96.50844	0.95003	6.78148	0.21520	191.03454	0.46236	1229.349	1.51433	23.454	1.620
0.91386	2000	2.18981	0.16016	122.92179	1.23770	7.91217	0.21902	255.80899	0.62833	1677.087	2.75547	25.513	1.168
0.94399	2600	1.00173	0.13252	51.87609	0.96867	4.11833	0.13628	112.42828	0.57192	727.918	1.55942	24.350	2.198
0.98482	3200	1.42741	0.13087	59.83815	1.08974	5.49471	0.13609	152.31136	0.66548	1031.996	1.22384	25.386	1.602
1.00000	4000	0.78243	0.11205	27.10071	1.06289	1.36414	0.14399	56.65692	0.24812	408.489	0.82534	19.858	3.691
MC14-x14d A435-i Plagioclase													
mass=1		J= 0.00353724 +/- 0.00000743162				tot.gas.age= 313.781 +/- 0.743							
0.01446	150	8.76788	0.12720	20.27991	0.71194	11.98142	0.20067	25.48360	0.25157	5346.973	4.23593	584.400	8.441
0.02916	200	1.82594	0.08504	16.45287	0.57523	2.22436	0.13792	25.91984	0.14935	1704.014	2.55424	266.066	5.552
0.08166	300	2.80412	0.18549	49.19233	0.62752	2.19163	0.10587	92.54432	0.48081	5404.814	4.51933	290.805	3.517
0.16468	400	1.73862	0.11136	68.82864	0.81755	1.20801	0.11636	146.33550	0.42020	8459.178	4.52890	316.942	1.475
0.24415	500	1.42019	0.07415	81.39715	1.33574	1.22410	0.13190	140.08002	0.32134	8258.960	3.91597	325.844	1.089
0.30552	600	0.97240	0.08447	78.22068	0.72795	0.64903	0.08065	108.18316	0.31772	6040.216	3.61693	310.943	1.508
0.38804	800	2.33988	0.07495	145.11303	1.04759	1.97297	0.09111	145.46087	0.58001	8481.031	3.16133	312.951	1.413
0.46594	1000	1.28054	0.04956	131.62621	1.18277	0.98108	0.07819	137.31394	0.39299	7352.439	2.23926	298.070	0.980
0.54123	1200	0.61970	0.05962	125.78361	1.04389	0.50720	0.09172	132.72574	0.40812	6846.417	4.56213	294.900	1.119
0.60091	1600	0.33901	0.06140	153.98242	0.64459	0.48984	0.09661	105.19171	0.47006	5303.705	4.60096	290.905	1.542
0.63479	2000	0.37285	0.10425	82.54984	0.91942	0.38568	0.06076	59.73229	0.23900	2958.061	2.53595	281.159	3.012
0.69063	2600	2.52568	0.11597	169.36959	1.45473	1.96581	0.11351	98.42203	0.40883	5902.280	3.65906	306.689	2.220
0.90928	3200	12.30101	0.11832	1076.11450	2.49597	12.92691	0.13233	385.41917	0.23959	24806.658	5.77291	320.342	0.524
1.00000	4000	5.36098	0.13840	550.73558	3.01152	5.22654	0.14798	159.92163	0.56783	10413.116	4.15398	321.818	1.726
MC14-x14e A435-i Plagioclase													
mass=1		J= 0.00353724 +/- 0.00000743162				tot.gas.age= 321.867 +/- 0.737							
0.01248	150	1.90423	0.10311	3.76624	0.50924	3.03321	0.08815	26.16820	0.30236	1718.403	1.28438	261.873	7.023
0.03148	200	1.80674	0.11194	4.47396	0.67295	1.82630	0.13310	39.85742	0.30524	2615.936	3.45609	305.888	4.985
0.10982	300	3.10946	0.10175	22.56466	1.30980	2.35544	0.12079	164.26305	0.57214	9338.106	5.05744	300.588	1.392
0.27806	400	2.42822	0.10130	38.33598	0.48985	2.17143	0.09299	352.81349	0.72126	20352.287	9.89174	324.187	0.772
0.43943	500	1.37799	0.08718	33.97957	0.88784	1.34314	0.14570	338.41390	0.34518	19944.355	8.15442	335.241	0.526
0.54272	600	0.81842	0.09784	29.24914	0.45517	1.05859	0.09713	216.59568	0.86109	12474.813	4.38968	328.588	1.394
0.63425	800	2.18005	0.13100	54.91767	1.50054	2.19385	0.12781	191.94534	0.53831	11442.266	4.74847	327.404	1.370
0.69028	1000	0.83716	0.09632	47.75212	1.36026	0.86945	0.10363	117.50478	0.50043	6659.748	3.90288	318.415	1.805
0.72013	1200	0.12296	0.11073	28.59899	0.88099	0.20239	0.09585	62.59930	0.30130	3385.241	11.00901	312.663	3.267
0.74983	1600	0.77716	0.10152	38.86709	1.06555	0.80626	0.11136	62.26687	0.17158	3366.618	1.40952	295.853	2.719
0.81032	2000	2.34302	0.06306	116.31576	1.10160	2.82325	0.08861	126.86702	0.55550	7435.225	2.81458	310.792	1.484
0.91511	2600	7.38859	0.03423	394.50532	2.68856	9.18129	0.11865	219.74734	0.74247	14538.258	6.85561	327.231	1.054
0.95499	3200	2.79218	0.13067	165.16680	1.56695	3.53401	0.13455	83.61335	0.45368	5479.259	3.75537	324.246	2.952
1.00000	4000	5.13528	0.12442	174.24611	1.46427	4.23347	0.12865	94.39857	0.23226	6800.840	3.46248	325.875	2.209

F39	LasPowm	Vol36	Err36	Vol37	Err37	Vol38	Err38	Vol39	Err39	Vol40	Err40	Age(Ma)	AgeErr
MC14-x14f A435-i Plagioclase													
mass=1		J= 0.00353724 +/- 0.00000743162				tot.gas.age= 270.069 +/- 2.264							
0.01196	150	3.00560	0.11571	2.42188	0.72344	1.37541	0.10323	3.30385	0.12396	892.543	1.28977	8.453	65.784
0.02952	200	1.16580	0.07718	1.81705	0.72752	0.64311	0.12406	4.84865	0.11333	473.117	0.96793	161.806	27.703
0.07375	300	1.10836	0.14055	3.29171	0.88956	0.58011	0.09057	12.21788	0.21963	834.007	1.64671	246.854	19.383
0.17447	400	0.82806	0.11586	5.16842	1.07613	0.39445	0.08555	27.81966	0.37610	1557.761	0.57524	278.546	7.583
0.32753	500	0.22571	0.08157	6.09046	0.75657	0.26012	0.08018	42.27968	0.22098	2143.810	1.96288	289.062	3.409
0.46178	600	0.00716	0.07841	4.39188	0.72023	0.08322	0.08723	37.08030	0.17927	1796.932	2.17948	285.119	3.650
0.66639	800	0.38999	0.07955	34.36845	0.82967	0.20247	0.09535	56.51712	0.29167	2742.141	2.42241	274.606	2.642
0.82979	1000	0.34287	0.09510	221.40090	2.04575	0.07769	0.08059	45.13430	0.25865	2102.671	1.85335	262.854	3.717
0.88606	1200	0.09990	0.07915	64.45586	0.98720	0.17133	0.07926	15.54293	0.15002	759.045	1.17805	277.106	8.611
0.93830	1600	0.19591	0.10761	58.41513	1.30161	0.12214	0.11015	14.42719	0.17509	723.567	1.06161	272.746	12.484
0.98027	2000	0.49289	0.07264	55.89101	1.40485	0.16280	0.10119	11.59347	0.24478	665.968	1.21757	265.820	11.471
0.99036	2600	1.10409	0.08488	19.29757	1.33491	0.38119	0.09588	2.78849	0.16750	430.068	0.54473	223.175	52.282
0.99644	3200	1.16325	0.06291	6.13053	0.86149	0.33030	0.08504	1.67863	0.09420	432.146	0.97710	308.189	61.739
1.00000	4000	1.31396	0.10289	5.65053	0.73833	0.56363	0.10061	0.98323	0.06308	437.786	1.06022	295.728	168.516
MC14-x14g A435-i Plagioclase													
mass=1		J= 0.00353724 +/- 0.00000743162				tot.gas.age= 244.4 +/- 0.925							
0.00439	150	1.13218	0.12314	0.98148	0.81272	0.71596	0.09670	3.57143	0.10426	404.030	0.68827	120.049	60.940
0.01014	200	0.76982	0.08101	0.68558	0.77904	0.43912	0.13508	4.68245	0.16482	322.278	1.04050	124.777	30.767
0.08747	300	1.90858	0.07030	2.78273	0.86964	1.28052	0.11124	62.96623	0.42532	2953.559	1.77576	227.244	2.357
0.23614	400	0.68034	0.09053	6.39032	0.75945	0.48821	0.09611	121.05681	0.41481	5354.187	2.03117	253.040	1.472
0.33841	500	0.19100	0.09843	4.39115	0.88894	0.19787	0.11046	83.27807	0.29048	3567.184	1.45870	250.759	2.107
0.41161	600	-0.04249	0.12245	4.22751	0.97472	0.07666	0.09612	59.60413	0.32115	2550.236	2.16745	255.418	3.605
0.50135	800	0.14335	0.06427	66.52494	1.32467	0.16793	0.09644	73.06858	0.26524	3148.856	2.38722	252.745	1.687
0.55473	1000	0.31115	0.11352	22.72056	1.13629	0.30650	0.07384	43.46772	0.42869	1868.378	2.03301	243.586	4.862
0.60028	1200	0.03505	0.05905	11.08415	0.99198	0.09458	0.09123	37.09059	0.26414	1585.489	1.92123	252.481	3.117
0.67088	1600	0.42258	0.04526	19.07596	1.06713	0.33097	0.11770	57.48321	0.32857	2466.620	0.84784	242.862	1.839
0.87610	2000	2.34024	0.11679	15.44896	0.99366	0.93198	0.13186	167.10633	0.39192	7421.168	4.68204	240.258	1.278
0.96495	2600	2.12392	0.13660	16.70393	1.15728	0.87221	0.16592	72.34770	0.37606	3523.623	2.38951	238.903	3.334
0.99629	3200	2.07943	0.07545	6.84777	0.85649	1.08552	0.09485	25.52102	0.23682	1639.352	2.34017	239.625	5.333
1.00000	4000	0.51155	0.07297	2.34287	0.76971	0.33146	0.11855	3.01955	0.11062	316.389	0.60519	319.204	39.671
MC14-x16a A435-m Groundmass													
mass=1		J= 0.00354115 +/- 0.00000885507				tot.gas.age= 232.678 +/- 0.561							
0.00148	100	2.46779	0.07765	5.29163	0.20744	4.42949	0.16206	33.67555	0.25476	1101.703	1.66053	69.312	4.231
0.00458	150	6.41560	0.13436	9.83098	0.23324	6.30610	0.13012	70.36496	0.40930	2845.682	1.86997	84.242	3.477
0.00872	200	10.40059	0.13285	14.93149	0.16185	7.26562	0.16399	94.10926	0.42261	5152.070	3.14273	135.863	2.548
0.01415	250	5.34000	0.12180	16.58606	0.20034	4.61130	0.13766	123.40220	0.53253	4810.892	3.31207	160.053	1.836
0.02166	300	2.94883	0.13522	18.41171	0.25050	2.92512	0.09079	170.84543	0.47512	5464.676	4.25168	164.068	1.440
0.04175	400	6.17302	0.11645	32.50898	0.40427	3.82231	0.17021	456.67733	0.88059	16430.431	4.16877	193.564	0.562
0.07698	500	8.06739	0.12942	35.75948	0.30822	3.42207	0.17197	800.78814	1.45039	31605.150	10.02513	219.242	0.467
0.11652	600	5.31024	0.11990	32.65727	0.24540	2.69582	0.12443	898.67808	1.30375	37851.540	11.06346	241.074	0.401
0.15938	800	1.97035	0.06444	35.77665	0.33261	1.15195	0.19089	974.28879	0.91471	43760.474	10.48139	262.989	0.261
0.18741	1000	0.96352	0.09745	21.83000	0.33599	0.87750	0.15802	637.05921	0.75819	28552.947	6.54116	263.294	0.388
0.20875	1200	0.47640	0.05968	14.03926	0.24845	0.65499	0.13700	485.04752	0.76515	21142.476	6.00188	257.351	0.434
0.24099	1600	0.45474	0.12373	19.76904	0.32869	1.42895	0.15197	732.75742	1.91815	31544.230	7.58162	254.951	0.684
0.28654	2000	0.93214	0.13453	26.05305	0.30807	1.62988	0.18896	1035.45186	1.56033	42926.462	10.39212	245.639	0.411
0.38923	2600	1.61344	0.05318	51.17311	0.43766	2.88620	0.34336	2334.22016	1.78643	93180.361	21.32869	237.393	0.182
0.54191	3200	3.15168	0.08430	80.04533	0.51008	5.62875	0.16279	3470.42513	2.99605	136162.304	28.22854	233.197	0.199
0.68799	4000	3.22037	0.12573	82.37872	0.53981	6.12912	0.31007	3320.22966	3.48779	128800.782	8.45172	230.609	0.237
1.00000	4001	9.22780	0.08719	191.17589	0.88912	14.81699	0.35481	7092.14365	11.22803	272717.119	53.56593	228.150	0.343
MC14-x16b A435-m Groundmass													
mass=1		J= 0.00354115 +/- 0.00000885507				tot.gas.age= 231.945 +/- 0.549							
0.00198	100	1.05750	0.09957	1.18914	0.13751	0.64040	0.04895	43.79682	0.28820	918.002	1.74664	86.230	4.136
0.00513	150	1.24791	0.11411	1.66135	0.15600	0.78055	0.08273	69.61662	0.18473	1983.293	1.06878	142.391	2.884
0.01002	200	1.25290	0.07805	2.37977	0.22419	0.90006	0.08618	108.18785	0.38344	3363.443	2.92583	168.618	1.375
0.01792	250	1.01805	0.07747	3.50021	0.22841	0.97625	0.05995	174.76248	0.41279	5110.877	3.11205	167.783	0.858
0.02976	300	1.36207	0.08667	4.98639	0.21032	1.09344	0.06174	261.94947	0.44592	8423.371	3.91954	185.720	0.645
0.05951	400	4.54272	0.12830	13.35333	0.32188	3.25566	0.16184	658.04049	1.03763	23155.827	8.94362	200.238	0.452
0.09087	500	1.47743	0.08779	13.32761	0.27002	1.75695	0.15490	693.65507	1.05175	27006.293	6.20045	229.472	0.392
0.11733	600	0.70552	0.07452	11.09070	0.23009	1.20617	0.15148	585.40705	0.52048	24372.124	4.05866	246.118	0.296
0.14924	800	0.91137	0.06810	15.28510	0.37436	1.33827	0.15281	705.83981	1.07265	30116.922	8.10093	251.739	0.396
0.17515	1000	1.33562	0.05898	13.81994	0.22664	1.59243	0.10712	573.11660	0.97127	24437.165	6.85393	249.870	0.436
0.19748	1200	0.60459	0.07421	12.07822	0.16979	1.35084	0.09562	494.12356	0.83986	20621.351	6.32489	246.647	0.469
0.22082	1400	0.60136	0.06817	12.01743	0.24762	1.49179	0.13791	516.26684	1.09524	21562.311	7.61687	246.926	0.542
0.24848	1600	0.52615	0.07008	15.12232	0.32292	1.45935	0.17274	611.74963	1.36087	25205.158	7.31492	244.283	0.547
0.28313	1800	0.54336	0.07182	19.85283	0.26798	1.42317	0.09314	766.49123	0.85073	31168.422	5.16264	241.529	0.297
0.32911	2000	0.70717	0.08214	24.87711	0.19926	1.66453	0.26153	1017.18884	0.45562	40904.016	7.22791	239.029	0.172
0.39009	2200	0.97085	0.08963	32.07309	0.36301	2.54101	0.19336	1348.95413	1.78817	53601.152	13.28682	236.315	0.319
0.46487	2400	1.37715	0.07795	38.94060	0.31093	3.05108	0.09626	1654.01393	1.76878	64888.435	21.53980	233.299	0.258
0.53763	2600	1.62593	0.09980	41.02208	0.41947	2.94652	0.17461	1609.56790	1.89446	63426.418	11.09137	233.986	0.281
0.60342	2800	1.84074	0.10491	42.99634	0.43386	3.31147	0.31903	1455.41670	1.17484	57406.842	8.86175	233.776	0.216
0.65750	3000	1.15261	0.09337	35.10536	0.32949	2.95564	0.15967	1196.22945	0.84794	46714.689	14.79775	232.075	0.213
0.71132	3200	1.02196	0.07759	40.96271	0.36371	2.93942	0.20158	1190.57790	1.76329	46490.577	10.34250	232.233	0.344
0.75774	3400	0.63601	0.08134	32.63300	0.53612	2.27957	0.17009	1026.88225	0.92944	39854.679	11.51611	231.296	0.245
0.81948	3600	1.03215	0.08969	42.07807	0.22761	3.32260	0.13786	1365.60530	1.87952	52754.112	11.87950	230.053	0.321
0.90034	4000	1.29288	0.09009	49.62199	0.45165	4.90002	0.20294	1788.73977	1.40356	68710.894	22.51260	228.884	0.201
1.00000	4001	3.42187	0.05671	92.91590	0.54688	9.71010	0.24876	2204.55828	2.78093	84378.739	72.81017	226.725	0.330

F39	LasPowm	Vol36	Err36	Vol37	Err37	Vol38	Err38	Vol39	Err39	Vol40	Err40	Age(Ma)	AgeErr
MC14-x13a A471-i Plagioclase													
0.00082	100	0.20269	0.06729	0.93031	0.11834	0.41548	0.06657	0.96857	0.08910	98.933	0.54722	240.375	116.534
0.00323	150	0.51955	0.06032	1.98650	0.16358	0.89667	0.07488	2.85594	0.10645	252.295	0.62552	208.146	36.250
0.00797	200	0.87853	0.08186	4.05364	0.16094	1.32233	0.06446	5.59606	0.10118	621.053	0.60150	371.124	23.262
0.01452	250	1.44786	0.08523	6.64302	0.23711	1.27827	0.06421	7.74553	0.15781	820.693	1.79192	297.613	18.501
0.02461	300	1.14075	0.06332	9.24179	0.16657	0.80521	0.05911	11.93228	0.15321	787.670	0.96123	226.119	9.249
0.05254	400	1.71811	0.11550	23.96972	0.22467	0.93433	0.06116	33.03335	0.17561	2125.253	1.73201	288.109	5.802
0.09729	500	1.15638	0.16646	37.03014	0.29932	0.67558	0.05028	52.92644	0.26059	3443.431	1.65534	339.769	5.145
0.14552	600	0.53288	0.04634	45.23714	0.31934	0.27153	0.06546	57.03119	0.36492	3442.840	2.66292	334.489	2.346
0.20874	800	0.74388	0.15153	125.81279	0.55437	0.69928	0.10122	74.76320	0.45953	4761.611	3.73617	351.067	3.716
0.26225	1000	0.35958	0.06855	126.16546	0.59575	0.27344	0.07150	63.28573	0.34298	3445.296	4.11227	308.625	2.335
0.33861	1200	0.40240	0.06939	131.52015	0.37905	0.35835	0.07614	90.29929	0.34681	5170.814	2.83126	325.667	1.674
0.48311	1600	0.56574	0.04883	164.56868	0.64463	0.48883	0.08957	170.88935	0.58882	9661.699	5.05517	323.606	1.127
0.53485	2000	0.20004	0.05762	93.46424	0.66186	0.24507	0.11097	61.19620	0.33301	3469.186	3.00449	324.481	2.210
0.57415	2600	0.36498	0.05878	71.97957	0.25350	0.35500	0.08577	46.46733	0.23701	2967.284	2.59187	355.197	2.575
0.61415	3200	0.55453	0.06579	94.02086	0.42355	0.54357	0.09696	47.30587	0.32049	3823.144	4.60759	436.223	3.373
1.00000	4000	4.33389	0.08636	1571.26958	1.94941	5.98091	0.13681	456.31194	0.94998	34219.152	15.81988	410.140	0.834
MC14-x13b A471-i Plagioclase													
mass=1		J= 0.0035362 +/- 0.00000773497				tot.gas.age= 294.417 +/- 1.43							
0.00111	100	0.14635	0.08151	0.64295	0.15438	0.28968	0.06816	0.43458	0.09405	123.684	0.64684	908.369	263.763
0.00315	150	0.32156	0.06077	1.39752	0.14251	0.45676	0.08369	0.80227	0.09432	364.108	0.68810	1410.970	132.366
0.00771	200	0.56600	0.05723	2.45691	0.17820	0.55362	0.08366	1.79404	0.08113	551.776	1.01528	1017.742	49.115
0.01338	250	0.07849	0.06498	3.14476	0.25657	0.20926	0.10266	2.23208	0.13570	281.547	1.00953	618.967	50.359
0.02141	300	0.24016	0.09373	4.71039	0.27543	0.13158	0.06974	3.15581	0.10387	283.093	0.59650	384.719	46.664
0.04638	400	0.73310	0.09833	17.04643	0.25267	0.42283	0.06593	9.82281	0.19968	816.119	1.33634	352.543	16.849
0.08674	500	0.45353	0.06700	30.81897	0.14553	0.20074	0.05223	15.87071	0.17499	959.878	0.92604	304.725	7.406
0.14172	600	0.22987	0.06502	44.62062	0.50089	0.01212	0.05583	21.62386	0.18023	1164.131	1.37488	297.477	5.335
0.27677	800	0.50228	0.07208	116.21597	0.53357	0.54552	0.05089	53.11137	0.14798	2991.735	2.70402	312.779	2.311
0.38950	1000	0.22033	0.09403	98.72348	0.58025	0.10971	0.03591	44.33493	0.25119	2190.537	1.79853	282.516	3.733
0.50941	1200	0.10395	0.05428	111.95381	0.72968	0.17583	0.10012	47.15942	0.22682	2269.574	2.50131	279.972	2.257
0.67108	1600	0.27243	0.06100	147.71707	0.70199	0.23093	0.10787	63.57997	0.26174	2974.195	2.65029	269.225	1.882
0.78222	2000	-0.02399	0.07305	100.24640	0.39933	0.07777	0.10673	43.71162	0.11940	2026.227	2.47281	274.734	2.811
0.87676	2600	0.21162	0.08056	80.20965	0.82909	0.09108	0.08225	37.17904	0.23775	1718.567	2.57895	263.884	3.882
0.93885	3200	0.20754	0.07170	49.79460	0.41037	0.07654	0.10269	24.41839	0.14289	1160.340	1.52629	266.448	5.003
1.00000	4000	0.15919	0.06042	47.69744	0.42390	0.14684	0.11259	24.05042	0.27287	1146.152	2.36328	270.256	5.004
MC14-x13c A471-i Plagioclase													
mass=1		J= 0.0035362 +/- 0.00000773497				tot.gas.age= 310.026 +/- 9.829							
0.00489	150	-0.02550	0.05690	0.76263	0.56040	0.25009	0.08340	0.20679	0.06825	164.527	0.67876	2474.795	463.540
0.00646	200	0.03903	0.05643	0.18700	0.49589	0.05602	0.06491	0.06635	0.07040	50.524	0.58328	2028.280	1393.522
0.02141	300	0.14809	0.05261	1.39576	0.49101	0.09512	0.07353	0.63135	0.10921	121.212	0.71671	650.070	144.736
0.05158	400	0.14741	0.06964	1.05468	0.60532	-0.06350	0.07262	1.27473	0.07640	68.382	0.64343	120.133	96.655
0.09119	500	0.09297	0.05546	4.57014	0.44549	0.07812	0.07511	1.67363	0.10615	117.774	0.77390	315.037	55.636
0.14147	600	-0.02519	0.07273	4.63093	0.52029	-0.03042	0.06499	2.12450	0.08006	121.733	0.53869	351.354	54.480
0.26223	800	0.01515	0.10184	14.75647	0.56028	0.00053	0.06567	5.10225	0.13581	298.056	1.03643	334.132	32.323
0.37481	1000	0.02653	0.09371	13.26323	1.18808	-0.04136	0.06645	4.75637	0.11157	217.831	0.59979	261.719	32.638
0.51133	1200	0.06357	0.09660	17.15493	0.78265	-0.03786	0.07213	5.76813	0.20129	268.183	0.76043	256.677	28.640
0.66740	1600	0.17972	0.06775	21.01244	0.63692	-0.09164	0.05836	6.59415	0.10398	328.529	0.63308	248.526	17.278
0.79234	2000	0.09416	0.03040	16.27735	0.50702	0.04972	0.07450	5.27859	0.15376	283.042	0.82137	284.746	12.069
0.89368	2600	0.02849	0.04501	13.34142	0.70313	0.06631	0.04411	4.28197	0.15511	237.279	0.90871	312.311	19.676
0.95976	3200	0.06041	0.04452	7.87237	0.60453	0.01346	0.05669	2.79199	0.08985	154.234	0.48006	287.462	27.041
1.00000	4000	0.12920	0.03982	5.24276	0.66557	0.00085	0.05895	1.70002	0.07264	96.753	0.47593	207.409	40.274
MC14-x13d A471-i Plagioclase													
mass=1		J= 0.0035362 +/- 0.00000773497				tot.gas.age= 322.006 +/- 0.779							
0.00885	150	4.72657	0.10724	16.69537	0.60467	2.41876	0.07572	14.57593	0.13101	1982.986	1.50383	239.919	12.323
0.02161	200	4.45177	0.11345	25.89241	0.58194	1.25522	0.09732	21.02595	0.15677	2005.450	1.60515	198.060	9.231
0.05548	300	2.51410	0.08374	60.12509	0.65048	0.92089	0.07996	55.81780	0.35522	3544.672	4.03701	294.772	2.987
0.09293	400	0.79602	0.09923	95.51650	0.78727	0.29799	0.08074	61.70804	0.33745	3462.683	2.76416	306.154	2.996
0.13280	500	0.55222	0.07171	145.22932	1.35921	0.20062	0.07901	65.71036	0.38832	3440.889	2.63369	293.072	2.380
0.18662	600	0.63296	0.06716	174.99169	0.86511	0.33656	0.08294	88.68285	0.37836	4658.036	2.07615	295.968	1.686
0.32429	800	1.26063	0.08342	274.06250	2.02516	0.67152	0.10512	226.86090	0.68230	12258.739	2.73740	306.650	1.033
0.38053	1000	0.29821	0.07803	168.59857	1.46013	0.21790	0.12268	92.66448	0.19985	4806.365	3.12836	298.684	1.482
0.40663	1200	0.15897	0.07382	79.42277	1.05189	0.24060	0.09336	43.02006	0.18130	2268.692	2.03539	302.606	2.988
0.44775	1600	0.34590	0.06263	114.75389	1.02077	0.45518	0.10013	67.75384	0.47541	3831.128	3.04551	320.814	2.539
0.51471	2000	0.40329	0.07228	153.37489	2.16329	0.92134	0.11420	110.33686	0.64780	6495.497	2.63433	335.458	2.074
0.79674	2600	1.95606	0.11732	1126.26803	4.24827	4.42778	0.18273	464.74148	0.45043	28386.315	8.78524	346.266	0.508
0.98767	3200	1.13439	0.09266	883.30202	2.26766	3.13131	0.15949	314.62272	0.88072	18317.708	3.99210	332.097	0.970
1.00000	4000	-0.02936	0.09064	60.45592	0.60350	0.37360	0.07847	20.31246	0.22065	1273.394	1.31893	363.462	7.760
MC14-x13e A471-i Plagioclase													
mass=1		J= 0.0035362 +/- 0.00000773497				tot.gas.age= 298.905 +/- 1.179							
0.00352	150	0.43253	0.14605	0.22336	0.78115	0.56810	0.07162	2.62207	0.12787	153.566	0.83459	61.597	101.539
0.01420	200	0.79116	0.16335	1.14978	1.10008	0.73610	0.12688	7.95409	0.17556	570.166	1.41869	251.427	34.090
0.06837	300	1.51108	0.14930	8.88176	0.97593	0.80481	0.07514	40.34682	0.20354	2355.882	4.30319	279.149	6.145
0.23556	400	0.82895	0.13864	16.65909	0.93665	0.26912	0.10815	124.51654	0.40901	7266.655	4.82439	328.038	2.019
0.32690	500	0.26358	0.13327	16.23195	0.99905	0.13882	0.07418	68.02111	0.33168	3866.542	3.27501	324.346	3.419
0.36725	600	0.13716	0.09007	15.83976	1.17631	-0.41473	0.08839	30.05588	0.35690	1576.512	2.70161	299.693	5.822
0.49745	800	0.74790	0.07238	43.30041	1.15228	0.11154	0.09870	96.96558	0.35000	5169.524	3.24706	299.312	1.564
0.59864	1000	0.24366	0.07537	28.39261	1.01867	0.27799	0.09180	75.36096	0.31871	3851.691	2.53584	294.554	1.980
0.64564	1200	0.11394	0.08253	18.35604	0.83521	0.17930	0.07683	35.00378	0.32634	1689.938	1.37209	279.112	4.513
0.71614	1600	0.24309	0.08228	27.48295	1.06157	0.40214	0.10640	52.50588	0.18938	2510.666	2.61205	274.362	2.712
0.79703	2000	0.48747	0.08320	45.69531	1.22667	0.70928	0.10124	60.24521	0.30999	3042.789	1.67904	283.473	2.607
0.93027	2600	0.51692	0.11907	111.01532	1.25843	1.02046	0.11589	99.23438	0.55153	5257.166	2.56076	301.496	2.463
0.99762	3200	0.38213	0.12225	74.33704	0.74556	0.56320	0.11301	50.15965	0.20377	2556.860	1.64793	286.782	4.069
1.00000	4000	0.07786	0.08257	2.16108	0.63309	0.27137	0.11415	1.76901	0.12557	86.550	0.53010	215.725	79.415

F39	LasPowm	Vol36	Err36	Vol37	Err37	Vol38	Err38	Vol39	Err39	Vol40	Err40	Age(Ma)	AgeErr
MC14-x13f A471-i Plagioclase													
mass=1		J= 0.0035362 +/- 0.00000773497				tot.gas.age= 294.861 +/- 2.951							
0.02519	150	1.48980	0.10636	5.94242	0.98400	0.95286	0.11821	4.54483	0.08385	546.774	1.26819	143.673	40.852
0.08301	200	1.00316	0.07761	9.85057	1.10757	0.31959	0.08145	10.43246	0.17998	669.956	1.38619	215.068	12.954
0.19389	300	0.23988	0.09530	21.18083	1.36388	0.06206	0.08977	20.00590	0.13039	1088.708	1.96093	298.461	7.837
0.27682	400	0.08827	0.09653	32.39362	1.25396	0.06049	0.09374	14.96237	0.12068	761.288	1.34231	289.032	10.595
0.32299	500	0.10002	0.10604	18.25336	1.22077	-0.04564	0.13174	8.32958	0.13418	417.786	1.34934	275.237	21.029
0.42602	600	0.42966	0.06763	20.65084	0.78672	0.20376	0.07377	18.58965	0.20962	1127.493	1.38050	314.317	6.630
0.57317	800	0.10428	0.06471	20.67138	0.92548	0.13574	0.07693	26.54995	0.26944	1392.940	1.45389	300.774	4.809
0.60763	1000	0.05019	0.05272	5.62692	0.88263	-0.05900	0.08035	6.21602	0.23609	317.579	1.02752	286.680	16.983
0.62491	1200	0.05619	0.07985	1.46305	0.84328	0.00123	0.09534	3.11883	0.12573	162.889	1.01285	276.852	42.710
0.63316	1600	-0.03006	0.05974	1.56101	0.79294	0.05138	0.06761	1.48880	0.14581	78.445	0.55895	340.042	69.651
0.70425	2000	0.18958	0.07776	6.81536	0.78197	0.01292	0.07236	12.82510	0.17864	668.991	1.36100	281.721	10.448
0.77959	2600	0.27965	0.07584	23.13855	0.86310	0.13193	0.07334	13.59417	0.23280	777.325	1.28522	299.681	10.100
0.99895	3200	0.41703	0.07881	93.11511	1.50569	0.36503	0.11603	39.57816	0.28927	2375.075	2.53968	330.719	3.843
1.00000	4000	0.07202	0.07273	-0.40515	0.52932	0.08177	0.07663	0.18861	0.12858	0.754	0.38923	-876.060	1410.020
MC14-x13g A471-i Plagioclase													
mass=1		J= 0.0035362 +/- 0.00000773497				tot.gas.age= 276.086 +/- 7.606							
0.02779	150	0.67081	0.06490	2.60968	0.81387	0.36943	0.10399	1.92183	0.10968	268.575	0.83939	219.609	57.641
0.06634	200	0.28679	0.08859	2.98538	0.69182	-0.02892	0.11719	2.66564	0.09832	188.546	0.98860	232.739	55.694
0.14917	300	0.12897	0.07121	9.19235	0.79882	0.04065	0.10745	5.72764	0.15620	298.792	0.81828	269.225	21.327
0.24593	400	0.01317	0.06898	19.11973	0.68606	0.07168	0.11248	6.69065	0.12731	329.397	0.99474	286.388	17.351
0.33947	500	0.06592	0.06655	16.87469	0.67755	-0.01575	0.12458	6.46826	0.09205	333.500	0.90430	285.828	16.993
0.41324	600	0.12463	0.08549	9.85259	0.77474	0.04516	0.09347	5.10056	0.10173	253.950	1.03001	252.973	27.886
0.47314	800	0.13198	0.07253	9.90396	0.70498	0.08430	0.06591	4.14223	0.13580	202.344	0.70215	235.510	29.878
0.50033	1000	0.24434	0.09241	4.25718	0.98491	-0.03255	0.07707	1.87985	0.10150	97.412	0.56321	83.587	88.607
0.53400	1200	0.22204	0.08945	4.21932	0.77710	0.04479	0.07408	2.32863	0.10387	132.107	0.94932	173.551	66.229
0.64954	1600	0.16585	0.08115	17.70372	0.62563	0.18809	0.11502	7.98903	0.12192	446.086	0.97342	292.105	16.811
0.84605	2000	0.34283	0.08979	50.12282	1.26650	0.06049	0.11189	13.58844	0.19615	807.358	1.20350	304.310	11.285
0.92400	2600	0.18239	0.10609	21.62639	2.04402	0.07010	0.07398	5.39050	0.16368	343.626	1.03568	313.924	32.400
0.92560	3200	0.11743	0.08588	1.39167	1.18348	0.17440	0.08502	0.11049	0.08899	9.123	0.64008	-2837.072	10407.754
1.00000	4000	0.12883	0.10079	27.01538	1.27576	0.20568	0.09912	5.14454	0.18895	357.874	0.91644	358.481	32.564
MC14-x17a A471-m Groundmass													
mass=1		J= 0.00354215 +/- 0.0000100247				tot.gas.age= 242.341 +/- 0.654							
0.00002	100	0.11382	0.07223	0.06097	0.15274	-0.00243	0.06675	0.26064	0.12079	6.189	1.11803	-841.750	972.425
0.00001	150	0.09751	0.05691	0.12223	0.14972	0.03127	0.07548	-0.06495	0.07197	10.227	0.97997	1262.867	1300.261
0.00007	200	0.44269	0.05132	0.21876	0.16080	0.19001	0.07730	0.87006	0.07858	89.471	1.09824	-332.500	138.269
0.00028	250	0.98408	0.05082	0.54188	0.15970	0.25394	0.08697	3.29821	0.08814	302.905	1.36478	23.308	28.848
0.00070	300	1.74875	0.06272	0.78494	0.14825	0.58644	0.07630	6.37799	0.09668	520.958	1.40484	4.204	18.581
0.00203	400	3.83488	0.11812	1.65229	0.14609	1.19212	0.08044	20.61314	0.19948	1472.190	1.62477	102.142	10.281
0.00472	500	6.41334	0.11093	3.04493	0.15745	2.18030	0.08376	41.41707	0.33252	2965.197	2.62174	157.977	4.805
0.00739	600	3.45894	0.10111	2.59497	0.16591	1.12987	0.06750	41.07584	0.27482	2174.336	1.40268	170.899	4.372
0.01445	800	15.46361	0.18954	7.00759	0.22341	3.88586	0.14369	108.86776	0.34611	7482.494	4.41308	163.362	3.053
0.02664	1000	10.14998	0.13956	10.79778	0.23395	2.73436	0.10445	187.98054	0.38070	8364.051	4.91603	173.731	1.325
0.04453	1200	9.43942	0.12896	15.34846	0.22160	3.02905	0.11356	275.73830	0.55767	11710.084	6.23860	195.728	0.886
0.10100	1600	18.43387	0.19521	41.32210	0.26175	6.38675	0.21907	870.61598	1.10588	37346.162	11.50085	220.143	0.464
0.16448	2000	6.46789	0.12163	41.26007	0.23798	2.84746	0.18735	978.52838	1.09854	45101.317	4.91837	262.064	0.342
0.24795	2600	4.64492	0.12032	47.49832	0.29816	2.15297	0.16334	1286.90012	1.69628	59554.574	12.10954	267.985	0.366
0.33223	3200	3.42387	0.09739	48.27854	0.35384	2.26554	0.10025	1299.17703	1.57894	57498.792	9.23522	258.420	0.320
0.42260	4000	3.06252	0.10900	54.18349	0.33505	1.83206	0.21712	1393.22048	1.82553	59712.121	14.39872	251.376	0.338
1.00000	4001	21.86292	0.07886	481.64376	1.76780	31.90707	0.65621	8901.26441	6.27701	363922.301	106.35062	239.938	0.173
MC14-x17b A471-m Groundmass													
mass=1		J= 0.00354215 +/- 0.0000100247				tot.gas.age= 237.456 +/- 0.644							
0.00193	100	1.91048	0.06044	0.31704	0.14988	0.87784	0.06292	16.78582	0.19549	835.656	1.07887	100.366	6.543
0.00460	150	1.42322	0.08167	0.64887	0.17842	0.78626	0.09800	23.28940	0.29432	1009.250	1.08723	154.702	6.367
0.01031	200	2.07911	0.06888	1.85236	0.17809	0.80482	0.07212	49.69722	0.27733	1822.622	1.06231	149.033	2.542
0.02193	250	3.09229	0.09142	4.04040	0.29530	1.33004	0.06611	101.25844	0.27561	3689.240	2.08936	167.167	1.618
0.03744	300	1.79494	0.10262	5.20403	0.24257	0.85384	0.11279	135.04841	0.43898	5073.358	3.97909	203.094	1.436
0.06383	400	1.31685	0.08218	7.92604	0.20601	0.96940	0.13688	229.93546	0.47626	9843.843	2.63072	245.304	0.760
0.09262	500	0.51104	0.06938	7.21425	0.16762	0.43576	0.12912	250.70171	0.43561	11366.916	3.96497	265.378	0.629
0.12102	600	0.37353	0.08026	6.63302	0.20315	0.29785	0.13510	247.40856	0.45535	10927.423	3.74251	259.761	0.698
0.16084	800	0.49118	0.07742	11.12405	0.26826	0.52838	0.11439	346.82889	0.72680	14766.248	3.68987	251.082	0.616
0.20047	1000	0.53960	0.07129	13.07980	0.21614	0.74326	0.15940	345.16340	0.60491	14388.711	6.45693	245.893	0.538
0.24427	1200	0.54622	0.11564	17.58516	0.30720	0.84521	0.12193	381.50672	0.88713	15573.086	6.09683	241.271	0.732
0.29962	1400	0.93224	0.17250	26.20043	0.33056	0.98668	0.17215	482.11649	1.18523	19483.362	6.75400	238.160	0.811
0.36942	1600	1.10181	0.13090	41.48354	0.53562	1.63355	0.08854	608.03758	0.71714	24325.822	7.68484	236.091	0.448
0.43737	1800	0.99334	0.14220	29.44147	0.42518	1.84561	0.10662	591.81966	0.89581	23678.022	9.88360	236.322	0.529
0.51505	2000	1.16194	0.14631	25.91487	0.42841	2.07335	0.18218	676.63903	1.08098	26944.091	7.15424	235.202	0.506
0.59757	2200	1.16115	0.09931	33.43185	0.53486	2.59101	0.09931	718.79162	1.20616	28566.107	8.30745	234.930	0.440
0.67574	2400	0.84474	0.09974	30.67466	0.32945	2.74647	0.15433	680.85845	0.75409	27089.542	6.09090	235.806	0.349
0.73384	2600	0.64553	0.10799	23.71730	0.28078	1.98463	0.14719	506.04826	0.81321	19988.835	8.65826	234.135	0.509
0.79793	2800	0.63356	0.08351	30.54835	0.40341	2.99132	0.17556	558.24436	1.03701	22213.017	7.01618	236.001	0.485
0.87312	3000	0.78049	0.08948	38.99915	0.31069	3.28466	0.14543	654.92729	1.10423	26148.077	7.07304	236.660	0.442
0.91795	3200	0.44558	0.07156	35.60442	0.34010	4.38217	0.09809	390.52675	0.71454	15879.769	7.30537	240.871	0.523
0.96109	3400	0.54398	0.08135	29.16749	0.36105	3.08442	0.07652	375.72773	1.06839	15382.841	2.30139	241.924	0.738
0.98804	3600	0.40849	0.08751	10.40591	0.27203	0.92828	0.04490	234.79134	0.58126	9606.845	3.07672	241.302	0.835
1.00000	4000	0.21076	0.08888	5.22658	0.25017	0.56895	0.07021	104.15189	0.47183	4403.849	2.33371	248.458	1.759

F39	LasPowm	Vol36	Err36	Vol37	Err37	Vol38	Err38	Vol39	Err39	Vol40	Err40	Age(Ma)	AgeErr
MC14-x15a A493-i Plagioclase													
mass=1		J= 0.00353943 +/- 0.00000770415				tot.gas.age= 301.572 +/- 2.495							
-0.00046	100	0.10361	0.06335	-0.14296	0.16291	0.04845	0.05745	-0.11115	0.08658	18.230	0.49457	599.833	867.908
-0.00029	150	0.15773	0.05052	0.18369	0.18114	-0.03104	0.04970	0.04230	0.10743	45.023	0.46574	-257.048	2692.297
0.00061	200	0.22204	0.04700	0.30661	0.18803	0.18539	0.06194	0.21587	0.12024	122.612	0.76503	1190.458	530.028
0.00200	250	0.25824	0.05770	0.82209	0.19894	0.16207	0.08124	0.33610	0.10633	208.869	0.87818	1576.366	359.071
0.00478	300	0.39576	0.10792	1.41580	0.19704	0.17780	0.06544	0.67052	0.10909	169.068	0.85728	438.474	246.540
0.01574	400	0.59480	0.09861	5.53938	0.23960	0.31043	0.06871	2.64800	0.11182	348.119	1.22977	374.026	58.919
0.04241	500	0.45119	0.08281	14.36167	0.36710	0.15340	0.06740	6.44392	0.14567	419.125	0.89299	263.058	21.692
0.08449	600	0.33760	0.07276	24.58601	0.29522	0.18695	0.08196	10.16494	0.15287	587.069	0.90094	282.755	12.210
0.23251	800	0.48100	0.07039	97.40621	0.41223	0.40772	0.09829	35.75969	0.26336	2050.970	2.46033	312.207	3.790
0.41547	1000	0.32110	0.07792	124.37210	0.34138	0.03245	0.07319	44.19944	0.24506	2167.051	2.21778	276.970	3.201
0.58408	1200	0.08905	0.10526	115.76649	0.53637	0.07271	0.08264	40.73180	0.24095	1999.388	1.94181	285.485	4.454
0.71697	1600	0.14646	0.09259	87.55371	0.56745	0.14604	0.09176	32.10427	0.17707	1613.505	2.40775	288.043	4.883
0.78473	2000	0.08304	0.08678	43.40241	0.35283	0.11562	0.08960	16.36810	0.10969	854.976	1.38286	297.948	8.691
0.84599	2600	0.05963	0.10432	38.25414	0.39792	0.06082	0.08530	14.79978	0.16202	769.838	1.40618	298.442	11.680
0.90162	3200	0.02205	0.09111	35.31313	0.44612	0.24408	0.07763	13.43882	0.15649	735.607	1.74889	316.890	11.275
1.00000	4000	0.11236	0.13282	68.18549	0.20290	0.19151	0.05043	23.76753	0.19248	1442.423	1.38721	343.684	9.082
MC14-x15b A493-i Plagioclase													
mass=1		J= 0.00353943 +/- 0.00000770415				tot.gas.age= 330.221 +/- 1.027							
0.00009	100	0.16002	0.09493	1.98284	0.17648	0.27299	0.04034	0.06848	0.05956	155.305	0.66210	3399.774	1388.869
0.00072	150	0.27685	0.06654	2.20702	0.16362	0.34345	0.05168	0.47583	0.08092	198.519	0.81927	1127.441	200.789
0.00172	200	0.56190	0.07292	4.14752	0.16069	0.58938	0.06295	0.74763	0.09310	367.632	1.11914	1208.854	144.678
0.00291	250	0.43559	0.07062	5.45852	0.19507	0.49836	0.09117	0.89881	0.05425	286.769	0.74095	872.999	100.528
0.00522	300	0.27181	0.11437	8.28090	0.29354	0.36469	0.06341	1.73955	0.12620	225.586	0.77252	467.168	100.334
0.01295	400	1.01359	0.06806	24.93629	0.40645	0.73696	0.09142	5.82243	0.15573	684.639	0.77267	379.496	20.093
0.02552	500	1.22505	0.07099	39.51037	0.36877	0.48311	0.08442	9.46665	0.20248	891.866	1.05683	326.074	13.439
0.04459	600	1.22552	0.08598	61.61218	0.44547	0.99277	0.09087	14.36132	0.19005	1243.875	1.59693	354.758	10.230
0.09147	800	1.96508	0.08732	199.76043	0.58104	1.66049	0.11241	35.30798	0.21643	2857.345	2.33969	370.862	4.334
0.14562	1000	1.02008	0.06640	165.73426	1.10491	0.67417	0.11644	40.78273	0.35066	2506.448	3.88095	315.898	3.623
0.22682	1200	1.63702	0.07767	179.42706	0.65897	1.11451	0.09722	61.16050	0.27237	3683.877	3.73901	306.527	2.403
0.45123	1600	1.89402	0.08678	462.65127	0.93000	1.71895	0.10621	169.01565	0.55322	9158.990	6.26528	298.726	1.236
0.50707	2000	0.47906	0.05510	151.81583	0.64424	0.64172	0.10475	42.05354	0.37411	2203.048	2.14274	288.643	3.187
0.72794	2600	3.22305	0.06805	906.82169	2.04251	4.93710	0.15009	166.35105	0.33679	10673.200	9.70096	339.158	0.947
0.74529	3200	0.33708	0.04995	58.84528	0.79893	0.35138	0.06863	13.06280	0.21201	853.493	1.03611	335.329	7.796
1.00000	4000	4.52449	0.08914	1273.02539	1.67175	5.75074	0.16693	191.83636	0.38163	12734.941	12.43459	344.334	1.016
MC14-x15c A493-i Plagioclase													
mass=1		J= 0.00353943 +/- 0.00000770415				tot.gas.age= 287.469 +/- 1.163							
0.02161	150	0.84021	0.09752	2.58502	0.65156	1.57979	0.07958	11.17362	0.14593	1162.577	1.76362	458.860	13.846
0.05008	200	0.16012	0.06330	3.28680	0.62142	0.35519	0.05680	14.71848	0.23711	633.630	1.28548	237.958	7.985
0.16373	300	0.38438	0.11549	17.20389	0.72706	0.55575	0.14144	58.75426	0.32141	2945.647	3.30240	284.183	3.494
0.26787	400	0.19176	0.05808	30.67699	1.01295	0.48152	0.12799	53.83784	0.43157	2978.884	3.26529	317.027	2.909
0.32865	500	0.12158	0.06658	34.24936	1.02436	0.25561	0.07125	31.42020	0.24886	1543.225	2.30154	282.930	4.019
0.37415	600	0.30092	0.07399	32.83290	0.81331	0.05109	0.13559	23.52176	0.22428	1084.014	1.32036	251.728	5.637
0.45154	800	0.22136	0.06401	39.29029	0.63929	0.16247	0.13672	40.00687	0.21506	1855.282	1.49378	265.195	2.932
0.50927	1000	0.10077	0.05880	25.46569	0.80060	0.00509	0.14464	29.84723	0.26729	1332.879	1.38261	259.231	3.888
0.56520	1200	0.05089	0.06955	15.45863	0.50442	0.03314	0.10828	28.91560	0.19390	1251.553	1.07044	254.268	4.256
0.65460	1600	0.23205	0.06294	15.62828	0.76754	0.02680	0.12240	46.21648	0.32344	1977.508	1.80001	246.160	2.770
0.72206	2000	-0.06919	0.06409	13.51500	0.57118	0.22317	0.09589	34.87673	0.29176	1548.790	1.85501	266.598	3.652
0.76581	2600	0.05687	0.06233	21.08181	0.90001	-0.04859	0.09450	22.61750	0.20987	1122.760	1.85991	287.977	5.095
0.85013	3200	0.27129	0.06696	88.27110	1.13323	0.82147	0.10996	43.58705	0.31537	2491.500	2.02079	322.611	3.242
1.00000	4000	0.57809	0.05822	179.71800	1.32940	1.44497	0.11070	77.48132	0.45511	4319.497	2.04892	313.091	2.073
MC14-x15d A493-i Plagioclase													
mass=1		J= 0.00353943 +/- 0.00000770415				tot.gas.age= 328.52 +/- 1.075							
0.00346	150	0.66556	0.12602	6.21842	0.50396	1.32356	0.09441	2.69764	0.09694	813.949	1.70184	1070.304	56.733
0.00662	200	0.33006	0.06436	7.98233	0.56529	0.36861	0.10781	2.46907	0.11414	276.782	0.72897	412.576	42.714
0.01874	300	0.95350	0.10232	35.51610	0.45243	0.66934	0.09125	9.46193	0.18872	890.127	1.02913	369.906	17.922
0.04146	400	1.09089	0.09202	71.52793	0.77774	0.70865	0.08347	17.74160	0.12383	1353.482	1.65842	337.484	8.412
0.07002	500	0.50914	0.10737	119.14959	0.97086	0.43792	0.08124	22.29772	0.21470	1363.337	1.03702	317.653	8.123
0.09885	600	0.06909	0.06204	155.93594	1.24643	0.19503	0.08011	22.50609	0.15735	1191.107	1.03164	304.872	4.818
0.16000	800	0.70370	0.08592	321.94504	1.73727	0.60030	0.05942	47.74495	0.31144	2689.913	1.80772	304.696	3.408
0.25599	1000	0.85391	0.09676	330.18318	1.69684	0.56144	0.10317	74.94108	0.53230	4029.681	3.64915	296.157	2.849
0.32780	1200	0.41137	0.06465	283.68850	1.71553	0.37996	0.09338	56.06742	0.45210	2874.043	2.11768	289.034	2.850
0.39018	1600	0.45843	0.06724	288.27397	1.90205	0.44904	0.08175	48.69820	0.30938	2596.959	3.19605	296.924	2.836
0.44382	2000	0.75118	0.06430	238.01020	1.73611	0.77062	0.07652	41.88000	0.26480	2476.128	1.95584	314.593	3.053
0.51556	2600	1.71864	0.09633	260.14825	0.35772	2.06291	0.14821	56.00727	0.29430	3945.794	1.32388	354.691	3.161
0.81810	3200	4.31958	0.09268	1838.78199	2.61687	6.27091	0.08944	236.19978	0.83535	15465.815	6.28161	347.806	1.283
1.00000	4000	1.64687	0.05017	1298.20783	5.26536	4.59289	0.09885	142.01831	0.58761	8369.527	3.22879	323.592	1.353
MC14-x15e A493-i Plagioclase													
mass=1		J= 0.00353943 +/- 0.00000770415				tot.gas.age= 310.412 +/- 2.282							
0.00036	150	0.45882	0.07052	-0.69985	0.79398	0.09735	0.10765	0.09103	0.08502	125.194	0.59885	-932.523	2705.394
0.00090	200	0.46642	0.06078	0.43487	0.81205	0.07606	0.09292	0.13819	0.08316	158.375	0.98030	762.886	660.923
0.00360	300	0.54644	0.07652	0.53007	0.79778	0.25578	0.10324	0.68276	0.15351	366.091	1.15807	1304.465	232.740
0.00811	400	0.56741	0.08310	0.87753	0.86335	0.30228	0.09976	1.14199	0.09749	436.116	0.77211	1092.205	102.552
0.01317	500	0.27516	0.07430	1.93368	0.78453	0.26051	0.09440	1.28378	0.10915	199.122	0.66591	507.439	90.648
0.02627	600	0.27405	0.09009	3.02481	0.91228	0.38456	0.14222	3.31893	0.10776	239.147	0.57429	281.200	44.646
0.09523	800	0.63358	0.10063	29.03869	1.33303	0.30490	0.10448	17.47026	0.27456	1249.179	1.52167	351.555	10.269
0.22598	1000	0.35435	0.10266	73.39588	1.23220	0.36581	0.08888	33.12819	0.18856	1910.148	2.26026	318.207	5.189
0.37460	1200	0.06480	0.09374	89.39352	2.03860	0.03010	0.07742	37.65530	0.23920	1915.115	1.86953	295.866	4.356
0.59177	1600	-0.05725	0.09880	129.01470	0.85054	0.24424	0.06813	55.02280	0.13263	2820.854	2.09256	302.487	2.950
0.72665	2000	0.20760	0.08301	81.60987	1.19462	0.07805	0.12371	34.17334	0.23001	1741.914	1.50152	289.498	4.307
0.83570	2600	0.14100	0.09068	62.22795	1.10814	0.09265	0.07095	27.63074	0.23884	1400.348	1.53386	289.472	5.768
0.92266	3200	0.15508	0.09045	49.24869	0.75041	0.07098	0.07502	22.03106	0.14112	1145.820	1.01463	293.581	6.813
1.00000	4000	0.30288	0.10662	39.56204	0.88287	0.05033	0.09750	19.59561	0.17343	1029.726	1.64532	282.980	9.089

F39	LasPowm	Vol36	Err36	Vol37	Err37	Vol38	Err38	Vol39	Err39	Vol40	Err40	Age(Ma)	AgeErr
MC14-x15f A493-i Plagioclase													
mass=1		J= 0.00353943 +/- 0.00000770415				tot.gas.age= 350.025 +/- 1.067							
0.00031	150	0.27993	0.08529	-0.86349	0.70552	0.48261	0.11553	0.35765	0.07975	203.514	0.74282	1418.679	300.074
0.00103	200	0.14798	0.05466	0.73634	0.94687	0.43140	0.11741	0.82833	0.12859	222.305	0.85380	1023.006	140.363
0.00344	300	1.78411	0.09244	6.60953	0.90441	1.60594	0.17142	2.75934	0.16038	1146.297	1.72989	1054.508	58.321
0.00878	400	2.77403	0.10441	12.53070	0.84431	1.50086	0.10458	6.12305	0.15998	1480.578	1.96503	583.683	26.723
0.01996	500	3.34512	0.12332	30.41454	1.44261	1.27309	0.13363	12.81846	0.23586	1700.316	2.44705	323.730	16.155
0.04093	600	3.33609	0.09738	57.53091	1.07572	1.52324	0.09025	24.03503	0.23487	2422.294	1.83100	346.185	7.034
0.09048	800	7.98020	0.08810	189.41165	1.61629	3.31691	0.11836	56.80807	0.38792	6336.330	2.60075	399.478	3.398
0.13879	1000	1.16562	0.19687	143.06771	0.84299	0.56142	0.09121	55.38349	0.27870	3269.534	1.84367	309.174	5.832
0.19238	1200	1.21029	0.11211	129.16483	1.47395	0.60904	0.06922	61.43383	0.36297	3628.072	3.81337	311.431	3.371
0.37704	1600	6.60911	0.18601	257.53485	2.69428	3.44795	0.16147	211.69463	0.63757	13575.271	6.14469	320.361	1.654
0.49521	2000	2.20174	0.09886	198.82473	2.22073	1.10256	0.14425	135.47085	0.53286	7519.197	3.50370	297.767	1.597
0.60506	2600	4.09188	0.14257	269.31072	2.11155	3.71077	0.13089	125.92831	0.33534	8981.713	1.73175	356.465	1.955
0.75825	3200	8.61401	0.17009	674.39667	2.99164	7.02734	0.16340	175.62282	0.99283	14549.557	4.58858	390.878	2.477
1.00000	4000	8.17694	0.13856	1074.57789	3.04238	6.94071	0.17878	277.14479	0.88588	19599.870	5.79273	357.933	1.300
MC14-x15g A493-i Plagioclase													
mass=1		J= 0.00353943 +/- 0.00000770415				tot.gas.age= 301.585 +/- 1.313							
0.00188	150	1.47309	0.09922	2.06643	0.72293	1.42665	0.09495	1.05943	0.09820	800.165	1.52984	1437.935	121.658
0.00481	200	0.68511	0.08558	4.82430	0.66269	0.65406	0.09275	1.64511	0.07757	370.343	0.96642	556.344	75.611
0.01638	300	1.13342	0.12200	13.90670	0.86169	0.78184	0.09039	6.50786	0.07208	693.973	0.87581	321.806	29.783
0.04080	400	1.41686	0.08943	31.04969	0.96126	0.56988	0.11783	13.73281	0.15126	1042.601	1.73554	269.014	10.961
0.07954	500	1.45236	0.09194	60.76509	1.06133	0.55126	0.08004	21.78895	0.22106	1489.788	1.61658	286.771	7.317
0.12613	600	1.01865	0.09696	73.63161	1.47579	0.36826	0.07287	26.20573	0.25485	1488.303	1.50497	268.320	6.496
0.20779	800	0.96779	0.10618	130.17636	1.43609	0.49240	0.07988	45.92336	0.34443	2478.906	2.05671	281.726	4.221
0.28093	1000	0.59143	0.11992	119.46786	1.29477	0.29733	0.07545	41.13893	0.20932	2139.477	1.45950	281.760	4.893
0.33336	1200	0.28076	0.09383	79.50449	0.68472	0.16248	0.08011	29.48595	0.24458	1466.536	1.18985	277.194	5.578
0.38629	1600	0.29021	0.10597	71.60647	1.04768	0.11059	0.08752	29.76890	0.12283	1474.478	0.74437	275.699	5.863
0.42235	2000	0.24785	0.06032	42.06123	1.31634	0.08922	0.10722	20.28033	0.16443	1020.028	1.24432	275.890	5.256
0.46776	2600	0.51889	0.08273	52.47435	1.21480	0.11347	0.07182	25.54279	0.16900	1428.160	1.28807	293.474	5.502
0.97470	3200	4.61728	0.18030	937.56002	3.37710	3.85469	0.11522	285.11704	0.22313	16631.484	6.91665	313.105	1.036
1.00000	4000	0.27041	0.07253	37.56053	1.19662	-0.07245	0.08647	14.22680	0.15434	810.509	1.14092	301.296	8.690
MC14-x18a A493-m Groundmass													
mass=1		J= 0.00354243 +/- 0.0000106972				tot.gas.age= 237.728 +/- 0.678							
0.00025	100	0.60880	0.07793	0.87454	0.11988	0.36478	0.07963	5.86306	0.12410	273.932	1.10974	99.690	23.867
0.00171	150	2.07785	0.11155	2.80513	0.14645	0.90213	0.09375	33.93714	0.29135	1105.325	1.22773	90.228	5.957
0.00386	200	1.97349	0.08048	4.06327	0.17407	1.18841	0.06458	49.99365	0.29948	1441.067	0.89080	106.463	2.934
0.00674	250	1.86609	0.09840	4.85252	0.17990	1.02354	0.06262	67.28180	0.36987	1986.711	1.97103	131.426	2.667
0.01005	300	1.33002	0.09262	5.99638	0.19990	0.90702	0.08525	76.96344	0.12050	2317.607	2.09177	153.125	2.106
0.01800	400	3.56228	0.08667	13.59524	0.33214	2.41073	0.12450	185.25172	0.51626	6015.588	3.30760	163.567	0.923
0.03152	500	4.77158	0.12458	20.41676	0.25708	2.37878	0.09557	314.96000	0.68138	10148.112	2.43073	169.123	0.766
0.05345	600	5.85649	0.08351	32.58379	0.25075	2.51763	0.19580	510.72445	1.09572	17168.198	6.19213	183.516	0.473
0.10733	800	10.78794	0.21134	78.27718	0.35193	5.54022	0.18939	1254.99919	0.96236	46636.411	13.75924	208.701	0.327
0.17270	1000	6.34575	0.08227	88.06919	0.53765	3.67450	0.17007	1522.68508	1.92608	63784.250	20.38979	242.747	0.310
0.22890	1200	2.54424	0.08219	75.63368	0.24339	1.49306	0.20881	1308.89884	1.38643	58189.146	13.48238	260.670	0.283
0.30111	1600	3.05578	0.06107	114.67950	0.52544	1.67536	0.16271	1682.00578	1.85549	73819.702	16.22611	257.730	0.277
0.36547	2000	2.21038	0.03659	107.22194	0.41384	1.73135	0.16274	1499.01378	2.31428	63534.804	17.96196	249.944	0.369
0.44411	2600	2.46662	0.06931	141.42961	0.51214	2.59758	0.24154	1831.64538	2.46100	75683.262	21.10168	244.222	0.320
0.53232	3200	2.70620	0.10685	144.03900	0.80223	3.00010	0.19744	2054.57393	2.70951	83814.300	21.58621	241.333	0.316
0.64583	4000	3.65753	0.09658	204.22599	0.55096	5.77030	0.29151	2644.06445	1.83136	106870.139	39.81064	239.125	0.187
0.84593	4001	8.95244	0.10684	521.45452	1.50273	16.81056	0.28039	4660.59942	4.37290	188094.780	28.27888	237.898	0.215
1.00000	4002	6.25375	0.07731	655.50087	1.48215	12.50043	0.19922	3588.73796	4.07607	146216.605	48.63209	240.346	0.269
MC14-x18b A493-m Groundmass													
mass=1		J= 0.00354243 +/- 0.0000106972				tot.gas.age= 240.952 +/- 0.686							
0.00015	100	0.35735	0.11745	0.13223	0.14939	0.31475	0.08591	3.14453	0.10444	166.969	0.80093	120.606	66.105
0.00107	150	1.06384	0.12573	1.00078	0.18127	0.56602	0.10467	18.64493	0.15830	537.667	1.25194	74.961	12.239
0.00370	200	1.47166	0.09726	2.51425	0.20466	2.34402	0.12146	53.61918	0.05140	1802.526	3.00320	156.060	3.162
0.00627	250	1.03981	0.09205	2.39147	0.16930	1.10489	0.08947	52.35696	0.26679	1552.230	1.25296	145.901	3.148
0.00946	300	1.23695	0.09141	3.14637	0.20843	0.86333	0.09795	65.05898	0.32396	2101.622	2.64850	162.953	2.557
0.01953	400	4.08956	0.10723	9.32385	0.24397	2.68890	0.17104	205.25972	0.51339	6811.039	2.03788	166.511	0.986
0.03940	500	7.87278	0.12418	17.24058	0.21405	3.54486	0.16138	405.01163	0.91118	13269.779	5.67534	164.907	0.642
0.06611	600	4.29641	0.11041	23.65102	0.33647	2.79123	0.13740	544.22883	0.73948	19550.768	5.38012	202.832	0.434
0.12869	800	7.37195	0.08393	59.12322	0.38717	5.24549	0.19488	1275.54593	1.68689	51621.256	5.16232	232.126	0.309
0.18281	1000	2.04277	0.08940	52.91466	0.35456	2.19937	0.20122	1102.97729	1.37238	50238.824	13.87387	266.848	0.343
0.22850	1200	1.43437	0.10111	50.73210	0.56710	1.17396	0.14728	931.14263	1.12538	42508.770	8.16980	267.928	0.353
0.26974	1400	1.27853	0.08659	51.55966	0.34927	0.97221	0.21637	840.54992	1.57477	37179.542	9.04764	260.121	0.488
0.30676	1600	0.81322	0.06114	49.41002	0.17937	0.73659	0.14701	754.49705	1.15793	32313.649	8.90345	253.062	0.392
0.34026	1800	0.85120	0.07968	45.83361	0.41717	0.82875	0.15191	682.78677	1.47373	28852.825	5.59414	249.612	0.541
0.37489	2000	0.97262	0.07506	45.76625	0.29384	0.98913	0.13241	705.88870	0.96948	29804.724	7.20175	249.204	0.369
0.41294	2200	0.70138	0.13621	47.18140	0.30988	1.23730	0.13319	775.41664	0.95050	32461.844	6.21120	247.983	0.408
0.45602	2400	1.12296	0.09131	55.86682	0.55253	1.88142	0.14477	878.07001	0.83339	36385.791	8.25516	244.995	0.282
0.50219	2600	1.14142	0.09718	58.58911	0.36982	1.78572	0.23633	940.96733	0.92620	38688.276	8.36982	243.301	0.286
0.55376	2800	1.17701	0.12246	62.09009	0.35870	1.73775	0.19508	1051.11533	1.73876	43056.884	20.08317	242.604	0.436
0.60963	3000	1.47422	0.09222	71.35436	0.38465	2.68681	0.12416	1138.64672	0.99623	46362.361	6.14181	240.940	0.241
0.66850	3200	1.26605	0.07998	87.97516	0.43029	2.85683	0.16484	1199.88440	1.02695	48886.034	6.35148	241.477	0.225
0.73483	3400	1.54018	0.07008	110.50178	0.42140	3.99363	0.18675	1351.94546	1.64497	54893.285	12.08752	240.560	0.292
0.79925	3600	1.43892	0.04848	108.74069	0.42536	3.78111	0.20596	1312.74966	1.39435	53109.560	7.72312	239.812	0.249
0.86666	4000	1.43345	0.07963	131.50284	0.38852	4.98980	0.23166	1374.08245	1.16606	55575.586	12.36629	239.837	0.219
1.00000	4001	3.06481	0.12051	304.85098	0.89237	12.64014	0.22108	2717.53047	2.87334	109311.053	92.40700	238.459	0.312

Legend and explanation for Table A1. The volumes are in units of 1E-13 ccSTP. All data have been corrected for isotope interference reactions. Uncertainties are one standard deviation.

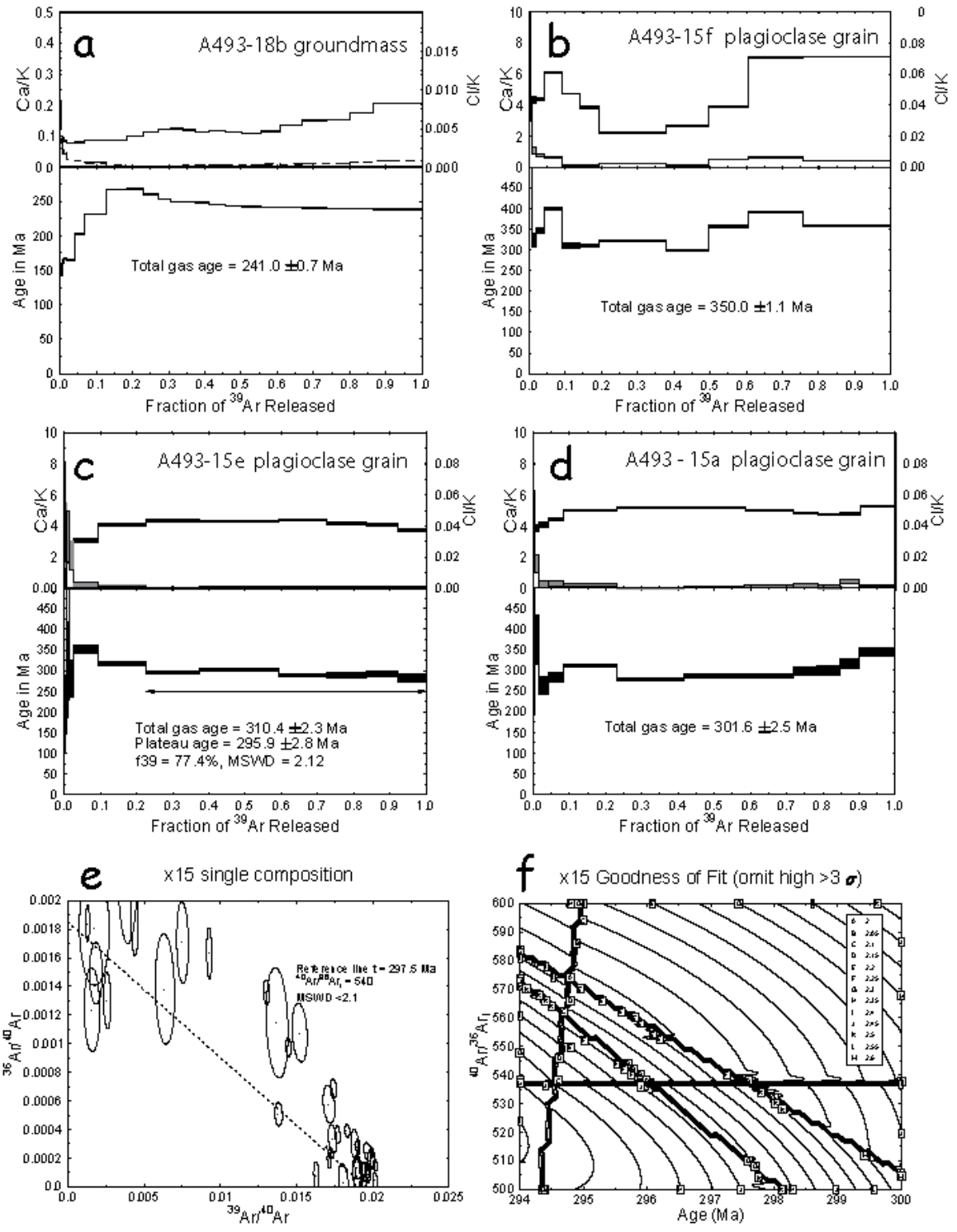

Fig. A1. Examples of Ar release spectra and element ratios for several samples from the paleomagnetic site A493. a) groundmass sample; b) plagioclase grain, likely a xenocryst, showing an Ar/Ar age that is significantly older than stratigraphic age of the rock; c) and d) plagioclase grains; e) inverse isochron for three samples showing the least evidence for the contamination; f) a goodness of fit plot.

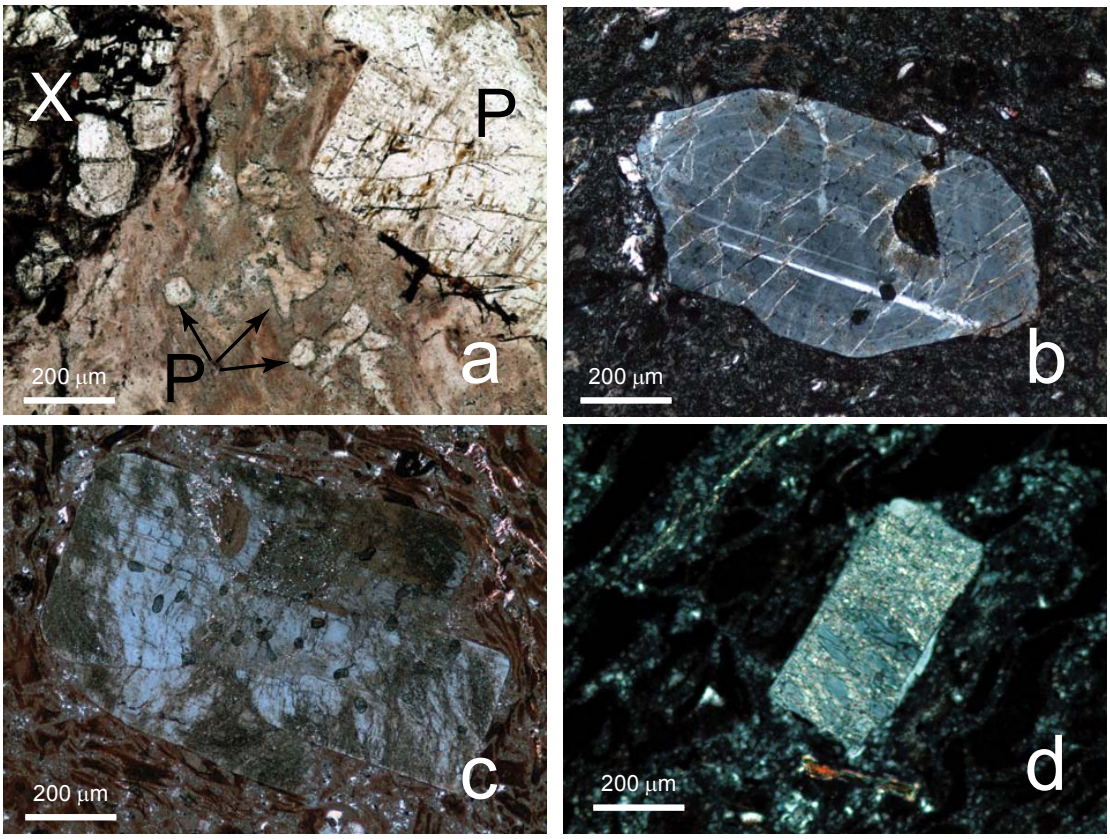

Fig. A2. Micrographs of plagioclase grains. (a) different sources of plagioclase grains: lithic clast (x) with plagioclase and plagioclase phenocrysts (P); (b-d) plagioclase grains showing different degrees of alteration from relatively light (b), to severe (c, d).

References

Fleck, R.J., Mattinson, J.M., Busby, C.J., Carr, M.D., Davis, G.A., Burchfiel, B.C. 1994. Isotopic complexities and the age of the Delfonte volcanic rocks, eastern Mescal Range, southeastern California; stratigraphic and tectonic implications. *Geological Society of America Bulletin*, 106 (10), 1242-1253.

Gansecki, C.A., Mahood, G.A., McWilliams, M.O. 1996. ^{40} Ar/ ^{39}Ar geochronology of rhyolites erupted following collapse of the Yellowstone Caldera, Yellowstone Plateau volcanic field; implications for crustal contamination. *Earth and Planetary Science Letters*, 142 (1-2), 91-108.

Hall, C.M., Kesler, S.E., Simon, G. and Fortuna, J., 2000, Overlapping Cretaceous and Eocene Alteration, Twin Creeks Carlin-Type Deposit, Nevada. *Economical. Geology*., 95, 1739-1752.

Miller, J.S., Heizler, M.T., Miller, C.F. 1998. Timing of magmatism, basin formation, and tilting at the west edge of the Colorado River extensional corridor; results from single-crystal ^{40}Ar/ ^{39}Ar geochronology of Tertiary rocks in the Old Woman Mountains area, southeastern California. *Journal of Geology*, 106 (2), 195-209.

Samson, S.D. and Alexander, E.C., 1987, Calibration of the interlaboratory 40Ar-39Ar dating standard, MMhb-1. *Chemical Geology*, 66, 27-34.

Smith, M.E., Singer, B., Carroll, A. 2003. ^{40}Ar/ ^{39}Ar geochronology of the Eocene Green River Formation, Wyoming. *Geological Society of America Bulletin*, 115 (5), 549-565.

Spell, T. L., Smith, E.I., Sanford, A., Zanetti, K.A. 2001. Systematics of xenocrystic contamination; preservation of discrete feldspar populations at McCullough Pass Caldera revealed by ^{40}Ar/ ^{39}Ar dating. *Earth and Planetary Science Letters*, 190 (3-4), 153-165.

Appendix B

Overview of previous studies on stability of iron (oxyhydr)oxides towards reductive dissolution

For a good review on dissolution studies of magnetic minerals see Cornell and Schwertmann, (2003). The next section only briefly summarizes information relevant to our study. Dissolution behavior of iron oxides has been studied extensively, but most of those studies were aimed primarily at elucidating the main principles of dissolution mechanisms and factors controlling the rate of the reaction (Cornell and Schwertmann, 2003, and references herein). The common approach in dissolution studies is to add known chemical reagents or bacterial cultures to a known iron oxide (usually a single-phase suspension, or a mixture of minerals with widely differing reactivities) and monitor the change in iron released into the solution. The data (the concentration of the Fe^{2+} in the solution as a function of time) then is tested against several theoretical models (concentration or a surface-controlled diffusion, etc.). As criteria of suitability of the particular model, the correlation coefficient between measured and predicted values is usually used. According to a chosen model, a parameter related to stability, either a rate constant or a half-life can be calculated for a specific iron oxide mineral and specific experimental conditions.

It has been well established that multiple factors influence the rate of dissolution of Fe oxides, among them temperature, composition of the solution (pH, concentration of acids, reductant and complexing agents), and properties of the oxide (specific surface area, stoichiometry, crystal habit, presence of defects or guest ions). Currently, there are no models that take all of these factors into account. In general, only the specific surface area, the composition of the solution and in some cases the tendency of the ions in the

solution to form surface complexes are considered. Even when those factors are included into calculations, they are, by necessity, simplified. For example, the change in the specific surface area during dissolution is modeled on the assumption of what is called shape-preserving dissolution. Each crystal face is assigned its own dissolution rate, and during dissolution, the reacting interface is considered as moving inwards at a constant rate, thus preserving the overall shape of the oxide crystal. As laboratory studies have shown, this is rarely the case (e.g. Schwertmann, 1984).

There are a number of rate equations that are commonly applied to dissolution processes (Brown et al., 1980). Often, the data obtained during the laboratory experiments could either fit reasonably well by more than one physical model or by none of them, suggesting that an apparent rate law is the result of the interaction between several counterbalancing processes (Cornell and Schwertmann, 2003). Thus, there is a significant uncertainty in an absolute value of a stability parameter, calculation of which depends on the physical model chosen.

According to previous studies (see a review in Cornell and Schwernmann, 2003), iron oxides could be divided into two groups based on their reactivity. Poorly-crystalline oxides such as ferrihydrite, lepidocrocite, and green rust have rate constants ~two orders of magnitude higher than well-crystalline oxides, magnetite, hematite and goethite. The relative stabilities of the last group are poorly defined, especially those of goethite and hematite. Although goethite and hematite have similar thermodynamic stabilities, their dissolution rates relative to each other and to magnetite can vary significantly depending simply on whether the rates are expressed in terms of surface area (goethite < hematite < magnetite), or in terms of mass (hematite < magnetite < goethite) (e.g. Poulton et al., 2004). It is not clear how applicable these stability schemes are to rock magnetic studies, as magnetic properties of mineral grains depend on both their volume and shape.

References

Cornell, R. M., Schwertmann, U. 2003. The iron oxides: structure, properties, reactions, occurrences, and uses. Weinheim: Wiley-VCH, 664 pp.

Schwertmann, 1984. The influence of aluminiun on iron oxides. IX. Dissolution of Al-goethites in 6 M HCl. *Clay minerals*, 19, 9-19.

Brown, W.E.B., Dollimore, D. and Galwey, A.K. 1980. Reactions in the solid state. In: Bamford, C.H. and Tipper, C.F.H. (eds.) Comprehensive chemical kinetics. Elsevier Amsterdam, 22, 41-109.

Poulton, S.W., Krom, M.D., Raiswell, R. 2004. A revised scheme for the reactivity of iron (oxyhydr)oxide minerals towards dissolved sulfide. *Geochimica et Cosmochimica Acta*, 68(18), 3703-3715.